AN INVESTIGATION OF THE ACTIVITY OF COMPOSITE CATALYST BEDS FOR HYDROTREATMENT OF A COAL-DERIVED LIQUID

By

OPINDER KISHAN BHAN

Bachelor of Engineering
University of Kashmir
Srinagar, India
1978

Master of Science
Oklahoma State University
Stillwater, Oklahoma
1981

Submitted to the Faculty of the Graduate College
of the Oklahoma State University
in partial fulfillment of the requirements
for the Degree of
DOCTOR OF PHILOSOPHY
December, 1983

AN INVESTIGATION OF THE ACTIVITY OF COMPOSITE CATALYST BEDS FOR HYDROTREATMENT OF A COAL-DERIVED LIQUID

Thesis Approved:

Billy L Hynes
Thesis Adviser

Jerald D Parker

Mayis Seapan

Norman N Durham
Dean of the Graduate College

PREFACE

Two different nickel-molybdenum on alumina catalysts, Ketjen KF-153 S and Harshaw HT-115 E were used for hydrotreatment of a coal-derived liquid. Four experimental runs were conducted using different temperatures and liquid volume hourly space times, hydrogen pressures and gas flow rates were held constant. Product liquid samples were analyzed for nitrogen and hydrogen content, some selected liquid samples were also subjected to ASTM distillation and solvent residue analysis. Spent catalysts were analyzed for their surface area, pore volume, pore diameter and metal content.

For all the experimental runs conducted during this study, no equipment operation problems were encountered even while hydroprocessing a highly viscous coal liquid over extended periods of time. A trickle-bed reactor system, with two reactors in series, was constructed for conducting this study. This system was designed with major emphasis on avoiding reactor and exit liquid line plugging. This work is a first step in the development of the concept of composite catalyst beds, considerably useful data has been generated for design of such reactors.

I am deeply indebted to my thesis adviser, Professor Billy L. Crynes, who inspired and guided me through this thesis and also through my entire graduate work. I am also thankful to Dr. M. Seapan, Dr. J. Parker, Dr. J. Wagner and Dr. R. N. Maddox for their excellent guidance and cooperation during the various phases of this project. A special

note of thanks is due Mr. Preston Wilson, for his cooperation in building the apparatus, and Ms. Elizabeth Struble, for her invaluable assistance in locating library materials.

I am very grateful to Messrs. Shaun Pearson, Steve Smith, Jana Patterson, James Wolfe and Ale Nugyen for their help in operating the equipment and analytical instruments. I would also like to take the opportunity to thank all of the staff at the School of Chemical Engineering, especially Mrs. Dee Maule, Mrs. Marcia Kitchens, and Mr. Charles Baker, the store manager, for their cooperation in completing the needed paperwork for this research. A special note of thanks for Ms. Teresa Tackett for typing this manuscript.

Financial support from the Department of Energy and the School of Chemical Engineering is sincerely appreciated.

Finally, I would like to dedicate this work to my father, Professor Brij K. Bhan, who introduced me to science and scientific thought. I would also like to express my deepest gratitude to my parents and my brother, Mr. Roop K. Bhan, for their constant support and encouragement throughout the duration of this work.

TABLE OF CONTENTS

Chapter Page

LIST OF TABLES

LIST OF FIGURES

Figure Page

CHAPTER I

INTRODUCTION

Coal-derived liquids produced by the various coal liquefaction processes (H-Coal, Solvent Refined Coal, Synthoil, Exxon Donor Solvent) are low in hydrogen and high in heteroatom content (nitrogen, oxygen, sulfur). Catalytic hydroprocessing has been used to reduce the heteroatom content and also to increase the hydrogen content.

During hydrotreatment, sulfur, nitrogen, and oxygen are removed as hydrogen sulfide, ammonia, and water, respectively. Sulfur must be removed from the coal liquids to meet the low levels required for further catalytic processing, and also to meet the environmental emission standards. Nitrogen removal is necessary for the following reasons:

1. Nitrogen-containing compounds severely reduce the activity of cracking, reforming, hydrocracking, and isomerization catalysts.

2. Coal liquids are highly carcinogenic due to the high aromatic nitrogen content.

Certain oxygen-containing compounds are acidic, and their presence is unwelcome. Further, upon storage coal liquids increase in viscosity and gum deposits occur; hydrotreatment results in more stable product.

Coal-derived liquids differ in composition and properties from the petroleum-derived fuels; they possess higher concentrations of

heteroatoms, polyaromatics, metals and asphaltenes, and lower concentrations of hydrogen. Commercial petroleum feedstock hydrotreatment processes have been used to upgrade coal liquids. The catalyst types usually employed are cobalt-molybdenum or nickel-molybdenum on alumina support. These catalysts, however, deactivate significantly over short periods of time, rendering such processes commercially infeasible.

A coal-derived liquid (Solvent Refined Coal), representative of the various coal liquids presently being produced, was selected for hydroprocessing over various commercially available nickel-molybdenum on alumina catalysts (Ni-Mo-Al_2O_3). The following were the principal objectives of this study:

1. Design, construct, and test a trickle-bed reactor system with multiple catalyst zones.

2. Study the effect of catalyst properties (pore diameter, pore volume, surface area) on hydrotreating activity.

3. Study the effect of catalyst zoning (employing two or more different catalysts) within the reactor on overall hydrotreatment activity.

4. Investigate the concept of guard-chambers for improving catalyst life in the main reactor bed.

This study is the first step in the direction of developing the concept of composite catalyst bed reactors. With the advent of heavy petroleum and alternate crude processing, hydrotreating catalysts will be hydroprocessing feedstocks high in metal, aromatic and heteroatom content. These catalysts would thus be more susceptible to deactivation. Composite catalyst beds, with different catalysts in different sections of the reactor, can reduce the overall bed deactivation by introducing

metal and coke resistant catalysts in the top reactor sections, and high heteroatom removal activity catalysts in the lower sections. Considerable amount of data has been generated during this study. In all, four experimental runs were conducted on a newly constructed trickle-bed reactor system. Two different Ni-Mo-Al_2O_3 catalysts (small and large pore diameter) were used separately, and in combination in composite catalyst beds. One of the composite catalyst bed experiments was conducted using temperature zoning within the reactor bed.

Liquid sample elemental analysis revealed that the catalysts lost significant fraction of their initial activity during the first 12-36 hours of oil-catalyst contact, the loss in activity was less severe during the remaining period of the experimental run. Pore volume and surface area analysis of the coked catalysts revealed significant reduction in the pore volume for both the catalysts tested, the loss in surface area of the two catalysts, however, was different. The small pore catalyst lost approximately 40% of its fresh surface area, the loss for the large pore diameter catalyst was less than four percent.

Significant carbonaceous residues were deposited on the aged catalyst samples. On a surface area basis, the large pore diameter catalyst deposited twice the amount of coke deposited on the small pore diameter catalyst. The coke deposition profiles within the catalyst bed were also different for the two catalysts. The difference in the mechanism of coke deposition on the two catalysts is hypothesized to occur due to the difference in the catalyst physical properties. The two catalysts used in this study contained different amounts of silica in the alumina support, the small pore diameter catalyst contained 4.1 wt% silica compared to only 0.1 wt% silica in the large pore diameter catalyst.

Contrary to the popular belief of higher hydrocracking activity and subsequent higher coke deposition on the high silica catalysts, the small pore diameter catalyst deposited less coke than the large pore diameter catalyst; further strengthening our hypothesis of coke deposition being a function of catalyst physical properties.

The composite catalyst bed combination used during this study did not show a significant improvement in the bed hydrotreatment activity. This should not, however, discourage further research using other catalyst combinations. Several reasons can be attributed to the lack of response of the composite catalyst bed combination during this study, the most significant being the rapid catalyst deactivation during the initial oil-catalyst contact time.

CHAPTER II

CONCLUSIONS AND RECOMMENDATIONS

Conclusions

A multiple trickle-bed reactor system was successfully constructed and operated to hydroprocess a coal-derived liquid. The reactor system was capable of being operated at pressures upto 17 MPa (2500 psig), and temperatures upto 450°C. This system was specially designed for processing highly viscous feedstocks, prone to liquid line and reactor plugging. A series of experimental runs were conducted using single, composite and temperature zoned catalyst beds. A global kinetic model was developed to facilitate design of catalytic reactors for coal-derived liquid hydrotreatment. An intrinsic kinetic model was also developed to study the effect of catalyst and feedstock properties on overall hydrotreatment activity. The following conclusions can be drawn from this study:

1. The multiple reactor zone hydrotreating system constructed during this study operated satisfactorily in terms of stabilities of temperature, pressure, liquid and gas flow rate controls. No operational problems were encountered while processing highly viscous SRC coal liquid over extended periods of time.

2. Substantial carbonaceous residues were deposited on the hydrotreating catalysts used during this study. These deposits consisted primarily of C, H, N, O, and sulfur atoms. The low hydrogen

and high heteroatom content of these residues points to the polynuclear condensed molecular structure of these deposits. The residues were noticed to be deposited on the catalyst even when the catalyst and the coal liquid were contacted at low temperatures (27-100°C). Irreversible adsorption of basic nitrogen species is hypothesized to be responsible for this phenomenon.

3. Both on the basis of catalyst mass and catalyst surface area, the large pore diameter catalyst deposited more coke. The coke content in the large pore diameter catalyst bed was observed to decrease from the reactor inlet to outlet; the coke deposition profile in the small pore diameter catalyst bed was exactly reverse.

4. The amount of coke deposited on the catalysts showed negligible dependence on process temperature for the temperature range of 260 to 400°C. Considerable amount of coke was deposited on the catalysts even at temperatures as low as 260°C. The catalyst age beyond 120 hours of oil-catalyst contact, too, did not effect the catalyst coke content significantly, signifying attainment of equilibrium coke contact prior to 120 hours of oil-catalyst contact.

5. The small pore diameter catalyst showed consistently higher hydrodenitrogenation, hydrogenation, n-pentane and 454 C^+ residue reduction activity compared to the large pore diameter catalyst. The higher activity of the small pore catalyst can be attributed to the higher surface area of the small pore catalysts. The small pore diameter catalyst lost activity less rapidly than the large pore diameter catalyst.

6. All catalysts and catalyst combinations used during this study lost significant hydrodenitrogenation, hydrogenation, n-pentane

and 454 C^+ residue reduction activity over the experimental run duration. The activity loss was severe during the first twelve to thirty-six hours of oil-catalyst contact, the activity tended to level-off during the remaining run duration. The rapid carbonaceous deposition and basic species adsorption can be responsible for the initial catalyst deactivation, combined coke and metal deposition causes the gradual catalyst activity loss.

7. The composite catalyst bed combination offered no significant advantage in the hydrodenitrogenation, hydrogenation, n-pentane and 454 C^+ residue reduction activity over single catalyst beds. The amount of coke deposition and the rate of catalyst deactivation, too, were comparable to single catalyst beds.

8. The coked catalyst surface area and pore volume analyses revealed that the large pore diameter catalyst lost substantial pore volume and pore diameter with only negligible reduction in surface area. On the contrary, the small pore diameter catalysts lost significant fraction of their surface area and pore volume without a corresponding decrease in catalyst pore diameter. The coked small pore diameter catalyst pore size distribution remained unaltered compared to the significant reduction observed for the large pore catalyst.

9. The reactor temperature zoning offered several advantages over the conventional single temperature reactor beds. Approximately all the inorganic and heavy carbonaceous residues were removed in the low temperature reactor section, the high temperature zone was almost residue free. The hydrodenitrogenation, hydrogenation, and n-pentane residue reduction activity of the temperature zoned bed was

consistently higher than the single temperature catalyst bed when the catalysts were compared on the basis of high temperature catalyst reactor volume. No advantage, however, was noticed in the amount of coke deposited for the temperature zoned reactor beds.

10. The small pore diameter catalyst selectively excluded large molecular species from the catalyst interior. This was evidenced by the negligible dependence the THF insoluble fractions showed on the catalyst age. Exclusion of the large molecular species, which are known to be active coke precursors, from the small pore diameter catalyst interior may be responsible for its lower deactivation rate.

11. For all catalysts used during this study, a thin crust was deposited on the catalyst exterior, this crust was identified to consist primarily of Fe, Si and S. In addition to the external deposits, Fe and Ti were deposited in the catalyst interior; Ti was noticed to occur in clusters. The metal deposition occurred primarily in the catalyst periphery for both the small and the large pore diameter catalysts.

12. Residues consisting of inorganics and THF insoluble fractions were deposited on glass beads and catalyst interstices for all experiments conducted. These fractions were observed to contain 70 wt% ash, the remaining fraction being composed of low hydrogen, high heteroatom content residues. The amount of the interstitial residues decreased along the reactor length. The glass beads in the pre- and post- reactor sections had a uniform residue layer deposited on them.

13. The kinetics of coal liquid hydrodenitrogenation was adequately represented by a first order global model.

14. An intrinsic kinetic model revealed catalyst pore sizes five times the size of the diffusing molecule to be optimum for hydrodenitrogenation activity.

Recommendations

In the coming decade, the US refineries are expected to handle substantially higher amounts of heavy petroelum and synthetic crudes. Greater attention must thus be focused on the development of new generation of catalysts and processing techniques capable of avoiding early catalyst deactivation and high hydrogen usage. The present work is a first step in this direction. For the continuity of this project, the following recommendations are made based on the results and experience gained from this study:

1. The coke deposition on hydrotreating catalyst should be studied against the following:

   a. Process temperature in the range of 200-500°C.

   b. Process times less than 12 hours of oil-catalyst contact.

   c. Catalyst active metal content.

   d. Catalyst support chemical and physical properties.

   e. Boiling ranges of the feedstock. The feedstock should be separated into three boiling ranges (IBP-315°C, 315°C-450°C,>450°C), and each fraction separately hydrotreated.

2. The guard-bed reactor concept must be more thoroughly investigated. The effect of guard-bed reactor temperature and type of material should be determined. Temperatures in the range of 150 to 450°C must be studied. The following materials are recommended for testing in the guard-bed reactor: large pore size (>200 Å) alumina,

high silica content alumina, mill slag, glass beads, activated carbon, and low metal content high surface area catalyst spheres (Shell 524 catalyst).

3. The effect of introducing H_2S in addition to H_2 at the reactor inlet on the overall bed hydrodemetallation activity should be determined.

4. The concept of composite catalyst beds needs a more thorough investigation, the following configurations are recommended:

   a. Large pore diameter catalyst in the reactor top (>200 Å), followed by small pore diameter catalyst (<60 Å).

   b. Shape selective composite catalyst beds. Spherical pellets in the top reactor section (high mechanical strength) followed by small diameter extrudates.

5. Following experiments should be conducted to investigate reactor temperature zoning effect: high temperature (500°C), low space time (0.1 hrs) hydrocracking over Ni-W-Al_2O_3 or high silica content Ni-Mo-Al_2O_3 catalyst followed by hydrotreating at 350°C and one hour space time over a high hydrogenation activity Ni-Mo-Al_2O_3 catalyst. This experiment should be conducted in conjunction with a suitable guard reactor bed.

6. A catalyst deactivation mathematical model should be developed which takes both the initial carbonaceous and basic species adsorption, and subsequent combined metal and carbonaceous deposition into account.

7. Based on the prediction of the intrinsic mathematical model developed during this study, activity of a 120 Å pore diameter catalyst with approximately 3 wt% NiO and 15 wt% MoO_3 must be determined using 15 wt% SRC/Process Solvent mixture.

8. Catalyst poisoning by basic species adsorption should be thoroughly investigated. The effect of adsorbing species aromatic ring number, nitrogen content, molecular weight and nitrogen heteroatom location in the molecular structure should be studied. This study should also be extended to oxygen containing compounds.

9. Realistic measurements of coal liquid average molecular weight, molecular size, viscosity and density at reactor process conditions should be made to develop more effective mathematical models.

CHAPTER III

LITERATURE REVIEW

Considerable literature is available regarding coal-derived liquid hydroprocessing. In this review, only the topics most closely related to the present study are discussed. Considerable attention has been focused on the aging of hydrotreating catalysts to bring forth the urgency of developing catalysts specifically tailored for coal-derived liquids. Available literature on graded (two or more different catalysts contained within zones in a single reactor bed) catalyst beds, and catalyst guard beds has been thoroughly reviewed; attention has also been focused on the nature of coal-derived asphaltenes and their hydroprocessing.

Coal-Derived Liquid Hydrotreatment

Coal-derived liquids consist mostly of aromatic compounds, the most common being benzene, naphthalene, anthracene, phenanthrene, acenaphthylene, pyrene, chrysene, and fluorene. In addition, coal-derived liquids contain significant heterocyclic compounds. Sulfur containing compounds most commonly found in the coal-derived liquids are thiophene, benzothiophene, dibenzothiophene, benzonapthothiophene. Common nitrogen containing compounds are quinoline, carbazole, indole, acridine, benzacridine, and dibenzacridine. Coal-derived liquids are

also high in metals, which may be present in the oil soluble organo-metallic compounds, and/or in the inorganic fraction. The major metals in coal liquids are Fe, Ti, Al, Ca, Mg, and K.

Hydrotreatment of coal-derived liquids is typically achieved in trickle-bed reactors, at temperatures in the range of 300-425°C, and hydrogen gas pressures in the range of 10-20 MPa (Satterfield, 1975). Coal-derived liquid hydrotreatment in trickle bed reactors suffers from two major drawbacks: rapid catalyst deactivation due to coke and metal deposition, and severe reactor plugging due to residue deposition. For coal-derived liquids to commercially compete with petroleum crudes, the incidence of reactor plugging must be greatly reduced, and the life of hydrotreating catalyst improved. The following general reaction steps occur during hydrotreatment:

Hydrogenation and Hydrocracking: Preasphaltenes → Asphaltenes → Resins → Oils
Unsaturates → Saturates

Hydrodemetallation: Organometallic Compounds → Metal Deposits + Hydrocarbons

Hydrodenitrogenation: N-Compound → Hydrocarbon + NH_3

Hydrodesulfurization: S-Compound → Hydrocarbon + H_2S

Hydrodeoxygenation: O-Compound → Hydrocarbon + H_2O

Numerous studies have been devoted to the understanding of the mechanism of the heteroatom removal reactions. The coal liquids contain a myriad of chemical species, which precludes detailed study of the kinetics and mechanism of a particular species. Various researchers have attempted to gain better understanding of these reactions by

studying pure compounds representative of the heterocycles. The following works present detailed information on kinetics and reaction mechanisms of these reactions: Veluswamy, 1977; Gates et al., 1979a, 1979b; Stein, 1979.

SRC Liquid Processing

Solvent Refined Coal (SRC) feedstock has been used in various research laboratories. In all the investigations conducted with this feedstock, it has been diluted with a solvent (SRC being a solid at room temperature). Concentrations in the range of 15 to 90 wt% have been used. Severe reactor bed plugging and rapid catalyst deactivation have been reported by several authors while processing SRC coal liquids in trickle bed reactors (Chang, 1982; Ahmed, 1979; Stein et al., 1978; Bowman et al., 1980; Sullivan et al., 1981).

Considerable experimental work has been conducted at the Cities Service Company and the C. E. Lummus Company on hydroprocessing SRC-I in an expanded-bed reactor (LC- Fining process). Potts et al. (1980) reported stable, continuous operation over extended periods for this process (41 days). These reactor beds have an advantage over conventional trickle-bed reactors in that the turbulent action of the catalyst particles, due to extensive backmixing in the reactor, reduces the reactor bed-plugging tendency. These reactors, however, suffer from high catalyst attrition rates.

Mobil Oil Corporation under a contract from the Electric Power Research Institute (EPRI) has conducted considerable work on hydroprocessing SRC. A series of commercial and proprietary catalysts were

evaluated for hydroprocessing 50 wt% Kentucky, short contact time SRC (Angevine et al., 1979). All pilot plant lines and valves were reported to be heat traced to achieve smooth mechanical operation during hydroprocessing of the solvent diluted SRC solids. In an earlier report, Stein et al. (1978) reported post-reactor plugging and two-phase product formation while processing SRC over a small pore diameter Co-Mo-Al_2O_3 catalyst. These problems were, however, overcome by the use of a large pore diameter catalyst.

Chang (1982) studied the hydrotreatment of 30 wt% SRC-I mixture in process solvent, over Shell-324 Ni-Mo-Al_2O_3 catalyst. Severe catalyst deactivation was observed. Processing difficulties due to post-reactor plugging were also reported.

Greskovich et al. (1977) hydrotreated a 52 wt% SRC blend in Kopper's tar cresote oil over Ni-Mo-Al_2O_3 and Ni-W-Al_2O_3 catalysts. At both temperatures of operation, 400°C and 427°C, the Ni-Mo-Al_2O_3 catalyst was reported to be more active than the Co-Mo-Al_2O_3 catalyst. Severe equipment problems were reported by the authors while processing the SRC feedstock. Crynes (1981) hydroprocessed 30 wt% SRC/Process Solvent mixture over inert glass-beads; severe down-stream line plugging was reported to cause experimental run termination.

Coal-Derived Liquid Hydrotreatment Kinetics

Simple first-order kinetics has generally been used to mathematically model coal-derived liquid hydrotreatment over Ni-Mo-Al_2O_3 and Co-Mo-Al_2O_3 catalysts. These models are global types; the effect of various factors (diffusion resistance, external mass transfer resistance,

etc.) are lumped together in the reaction rate constant (White et al., 1968; Jacobs et al., 1971; deRosset, 1976). Several authors have separated the effects of physical properties and determined intrinsic kinetics of the hydrotreatment reactions (Chang, 1982; Ahmed, 1979). For coal-derived liquids, second-order models have also been reported. The second-order models may result in a better fit for some heavy feedstocks due to the different rates of reactions of the heteroatom species.

The following authors have used second-order kinetics to model coal-derived liquid hydrotreatment: Heck and Stein, 1977; Stein et al., 1978; Mehta, 1978; Shih et al., 1980; Soni, 1977; Angevine et al., 1979; Thakkar et al., 1981; Ternan and Brown, 1982. An excellent review of the kinetics of coal-derived liquid hydrotreatment has been conducted by Seapan and Crynes (1983); the reader is referred to this work for detailed information on coal liquid hydrotreatment kinetics.

This section can be summarized as follows:

1. Coal-derived liquids consist of highly aromatic compounds, low in hydrogen and high in heteroatom and metal content.

2. Catalytic hydrotreatment of coal liquids is usually conducted in trickle-bed reactors; this process suffers from the disadvantage of catalyst bed-plugging and rapid catalyst activity decay.

3. In addition to the trickle-bed reactors, ebullated bed reactors have also been used for hydrotreatment. These reactors are reported to avoid bed-plugging due to ebullition of the catalyst pellets.

4. Solvent Refined Coal has been used widely as a representative coal-derived liquid feedstock. In all the studies conducted, SRC has been diluted with a solvent (15 to 90 wt% SRC).

5. Severe equipment problems have been reported while processing SRC mixtures. The problems range from severe reactor bed plugging to exit-gas line plugging.

6. First- and second-order kinetics have been used to model coal-derived liquid hydrotreatment; second-order models have had more success due to the myriad of chemical species present in the coal liquids

Hydrotreating Catalysts

The oxides and sulfides of molybdenum, tungsten, and promoted by cobalt, nickel, zinc or manganese have been found to be effective hydrotreating catalysts. The most frequent metal combinations have been Co-Mo, Ni-Co-Mo, Ni-Mo, and Ni-W, with Co-Mo combination being generally preferred for hydrodesulfurization (HDS), and Ni-Mo combination being used when hydrodenitrogenation (HDN) is required. Sulfided metal species are believed to be the active hydrogenation sites.

High purity alumnia and alumina silicates have been widely employed as supports for hydrotreating catalysts. The alumnia support typically has surface areas of the order of 100-325 m^2/gm, pore volumes of 0.3-0.6 cm^3/gm, and average pore diameters of 40-150 $\mathring{A}$.

Alumina usually occurs in eight different phases, gamma phase being the most popular for use as catalyst support. The catalyst support not only provides the large surface area for contact between the molecule and the active metal, but also provides active acid sites for cracking activity. When sufficiently pure, alumina is acidic, the activity is generally characterized as of the Lewis type;

with passive Bronsted sites. Silica-alumina, too, exhibits surface acidity. Misserov (1969) attributed the catalytic activity of alumnia silicates to the appearance of acid sites of Bronsted type through the formation of exchangable alumina-water complex.

Conflicting evidence regarding the effect of the catalyst support composition and active metal concentrations has been reported in the literature. Brunn et al. (1975) investigated the effect of catalyst properties on the coke formation. The coking tendency of the HDS catalyst was primarily controlled by the intrinsic surface properties rather than the catalyst pore structure. Coke resistant catalyst supports were reported to contain two to three times higher Bronsted acidity compared to the high coking catalysts.

Kwan et al. (1975) investigated the effect of support properties on the hydrodesulfurization activity of Khafji residues. Various catalyst supports were selected: SiO_2-Al_2O_3, Al_2O_3, MgO-Al_2O_3, and CaO-Al_2O_3. Cobalt-Molybdenum active metal combination was used. It was observed that coke deposited on SiO_2-Al_2O_3 catalyst was slightly higher than for MgO-Al_2O_3 and CaO-Al_2O_3 supports. These findings are contrary to those of Brunn et al. (1975), and point out that greater attention should be paid to the physical properties of the catalyst support.

Co-Mo-Al_2O_3 and Ni-Mo-Al_2O_3 catalysts have been extensively used for petroleum hydrotreatment; the preferred industrial catalysts contain 2-4% Co or Ni as CoO or NiO and 8-15% MoO_3. Commercial preparations use metal ratios in the range of 0.1:1.0 to 1.0:1.0. Recently, catalysts with much higher metal loadings have been produced (Shell-324, American Cynamid HDN-30).

Catalyst Pore Size Effect

Most of the surface area of a catalyst is contained within the catalyst pore structure. For efficient utilization of the catalyst, the molecules must diffuse into the catalyst pore structure and react on the active sites. For the heteroatom removal reactions, the rate of chemical reaction is almost instantaneous compared to the rate of diffusion of the molecules into the catalyst interior. The diffusion of the reactants, thus, being the rate controlling step (LeNobel, 1959). For the molecular sizes of the species normally encountered in petroleum residua and coal-derived liquids, the diffusion of the molecules into the catalyst pores can be seriously impeded by collision with the catalyst pore walls. (Comparable size of the diffusing molecule and the catalyst pore.) Diffusion of the molecules into the catalyst pores can be increased by increasing the catalyst pore diameter; however, increase in catalyst pore size results in a corresponding decrease in the catalyst surface area, which results in lower catalyst activity due to fewer active sites being available for the diffusing molecule per unit weight of the catalyst. The two opposing effects result in the existence of an optimum pore size.

Hardin et al. (1978) prepared a series of catalysts with different surface areas, pore volumes and pore diameters. Each catalyst was reacted with Athabasca bitumen, to determine the effect of catalyst pore size on sulfur removal. Constant conversion was obtained for catalysts having pore diameters in the range of 75 to 500 Å; this was hypothesized to occur due to the decrease in surface area of the catalyst which negated any benefits of the decreased mass transfer resistance due to increased pore size.

Steigel et al. (1983) observed the hydrogenation activity of Ni-Mo-Al_2O_3 catalyst to be independent of the catalyst pore size distribution. Oxygen and nitrogen removal from the SRC liquid, however, improved with increase in catalyst pore size. Ahmed and Crynes (1978) reported a decrease in heteroatom removal of coal-derived liquids when the catalyst pore diameter was reduced from 66 Å to 50 Å. Similar resutls were reported by Sooter (1975) for another coal-derived liquid. For both of these studies, the pore diameter was varied only from 50 Å to 66 Å.

For both coal-derived liquids and petroleum residua, the predominant fraction of the metals and heteroatoms are contained in the asphaltic portion. Asphaltenes are considered to be highly condensed molecular species, low in hydrogen and high in metals and heteroatoms. The asphaltenes are considered to be active coke precursors and thus their presence in the catalyst pores is unwelcome. It is still debated, whether asphaltene fraction should gain access into the catalyst interior. Several researchers have recommended decreasing the catalyst pore size to exclude the asphaltenes from the catalyst interior. Large catalyst pores, to accommodate the large asphaltene molecules, have also been recommended.

Drushel (1972) proposed that the reason for high activity maintainance of the small pore diameter catalysts was their ability to reject the high molecular weight asphaltenes. The high desulfurization of the residuum being due to the dissociation of the asphaltene molecules outside the catalyst pore structure and the subsequent hydrotreatment of the smaller fragments in the catalyst pore structure. Richardson and

Alley (1975) thoroughly investigated the phenomenon of exclusion of asphaltene molecules by small catalyst pores. For catalysts of 60 to 95 Å most frequent pore diameters, exclusion of asphaltenes for Kuwait residua was observed at 100°C. Exclusion was also observed at higher temperatures; however, the fraction excluded decreased with increase in temperature.

Ohtuska et al. (1968) investigated the effect of catalyst pore structure on hydrodesulfurization of Khafji crudes. Three catalysts of different pore sizes and different active metal contents were used. Two catalysts were of similar pore size distribution (200-250 Å), but different active metals (Co-Mo-Al_2O_3 and Ni-Co-Mo-Al_2O_3); the third catalyst was of Co-Mo-Al_2O_3 type and had its pores in the size range of 2000 to 5000 Å. The large pore diameter catalyst removed approximately 70% sulfur compared to 55-66% removal for the small pore catalysts. The large pore catalyst was reported to have high asphaltene conversion selectivity, obviously the pore sizes in the range of 2000-5000 Å offered the least resistance to the diffusion of the large asphaltene molecules into the catalyst interior.

Contrary to the findings of the above authors, U.S. Patent 3,531,398 favors the exclusion of asphaltenes and metal bearing molecules by maximizing the surface area contained by pores in 30-70 Å size range. U.S. Patents 3,563,886 and 1,122,522 recommended an average pore size of 140-180 Å to avoid blocking of catalyst micropores by asphaltene molecules.

Riley (1978) prepared a series of catalysts with narrow pore size distributions. Catalysts of pore diameters less than 100 Å were classified as small pore catalysts, 100-150 Å as intermediate size, and above 150 Å as large

pore size. All catalysts were prepared in a similar manner; impregnation of Co and Mo on the calcined alumina extrudes; two metal loading were used. Surface areas of the two catalysts varied from 100-325 m^2/gm, pore volumes varied from 0.45 to 0.65 cm^3/gm. The catalyst activity was noted to increase to a maximum and then decrease with increase in the pore size. The increase in activity was due to the increase in the effectiveness factor; a continued increase in pore diameter resulting in loss in surface area, leading to an ultimate decrease in reaction rate.

Metals in coal-derived liquids and petroleum residua are contained in the oil soluble fraction (metal porphyrins), asphaltene fraction (within the asphaltene molecular structure), and the inorganic fraction (mostly ash fraction). Metal deposition on the catalyst causes permanent catalyst deactivation, and should be avoided. With the advent of high metal petroleum residua hydroprocessing, hydrodemetallation selective catalysts are being developed by altering the catalyst pore structure.

Hardin et al. (1978) reported an advantage in the use of large pore diameter catalysts, the deposited metals were more thoroughly dispersed in the large pore catalysts than in the small pore catalysts. For small pore catalysts, vanadium was predominantly deposited on the exterior surface of the catalyst; with increase in pore diameter, vanadium was reported to disperse more evenly throughout the catalyst.

In general, demetallation is more severely diffusion limited than desulfurization. The size of catalyst pores influences how deeply the metals shall penetrate the catalyst pore structure. The metal-bearing molecules tend to deposit on the catalyst pore mouth, thereby, making the catalyst interior inaccessible to the diffusing molecules.

Major pore-mouth plugging occurs predominantly in the catalyst periphery. In order to increase catalyst active life, the metals should disperse more evenly over the catalyst interior. A low activity, large pore diameter catalyst can prove valuable for such service.

Tamm et al. (1981) showed demetallation reactions to be severely diffusion controlled. The radial distribution of vanadium in the catalyst was compared for a small pore and a large pore diameter catalyst (petroleum residua); vanadium was reported to be deposited more evenly in the large pore catalyst, compared to the small pore catalyst. Riley (1978) observed an increase in the metal removal with increase in catalyst pore size, vanadium removal activity increased from 42% for small pore catalyst to 70% for large pore catalyst.

Inoguchi (1976) observed different effects of catalyst pore structure on hydrodesulfurization (HDS) and hydrodemetallation (HDM). The HDS activity, decreased with increase in pore size (80 to 165 Å). HDM activity reach a maximum at 120 to 140 Å. Montagena et al. (1975) hydroprocessed Ceuta crudes using catalysts of small and large pore diameters. The demetallation reactions were reported to be suppresed by using small pore catalysts.

Hydrotreatment catalysts have also been utilized for primary coal conversion processes. The H-coal liquefaction process employs a catalyst with a bimodal pore distribution. Bertolacini et al. (1979) reported for primary coal liquefaction, the desirability of using catalysts consisting of micropores, narrowly distributed around 120 Å, with larger macropores of greater than 1000 Å diameter acting as feeder pores.

The optimum catalyst pore size for primary coal liquefaction does not necessarily mean improved performance of the catalyst for coal-derived liquid hydrotreatment. Steigel et al. (1983) reported bimodal catalysts to accumulate more metals compared to the unimodal catalyst, while hydroprocessing SRC liquids. Upon regeneration, unimodal catalysts were restored to their original activity, while bimodal catalysts lost some surface area and pore volume. Kang and Gendler (1978) observed that a Ni-Mo-Al_2O_3 catalyst with a unimodal pore size distribution and one with a bimodal distribution had the same activity for hydrodenitrogenation (HDN) of an SRC liquid on the volumetric basis, however, on the weight basis, the unimodal catalyst contained more metal due to its higher density and thus had lower activity per unit weight of the catalyst.

Brooks et al. (1976) found that Co-Mo-Al_2O_3 catalysts with 100-200 Å pores, were the most optimum for coal liquefaction. Ho and Weller (1981) reported higher coal to asphaltene conversion with increase in catalyst pore size from 100 to 500 Å, no improvement in the oil fraction of the liquids was observed.

Optimum Catalyst Pore Size

Various theoretical models have been developed to determine the most optimum pore diameter for hydroprocessing. The optimum pore size is strongly dependent upon the feedstock properties: asphaltene content, average molecular size, metal content. The models developed are highly speculative and are not generally based on actual laboratory data.

Beuther and Schmid (1963) determined the catalyst activity as a function of pore volume, pore diameter and surface area, for petroleum residua hydroprocessing. They determined the following relationship:

$$\% \text{ Desulfurization} = K + 0.0589A + 13.2V + 0.012R$$

where:

K = a constant depending upon reaction conditions

A = surface area of catalyst, m^2/gm

R = pore radius, $\mathring{A}$

V = pore volume, cm^3/gm

Ruckenstein and Tsai (1981) determined for a partition coefficient of one, the optimum pore size to be about twice the size of the diffusing molecule. For petroleum molecules, a pore diameter of 100 $\mathring{A}$ was recommended on the basis of petroleum residua being of an average size of 50 $\mathring{A}$. Rajagopalan and Luss (1979) determined from theoretical analysis that the catalyst pore diameter for optimum initial activity to be never larger than five times the diameter of the diffusing species. Spry and Sawyer (1975) reported that the hydrotreating catalyst pore diameter was dependent upon the molecular size of the reactant, catalyst pore size ten times larger than the size of the diffusing molecules were recommended.

This section on hydrotreating catalyst can be summarized as follows:

1. Oxides of molybdenum and tungsten promoted by cobalt or nickel, impregnated over alumina or silica-alumina supports, have found widespread use as hydrotreating catalysts. The metal species are believed to be active hydrogenation sites, the support provides the large area of contact for the reaction and also has some catalytic activity due to the acid sites present.

2. Commercial hydrotreating catalysts usually contain 2-4 wt% CoO or NiO and 8-15 wt% MoO_3.

3. The support pore size has been reported to affect the hydrodesulfurization, hydrodenitrogenation, hydrodemetallation, and asphaltene conversion activity of hydrotreating catalysts.

4. Large catalyst pores (150-2000 Å) are generally preferred when selective hydrodemetallation and asphaltene conversion activity is preferred; small pores (50-120 Å) are preferred for heteroatom conversion.

5. An increase in catalyst pore size results in lesser pore diffusional resistance. An increase in pore diameter is also accompanied by a corresponding decrease in catalyst surface area. The two opposing effects result in the existence of an optimum pore size.

6. Optimum catalyst pore sizes, two to ten times greater than the size of the diffusing molecules have been recommended based on the mathematical model studies.

7. Contrary to the theoretical recommendations, the small pore catalysts have been reported to exclude asphaltene and metal-bearing molecules from the catalyst interior; thereby, improving the catalyst active life.

8. For primary coal liquefaction, bimodal catalysts with 120 Å micropores, and macropore channels of >1000 Å size have been shown to result in optimum activity.

9. Low activity, large pore size, large pellet diameter catalysts have been recommended for demetallation service.

Catalyst Deactivation

Long catalyst life is essential for commercial hydrotreating. Catalyst deactivation rates often determine the commercial feasibility of a process. With the advent of coal-derived liquid and petroleum residua hydroprocessing, considerable attention is being devoted to the mechanism of catalyst deactivation. Four principal mechanisms are generally accepted to be responsbile for hydrotreating catalyst decay: metal deposition, coke deposition, high-temperature sintering, and basic species poisoning. Metal deposition on the catalyst causes irreversible deactivation. In contrast, coke deposition is a reversible process; the catalyst can be regenerated by controlled combustion of coke deposits.

The major metal types present in the coal-derived liquids are different from those present in petroleum feedstocks. Coal-derived liquids contain high concentrations of iron and titanium, whereas, petroleum feedstocks contain significantly higher levels of nickel and vanadium. Deactivation in catalysts processing coal-derived liquids is more severe compared to petroleum fuels; coal liquids being principally composed of polynuclear aromatics and asphaltenes, which are considered to be active coke precursors.

Metal Deposition

The prediction of catalyst age is essential to the successful design of heterogenous catalytic reactors for processing coal-derived liquids, and petroleum residua. The mechanism of catalyst deactivation must be understood prior to the development of mathematical models to predict catalyst active life. Recently complex analytical techniques

like Scanning Electron Microscopy (SEM), Energy Dispersive X-ray Analysis (EDAX), Electron Microprobe, Auger Electron Spectroscopy, Ion Scattering Spectroscopy, to name a few, have been used to analyze the nature of deposits found on aged catalysts.

Stanulonis et al. (1976) analyzed aged Co-Mo-Al_2O_3 catalysts from the Synthoil coal liquefaction process using an electron microprobe and scanning electron microscope equipped with an energy dispersive X-ray analyzer, and observed organic and inorganic deposits on and inside the catalyst. Relatively higher inorganic deposits were observed in the upstream end of the fixed-bed reactor. These deposits were identified as $Fe_{14}S_{15}$ and they covered up to 70% of the catalyst peripheral surface. Inorganic deposits penetrated the catalyst pellet to a depth of 100 microns. The catalyst pellets were firmly cemented by an organic residue. The iron sulfide crust was present in the upstream reactor section only, downstream the ferrous sulfide crust was replaced by an aluminum and silicon crust. A difference in the metal constituents of the catalyst crust for upstream and downstream catalysts was also noticed. Upstream, the pore mouth accumulated major quantities of iron and sulfur, downstream large quantities of titanium and silicon were deposited. Both upstream and downstream catalysts showed considerable loss in surface area and pore volume.

Halloway and Nelson (1977) studied commercial Co-Mo-Al_2O_3 catalysts from primary coal conversion in fixed-bed reactors. Toluene extracted catalyst samples were analyzed by emission spectroscopy and electron microscopy. The surface of the used catalyst was observed to be partially covered by a residue, considered to be carbon rich with

embedded metals.

Wukash and Rase (1982) reported large deposits of iron in residues found in the interstitial spaces between catalyst pellets, and identified them as FeS_x ($x = 0.877$ to 0.94). The deposits were hypothesized to orginally occur on the pellet surface and fall off due to attrition into the spaces between the catalysts.

Tamm et al. (1981) also employed microprobe techniques to study the deposition of metals on petroleum residuum hydroprocessing catalysts. They observed Fe removal from the residuum to be reaction rate controlled; removal of Ni and V was observed to be diffusion controlled. They postulated two distinct mechanisms of catalyst deactivation by metal deposition; poisoning of catalyst active surface, and physical obstruction of catalyst pores. Iron depositions were found primarily outside the catalyst pellet as a thin crust. Ni and V penetrated into the catalyst interior, Ni penetrating to a greater depth than V. The difference in the metal deposition profile could be the result of difference in diffusivity and reactivity of Ni and V bearing organometallic molecules. Shah et al.(1975) observed greater V removal compared to Ni in petroleum residuum hydroprocessing. They inferred that the accelerated V removal occured due to the V porphyrin combining with oxygen, the latter being strongly adsorbed to the surface.

Furimsky (1978) reported high accumulation of metals and coke during hydrotreatment of gas-oil, and bitumen over commercial Co-Mo-Al_2O_3 catalysts. Consistent with the other authors observations (Shah et al. 1975), V was noted to deposit to a much higher extent compared to Ni,

the ratio being as high as nine. Metal V was hypothesized to play a dominant role compared to Ni. This hypothesis is further supported by the work of Beuther and Schmid (1964), who reported relative ease of vanadium removal compared to the considerable difficulty of removing Ni. They postulated that the micellar nature of asphaltenes does not persist at high operating temperatures, nickel concentrates on the inside of the micelles, hence its refractory nature, whereas, vanadium concentrates on the exterior and is easily removed.

Sivasubramanian et al. (1980) analyzed by scanning electron microscopy (SEM) aged Ni-Mo-Al_2O_3 catalyst from a coal-derived liquid hydrotreatment step. The results were consistent with the past studies by Stanulonis et al. (1976). A thin inorganic crust covered the catalyst pellets. Cracks ranging in size up to five microns were noticed on the inorganic crust; which was mainly composed of FeS_x and was cemented to the catalyst surface by the coke. Silicon, the major constituent of clays, penetrated into 100 microns of the catalyst periphery. It was also reported that a titanium crust was formed below the inorganic crust.

Kovach et al. (1982) investigated the deactivation of HDS catalysts under coal liquefaction conditions. They observed the carbonaceous deposits to be the major cause of catalyst deactivation; however, organometallic titanium compounds and other metals from inorganic salts in ash (K, Na, Mg, Ca, P, Fe) deactivated the catalyst permanently. Carbonaceous deposits on catalyst surfaces were observed to suppress adsorption of coal-liquid insoluble constituents, whereas soluble organometallics adsorbed and deactivated the catalyst in high concentrations.

Inoguchi (1976) compared petroleum feedstock hydrotreating catalysts aged up to 2000 to 3000 hours with fresh catalysts. Metals were observed to have a greater tendency than coke to form deposits when catalyst pore-size was large. Metal deposition being diffusion controlled, large catalysts pores offer less diffusional resistance to the organometallic molecule, leading to greater deposition.

The nature of the metals depositing on hydrotreating catalysts is not clear; Ti and Fe, major metal constituents of coal-derived liquids, can have their origin in inorganic constituents and/or the oil-soluble components. The deposits on the catalyst periphery occur due to reaction of inorganic constituents with hydrogen sulfide and their subsequent deposition. The internal catalyst pore depositions come from oil-soluble fractions, chiefly composed of organometallics.

Kang and Johnson (1976) reported titanium deposits on approximately 10% of the radius of the spent catalyst pellet (1/16 - inch extrudates) from the H-Coal liquefaction process. Iron was found in clusters on the extrudate surface; approximately 10 to 35% carbonaceous deposits were reported on the spent catalyst. Berry et al. (1977) reported the depth of metal (Ti, Fe, Cr, S) penetration to be insignificant compared to the pellet dimensions (1/8 - inch); suggesting high internal mass transfer resistance for the diffusion of metal-bearing molecules.

Cable et al. (1981) studied radioactively tagged Co-Mo-Al_2O_3 catalyst samples from the H-Coal liquefaction process, obtained at various times. Coke content and metal deposits were noticed to first increase rapidly and then gradually with exposure time. Catalytic activity, too, followed a similar pattern; the activity decreased rapidly for the first day, decline being gradual for subsequent

exposure times. Regenerated catalyst samples showed lesser recovery of activity with increased processing time; some permanent deactivation due to blocking of catalyst pores by metal deposition was noticed. These authors further observed regenerated crushed catalyst activity to be no higher than extruded regenerated catalysts, thereby concluding that metal deposits alone do not increase the diffusional resistance in the pores.

Cable and McCaskill (1979) identified ten different organometallic compounds in a coal-derived liquid. They observed that the removal of organometallic compounds by metal oxide adsorbents was effective in improving subsequent hydrotreatment catalytic activity; the extent of removal of organometallics being a function of adsorbent surface area. A similar experiment was conducted by Chang and Silvestri (1974), where naturally occuring manganese nodules were found to possess catalytic activity for demetallation of topped crudes in the presence of hydrogen.

This section on metal deactivation can be summarized as follows:

1. Ti and Fe are the most abundant metals in coal-derived liquids; Ni and V occur in high concentrations in petroleum feedstocks.

2. Metals frominorganic sources deposit on the surface of the catalyst pellets forming a thin crust; whereas, organometallic compounds penetrate and deposit inside the catalyst pellet.

3. Metal deposition occurs monotonically; catalyst deactivates by progressive deposition on catalyst surface, thereby reducing pellet pore-diameters, and hence, accessibility of molecules into the catalyst interior.

4. Metal sulfide formation in the catalyst interstitial spaces is very critical to hydroprocessing operation in packed bed reactors.

High pressure drop across the fixed-catalyst bed can lead to premature reactor shutdown. The need for removal of inorganic metals prior to hydrotreatment is obvious.

5. Considerable losses in catalyst pore-volume, surface area, and activity occur due to metal deposition. Contrary to carbonaceous deposition, catalysts cannot be regenerated to their virgin activity.

Coke Deposition

Coke deposition occurs through a complex mechanism, which is not yet fully understood. Considerable study has been devoted to determine the nature of coke deposits; most of the work has been conducted on cracking catalysts, which deactivate primarily by coke deposition. The physical and chemical nature of the coke deposits varies with the nature of feedstock, process temperature, and catalyst type. For coal-derived liquid processing, coke is believed to form from polyaromatic compounds, concentrated in the asphaltic fraction (Ternan et al., 1979). These compounds are deficient in hydrogen and contain considerable heteroatom and metal content.

Asphaltic fractions alone cannot be solely responsible for coking reactions. Feeds with very low asphaltic content are no less susceptible to coke formation. Generally, catalysts in fresh states possess high cracking activity; the cracked molecules tend to polymerize, the basic nitrogen and/or metals forming the link between the catalyst active site and the polymerized molecule.

Early work by Halderman and Botty (1959) for catalytic cracking of gas oils over silica-alumina catalysts revealed finely divided coke

deposits present within the ultimate pore structure of the catalyst. Their results from X-ray diffraction indicated coke deposits consist of large pseudo-graphitic structures together with considerable amounts of poorly organized carbonaceous materials.

Coke deposits on cracking catalysts almost instantaneously, coke deposits comparitively slowly on hydrotreating catalysts. Coke deposits on hydrotreatment catalysts processing coal-derived liquids and petroleum feedstocks have been found to consist of condensed polyaromatics, having low H/C atomic ratios, and high heteroatom content. Various techniques ranging from extraction with different solvents to the use of sophisticated techniques like ESCA (Electron Spectroscopic Chemical Analysis), have been used to characterize these deposits.

Furimsky (1981) attributed the loss in activity of coal-derived liquid hydrotreating catalysts to the formation of polynuclear aromatic structures on a catalyst surface. The deposits contained N and O heteroatoms, their presence being attributed to the precursor properties of hetero-compounds. The H/C atomic ratio of the deposits on the catalyst decreased with the severity of the solvent used for extraction. Polynuclear ring compounds like chrysene, benzochrysene, benzophenathrene, benzofluroanthene, perylene, benzoperylene, benzacridine, benzacarbazole, and coronene were identified by GC/MS techniques. The presence of these compounds on the catalyst (not present in feed) support the hypothesis of a chemical route for the species formation. The authors speculated that the heavier fractions on the catalyst surface formed from coupling of anthracene, naphthalene and other polyaromatics present in the coal-derived liquid. Phenols, too, were considered to be an

additional source of deposits due to their tendency of forming poly-aromatic structures containing furanic rings and their resistance to hydrogenation and deoxygenation.

Wukash and Rase (1982) analyzed the deposits on commercial hydro-treatment catalysts (petroleum feed) using X-ray photoelectron spectroscopy, scanning electron microscopy, and mass spectroscopy. Definite differences were noted in the deposits on the catalyst exterior and interior; the inner portions contained materials of higher N/C atomic ratio, molecular weight, and saturation. Deposits formed on the catalyst exterior were easily attritable. The authors believed the attritable coke to be formed from non-catalytic pyrolysis, outside the catalyst pellet, of large hydrocarbon precursors (the feed did not contain any asphaltenes). The H/C atomic ratio of the external and internal coke revealed that the internal deposits were more saturated. This was concluded to occur due to the hydrogenation activity of the catalyst compared to non-catalytic pyrolysis of external coke. The N/C atomic ratios were noted to be higher inside the catalyst, obviously the large nitrogen containing molecules were thermally decomposed exterior to the catalyst, smaller fragments gained access to the interior, and ultimately formed coke. The external coke was reported to be composed of large molecules which could not gain access to the catalyst interior.

Stiegel et al. (1983) analyzed coke deposited on several Ni-Mo-Al_2O_3 catalyst used for hydroprocessing SRC liquids. The H/C atomic ratio of the coke was reported to decrease with time, signifying a change in the nature of coke deposits with increase in process time. Large reductions in surface

area, pore volume, and average pore diameter were noted for both unimodal and bimodal pore-size distribution catalysts.

Ternan et al. (1979) suggested the formation of two types of coke; reactive coke, which subsequently forms into reaction products and nonreactive coke, which blocks catalyst active sites for hydrotreatment catalysts (petroleum feedstock). Deactivation was reported to occur primarily due to coke deposition. Coke formation was reported to be inversely proportional to the catalytic activity, maximum activity catalysts producing the least amount of coke. Assuming the coke deposition thickness to be of an aromatic molecule, the authors concluded the coke content of 0.2 mg/m^2 to constitute a 0.49 statistical monolayer of coke. According to the same reasoning, 8 wt% coke on 200 m^2/gm catalyst surface area would be sufficient for one monolayer coverage of the catalyst surface. This would mean complete loss of catalyst activity in very short process times. There is little evidence to suggest catalyst monolayer coverage. High heteroatom content in coke suggests coke adsorption on catalyst active sites which could lead to multilayer coke formation (patch formation on the catalyst surface).

Several researchers have reported negligible loss in catalyst activity even when catalyst coke content exceeded theoretical amounts for monolayer coverage. Ternan et al. (1979) reported no activity loss for the first hundred hours of operation with a heavy gas oil. Chang (1982) reported negligible loss in catalytic activity while processing an EDS (Exxon Donor Solvent Process) liquid over a Ni-Mo-Al_2O_3 catalyst; coke content as high as 17 wt% were reported. Bhan (1981) reported only slight catalyst deactivation over 100 hours of oil-catalyst contact

while hydrotreating an SRC Process Solvent. The feedstocks used in these studies contained low asphaltene and ash content.

Brunn et al. (1975) reported that catalyst deactivation during petroleum residue desulfurization occurred due to both coke and metal deposition, the severity of deactivation due to coke deposition increasing with the asphaltene content of the feed. They further concluded that although initial catalyst deactivation rate is determined by coke deposition rate, the ultimate catalyst life depends upon the extent of metal deposition, with a theoretical maximum of metal deposition with complete filling of pore space by the deposits.

Furimsky (1978) reported that differences in feedstock properties resulted in coke of different structures. Heavy gas oil, deposited more nitrogen and oxygen in coke compared to the bitumens. This was attributed to coke formation from different precursors - heterocyclic compounds in gas oil, and heavy asphalteneous species in bitumen. The hetero ring-containing compounds are adsorbed strongly on the surface due to their polar nature, the subsequent coupling mechanism leading to higher molecular weight species formation. Further evidence of heteroatom precursor activity was reported by Mochida et al. (1977). The authors reported heteroatom multiring hydrocarbon compounds like dibenzofuran, carbazole and dibenzothiophenene to be easily converted to coke in the presence of Lewis acid sites.

Beuther and Schmid (1964) reviewed the factors influencing catalyst deactivation during petroleum residue hydrodesulfurization. Asphaltenes were found to have a profound effect on the rate of desulfurization. The authors reported a four fold increase in the reaction rate upon removal of 20 wt% residues as asphaltenes. The authors further reported asphaltenes not to contribute materially to the coke formation. Contrary

to Furimsky's (1978) conclusions, the authors reported little difference in coke yields from reduced crudes and their deasphalted counterparts, the increase in coke formation being only slightly greater for asphaltic stocks. Coke deposition on the catalyst was reported to occur due to uncontrolled hydrocracking of large, easily cracked molecules; surface defects on the catalyst contributing to hydrocracking activity. Pazos et al. (1981) confirmed the above findings for processing high metal content Venezuelan crudes; the coke deposition was independent of the ashpaltene and conradson carbon content of the feed.

Catalyst active-species type has been reported to have a definite effect on coke deposition on the catalyst surface. Relatively lower coke deposition has been reported for catalysts containing Ni metal promoter compared to Co metal promoter. The lower coke content on Ni-Mo-Al_2O_3 catalyst could be the result of improved hydrogenation activity of Ni metal. Several researchers have reported findings in this direction. Ahmed (1979) reported more carbonaceous materials deposition on a Co-Mo-Al_2O_3 catalyst compared to a Ni-Mo-Al_2O_3 catalyst. Similar results were reported by Brito et al. (1982), who reported greater deactivation in Co-Mo-Al_2O_3 catalysts compared to Ni-Mo-Al_2O_3 catalysts. Kang (1977), too, reported greater coke deposition on Co-Mo-Al_2O_3 catalysts compared to Ni-Mo-Al_2O_3 catalysts.

Cable and Massoth (1981) studied H-Coal catalysts in their fresh, aged, and regenerated form. The aged catalysts contained approximately 20 wt% coke and 5 wt% metals, the coke was evenly distributed throughout the catalyst, whereas the metals were distributed in a 100-200 micron catalyst crust. Catalyst deactivation caused about 50% reduction in

pore volume and surface area of the catalyst. The aged catalyst was reported to have 20% intrinsic hydrodesulfurization and hydrogenation activity compared to virtually no cracking activity. The authors concluded that catalyst aging affected various activities differently; coke deposition had the greatest effect on cracking activity, while metal deposition affected desulfurization activity the most. Regeneration of the catalyst did not restore HDS activity completely. Hydrodesulfurization, hydrogenation, and cracking on the catalyst surface were reported to occur on different active sites, HDS and hydrogenation taking place on molybdenum sulfide phase, whereas cracking mostly occurred on the alumina support active sites. Regeneration removes coke from the active acid sites and thus regenerates catalysts for cracking activity.

Effect of Temperature on Catalyst Coke Content

No systematic study has been carried out to study the effect of temperature on coke deposition in hydrotreating catalysts. Ternan et al. (1979) reported substantial increase in catalyst coke content with temperatures up to approximately 375°C for hydroprocessing bitumen. The coke content remained constant from 375°C to 440°C; above the temperature of 440°C, the coke content increased markedly with temperature.

El'bert et al. (1970) studied the kinetics of coke formation on a Co-Mo-Al_2O_3 catalyst in the temperature range of 450-500°C for hydrocracking coal-tar distillates. The coke formation passed through a maximum at 510°C. Lower coke yields were reported by Panfilov et al. (1973) at 550°C for hydrocracking coal-tar fractions at low pressures.

Kang (1977) reported an increase in coke deposits with temperature increase while processing 40 wt% blend of SRC in Recycle Solvent. A 10 to 15% increase in the carbon content on the catalysts was reported for a temperature increase from 432 to 452°C. Maximum coke deposition was reported to occur on Co-Mo-Al_2O_3 catalysts (approximately 40%), compared to approximately 25 wt% for Ni-Mo-Al_2O_3 catalysts.

Determination of Catalyst Coke Content

In spite of the considerable research conducted to determine the nature of coke deposits, no standard method exists for determining the coke content of aged catalysts. The coke content varies with the solvent used for removal of the oils from the catalyst surface. Strong solvents like pyridine and THF dissolve and remove some of the condensed molecules from the catalyst surface and thus affect the final coke content. There is a need to standardize the method for coke determination on hydrotreating catalysts. Furimsky (1979) argued that determination of true coke content on the catalyst is impossible unless the chemical form of the active species is clearly known. Metal deposition, too, can change the weight percent coke on the catalyst due to the change in the catalyst pellet density.

This section on coke deposition can be summarized as follows:

1. Carbonaceous deposits on hydrotreating catalysts are believed to occur due to uncontrolled cracking of polyaromatic compounds on the catalytic surface, and subsequent polymerization and condensation of cracked molecules to form residues lower in hydrogen content than the parent molecules.

2. Heteroatom and metal containing molecules are believed to act as precursors for coking reactions and may also form a bond between the catalyst surface and the polycondensed molecules.

3. Considerable loss in catalyst surface area, pore volume, pore size, and activity occurs due to carbonaceous depositions on catalyst surfaces.

4. Coke depositions as high as 40 wt% have been reported on hydrotreating catalysts.

5. The analytical methods and procedures used for determining coke content vary among the various research laboratories: a need for a standard procedure for coke deposit determination exists.

6. Most of the studies on coking mechanism in the past have been conducted on silica-alumina cracking catalysts, only recently has the focus shifted to hydrotreating catalysts. There is a need for systematic study of coke deposition as a function of temperature, catalyst type, and nature of feedstock.

Mathematical Modeling

As discussed in the previous sections, coke and metal deposition are the principal causes of catalyst deactivation. Lack of reliable experimental data, regarding coke deposition on hydrotreating catalysts, has been responsible for lack of good catalyst performance prediction models. Most of these models can explain only specific data sets, none of them has any universal application. Catalyst deactivation is usually assumed to occur either by carbonaceous or by metal deposition, however, in actual practice, coke and metal depositions tend to occur simultaneously.

Coke formation on hydrotreating catalysts can occur due to three principal mechanisms: parallel, and/or in series to the desired reaction, and/or independently from precursors.

1. Series Reaction: coke formation occurs from the desired reaction products and is generally represented as:

$$A \xrightarrow{k_1} P \xrightarrow{k_2} C$$

(Reactants) (Products) (Coke)

2. Parallel Reaction: Coke formation occurs by a side reaction involving the main reactants and is represented as:

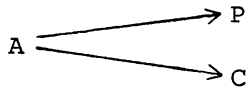

3. Independent Reaction: Here the coke formation is assumed to occur independent of the desired reaction, say from a precursor.

$$A \longrightarrow P$$

$$\text{Precursor} \longrightarrow C$$

Voorhies (1945) presented an empirical correlation for coking on cracking catalysts processing gas oil.

$$C = At^n$$

where t = time on stream

C = carbon weight percent per unit weight of catalyst

A = constant depending upon catalyst type, temperature and nature of feedstock

n = constant ranging from 0.5 to 1

This equation has been widely used in spite of its limited scope. This equation considers an independent coke formation mechanism, where the coke content is a strong function of the time on stream.

Froment and Bischoff (1981) related coke deposition on cracking catalyst to the composition of the reacting mixture. The authors

considered coke to form either by a path parallel to, or in series to the main reaction. Two forms of activity decay functions, exponential, and hyperbolic were used. For the system investigated by the authors, the carbon profile in the reactor descended from the entrance for parallel fouling and ascended for series fouling.

Similar models have been presented by Masmune and Smith (1966), Murakami et al. (1968), vanZoonen (1965), Ozawa and Bischoff (1968), Lee and Butt (1973), Beeckman and Froment (1979, 1980). All these models have been developed to explain data where only one chemical species is present. Coal-derived liquids on the contrary, contain a myriad of chemical species. The picture is still complicated by the molecular-size of the reactant species, which approaches the catalyst pore size, thereby bringing strong diffusional resistance into play. Metal deposition, too, reduces the catalyst pore diameter and increases diffusional resistance.

Rajagopalan and Luss (1979) developed a model for deactivation of hydrotreatment catalysts by metal deposition. The metal sulfide was assumed to deposit uniformly on the catalyst surface and reduce the effective radius of the pores, thus increasing the diffusional resistance offered to the movement of the molecules. The effective diffusivity of the reactant metal molecules was determined using the procedure developed by Spry and Sawyer (1975). The model predicted the influence of catalyst pore size on the rate of demetallation, which accounted for restricted diffusion of large reactant species in the pores. The model completely ignored coke deposition on the catalyst surface and assumed catalyst deactivation to occur only by metal

sulfide deposition. For the same catalyst surface area and porosity, the model predicted a uniform pore size distribution to attain the maximum activity. The model predicted the catalyst pore diameter for the maximum initial activity to be never larger than four times the diameter of the diffusing species. The model assumed a constant molecular diameter of the diffusing species, and first-order demetallation kinetics.

Chiou and Olson (1978) theoretically modelled the effect of coke formation on the performance of primary H-Coal liquefaction catalysts. The combined effect of pore plugging and geometrical exclusion of molecules was developed to explain the loss of catalyst activity. In their development, all three mechanisms of coke formation; series, parallel, and independent were considered. A quasi-steady state assumption was made, where catalyst deterioration time was assumed to be relatively long compared to either the residence time or reaction time. The model predicted choking of catalyst pores to decrease in the following order of fouling reaction mechanism: independent, parallel, series. Large pore catalysts were predicted to have longer life and higher conversion. A peak in coke profile was predicted inside the catalyst pellet for series coking mechanism, for independent mechanism rapid coke buildup was predicted. Coke deposition was assumed to be a function of the extent of coking on the catalyst and would cease when maximum coke deposition occurred. This model completely ignored the deactivation due to metal deposition on the catalyst.

Ahmed (1979) studied the hydrotreatment of a coal-derived liquid over commercial Co-Mo-Al_2O_3 and Ni-Mo-Al_2O_3 catalysts. He observed

that the catalyst most frequent pore size remained unchanged in spite of large reduction in surface area and pore volume. The author proposed an independent coking mechanism model by which he satisfactorily explained his experimental results.

Chang (1982) formulated a parallel fouling model to represent his experimental data. Second order differential equations were solved numerically to yield coke profiles within the catalyst pellet and the reactor length. The model also predicted higher activity and longer life for catalysts with lower diffusional resistance.

Newson (1970) presented approximate methods for prediction of catalyst life for residuum desulfurization. Metal deposition was assumed to cause catalyst deactivation by the pore plugging mechanism. No consideration was given to the decrease in catalyst pore diameter due to coke deposition. In a later paper, Newson (1975) considered catalyst deactivation in residuum hydrotreating catalysts to occur by a pore-plugging mechanism, due to the combined metal and coke deposition. In this model, loss in catalyst porosity was considered to occur due to three distinct mechanisms: fast coke deposition, slow coke deposition, and metal sulfide plugging. The flux of heteroatom containing molecules being progressively impeded by deposition of metal sulfides in catalyst pores. The model predicted little effect of the change in pore size distribution on catalyst life. Macropores and decreasing pellet diameter were reported to contribute to longer catalyst life, the effect in both cases being an increase in the number of pores available for coke deposition.

Hughes and Mann (1978) proposed a model to predict catalyst activity loss by accounting for the change in pore geometry due to foulant

deposition. These authors assumed the catalyst to consist of a set of idealized, parallel, non-intersecting pores of variable radius, and equal length. The foulant accumulated within the pores by simultaneous penetration and deposition. The authors studied the hydrodesulfurization of thiophene using Co-Mo-Al_2O_3 catalysts, which were aged to different coke levels. They concluded that the pore diffusional effect was negligible and activity loss occurred mainly by pore-mouth plugging.

Dautzenberg (1978) presented a model to account for the loss in activity of residual oil hydroprocessing catalysts. This model considered metal deposition to be detrimental to catalyst life. The model predicted greater metal deposition on the catalyst periphery compared to the catalyst center.

This section on deactivation modeling can be summarized as follows:

1. Mathematical models have been developed to predict activity loss of hydrotreating catalysts processing coal-derived liquids and petroleum residua. These models tend to be highly complex and seem to have very little or no actual industrial applicability.

2. Demetallation reactions like the heteroatom removal reactions have been modeled using first- and second-order reaction kinetics. Both demetallation and heteroatom reactions are diffusion controlled due to the comparable size of the diffusing species and the catalyst pore sizes.

3. The mathematical models differ widely regarding the effect of catalyst pore size on catalyst activity decay. Some models predict lesser deactivation for large pore catalysts, whereas others predict

lower deactivation in small pores due to exclusion of large molecular species.

4. Models developed for petroleum residua catalyst activity loss base deactivation solely on metal deposition, such models result in catalyst life of several thousand hours. Coal-derived liquids catalyst deactivation models consider deactivation by coking only, metal deposition being completely ignored.

Asphaltenes

Asphaltenes are an intermediate between coal and the final liquefied product; they convey by their chemical composition and physical structure, the extent of change suffered by coal during liquefaction. Asphaltenes are difficult to hydroprocess, due to their high aromaticity, hetero-atom and metal content. They also contain higher molecular weight species compared to the oil fraction, and thus represent the more refractory species of the feedstock. They are considered to impart high viscosity to the coal-liquid products; their removal/reduction being imperative to the commercial success of coal-derived liquids.

Asphaltenes also exist in naturally occuring crudes; in fact, the term "asphaltene" has been taken from the petroleum industry, where it represents the fraction of the crude soluble in benzene and insoluble in pentane. Essentially similar definitions have been used to characterize asphaltenes in coal-derived liquids. Asphaltenes can be defined as that fraction of the liquid that is soluble in benzene and precipitates on addition of non-polar solvents like pentane, heptane, cyclohexane. Asphaltenes can be precipated by any solvent having a surface tension lower than 25 dynes/cm at 25°C, and will dissolve

in liquids of surface tension above 25 dynes/cm (Speight and Moschopedis, 1979).

Nature of Coal-Derived Asphaltenes

Coal-derived liquids consist essentially of five fractions, which are generally defined as follows:

Oils - Pentane and propane soluble.

Resins - Pentane soluble, propane insoluble.

Asphaltenes - Benzene soluble, pentane insoluble.

Preasphaltenes - Benzene insoluble, pyridine soluble.

THF/Pyridine Insolubles - Essentially ash and unconverted coal.

Until recently the preasphaltene fractions were catagorized as a general class of benzene insolubles and were assumed to be composed mainly of the unreacted coal. This picture, however, has completely changed, the important role the preasphaltenes play in coal liquefaction is being realized. Preasphaltenes are the primary product of coal dissolution and are converted to asphaltenes, resins, and oils during liquefaction.

Preasphaltenes and asphaltenes exist in coal liquids and are not artificial products of the separation procedure: association of unstable, reactive species upon their concentration. Roberto et al. (1981) concluded from their gel permeation chromatography (GPC) and solvent extraction studies that preasphaltenes and asphaltenes exist in coal liquids and are not formed during the separation process.

Aczel et al. (1979) defined coal-derived asphaltenes to be a complex mixture of hydrocarbons and heterocyclic molecules. The basic structural unit of the asphaltenes was reported to consist of 2-8

ring condensed aromatic hydrocarbons, associated with 1-3 functional groups and/or naphthenic rings and short-side chains. High resolution mass spectroscopic (MS) analysis of the light asphaltenes were reported to reveal two oxygen containing molecules to be more abundant than one oxygen containing molecule. Considerably higher oxygen content was reported for the EDS distillates compared to the Synthoil liquid products. The higher oxygen content of the EDS asphaltenes was speculated to be responsible for their lower molecular weight and higher volatility.

Size of Asphaltene Molecules

Asphaltene microstructure has been analyzed by various physical techniques such as: X-ray diffraction, mass spectroscopy, infrared spectroscopy, vapor pressure osometry, densimetric methods, electron microscopy, and solvent elution chromatorgraphy. Yen (1979) reported for asphaltenes of simple structure, a microstructure to be sufficient to characterize the molecules; but for complex systems, the information required included association and micelle formation. The microstructures were reported to consist of distances in the range of 0.5 to 20 Å, the macrostructures containing distances from 20 to 2000 Å.

Schwager and Yen (1979) used X-ray diffraction method to investigate the crystalline structure of the Synthoil liquid asphaltenes. Asphaltenes consisted of condensed aromatic sheets, stacked parallel on top of each other, with aliphatic chains and naphthene rings protruding from the edges.

Petroleum asphaltenes are assumed to occur in clusters within a micelle; individually oriented clusters being suspended and distributed

within lower molecular homologs. Yen (1979) described petroleum clusters to consist of a number of planar aromatic molecules stacked in layers via a π-π interaction. A 5-6 layer stacking was reported to be common; essentially similar structure was reported for coal-derived asphaltenes (CDA).

A similar model for CDA was presented by Ho and Briggs (1982). Small angle X-ray scattering measurements were used to determine the size and shape of asphaltene and preasphaltene micelles. The micelle formation in coal liquids was considered to occur due to π-π and/or hydrogen bonding of the mixtures. For most of the systems studied, the micelles were reported to be spherical and of 22-38 Å diameter. Micelles in the 80-100 Å size range too were reported, their concentration being very low. Colloidal-sized particles were reported to form due to the association of asphaltene and preasphaltene molecules through π-π and hydrogen bonding. Strong forces of attraction were reported to exist between the asphaltenes and preasphaltenes due to their molecular structure, which also produced residual attraction for other molecules. Depending upon the residual attraction, three to four, polyaromatic molecules were reported to associate into a stacked arrangement to form a nominally spherical colloidal-sized particle.

Ho and Briggs (1982) further reported London - van der Waals' electromagnetic forces to be responsible for attraction between the clusters of molecules. The residual molecular repulsive forces provide stability to the coal liquids, and steric hinderance was reported to greatly limit the freedom of movement of the molecules. At the

molecular level, the π-π bonding atraction was considered to be the strongest; the force of attraction being greatest for hetero-atom molecules. Colloidal sized particles were considered to be formed from inter-molecular association of 3-5 polyaromatic molecules with diameters in the range of 22-38 Å. Micelles or flocks were formed by the association of the colloidal particles.

Hall and Heron (1979) determined the molecular size distribution of asphaltenes and oils for a series of petroleum residua using Gel Permeation Chromatography (GPC). A decrease in the mean size of the molecules was determined with the fractions eluted. The petroleum asphaltenes were determined to be of mean size ranging from 62-75 Å. The maltene fraction (resins) comprised of 33-43 Å size range. Metal and sulfur containing molecules were determined to be larger than the hydrocarbon molecules.

Pfeiffer and Sall (1940) assumed petroleum asphaltenes to be centers of micelles, formed by the adsorption of the part of the maltenes onto the surface or the interior of the asphaltene particle. The substance of greatest aromatic structure being closest to the center. Moschopedis and Speight (1976) considered petroleum asphaltenes to occur in clusters within the micelle. Dickie and Yen (1967) hypothesized the macrostructure of petroleum asphaltenes based on their divergent results for asphaltene molecular weight. Both resins and asphaltenes were considered to be composed of condensed aromatic layered sheets, which associated to form larger micelles. Resins were reported to be of the same size as the asphaltenes but differed in the extent of their condensation.

Asphaltene Molecular Weight

Determination of the molecular weight of asphaltenes is difficult due to their association even in dilute solutions. Moschopedis et al. (1976) reported that the molecular weight determined by vapor pressure osometry (VPO) was dependent not only on the nature of the solvent, but also the solution temperature at which the determination was made. Hydrogen bonding, involving asphaltene association, was reported to have a significant effect on the molecular weight determination.

Yen (1979) reported coal-derived asphaltenes to have molecular weights in the range of 500-600. The nuclear magnetic resonance studies of CDA revealed no paraffinic substituents; asphaltenes were reported to appear associated both in concentrated and dilute solutions.

Speight (1981) reported discrepencies in molecular weight of petroleum asphaltenes due to their low solubility in the liquids used for their solvation. The molecular weight was reported to vary from 600 to 300,000, for the various methods used. The molecular weight determined by the Vapor Pressure Osometry (VPO) was reported to be dependent on the temperature, in addition to the solvent used. A decrease in molecular weight with increase in the dielectric constant of the solvent was also noted.

Schwager et al. (1979) determined the VPO molecular weights of CDA as a function of their concentration in two different solvents, benzene and THF. Their results supported the hydrogen-bonding, donor-acceptor model of Sternberg et al. (1975). Complete dissociation was reported for CDA at infinite dilution in both THF and benzene; on the contrary, petroleum asphaltenes did not completely dissociate in

benzene.

Differences in the molecular weight of the acid/base asphaltene components have also been reported. Sternberg et al. (1975) reported asphaltenes from Kentucky coal contain acid fractions with molecular weight of 550 and basic fractions of 368 molecular weight. Bockrath et al. (1978) reported contrary results for Pittsburgh seam coal asphaltenes. Asphaltene basic fractions to be composed of larger molecules than the acid/neutral fractions.

Roberto et al. (1981) reported the molecular weights of CDA to increase in the following order:

Preasphaltene > Asphaltene > Oil

Yen (1980) reported molecular weight determined by VPO in benzene to increase from oils to carboids (undissolved coal).

Asphaltene Processing

Conversion of coal to liquid products in the presence of a hydrogen donor and high temperatures involves the following sequence of reactions:

Coal $\longrightarrow$ Preasphaltenes $\longrightarrow$ Asphaltenes $\longrightarrow$ Resins $\longrightarrow$ Oil

Weller et al. (1951) modeled the above sequence as two consecutive first-order, series reactions of the form:

$$\text{Coal} \xrightarrow{k_1} \text{Asphaltene} \xrightarrow{k_2} \text{Oil}$$

The conversion of coal to asphaltene was fast compared to the oil formation from asphaltenes. The reaction rate constant (k_1) for coal conversion to asphaltenes was reported to be 25 times the rate constant (k_2) for asphaltene conversion to oil.

Liebenberg et al. (1973) represented coal conversion as a series-parallel reactions, which were represented as follows:

Coal ⟶ Asphaltenes ⟶ Oil

Coal ⟶ Asphaltenes

Coal ⟶ Oil

Note that coal conversion to oils was represented as an independent reaction.

Stein et al. (1978) modeled the conversion of SRC asphaltenes to oils by the following series-parallel reaction.

Asphaltene ⟶ Resins ⟶ Oils

Asphaltene ⟶ Oils

Yen (1980) considered the following scheme for conversion of coal to liquified products

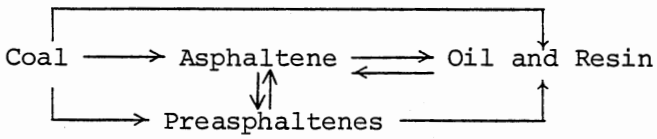

The conversions of preasphaltenes to asphaltenes, and asphaltenes to oils and resins were represented as reversible reactions. The formation of preasphaltenes was hypothesized to occur either by dehydrogenation of coal during liquefaction, or by polymerization of such reactive coal depolymerization species which were not stablized by the added hydrogen. The author further reported formation of asphaltenes even when liquids containing only oils and resins were heated. This experiment suggests that for coal liquids containing negligible asphaltene content, the reaction of oils and resins can result in formation of asphaltenes.

Speight and Moschopedis (1979) reported the importance of petroleum resins to keep asphaltenes dispersed in oil. Koots and Speight (1975)

reported petroleum asphaltenes to be essentially insoluble in the oil, but addition of resins dispersed the asphaltenes. The degree of aromatization and proportion of heteroatoms, were reported to play an important role in the ability of these materials to solublize asphaltenes. It seems that petroleum crudes and coal-derived liquids are a complex system, where each fraction depends upon the other for complete solubility and mobility.

The position of the heteroatoms in the asphaltene molecule determines their ease of removal. Speight and Moschopedis (1979) reported only 1% nitrogen removal, compared to 23% sulfur and 83% oxygen removal during thermal decomposition of bitumens. The lower removal of N and S was reported to occur due to their location in the asphaltene molecule. Bockrath et al. (1978) investigated the effect of coal liquefaction conditions on the chemical and physical nature of the asphaltenes. Asphaltenes were isolated from three different liquids produced using the same coal, but employing three different reaction conditions: catalyst packed bed, inert pellet packed bed, and batch autoclave. The first two experiments were conducted in the Synthoil reactor and the third in an autoclave from the Synthiol feed slurry. Highest asphaltene conversion was noted with the catalyst bed, next with the inert-pellets and least with the autoclave. Moschopedis et al. (1978) reported little or no asphaltene conversion below 340°C for Athabasca bitumens. Above 340°C, S-C bond cleavage was reported to occur as evidenced by H_2S evolution; above 400°C, C-C bond cleavage occurred. Drushel (1976) observed a shift in the average asphaltene molecular size of Arabian Light Vacuum oil asphaltenes with an increase in processing severity.

Hall and Heron (1979) reported no significant change in asphaltene size while processing petroleum asphaltenes over a small pore catalyst at temperatures up to 413°C, however, above this temperature, a dramatic reduction in size was reported to occur due to C-C bond thermal cracking. The small pore diameter catalyst was noted to selectively convert small asphaltene molecules to n-pentane solubles. A decrease in asphaltene content from 5.4 to 2.6% was reported to occur for a temperature increase from 357 to 385°C. At lower temperatures(357-385°C), theasphaltene molecules were seen to comprise of larger molecules. Above 400°C, catalytic cracking was reported to reduce average asphaltene size to 46 Å, which was not any smaller than for thermal cracking, 51 Å. From these observations, the authors concluded large asphaltene structures are processed external to the catalyst. Thermal cracking of the large asphaltene molecules occurs only on the catalyst surface, and the smaller molecules only, are able to gain access into the catalyst pore structure.

Drushel (1975) studied the effect of thermal treatment and catalytic hydrotreatment on the molecular weight distribution of petroleum asphaltenes. Pronounced decrease in molecular weight distribution was noticed for both thermal treatment and catalytic hydrotreatment. The NMR analysis of the treated fractions indicated dealkylation and decrease in the size of the aromatic sheet.

The results from this section are summarized as follows:

1. Coal-derived liquids are complex mixtures, consisting of five principal fractions: oils, resins, asphaltenes, preasphaltenes and THF insolubles, which can be separated into individual fractions by

addition of suitable solvents.

2. The following definitions are used to characterize these fractions.

Oils: pentane soluble, propane soluble

Resins: pentane soluble, propane insoluble

Asphaltenes: benzene soluble, pentane insoluble

Preasphaltenes: THF soluble, benzene insoluble

THF insolubles: THF insoluble fraction

3. Petroleum-and coal-derived asphaltenes differ in their chemical structure and physical properties. Coal derived asphaltenes have molecular weights in the range of 500-800, petroleum asphaltene molecular weights are approximately ten times higher.

4. Molecular weights determined by various techniques differ significantly due to the tendency of asphaltenes to associate in solution.

5. Asphaltenes are generally believed to consist of condensed aromatic layers, stacked one on top of the other, with naphthenic, and functional group side chains. Hydrogen bonding and π-π interaction is considered to be responsible for asphaltene formation. The individual molecules usually occur in clusters (micelle), which may range in size from 20-1000 Å.

6. Thermal and catalytic processing of asphaltenes reduces their size and also converts them into resins and oils.

Composite Catalyst Beds

With the recent upsurge in processing heavy petroleum residua and also the advent of coal-derived liquids, considerable attention has been

focussed on development of catalysts tailored for processing heavy feedstocks. Both petroleum residua and coal-derived liquids are high in asphaltene, metal, and heteroatom content. Processing these feedstocks over conventional catalysts results in very short catalyst life. Recently catalysts with high activity for metal or heteroatom removal have been developed. A reactor bed composed only of highly active demetallation catalyst would suffer from low heteroatom removal activity; a catalyst developed specifically for high heteroatom activity would deactivate rapidly due to metal deposition. A graded catalyst bed, where enough catalyst volume of each type is provided, would achieve specific processing objectives and, thus, optimize the catalyst bed operation.

The metal deposition in fixed bed reactors which process high metal content feeds, occurs mostly in the reactor inlet section. Demetallation reactions are usually of first- or second-order. Excessive deposition occurs on the catalyst surface due to the conversion of highly reactive metals into metal sulfides. These sulfide subsequently deposit in the catalyst intersticies leading to high pressure drops and premature reactor shutdowns. It would be prudent to replace the top reactor catalyst section by a catalyst having high intersititial deposit capacity and also a tolerance towards metal deposition.
Such a catalyst bed would offer reasonable protection to the downstream catalysts which would be tailored for heteroatom removal, asphaltene conversion, and molecular weight reduction.

With graded catalyst beds, the reactor can be tailored for processing different types of feedstocks. Development of catalyst beds, using different pore sizes, activities, and selectivities, would thus

result in optimized utilization of the catalyst bed.

The application of the graded catalyst reactor bed concept has been mostly restricted to the petroleum processing industry. Nielsen et al. (1981) used three catalytic reactors in series to study the effect of catalyst property change within the catalyst bed for hydroprocessing petroleum resids. Interstage sampling capability within the reactors was provided to study the extent of reaction in each reactor bed. Three different catalysts of large, medium and small pore diameter were used. With the small pore diameter catalyst in all three reactors, accelerated deactivation was reported in the top reactor bed, and thereafter in the second, and least in the third catalyst bed. Metal deposition, too, was reported to follow a similar pattern. The large pore diameter catalyst was observed to be the least active of the three catalysts tested, but it had the highest capacity for metal deposition. Rapid initial deactivation was also observed for this catalyst.

Various experiments were conducted with different catalyst sequencing and volumes to arrive at an optimized combination for a particular feedstock. A graded catalyst bed, comprising of large pore diameter catalyst in the top 25% of the bed, a medium pore size catalyst in 50% of the bed, and a small pore catalyst in the remaining section was observed to give 20% better HDS activity over that for the large pore catalyst, 65% HDS activity over that for the medium pore catalyst, and 30% over that for the small pore catalyst.

Brunn et al. (1975) reported hydrodesulfurization (HDS) of residua over two different catalyst beds placed in series. The top bed contained catalyst tailored specifically for hydrodemetallation

(HDM), the second bed contained an improved HDS catalyst resistant to coking. About 55% sulfur was removed in the first bed, and 70% of the remaining sulfur in the second bed. Most of the HDM occurred in the first bed; life of the catalyst in the second bed was improved by approximately 50%.

The Amoco Oil Company has developed proprietary catalysts for processing high metal, high asphaltene content crudes. In an experiment, two different proprietary catalysts were loaded in a reactor, the catalyst in the top bed of the reactor had a high Ni and V accumulation capacity. The catalyst in the bottom bed had high HDS activity, but low capacity for metal uptake. The combination of these two catalysts was reported to provide good activity and activity maintenance (Mosby et al., 1973).

Ramírez de Agudelo et al. (1982) recommended the use of composite catalysts for hydroprocessing high metal content petroleum residua. An inexpensive catalyst in the first section of the reactor was hypothesized to selectively remove the metals and thus protect the more expensive HDS catalyst. Schuit and Gates (1973) suggested the use of catalysts with molecular seiving properties, which could seive the metal-containing asphaltenes, while letting the sulfur-containing molecules to enter the catalyst pores. Small pore diameter (40 Å or lower) catalysts were recommended.

Green and Broderick (1981) reported a dramatic increase in catalyst useful life when one of the hydrocrackers at the Chevron Oil Company's Richmond refinery was replaced by a graded catalyst hydrotreater. The petroleum feedstock was reported to contain 30 ppm metals, of which 10 ppm were soluble iron compounds. The hydrocracker

suffered from excessive pressure drop due to the metal deposition in the top reactor section. This tendency was considerably reduced when graded catalysts were used in the reactor. No information was provided on the type of catalysts used. The Chevron Oil Company also investigated the use of graded catalyst hydrotreater for application in the 96 MBPD residue desulfurization plant under construction at Chevron's Pacagoula refinery, graded catalyst beds increased the reactor bed life considerably.

Two-Stage Hydroprocessing

Various two-stage hydrotreating processes have been developed in the past. These process schemes cannot be catagorized under the graded catalyst bed processes, because each of the specific processes is conducted under different conditions in separate reactors. A brief mention of these processes is made here:

Schmid and Beuther (1967) reported beneficial effect of visbreaking petroleum residua prior to their hydrotreatment. Lower coke deposition on the hydrotreating catalysts was reported.

Panfilov (1974) established the conditions for hydrocracking of coal-tar fractions. Preliminary hydrogenation of the feed was conducted over Mo-Al_2O_3, followed by hydrocracking over W-Al_2O_3 catalyst at 550°C. Elbert et al. (1970) also reported two-stage processing of low temperature (LT) coal-tar to be advantageous. In this process, the feed was first hydrocracked at 500-650°C over a Mo-Al_2O_3 catalyst, the 200-300°C fraction was hydrogenated over a Ni-Mo-Al_2O_3 or a Co-Mo-Al_2O_3 catalyst at 260-320°C.

Jankowski et al. (1982) reported hydrotreating of synthetic

crudes from coal to be most effective when two reactors containing different catalysts were used. The first reactor contained a Co-Mo-Al_2O_3 catalyst; the second reactor contained a Ni-Mo-Al_2O_3. The first and second stages were operated at 360 and 390°C, respectively.

Arey et al. (1966) described a two-stage residuum hydrocracking process: in the first stage, metals and other contaminants were partially removed by reaction catalyzed by a Co-Mo-Al_2O_3 catalyst having a pore diameter of 80 Å; a palladium loaded zeolite with a pore diameter of 13 Å was used in the second stage. The second stage further catalyzed the reaction of the smaller molecules.

Two-stage hydroprocessing of coal-derived liquids was reported by Fu et al. (1978). In the first stage, the SRC blend was hydrotreated in a 5 liter rocking autoclave at a temperature of 415°C and hydrogen pressure of 15 MPa (2200 psig). The catalyst was of the Ni-Mo-Al_2O_3 type. The product was hydrocracked over a Ni-W-Al_2O_3 catalyst, temperatures in the range of 377-433°C and reaction times in the range of 40-180 minutes were used. Effective upgrading of the liquid was reported in the second stage.

A combination of catalytic hydrotreating and solvent deasphalting was employed by the Chiyoda Chemical Company, Japan, for processing petroleum residua (Takeuchi et al., 1979). Asphaltene fractions of the hydrotreated product were separated by solvent deasphalting, and the asphaltene fractions recycled to the hydrotreating reactor. An overall improvement in the efficiency of the unit was reported.

This section on graded catalyst beds and two stage processing can be summarized as follows:

Composite catalyst beds have been successfully used for processing high metal petroleum residua. Usually two types of catalysts have been used: catalyst resistant to coke and metal deposition, and catalysts high in HDS activity. Reactors with top sections containing highly HDM selective catalysts and the lower sections containing highly active HDS catalysts have been used.

Guard Reactor Beds

Guard reactor beds differ from the graded catalyst beds in that the former bed is separated from the main reactor and can thus be taken off stream without affecting the normal operation. Guard reactors are usually filled with hydrodemetallation (HDM) or hydrodesulfurization (HDS) catalysts. Guard beds using inexpensive disposable materials have been used. The guard bed is usually run until the pressure drop reaches a maximum limit and then the bed can either be refilled or the flow rerouted through another guard bed.

Guard beds are desirable for extending catalyst life of the main reactor; they remove undesirable materials (particulates, metals, heavy coke material, inorganics) from feedstocks prior to contact with expensive catalysts in the main reactors. The guard beds also provide a very efficient means of direct heat transfer, thus eliminating the need for feedstock pre-heaters.

Various types of guard reactor beds have been used for processing petroleum residua. The Shell Oil Company developed a guard bed reactor where the catalysts was discontinuously replaced at the top of the reactor, and removed at the bottom as a slurry; catalyst

and feed moving concurrently. Langhout et al. (1980) reported 80% HDM of Venezeulan crude using this type of reactor. A special series of catalysts, tailored for high HDM activity, was developed at the Shell Laboratories, Amsterdam, for use in the guard reactor beds (van Glinneken et al., 1975).

Christ et al. (1979) reported the use of guard catalyst beds prior to hydrotreating reactors in the Exxon Oil Company's Baytown refinery. The guard beds were bypassed upon excessive pressure drop, recharged with fresh catalyst, and returned to service (7 days change-out time). Agglomeration of catalyst pellets was reported for the guard bed reactors; carbon, iron scales, and salts were identified to be deposited in the catalyst interstices. The hydrotreatment reactors were replaced after 16 months, and during this time, two guard chambers were used.

The Standard Oil Company of Ohio conducted extensive studies in the use of guard beds for hydroprocessing a shale-derived oil (Robinson and Evin, 1982). The process scheme for hydrotreating involved two reactors in series, the first reactor (guard bed) contained alumina pellets and was operated at a low temperature (216-271°C), the second reactor contained Shell 324 (Ni-Mo-Al_2O_3) catalyst and was operated at 385°C. The guard bed contained 1/16 inch alumina extrudates. At the reactor top, trash baskets were embedded within 1/2 inch alumina balls. Neither the extrudates nor the alumina balls contained an active metal. The pressure drop in the guard bed was reported to increase steadily over the run length; excessive pressure drop forced

shutdown after 24 days of operation. A heavy black residue was noticed to be deposited within the extrudates and the alumina balls. A fine powdery material, composed mainly of iron, sulfur, alumina, sodium, arsenic, and calcium was deposited in the interstices. At the low temperature of operation, no arsenic deposited on the alumina extrudates. The catalyst activity was observed to decline significantly for the hydrotreating catalyst during the 24 days of operation. Incomplete removal of metals (Fe, As) in the guard bed due to the low operating temperature was cited to be the cause of catalyst deactivation in the main reactor. The guard bed reactor was operated at a low temperature due to the low temperature rating of the reactor shells, and not for any processing advantage.

The Union Oil Company and the M. W. Kellog Company jointly developed a process for hydrodesulfurization of petroleum residua. The process used fixed bed reactors containing tailored catalysts to provide high desulfurization activity with minimal effects of coke and metal accumulation. A catalytic guard bed reactor was used to remove fine entrained materials. The catalyst used in the main reactors was specifically tailored for small pore size to inhibit the diffusion of asphaltenes and metals into the catalyst pore structure (Murphy and Treese, 1979). Richardson and Ishikawa (1979) reported 27 month service using this process for petroleum residua hydrotreatment. Approximately 44% coke and metals was reported deposited on the guard bed catalyst. The guard bed reactor was used in service with four other reactors placed in series. The metal deposition decreased downstream through the reactor train, 38% metal deposition occurred in the guard bed. No pressure drop problems developed in the guard

bed or in any of the reactors.

Extensive work was conducted on the concept of using guard bed reactors for processing COED coal oil. The FMC corporation and the Office of Coal Research jointly developed the COED process in the late 1960's. A 30 barrel-per-day fixed bed hydrotreater was constructed for upgrading these liquids, the pilot-plant design was based on the results obtained from bench-scale hydrotreater tests conducted by the Atlantic Richfield Company. One of the major objectives of this study was to demonstrate fixed bed hydrotreating as a viable processing step for converting heavy oils to synthetic crudes.

The hydrotreater reactor consisted of two reactors in series, the first reactor was used as a guard bed. Several materials and combination of materials were tested in the guard chamber: Koch stainless steel flexi-rings, alumina pellets and spheres, HDS-3 catalyst. The use of catalyst in the guard chamber was reported to result in significantly better performance than the use of alumina and flexi-rings. The use of high voidage material in the guard bed was reported to increase the operating time between reactor catalyst replacements(Jones et al., 1975).

Various patents have been awarded for processes employing guard bed reactors: U.S. Patents 4,102,779; 2,771,401; 3,901,792. A recent Gulf Oil Company patent (U.S. Patent 4,118,310) describes a process for upgrading petroleum liquids, high in asphaltene and metal content. A combination of guard bed and HDS main reactor was employed. The main reactor contained Ti promoted Ni-Mo-Al_2O_3 type catalyst (cylindrical shape). The guard bed catalyst was a

specially developed Co-Mo-Ni-Al_2O_3 catalyst. The catalyst surface had grooves and protrusions, possibly to improve the outside surface area of the catalyst.

Various researchers have recommended cheap, disposable materials for use in guard beds: Katzer and Sivasubramanian (1979); Schuit and Gates (1973). Huang et al. (1981) reported a two-stage process for primary coal liquefaction. The first stage was operated using a cheap disposable material, while the second stage was operated using commercial Ni-Mo-Al_2O_3 catalyst (Harshaw HT-500E, 1/16- inch extrudates). The cheap disposable material used in the first stage consisted either of pyrite (FeS_2), clays (Kaolinite, Illite, Montmorillonite) or SRC pilot-plant residues ashed at 700°C. The SRC ash was reported to be the most active for hydrogenation of model compounds. Use of pyrite in the first stage improved the yield of oil appreciably. Anderson (1980) investigated the catalytic activity of pyrite, mill scales (Fe_3O_4, formed during mill rolling), and coal liquefaction mineral residues from SRC liquefaction process, for both SRC-I and SRC-II primary coal liquefaction processes. Total oil yield in the SRC-II increased from 37 to 45% on addition of pyrite. In contrast, the addition of pyrite to SRC-I did not improve the desulfurization activity, however, mill scale addition improved desulfurization of both recycle solvent and SRC in the SRC-I process.

Wells (1977) observed a maximum of 51% sulfur removal and 29% nitrogen removal, using pure gamma-alumina to hydrotreat raw anthracene oil at 400°C and 10.2 MPa (1500 psig). Chirakaparambil (1974) observed negligible hydrodesulfurization in the presence of nonporous chips. Crynes (1981) reported negligible hydrodenitrogenation and

hydrodesulfurization upon hydrotreatment of a 30 wt% SRC mixture in SRC Process Solvent at 400°C and 10.2 MPa (1500 psig) over 1 mm size nonporous glass beads. Chang and Silvestri (1974) observed a demetallation rate of more than 80% using manganese nodules as a pretreatment demetallation catalyst.

This section on guard beds can be summarized as follows:

1. Guard beds containing catalysts have been used with commercial success in the petroleum industry.

2. Guard beds effectively remove the particulate fractions, metals, and coke particles from the feed prior to its contact with more expensive catalyst in the main reactor.

3. Cheap, disposable materials like alumina, pyrite, mill scales, mineral residue from the SRC liquefaction process, and various clays have been used for primary coal liquefaction, shale oil, and coal-derived liquid hydroprocessing.

Literature Summary

This literature review can be summarized as follows:

1. Coal-derived liquids are hydrogen deficient, high molecular weight hydrocarbons, containing significantly high concentrations of condensed aromatics, heterocyclic compounds, and metals. For coal liquids to be commercially successful, the heteroatom and metal contents need to be reduced to acceptable levels. Reduction in heteroatom content is usually accomplished by reacting these liquids with hydrogen in the presence of a catalyst, usually consisting of Ni-Mo or Co-Mo active metals, impregnated on a high surface area alumina support.

2. Coal liquid hydrotreating is usually accomplished in trickle-bed reactors. Catalytic hydroprocessing of coal liquids in trickle-bed reactors suffers from the disadvantage of early catalyst activity loss and catalyst bed-plugging. Catalyst deactivation occurs due to the following reasons: coke and metal deposition, basic species adsorption, and high-temperature catalyst sintering. Coke deposition occurs rapidly in the initial stages of oil-catalyst contact; metal deposition occurs monotonically through the entire catalyst process life.

3. Coke and metal depositions deactivate catalysts by two principal mechanisms; blockage of catalyst pores, and/or coverage of active catalyst sites due to uniform pore deposition. Diffusion of the reacting molecular species is progressively impeded by the reduction in catalyst pore size. Pore blockage renders the catalyst interior inaccessible to the diffusing molecules. Coke deposition on catalysts is reversible, the carbonaceous deposits can be removed by controlled combustion of the residues; metal deposition, on the contrary is irreversible and leads to permanent catalyst deactivation.

4. Coal-derived liquids are principally composed of five fractions: oils, resins, asphaltenes, preasphaltenes, and THF insolubles. The molecular weight increases, and hydrogen content decreases in going from oils to preasphaltenes. The major fraction of the heteroatoms and metals is contained in the asphaltene fraction. During hydroprocessing, preasphaltenes and asphaltenes are converted into oils and resins.

5. Asphaltenes consist of highly condensed aromatics, stacked in layers with naphthenic side chains. The position of the heteroatom within the asphaltene molecule determines its ease of removal. Coal-derived asphaltenes usually are of 15-35 Å size. In liquid, they form micelles due to the intramolecular attraction, these micelles are of 50-80 Å size. Coal-derived asphaltenes range in molecular weight from 300-800. Petroleum-derived asphaltenes, on the contrary, have approximately ten times higher molecular weights and are usually of 100-2000 Å size range.

6. Coal-derived liquids cause premature reactor shutdown when processed in conventional trickle-bed reactors, due to the deposition of residues in the catalyst interstices. These residues mostly consist of the inorganic fractions present in the coal-derived liquids. Attempts have been made to remove the inorganic fractions in a separate reactor (guard reactors), prior to processing these liquids over expensive hydrotreating catalysts. Guard reactor beds containing both catalysts and disposable material have been used; use of catalysts resulting in better performance.

7. Coal-derived liquids contain Fe and Ti as the principal metal contaminants; these metals occur both in the inorganic fraction (ash) and in the oil-soluble organometallic compounds. The metals in the inorganic fraction tend to accumulate outside the catalyst pellet as a thin crust. The oil-soluble metals deposit in the catalyst pore structure, most of the deposition occurring in the catalyst periphery (100-200μm).

8. Coke deposits on the catalyst have been observed to consist of highly condensed, polyaromatic structures, high in heteroatom content. Coking of the catalyst surface is considered to occur due to the uncontrolled hydrocracking of the large molecular species, polymerization of the cracked species, and their subsequent deposition on the catalyst surface; heteroatoms and metals forming the bond between the condensed molecule and the catalyst surface.

9. Most of the active sites in the catalyst are contained within its pore structure; increase in the catalyst pore size decreases the diffusional resistance offered to the diffusing species, however, this increase also decreases the catalyst surface area. These opposing effects result in the existence of an optimum catalyst pore size for hydrotreatment. The optimum catalyst pore size varies with the process objectives, heteroatom, and metal content of the feedstock.

10. Large, polycondensed, heteroatom and metal containing molecules are considered to be active coke precursors. Several researchers have recommended the use of small catalyst pores, which would selectively eliminate the large molecules from the catalyst interior; thereby, increase the catalyst life. Conflicting evidence is present in the literature regarding the catalyst pore size effect on the hydrotreatment activity. Demetallation activity is reported to increase with increase in catalyst pore size; heteroatom removal activity decreases with increase in catalyst pore size.

11. With the advent of coal liquid and petroleum residua hydroprocessing, new catalysts specifically tailored for selective demetallation or heteroatom removal activity have been developed. A catalyst

bed consisting of demetallation selective catalyst would suffer from low heteroatom activity and vice versa. A graded catalyst bed, consisting of demetallation catalyst in the top reactor section and highly active HDS or HDN catalyst in the bottom section would result in optimized catalyst bed activity. Such catalyst beds are being increasingly considered for conventional petroleum crude processing.

CHAPTER IV

EXPERIMENTAL EQUIPMENT

A special reactor system was constructed to meet the following objectives:

1. The reactor system should consist of multiple reactors, placed in series, each capable of being operated at a different temperature.

2. Provision should be made for removing small liquid samples (3-5 ml.) within the multiple reactors without distrubing the normal reactor operation. In addition, normal sampling capability should also be provided.

3. The system should be capable of processing heavy, viscous, coal-derived liquid feedstocks, with no liquid feed and exit line plugging.

4. The system should be capable of operating at constant pressures up to 17.0 MPa (2500 psig).

5. The reactor heating system should be able to provide flat axial temperatures profiles up to 450°C.

6. The liquid feed pump should be capable of delivering low flow rates (10 cc/hr upwards) accurately.

7. Adequate safety procedures such as: auto pump shut-off upon excessive pressure buildup; hydrogen concentration sensing audible alarm; hydrogen gas supply shut-off upon pressure surge, should be incorporated into the reactor system.

8. Inlet and exit gas flow rates should be measured and controlled accurately.

A trickle-bed reactor system was constructed to meet the above stated requirements. Figure 1 presents a simplified diagram of this experimental system. Coal-derived liquids were mixed thoroughly in a feed tank prior to their transfer into the Ruska pump. Because of the high viscosity of the feedstock used for this study, the liquid transfer from the feed tank to the Ruska pump was accomplished with 0.21 MPa nitrogen gas pressure. As can be seen from Figure 1, coal liquid and hydrogen gas were fed at the reactor top, and allowed to flow cocurrently down the catalyst bed. Hydrogen gas was supplied on a once through basis. The catalyst bed was maintained at a constant desired temperature by surrounding the tubular reactor with tight fitting aluminum cylindrical blocks having heating bands wrapped around them. Two temperature controllers were used to maintain the temperature of the reactor heating blocks. Thermocouples were placed inside and outside the reactor to accurately monitor the reactor temperature.

Separation of the liquid and gaseous products was accomplished in two consecutive high pressure sample bombs. The hydrogen gas flow rate was controlled downstream of the reactor by adjustment of a needle valve. Upstream hydrogen pressure was maintained by a Mity-Mite pressure regulator; hydrogen gas pressure was measured on a Heise gauge upstream of the reactor. The effluent gases from the separation bombs were scrubbed in 50% ethanolamine solution. Scrubbed exit gas flow rate was determined using either a bubble flow meter, or a low pressure rotameter. High pressure gas was metered through a high pressure (34.0 MPa) rotameter.

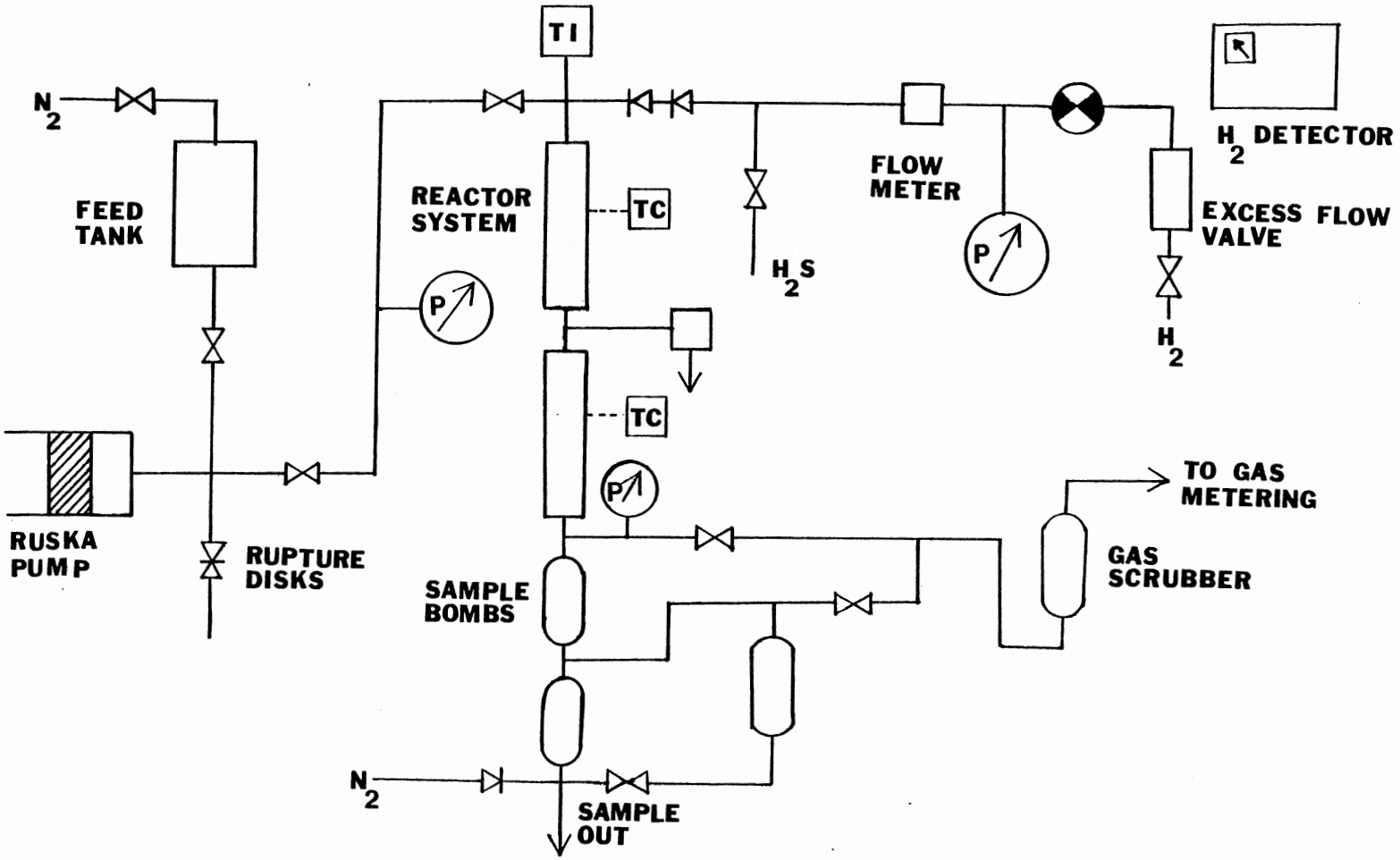

Figure 1. Experimental System

A list of the major equipment used in the reactor system is presented in Appendix B. Detailed experimental setup and procedures are described in Appendices A and C. In the following section only a brief description of the principal subsystems of the reactor system are presented.

Oil Feed System

Figure 2 presents a schematic of the oil feed system. The oil was fed through a high pressure, single displacement Ruska pump, capable of delivering liquid flow rates in the range of 2 to 250 cc/hr, at pressure as high as 68.0 MPa (10,000 psig). A pressurized liquid feed tank was used to store the oil prior to its transfer into the pump, the oil in the feed tank was always blanketed with N_2 to avoid oxidation. The feed tank was heated with band heaters; a thermocouple inside the tank was used to control the oil heating. The oil was thoroughly mixed prior to its transfer into the Ruska pump. In order to reduce the incidence of reactor plugging, a 50 mesh screen was placed at the feed tank outlet to remove any undissolved coal or any gun deposits formed during liquid storage. The Ruska pump feed cylinder and exit gas lines were heat traced to facilitate pumping viscous oils.

A pressure switch and an alarm would be activated in case of over pressure in the liquid feed system. The pressure switch was set to activate at 17.0 MPa (2500 psig). The Ruska pump power supply would automatically shut-off, whenever the pressure exceeded the set limit. In addition to the pressure switch, two rupture discs rated at 18.4 MPa (2700 psig) and 21.8 MPa (3200 psig), respectively, were incorporated into the system to guard against pressure switch malfunction.

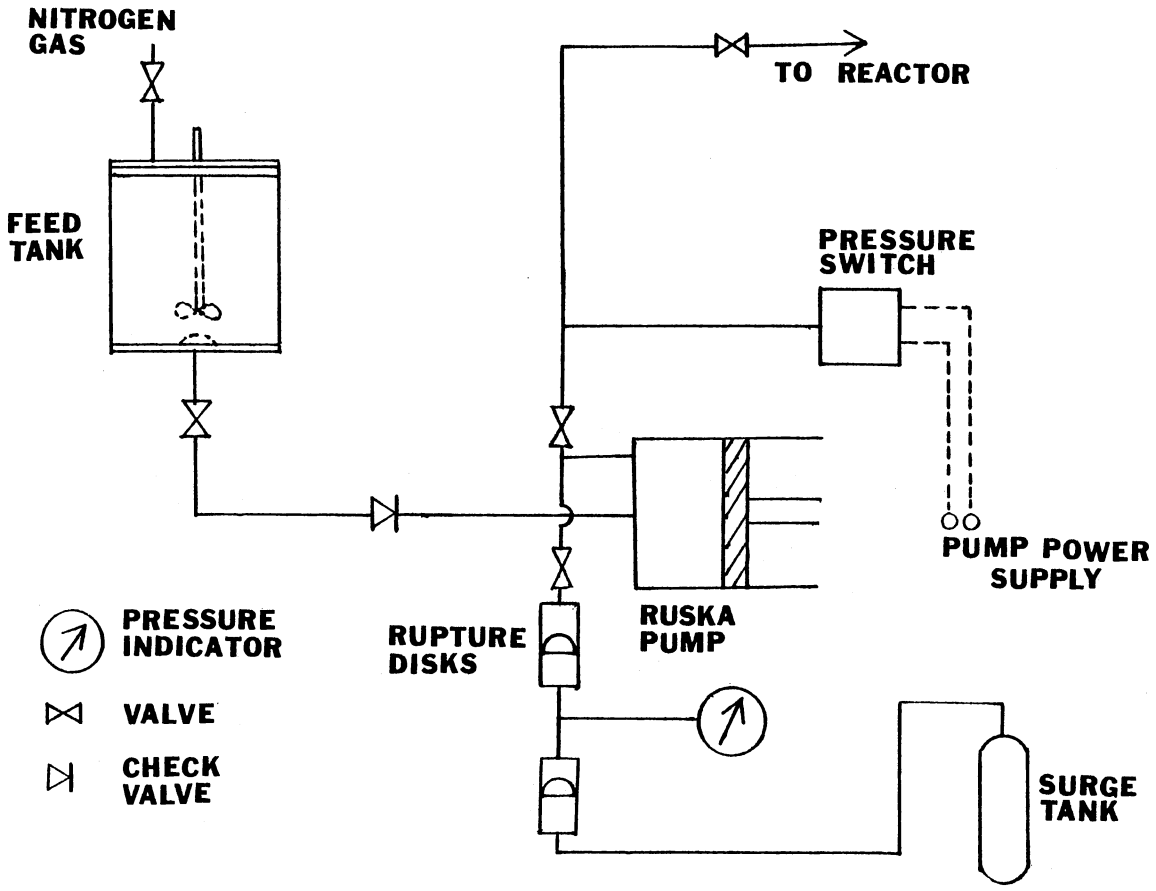

Figure 2. Oil Feed System

Gas Feed System

Figure 3 presents a schematic of the reactor gas feed system. Hydrogen gas was fed to the reactor directly from the hydrogen cylinders. A high pressure manifold was used to switch hydrogen cylinders; thus, avoiding interruption of normal gas flow.

To guard against any hydrogen surges due to equipment failure, a ball flow-check valve was placed in the inlet gas feed lines. In addition, a toggle switch was provided close to the gas manifold to manually cut the hydrogen feed supply in case of emergency.

A high pressure flow meter was placed upstream of the reactor to measure the hydrogen gas flow rate; the flow meter could be operated at pressure up to 34 MPa (5,000 psig). The hydrogen gas pressure was measured on a Heise gauge upstream of the reactor. In order to avoid the diffusion of light coal liquids into the gas feed lines, a liquid trap was placed immediately before the reactor; spherical alumina balls were packed in the trap to adsorb any diffusing liquid. In addition, two flow check-valves were placed in the hydrogen feed lines to avoid the flow of liquids into the gas lines.

Reactor System

Two reactor configurations were used during this study. A single reactor bed was used for one set of experiments, and two reactors placed in series were used for another set of experiments. For the multiple reactor system, provisions were made for removing product liquid samples between the reactors. Figure 4 is a schematic of the multiple reactor system and the reactor micro-liquid sampler; detailed drawings are

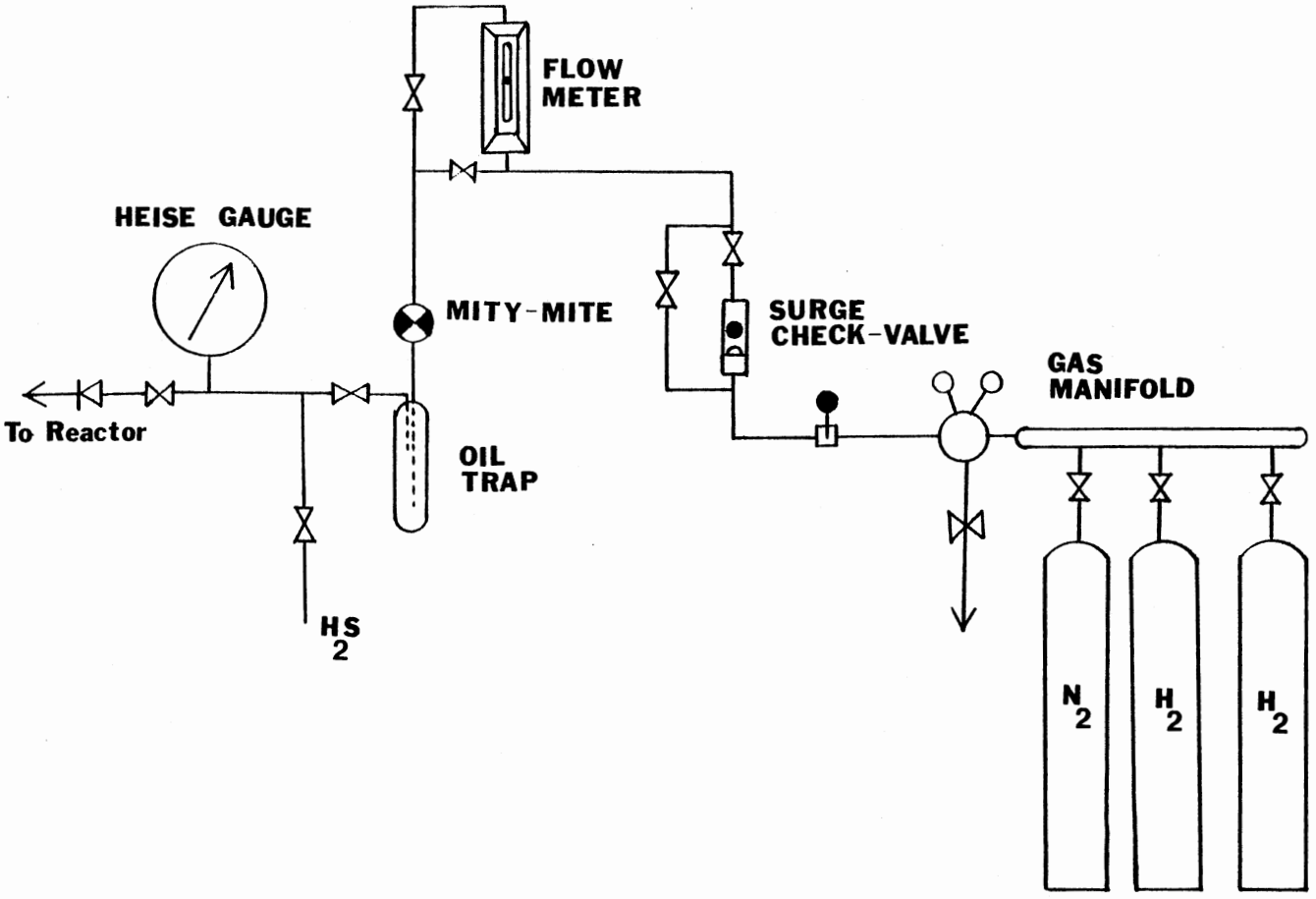

Figure 3. Hydrogen and Nitrogen Gas Feed System

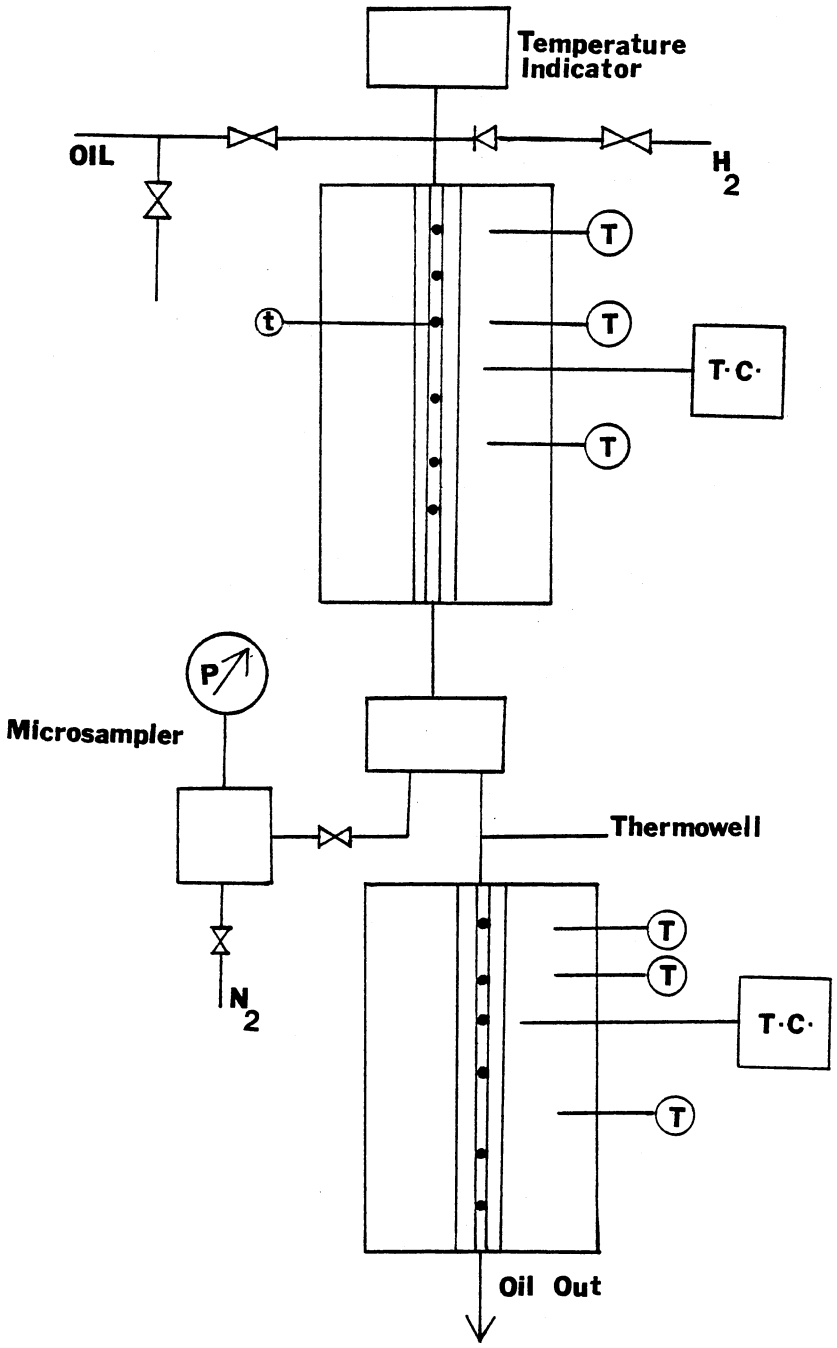

Figure 4. Trickle-Bed Reactor System

presented in Appendix A.

The reactor consisted of 76.2 cm long, 1.27 cm O.D., and 0.089 cm thick stainless steel tube, fitted with a half-inch Swagelok cross and union at the top and bottom, respectively. For the multiple reactor system, 38.1 cm long tubes of similar dimension as above were used. Two monolithic aluminum blocks of the reactor length, with grooves of reactor diameter running across the entire length, were tightly secured around the reactor tube. Heating bands were wrapped around the aluminum blocks to obtain a flat temperature profile along the reactor length. Two controllers were used to maintain the temperature profile in the reactors. Detailed drawings of the reactor heating system are presented in Appendix A.

The temperature inside the reactor was measured using ten hairline thermocouples (0.0254 mm diameter). These thermocouples were placed five centimeters apart, inside a thermowell, along the entire catalyst bed length. Thermocouples were also placed outside the reactor wall to determine the reactor wall temperature. These thermocouples were placed in holes drilled along the entire aluminum block length. Some of the outside thermocouples were aligned with the thermocouples placed inside the reactor bed to determine the temperature drop across the catalyst bed. The temperature was read on an Omega temperature read out.

Micro-Liquid Sampler

In addition to the regular liquid samples, micro-liquid samples were removed between the reactors in the multiple reactor system. Approximately, 3-5 ml liquid samples were collected. The normal gas-liquid flow was interrupted for approximately three minutes while taking the

micro-liquid sample. The micro-liquid sampler mainly consisted of a three-way valve to divert the normal liquid flow, and a high pressure bomb, containing the sample vial, for collecting the liquid sample. The details of this system are presented in the Appendix A.

Pressure and Gas Flow Control System

Figure 5 is a schematic of the gas-liquid separation system. The two-phase products from the reactor bottom were separated in two consecutive high pressure sample bombs. Two separation bombs were necessary to allow normal operation during sampling. The first sample bomb was placed close to the reactor exit to avoid plugging of the exit liquid lines. A long-stem, high temperature valve separated the first and the second sample bomb. Two additional high pressure bombs were used to avoid liquid carry-over into the gas exit lines. One bomb was filled with alumina pellets, which adsorbed any entrained liquid.

Gas flow through the system was controlled by a micrometer valve. The exit gas flow rate was measured, after ethanolamine scrubbing, by a low pressure flow meter. A bubble meter was also provided to fine adjust the gas flow rate.

Safety System

The safety system was designed to detect hydrogen gas leakage, and to avoid Ruska pump overpressurization. Diffusion cells were placed above the reactor system and the hydrogen gas supply system to detect hydrogen gas concentration. An alarm would sound, in case the hydrogen gas concentration in the room exceeded 40% of the lower explosive limit for hydrogen. Excess gas flow check valves were also incorporated into

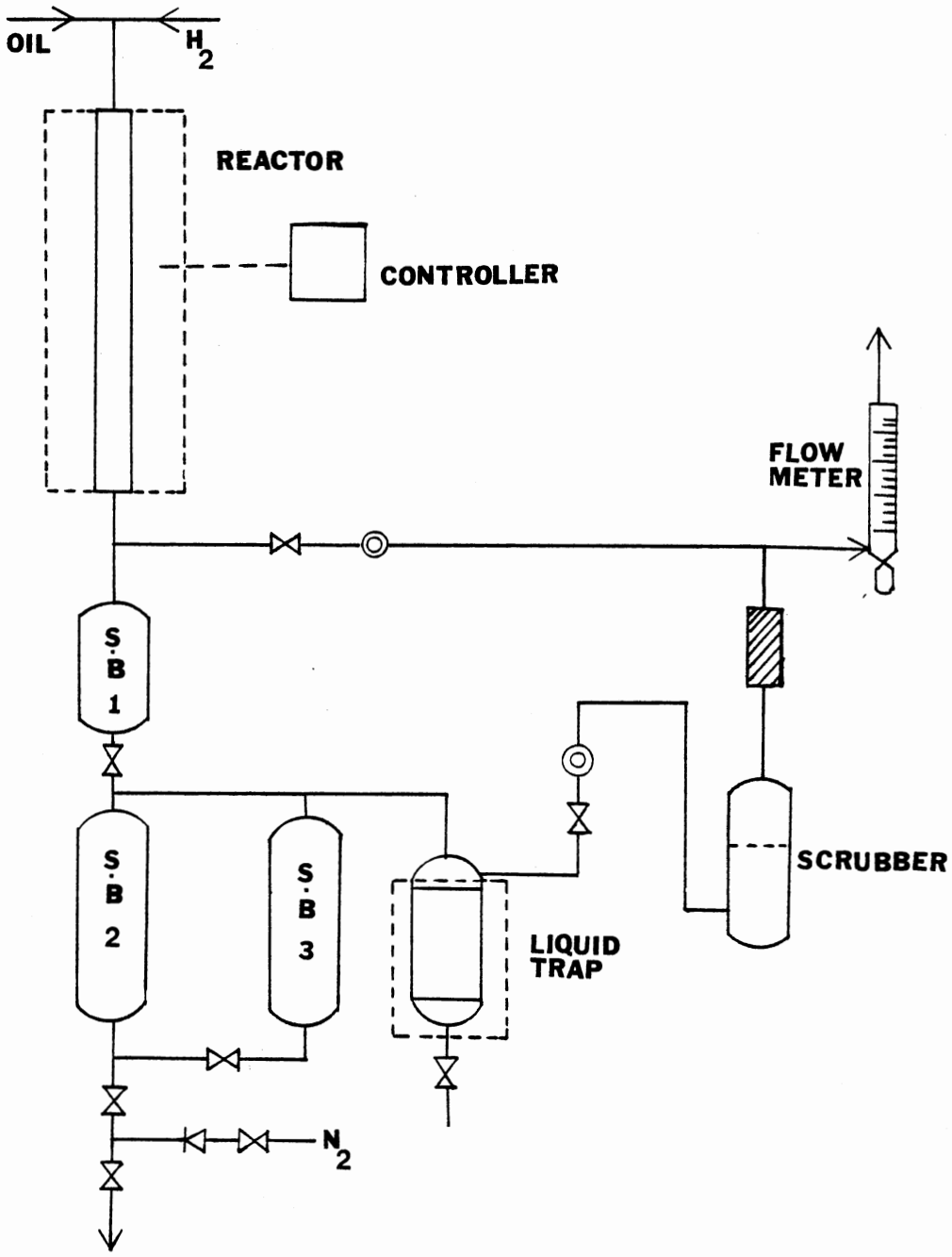

Figure 5. Gas-Liquid Separation System

the system to shut the gas supply in case of a flow surge. A manually operated, quarter-turn shut-off valve was placed close to the gas manifold for quick gas shut-off in case of emergency.

In case of overpressurization in liquid feed lines, the Ruska pump would automatically shut-off, in addition, an alarm would sound to inform the attendant. Two rupture disks were also connected to the oil feed system to avoid the Ruska pump overpressurization.

CHAPTER V

EXPERIMENTAL PROCEDURE

In this chapter, the experimental procedures used during this study will be discussed. Details of the experimental procedures are presented in Appendix C; gases and chemicals used are listed in Appendix E.

Catalyst Calcining and Loading

All catalyst samples were calcined in a muffle furnace at a temperautre of 475°C $\pm$ 25, for a period of six hours, to remove adsorbed and chemically bound water from the catalyst alumina support. The calcined catalysts were stored in a desiccator until further use.

Weighed calcined catalyst was packed into the middle of a tubular reactor, the remaining empty reactor sections were filled with glass beads, which acted as pre- and post-heat reactor zones. The reactor packing procedure differed for the various experiments conducted, details are present in Chapter VIII.

A thermowell, containing a thermocouple sheath, was placed in the middle of the reactor to monitor the reactor internal temperature. A number of stainless steel discs, with holes along the periphery, were snugly fit into the reactor at different positions to improve the solid-liquid contacting efficiency in the reactor. Two screens of

50 mesh-size were placed at the reactor inlet and outlet to avoid the entry of large, undissolved coal particles into the reactor.

The catalyst loaded reactor was pressure tested with nitrogen gas prior to its being installed in the reactor system. Pressure testing was next carried out by pressurizing the reactor system and closing all inlet and exit valves. The pressure drop was monitored for two hours; a pressure drop of greater than 136 KPa would warrant checking and tightening leaking fittings.

The reactor pressure was gradually reduced and nitrogen gas allowed to flow through the reactor system. The temperature programmers were adjusted to raise the reactor temperature to 400°C at a rate of 2°C per minute. The temperature was stabilized at 400°C, and a temperature profile inside the reactor taken; less than $\pm$ 5°C deviation in the catalyst bed temperature was considered satisfactory for catalyst presulfidation to begin.

Catalyst Presulfiding

Catalysts were presulfided "in-situ" using 5 vol.% H_2S/H_2 gas mixture, at a temperature of 400°C, for a period of four hours. A 500 cm^3/min, H_2S/H_2 gas mixture flow was maintained through the system at a pressure of 0.54 MPa (80 psig). A large excess of H_2S was provided to completely sulfide the catalyst active species. This procedure for catalyst sulfidation was reported by Laine et al. (1979).

Startup Procedures

The reactor was brought to operating pressure with hydrogen gas. The pump was next turned on, proper valves opened for liquid and gas to

flow into the reactor. Care was taken that coal liquids and hydrogen gas encountered the catalyst simultaneously.

The temperature in the catalyst bed was gradually raised to 400°C, and adjusted until the nominal bed temperature of 400°C $\pm$ 3 was achieved. Lower than normal operating temperature during the startup was used to reduce the incidence of hot-spots, which occurred due to high initial catalyst activity. The hot-spot formation can result in accelerated catalyst deactivation, due to excessive coke deposition.

Sampling Procedure

Product liquid samples were removed from the sample bombs at regular intervals; intermediate samples were removed whenever the reactor process conditions (temperature, liquid flow rate) were changed. Usually a through put of three reactor volumes (150 cm^3) was considered to be sufficient for the reactor to stabilize at the new process conditions. The details of the sampling procedure are given in Appendix C.

Shutdown Procedures

During shutdown, the oil supply to the reactor was cut by switching-off the feed pump. The hydrogen pressure was maintained, and its flow rate increased to quench the reactor; reactor insulation was removed to serve the same purpose. The hydrogen gas flow rate was maintained until the reactor reached ambient temperature. The last liquid sample was always withdrawn before the shutdown procedures were implemented. The reactor was cut into six sections, and the catalyst removed

from each section for further analysis.

Sample Analyses

The product liquid samples were analyzed for their sulfur, nitrogen, carbon, and hydrogen content. Some selected samples were analyzed for asphaltene content, and $454°C^+$ residue content. The analytical procedures are discussed briefly in this section; Appendix D contains the complete details.

Sulfur Analysis

The sulfur content of the liquid samples was determined by means of a Leco Automatic Sulfur Analyzer, consisting of a Model 532-000 Automatic Titrator, a Model 521-500 Induction Furnace, and an oxygen purifying train. The general procedure for operation of these instruments is given in the Leco Bulletin. In this system, the induction furnace is used to burn the sample in an atmosphere of purified oxygen. The SO_2 and other combustion products are passed to an automatic titrator, where they are titrated against a standard KIO_3 solution, using starch as an indicator. The amount of KIO_3 titrated, is used to determine the sulfur content of the sample.

Nitrogen, Carbon and Hydrogen Analyses

The complete analytical system consisted of a Model 240B Perkin-Elmer Elemental Analyzer, a Model AD-2 Perkin-Elmer Autobalance, a Model 56 Perkin-Elmer one millivolt Range Recorder, and a Model 04-1280 Perkin-Elmer Sealer. This system could analyze for three elements - carbon, hydrogen, and nitrogen, simultaneously. The Perkin-Elmer

instruction manual describes the general procedures for analyses with this equipment.

ASTM Distillation of Oil Samples

The feed oil and selected product oil samples were subject to ASTM D-1160 distillation (Annual Book of ASTM Standards, Part 23, 1979). The fractionation was carried out at 20 mm Hg pressure. One hundred mls of the sample to be distilled were taken in a distillation flask and heated by a mantle controlled by a powerstat. The vapor and the pot temperatures were recorded against the volume distilled. The distillation was stopped, when the vapor temperature reached 310°C (20 mm Hg). The weight percent residues remaining in the flask represented the fraction of oil boiling above 454°C (760 mm Hg).

Asphaltene Content of Oil Samples

The procedure for asphaltene determination, used in this study, was originally developed at Amoco laboratories by Bertolacini et al. (1977), and was later modified at Pittsburgh Energy Technology Center (PETC) by Utz et al. (1982). The procedure involves pressure filtration, compared to the conventional Soxhlet extraction. The major advantage this procedure offers lies in the time it takes to completely analyze a sample. A sample can be analyzed, without any loss in precision, in 30 minutes, compared to several hours or days it takes for Soxhlet extraction. Detailed description of the various separation methods used in different research labortories is presented in Appendix F.

In this study the asphaltene fraction is identified as the n-pentane insoluble fraction in the coal liquids. For some samples, the

tetrahydrofuran (THF) insoluble fractions were also determined. Figure 6 presents the scheme of fractionation used during this study.

The procedure involves mixing the liquid samples with the designated solvent (n-pentane, ethyl acetate, THF) and subjecting the mixture to ultrasonic mixing in an ultrasonic bath. The mixture is pressure filtered over a teflon filter in a pressurized filter cell using dry nitrogen gas pressure. The residues remaining on the filtered paper are removed, dried and weighed to determine the fraction residues. Details of this separation scheme are presented in Appendix D.

Ash Content of Oil Samples

The feed oil samples were analyzed for ash content by a procedure developed in our laboratory. The standard ASTM D-482 procedure (Annual Book of ASTM standards, Part 23, 1979) was found unsuitable for determining the ash content of coal liquids because of the large amount of liquid sample (100 mls) needed for analysis. In the present method, n-pentane insolubles were removed from 10 gms of the liquid sample using the procedure described earlier. The n-pentane insolubles were combusted in a muffle furnace at 500°C $\pm$ 25 for 12 hours, and residues weighed to determine the ash content. Care was taken to weigh the residues at a temperature higher than the ambient to avoid moisture adsorption.

Catalyst Characterization

The spent catalysts from each reactor section were removed and characterized individually. For those sections, where catalyst particles

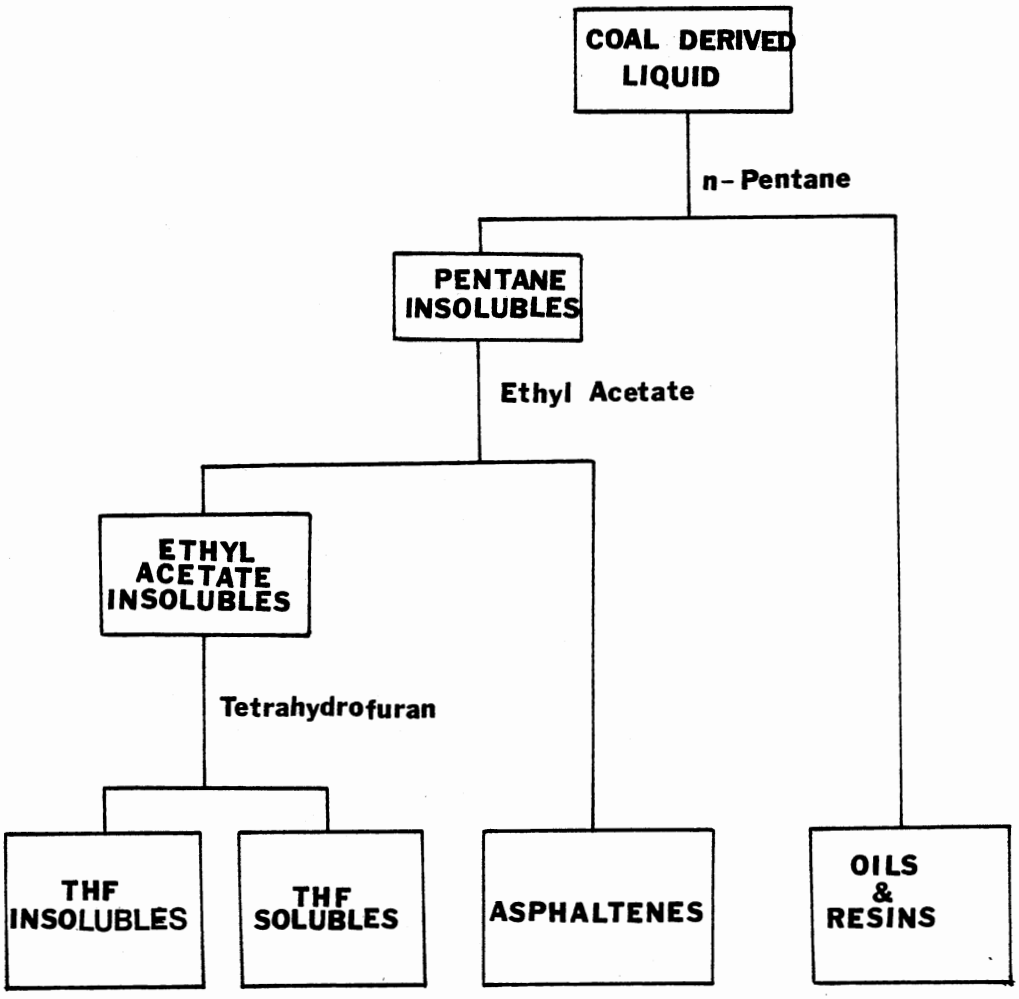

Figure 6. Solvent Fractionation Scheme for Coal-Derived Liquids

were cemented together by residues, each catalyst particle was carefully chipped off to avoid excessive catalyst fracturing. The catalysts were extracted in a Soxhlet apparatus with tetrahydrofuran (THF) to remove soluble material adhering to the catalyst. The catalysts were usually extracted for 24 hours, the solvent generally became clear after only a few hours of extraction. The extracted catalysts were vacuum dried at 125°C for 12 hours.

The catalysts and residues (contained in extraction thimble) were passed through a 20 mesh-size screen to separate the catalysts from the residues. The residues and catalysts were stored separately in a desiccator until further analysis. The residues were characterized in terms of coke content, ash content, elemental composition, and metal type. The catalyst samples were analyzed for coke content, surface area, pore volume, pore size distribution, metal content, and elemental composition of the residues deposited on the catalyst.

Coke Content

Coke content on the spent catalysts was determined by combustion in a muffle furnace at 475°C $\pm$ 25 for 24 hours. The catalyst coke content was defined on the basis of the regenerated catalyst weight. The catalyst samples can adsorb an appreciable quantity of moisture from air leading to erroneous results. The moisture adsorption was avoided by evacuating the catalyst samples at a temperature of 100°C for several hours, and sealing in a helium atmosphere before weighing.

The coke content in this study is defined as the THF insoluble, combustible carbonaceous material, deposited on the catalyst during hydrotreatment. Note that the solvent type used for catalyst washing

can have a significant effect on the final coke content. Pyridine was found unsuitable for catalyst washing; high nitrogen content in pyridine can mask further catalyst elemental analysis.

Elemental Analysis

The elemental composition of the residues on the catalyst pellet was determined by the Perkin-Elmer 240B elemental analyzer. Hydrogen on aged catalyst pellets can exist in two forms: that in the residues, and that as adsorbed/chemically bound water in the catalyst support.

The hydrogen content on the residues was corrected for hydrogen present in the catalyst support. Fresh catalyst pellets of an average weight of 10 mgs were analyzed, and their hydrogen content determined on the basis of the unit weight of calcined pellet. Note that the combustion in the Perkin-Elmer elemental analyzer occurred at 950-1000°C, in an atmosphere of oxygen. All the hydrogen can be assumed to be removed under these conditions. Correction was applied to the aged catalyst hydrogen content on the basis of the regenerated catalyst weight.

The hydrogen content on the catalyst determined by this method is only approximate, it does not take into account the water that chemically binds to the alumina support during hydrotreatment. The nitrogen and carbon content on the aged catalyst, however, can be determined with considerable accuracy.

Surface Area

The surface area of fresh and aged catalyst samples were determined using a Model 2100D ORR Surface Area - Pore Volume Analyzer. This

instrument determines the nitrogen adsorption isotherm, at liquid nitrogen temperature, which is used to obtain the B.E.T. plot.

Catalyst samples were degassed for over 12 hours at a temperature of 300°C, under high vacuum. Helium, an inert gas, was used to measure the dead space in the sample flask. The amount of nitrogen adsorbed by the catalyst, at liquid nitrogen temperature, was measured from the decrease in pressure, and used to determine the surface area of the catalyst.

Pore Size Distribution and Pore Volume

A Micromeritics Model 900/910 Series Mercury Penetration Porosimeter was used to determine catalyst pore size, pore volume, and pore distribution.

Mercury was forced into the catalyst pores under pressure, the volume of mercury penetrated into the catalyst pores was measured by the distance travelled by a movable probe at various pressures applied (atmospheric to 340 MPa).

Contact angles in the range of 128-130° have been reported for mercury and alumina catalyst (Baker and Relthaar, 1982). No study has been reported for the catalyst contact angle on coked catalyst surface. In this study, it has been assumed that the contact angle for mercury and alumina remains constant at 130°, and does not change with catalyst surface coking.

EDAX Analysis in Scanning Electron Microscope

Both aged and fresh catalyst samples were analyzed for metal deposits in a JEOL Electron Scan Microscope (SEM), Model JFM-35, fitted

with an Energy Dispersive X-ray Analyzer (EDAX). The electron beam conditions were 100 μA at 25 kV, focussed to a diameter of 10 μm; 60 seconds of counting time were spent on each scan, and the output fed to a Tracor Norther Model 2000 computer, which identified the metal type and count distribution. The results from this analysis are only semi-quantitative, and are present as area fraction of each element present. The area fractions are indicative of the ratio of the metals present and not the absolute metal content.

Usually overall scans of the catalyst pellet at x1000 magnification were taken to identify the metal deposits on the catalyst surface. The catalyst pellet was also radially fractured, and radial scans taken at catalyst periphery, 10 μm, 60 μm, and inside the catalyst center.

CHAPTER VI

PROPERTIES OF FEEDSTOCK AND FRESH CATALYST

The properties of the coal liquid and the catlysts used during this study are presented in this Chapter.

Fresh Catalyst

Two different commercial Ni-Mo-Al_2O_3 catalysts were used during this study; the catalysts (Armak KF-153S and Harshaw HT-115E) were selected with approximately similar metal loadings (3.5% NiO, 15.5% MoO_3), but different physical properties. Harshaw HT-115E is a large pore diameter catalyst with the most frequent pore diameter of 177 Angstroms (Å), and a low surface area of 125 m^2/gm. Armak KF-153S is a small pore catalyst, with a most frequent pore diameter of 64 Å, and a high surface area of 275 m^2/gm. The alumina support for the KF-153S catalyst contained 4.1 wt% silica; whereas, Harshaw HT-115E contained approximately 0.1 wt% silica.

Figures 7 and 8 present the pore volume and pore size distributions of these catalysts. Note that the catalyst, KF-153S, has a very narrow pore size distribution; all its pores are distributed in the pore size range of 50-70 Å. Harshaw HT-115E catalyst has a very broad pore distribution, the pore sizes range from 80 to 280 Å. The physical and chemical properties of these catalysts are presented in Table I. Both catalysts are of similar physical shape

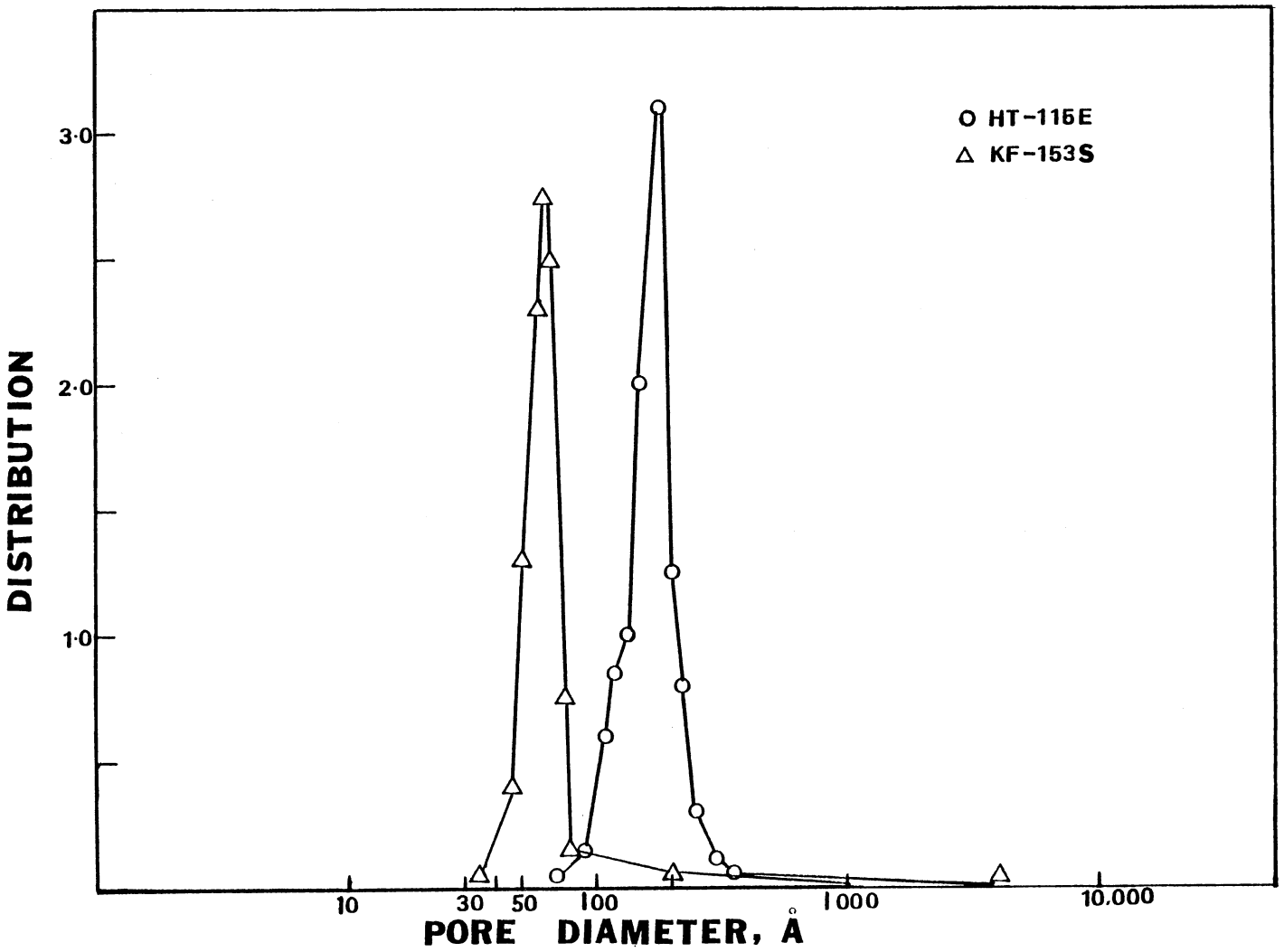

Figure 7. Fresh Catalyst Pore Distribution

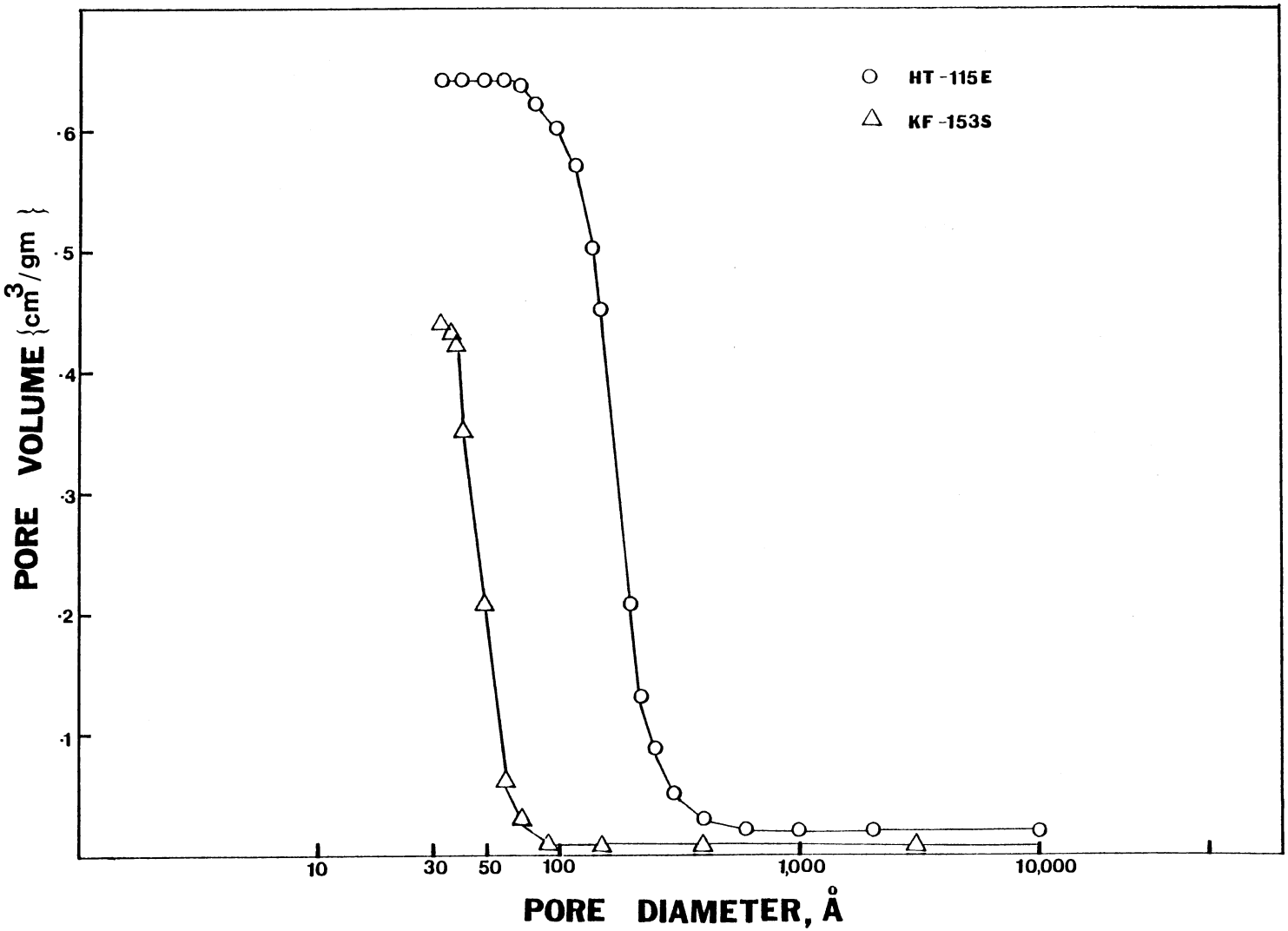

Figure 8. Fresh Catalyst Cumulative Pore Volume vs. Pore Diameter

TABLE I

CATALYST PROPERTIES

Catalyst Type	HT-115E	KF-153S
Manufacturer	Harshaw Chemical	Armak Chemical
Chemical Composition*, wt%		
NiO	3.6	3.3
MoO_3	16.4	15.5
SiO_2	0.1	4.1
P	1.1	--
Al_2O_3	78.8	77.1
Physical Properties**		
Geometry	1.6 mm Extrudates	1.6 mm Extrudates
Pellet Density, gm/cm^3	3.51	3.55
Reactor Density, gm/cm^3	0.54	0.63
Particle Density, gm/cm^3	1.12	1.24
Surface Area, m^2/gm	125	270
Pore Volume, cm^3/gm	0.63	0.49
Most Frequent Pore Diameter, Å	177	65
Pore Size Distribution, Å		
35- 70	0.01	0.87
70-100	0.04	0.02
100-150	0.36	0.02
150-200	0.40	0.01
200-400	0.13	0.04
>400	0.06	0.04
	1.00	1.00

* Vendor data.
** Values determined in our laboratory.

and size (1.6 mm extrudates), and contain approximately the same amount of active metals. Table II presents the Energy Dispersive X-ray Analysis data of these catalysts at various radial positions.

Feedstock

SRC-I solids and Process Solvent were received from Pittsburgh and Midway Coal Mining Company's SRC pilot plant at Dupont, Wyoming. A mixture of 15 wt% SRC-I solids in 85 wt% Process Solvent was used as a feedstock in this study.

Table III presents the properties of SRC-I solids, SRC Process Solvent, and 15 wt% SRC/Process Solvent mixture. The principal metal types identified in the 15 wt% SRC/Process Solvent mixture feedstock were (in order of their abundance): Fe, Cl, Ti, Si, S, Al, Ca, Cr, Cu, and K. The principal metal constituents, iron and titanium, can be present both in the inorganic fraction and in the oil soluble organo-metallic compounds.

A fifteen gallon mixture of 15 wt% SRC/Process Solvent was prepared for use during this study. Care was taken for complete dissolution of SRC-I solids in the Process Solvent; this was achieved by gradually adding SRC solids to the Process Solvent liquid, with constant agitation. The mixture was stirred for 12 hours at room temperature, after which the temperature was gradually raised and maintained at 125°C for a period of 24 hours. Precautions were taken for minimum light fraction loss. The hot mixture was filtered through a 50 mesh-size screen, and stored in five-gallon drums at room temperature.

TABLE II

FRESH CATALYST EDAX ANALYSIS AREA PERCENT

	KF-153S				HT-115E			
	Surface	10 μm	60 μm	Center	Surface	10 μm	60 μm	Center
Al	75.5	81.8	81.6	81.4	50.8	48.3	70.7	88.7
Ni	4.8	3.8	3.5	3.3	11.5	11.4	6.8	2.4
Mo	18.2	11.7	12.0	12.9	32.7	30.3	19.7	4.9
Si	2.2	1.9	2.1	2.4	0.3	--	--	--
P	--	--	--	--	2.6	2.8	2.7	3.8
Fe	--	--	--	--	2.5	1.0	--	--

TABLE III

PROPERTIES OF FEEDSTOCK

	SRC-I Solid	SRC Process Solvent	15 wt% SRC-I /Process Solvent
Total liquid density @ 21°C, gm/cm^3		1.003	1.058
Normal Boiling Point,* °C			
IBP	360	250	253
10 vol%	-	278	277
20	-	292	293
30	-	302	309
40	-	319	327
50	-	334	342
60	-	352	363
70	-	376	401
80	-	407	454
90	-	454	-
End Point,	-	454	-
Recovery, wt%	7	91	80
454C$^+$ Residues, wt%	93.0	8.5	20.4
n-Pentane Insol; wt%	97.9	7.7	22.1
Ethyl Acetate Insol, wt%	76.3	0.5	6.4
THF Insol., wt%	16.9	0.0	1.0
Elemental Composition, wt%			
Total liquid			
C	86.62	88.98	87.20
H	5.81	7.85	7.26
N	2.25	1.01	1.12
S	0.71	0.48	0.51
Ash	0.29	0.00	0.09
H/C	0.80	1.06	0.99
N/C	0.022	0.001	0.011
454C$^+$ Residues			
C	-	88.70	87.91
H	-	6.43	6.05
N	-	1.85	1.82
S	-	0.53	0.51
Ash	-	0.00	0.48

TABLE III (Continued)

	SRC-I Solid	SRC Process Solvent	15 wt% SRC-I /Process Solvent
H/C	-	0.98	0.82
N/C	-	0.020	0.018
$454C^-$ distillates			
C	-	89.43	88.89
H	-	8.41	7.41
N	-	0.93	1.08
S	-	0.48	0.52
Ash	-	0.00	0.00
H/C	-	1.13	1.01
N/C	-	0.009	0.010

* Determined by ASTM D-1160 procedure.

CHAPTER VII

PRECISION OF EXPERIMENTAL TECHNIQUES

The experimental results during this study are affected by the overall performance of the reactor system, and the precision of the liquid and catalyst sample analyses.

Reactor System Operation

Trickle-Bed Reactor Performance

This study was not intended to measure the effect of fluid dynamic parameters on the trickle-bed reactor performance. An attempt, however, will be made to analyze the extent to which these factors affected the reactor performance. Catalyst liquid holdup, effective catalyst wetting, external mass transfer, and axial dispersion have been cited by various authors to affect the reactor performance. The reader is referred to a review on the performance of trickle-bed reactors by Bhan (1981).

Consideration of the tube diameter to the catalyst particle diameter (D_t/D_p), liquid flux, and gas flux can give an insight into the reactor flow distribution effects. In this study, the D_t/D_p ratio was 6.4; the liquid feed flux was in the range of 0.007 to 0.015 gm/cm^2/sec. At these low flow rates, the liquid flow distribution is of negligible importance. Sooter (1974) and Satchell (1974) in their

hydrotreatment studies with raw anthracene oil on a similar reactor used a D_t/D_p ratio of 3.45 and varied the liquid flux in the range of 0.009-0.38 $gm/cm^2/sec$, they observed no significant effect on the hydrotreatment removal.

The evaluation of the kinetic data from fixed-bed catalytic reactors is usually based on the assumption of plug-flow. Mears (1971) reported substantial deviation from plug-flow model for shallow bed experimental reactors due to axial dispersion effects, and suggested a criterion for determining the extent of backmixing. Mears' (1971) correlation suggests an L/D_p ratio equal to 350 for less than 5% deviation at 90% conversion for first order kinetics in hydrotreating gas oil. The L/D_p ratio in the present study was 480, which is much higher than required by the Mears' criterion. Thus, the performance of the reactor used during this study did not involve any backmixing and can be safely assumed to behave as a plug-flow reactor.

Overall Reactor System Performance

In the trickle-bed reactors, temperature control can be an operational problem caused by exothermic hydrotreating reactions. In the present study, the reactor temperature distribution along the reactor outer wall was excellent; a variation of no more than 1°C with respect to both position and time was observed. The radial temperature difference across the catalyst bed, as measured by the inside and outside thermocouples, too, did not exceed 1°C. However, a temperature difference of 10°C between the center of the catalyst bed and the outer wall of the reactor was observed during the first few hours of oil-catalyst contact. This temperature differential

was caused by the exothermic reactions and was difficult to control. The outside aluminum block temperature was held within ± 0.5°C of the desired temperature through the entire run duration. The variations in the reactor bed temperature during this study were thus negligible to significantly affect the magnitude of reaction kinetic parameters determined.

Various researchers (Wan, 1974; Sooter, 1975) have reported negligible effect of pressure beyond 6.39 MPa (1000 psig) on heteroatom removal activity from coal-derived liquids. All experimental runs in this study were conducted at 11.7 MPa (1700 psig) with less than 34 kPa (5 psi) variation, thus the effect of pressure variation, too, on the heteroatom removal activity can be assumed to be negligible.

Analytical Precision

Liquid Analysis

Table IV presents the precision of analyses conducted on the feedstock. The percentage deviation, and the number of samples analyzed for each analysis are also presented. The maximum percentage deviation for the product liquid sample analyses are also shown.

The nitrogen content of the product liquid samples varied in the range of 0.25 to 1.12 wt%, with standard deviations of ± 0.011 to ± 0.084; the hydrogen content was in the range of 7.26 to 10.5 wt%, the standard deviation being ± 0.045 to ± 0.396 wt%. The percentage deviation increased with decrease in the magnitude of the measured variable.

TABLE IV

PRECISION OF THE ANALYTICAL TECHNIQUES
(LIQUID ANALYSES)

	Feedstock				Product Liquid
	Average	Standard Deviation	% Deviation	No. of Samples	% Maximum Deviation
Nitrogen	1.12	± 0.052	4.63	13	15.57
Carbon	87.20	± 1.220	1.39	13	6.73
Hydrogen	7.26	± 0.172	2.37	13	3.75
Sulfur	0.51	± 0.072	1.41	8	***
n-Pentane insol.	22.16	± 0.346	1.56	3	3.45
Ethyl Acetate insol.	6.39	± 0.583	9.12	3	7.77
THF insol.	0.99	± 0.054	5.45	3	***
454 C^{+} residues	20.41	± 1.730	8.47	2	***

The n-pentane insoluble content was determined with high precision and reproducibility. The Pittsburgh Energy Technology Center using a similar microfiltration technique for n-pentane separation determined the standard deviation to be in the range of ± 0.50 wt%; in our study the n-pentane insoluble standard deviation was ± 0.34 wt%, corresponding to ± 1.56% deviation. The ethyl acetate, THF residue, and 454 C^+ residue content could not be determined with very high precision, the percentage deviations were 9.12, 5.45, and 8.47%, respectively. Usually the n-pentane insoluble and ethyl acetate insoluble content for a product liquid sample were determined only once, only some of the liquid samples were anlayzed in duplicate to ascertain the precision of the separation. Due to the large liquid volume required for the ASTM D-1160 distillation, the product liquid samples were also subjected to distillation only once.

Catalyst Analyses

Table V presents the precision of the analytical techniques used for catalyst physical property characterization. The fresh catalyst samples were analyzed in triplicate for physical properties. The coked catalyst samples were anlayzed only once because of the small amount of catalyst sample available for analysis. The aged catalyst samples from Run ZBF were analyzed in triplicate for coke content. The standard deviation was ± 0.83 wt% for an average coke content of 18.36 wt%. Extreme precautions were taken to avoid moisture adsorbtion from the atmosphere.

The nitrogen content data of the aged catalysts were highly precise due to the absence of nitrogen in the solvent (THF) used for

TABLE V

PRECISION OF ANALYTICAL TECHNIQUES
(CATALYST ANALYSIS)

	Average	Standard Deviation	Percent Deviation	No. of Samples
Fresh Catalyst Samples				
Surface Area	125 m^2/gm	± 3.5	± 2.8	3
Pore Volume	0.63 cm^3/gm	± 0.04	± 6.3	3
Most Frequent Pore Diameter	177 Å	± 3.0 Å	± 1.7	3
Aged Catalyst Samples				
Coke Deposition	18.36 wt%	± 0.83	± 4.5	3
Coke Elemental Analysis				
N	0.334 wt%	± 0.014	± 4.25	14
C	9.122 wt%	± 1.248	± 13.63	14
H	1.169 wt%	± 0.218	± 18.64	14

catalyst washing; the percentage deviation of nitrogen content was less than 5.32%. The percentage deviation for the hydrogen content was high, ± 18.64 wt%, due to the hydrogen present in the fresh catalyst pellet.

The results for the surface area, pore volume, and pore size distribution determined for the fresh, coked and regenerated catalyst samples were highly reliable. The maximum standard deviation in surface area of catalyst samples was less than 3.0%, deviation in pore volume was less than 7.8%, and deviation in pore size less than 3.7%.

Reproducibility of Reactor Operation and Experimental Procedure

In a previous study (Bhan, 1981), the reproducibility of a reactor system similar to one used in the present study was determined, the experimental procedures, too, were exactly similar. It was observed (Bhan, 1981) that the nitrogen content of the product liquid samples for the two duplicate experimental runs varied within the range of the experimental error. During the present study, the response of the composite catalyst bed was determined to be similar to the response of the single catalyst beds. The analyses of the used catalyst samples from the single catalyst bed reactor and the composite catalyst bed revealed the used catalyst physical properties to be similar. The physical properties of a particular catalyst in the composite catalyst bed varied within the range of the experimental error for a similar catalyst in a single catalyst bed, suggesting the reactor performance and the experimental procedure in this study to be highly reliable and reproducible.

CHAPTER VIII

EXPERIMENTAL RESULTS AND DISCUSSION

The principal objective of this study was to assess the hydrodenitrogenation activity of composite catalyst beds (two or more catalyst zones in a single reactor bed). A total of four experimental runs were conducted, using catalysts separately, and in combination. Careful thought was given to the selection of catalysts and feedstock in this study. The catalysts were selected with similar metal loadings, but different pore diameters; the feedstock selection was based on oil asphaltene, and heteroatom (N, S, O) content. The properties of the catalyst and feedstock are given in Chapter VI.

Experimental Design

Four experimental runs were conducted in a trickle-bed reactor system. For all the experimental runs conducted, the pressure was maintained at 11.6 MPa (1700 psig); temperatures in the range of 260 to 400°C were employed. Liquid feed rates were changed to adjust liquid volume hourly space times (LVHST) at 0.94, 1.34 and 1.87 hours. Hydrogen flow rate was held constant at 1781 Std. m^3/m^3 of oil (10,000 SCF/Bbl.).

A 3^2 factorial experimental design was selected: for each catalyst temperature, three liquid volume hourly space times were employed. In all, 3 x 3 sequences of temperatures and LVHST were used. Table VI

TABLE VI

EXPERIMENTAL RUN SUMMARY

Reactor	EN-I Trickle-Bed Reactor Co-current gas-liquid flow.
Pressure	11.6 MPa (1700 psig)
Hydrogen Flow	1781 Std. $m^3 H_2/m^3$ of oil (10,000 SCF /Bbl.)
Feedstock	15 wt% SRC in Process Solvent

Run Series	Run Objective	Reactor Bed Sequence	Catalyst	LVHST hrs.	Temperature °C	Time On Oil hrs.
ZBF	Large Pore Diameter Catalyst Reference Run	Single Catalyst Bed	HT-115 E	0.94, 1.33, 1.87	350, 375, 400	240
ZBG	Small Pore Diameter Catalyst Reference Run	Single Catalyst Bed	KF-153 S	0.94, 1.33, 1.87	350, 375, 400	240
ZBH	Composite Catalyst Bed	Two Catalyst Composite Bed	KF-153 S (Top) HT-115 E (Bottom)	0.94, 1.33, 1.87	350, 375, 400	240
ZBI	Reactor Temperature Zoning Effect	Two Reactors in Series	KF-153 S	1.87	260 (Top) 400 (Bottom)	120

summarizes the experimental run conditions for all experimental runs conducted during this study.

Run ZBF and ZBG

These two experimental runs were conducted to assess the effect of catalyst pore size on catalyst hydrotreatment activity, and also to serve as a reference for further composite catalyst bed experiments.

Harshaw HT-115 E, a large pore diameter, Ni-Mo-Al_2O_3 catalyst was used for experimental Run ZBF; a small pore diameter Ni-Mo-Al_2O_3 catalyst (KF-153 S) was employed for Run ZBG. Both these experiments were conducted for a duration of 240 hours, the shutdown being scheduled. Glass beads were placed on both ends (10 cms) of the catalyst bed to serve as reactor pre- and post-heat, and distribution zones.

Run ZBH

The objective of this experimental run was to determine the hydrotreating activity and catalyst deactivation response of a composite catalyst bed. A small pore diameter catalyst (KF-153 S) was packed in the first-half of the reactor bed (30 cms), while a large pore catalyst (HT-115 E) filled the rest of the reactor. All the process conditions for this experimental run were the same as for Run ZBF and ZBG.

Run ZBI

This experimental run was conducted with two catalytic reactors placed in series, one on top of the other. The special inter-sampler was connected between the two reactors to withdraw liquid samples

from the first reactor. Both reactors were operated at a constant pressure of 11.6 MPa (1700 psig), and contained small pore diameter catalyst (KF-153 S). The nominal temperatures in the beds were different; the top reactor bed was operated at 260°C, the bottom reactor at 400°C. All other run conditions (pressure, LVHST) were similar to the experiments described earlier.

Run ZBI was conducted for a period of 120 hours, the shutdown being scheduled. Considerable pressure drop was noticed in the top reactor section during the last thirty hours of oil-catalyst contact. For experimental Runs ZBF, ZBG and ZBH, reactor plugging and pressure drop problems were encountered only after 210 hours of oil-catalyst contact time had elapsed. None of the runs conducted during this study had to be shutdown prior to the scheduled time.

Catalyst Sample Analyses

Coke Deposition

In this study, the catalyst coke content is defined as the percent loss in catalyst weight upon combustion at 475°C. Details of the coke determination method are presented in Appendix D.

Aged catalyst sample weight reduction occurs due to the combustion of carbonaceous deposits on catalyst surface. These deposits consist primarily of polynuclear condensed molecules, containing C, N, H, S and oxygen atoms. Some reduction in catalyst weight also occurs due to the oxidation of metal sulfides. Both the active metal species (Ni, Mo), and the metals deposited during hydrotreatment (Ti, Fe) are present on the catlayst in their sulfided form. Theoretically, 3.3 wt% reduction

in catalyst weight occurs upon oxidation of the sulfided active metal (Ni, Mo) species. The coke data reported in this study have been corrected for the sulfided active metal species oxidation. No estimate, however, could be made of the weight loss associated with oxidation of the deposited metal (Ti, Fe) sulfides.

Jepsen and Rase (1981) reported the presence of MoS_2 and Ni_2S_3 on the sulfided $NiO-MoO_3-Al_2O_3$ catalyst. Assuming complete sulfidation of Ni and Mo present, approximately 8.2 wt% stichometric sulfur is calculated to be chemically bound to the catalyst active metals. Correction for the loss in catalyst weight upon oxidation of the sulfided metal species was made assuming complete formation of Ni_2S_3 and MoS_2 during sulfidation.

Summation of the elemental content (C, N, H, O, S), determined by the elemental analysis of the aged catalyst samples can be a good measure of the catalyst coke content. Unfortunately during this study, the catalyst O and S content could not be determined accurately. The S, H, and O content determined from the elemental analysis of the aged catalyst may be contributed from the residues deposited on the catalyst, and/or the elemental content of fresh sulfided catalyst. About 3-4 wt% difference exists between the loss in catalyst weight upon combustion, and the summation of the elemental N, C, H, content. The difference may be contributed by the oxygen content of the residues, and/or the removal upon combustion of the water adsorbed during hydrotreatment.

Table VII presents the coke content analysis of the aged catalyst from Run ZBF (large pore catalyst). The elemental analysis of the catalyst residues for some selected samples is also presented. The coke content varied from 14.6 wt% in the bottom catalyst section of the

TABLE VII

LARGE PORE CATALYST COKE ANALYSIS
(RUN ZBF)

Sample Number		Total Loss In Catalyst Weight wt.%	wt.% C	wt.% N	wt.% H	wt.% S	Corrected Coke Content	Coke Per Unit Surface Area mg/m^2
(Top)	1	24.2	-	-	-	-	20.9	1.669
	2	20.5	9.12	0.34	1.17	8.75	17.2	1.376
	3	21.7	-	-	-	-	18.4	1.471
	4	19.6	9.67	0.34	1.27	8.75	16.3	1.301
	5	17.9	-	-	-	-	14.6	1.168
(Bottom)	6	19.0	10.45	0.35	1.03	8.75	15.7	1.258

reactor to 20.9 wt% in the top reactor section. The coke content of the catalyst decreased uniformly over the reactor length.

The coke content of the catalyst from Run ZBG (small pore catalyst) is presented in Table VIII. The coke content increased uniformly along the catalyst reactor length; 16.8 wt% coke was deposited in the top reactor section compared to 20.5 wt% in the bottom section. Figure 9 shows the difference in the coke profiles along the reactor length for the two experimental runs; linear regression lines have been drawn to indicate the trend.

The difference in the coke profiles for the large and the small pore diameter catalyst can be explained as follows: Due to the lower pore diffusional resistance of the large pore diameter catalysts, highly condensed polyaromatic molecules, containing high fractions of heteroatoms, gain access into the catalyst interior, and deposit on catalyst active sites to form carbonaceous residues. The concentration of these large molecular species decreases along the reactor length, resulting in a decreasing coke profile. In comparison, the small pore diameter catalyst offers considerable resistance to the diffusion of the large molecular species, this selective exclusion of large molecular species results in lesser coke formation in the top reactor sections. However, the large molecular species are thermally cracked external to the catalyst (Wukash and Rase, 1982; Richarson and Alley, 1975); a large fraction of these cracked molecular species gain access into the catalyst pore structures towards the lower reactor sections, and deposit relatively high amounts of coke.

TABLE VIII

SMALL PORE CATALYST COKE ANALYSIS
(RUN ZBG)

Sample Number		Total Loss In Catalyst Weight wt.%	wt.% C	wt.% N	wt.% H	wt.% S	Corrected Coke Content	Coke Per Unit Surface Area mg/m^2
(Top)	1	19.9	-	-	-	-	16.8	0.622
	2	21.3	9.62	0.42	2.03	8.26	18.2	0.672
	3	21.1	-	-	-	-	17.9	0.664
	4	21.6	8.95	0.41	2.17	8.26	18.5	0.684
	5	21.8	-	-	-	-	18.7	0.693
(Bottom)	6	23.6	7.82	0.40	2.06	8.26	20.5	0.759

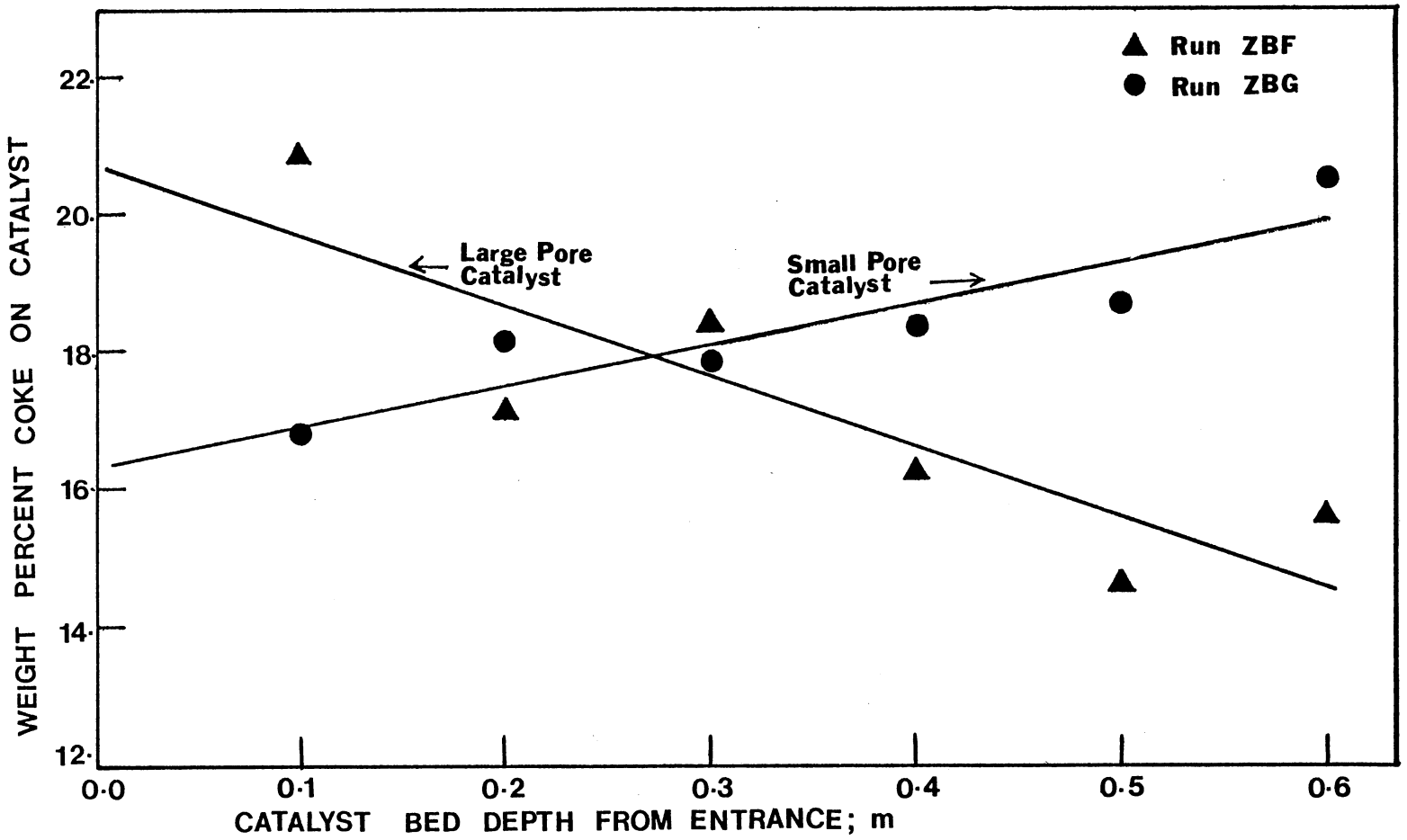

Figure 9. Coke Profiles in the Reactor Bed

Considerable difference in the coke content existed when the two catalysts were compared on a unit surface area basis. The large pore diameter catalyst deposited approximately two times more coke compared to the small pore diameter catalyst. On an average, 1.374 mgs of coke were deposited per square meter on the large pore diameter catalyst, whereas only 0.682 mgs/m^2 of coke were deposited on the small pore diameter catalyst. Similar results were reported by Beuther et al. (1980); coke deposition per unit surface area was reported to increase with increase in catalyst pore diameter. Hardin et al. (1978) reported higher per unit surface area coke deposition on a large pore diameter catalyst compared to a small pore diameter catalyst (Athabasca bitumen processing).

Figure 10 represents the coke deposition per square meter of the catalyst surface area as a function of the catalyst most frequent pore diameter. Note that the data reported by Chang (1982) for hydroprocessing SRC/Process Solvent mixture have been used to represent catalyst coke content for 118 Å most frequent pore diameter. The catalyst coke content increased gradually in the pore range of 65 - 120 Å, the rise in coke content was very steep for 177 Å pore size.

Coke deposition on the catalyst surface can occur in various physical forms: monolayer coverage; multilayer coverage; patch deposition. Ternan et al. (1979) assuming coke layer to have a thickness of an aromatic molecule, determined 0.2 mgs/m^2 of coke to be sufficient for a monolayer coverage of the catalyst surface. The assumption of the coke layer thickness to be equal to the size of an aromatic molecule is highly debatable. Coke consists of polycondensed molecules, which may contain four or five condensed aromatic rings. Considering

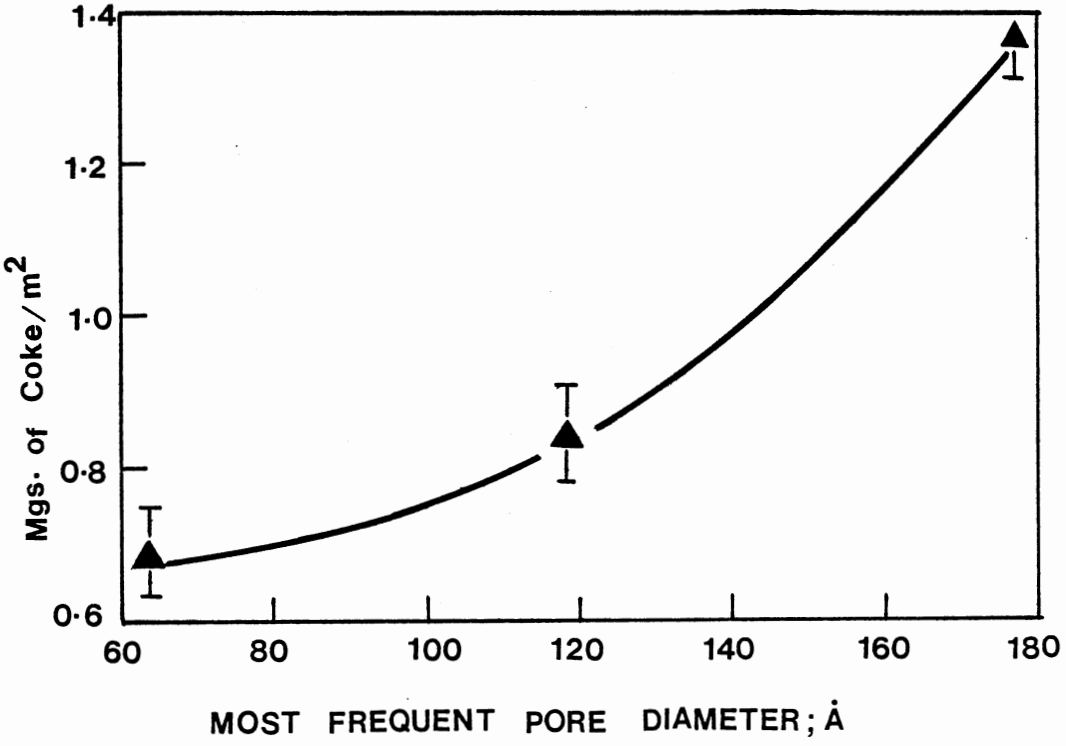

Figure 10. Coke Deposited per Square Meter vs. Catalyst Pore Diameter

the coke molecule to consist of four to five ring compounds of the azabenzopyrene or azacoronene type (N containing polyaromatic molecules), where the heteroatom forms the link between the catalyst and the condensed molecules, the thickness of the deposits can be estimated to be 10.4 Å (Satterfield and Sherwood, 1963). Mullendre et al. 1977, using ESCA sputter profiling, determined the thickness of the carbonaceous residue layer on a coal liquefaction catalyst to be 10 Å. For the present study, the most frequent pore diameter of the coked catalyst decreased from 65 Å to approximately 47 Å, suggesting the residue thickness to be 10 Å. Assuming the residue molecules to be of a 10 Å diameter, 4×10^8 molecules/m^2 would be necessary for a monolayer coverage. From the N/C and H/C ratio of the catalyst deposits in this study, the molecular weight of the residue molecules was calculated to be in the range of 240-260. Approximately, 1.66 mgs/m^2 of these deposits would be required for a monolayer coverage. According to this criterion, the large pore diameter catalyst would deposit a 0.83 monolayer, compared to 0.41 monolayer coverage for the small pore catalyst.

For a monolayer coverage of the catalyst surface, the catalyst hydrotreating activity would have to reduce to zero activity very rapidly. Total loss in catalytic activity does not occur even when the theoretical monolayer coverage is achieved. To suggest that the coke formation on the catalyst surface occurs as a perfect monolayer, is unrealistic. Multilayer coke coverage on the catalyst surface seems to be unlikely, too. If the coke is assumed to deposit by the adsorption of the heteroatoms on the catalyst acid sites, the coke molecule would most likely deposit on a fresh active site rather than on a second layer of carbonaceous deposits. Coke formation, most logically, occurs in patches

around the catalyst active site; the deposition being haphazard rather than uniform and predictable.

Table IX presents the coke analysis of the catalysts samples from experimental Run ZBH (composite catalyst bed). The coke data from this run did not show any improvement over the single catalyst bed. The top catalyst section (small pore diameter catalyst) contained an average of 16.7 wt% coke, which is comparable to the coke deposited on the same catalyst in Run ZBG. Similarly, 15.7 wt% coke was deposited in the bottom section (large pore catalyst). Here too, the large pore diameter catalyst deposited approximately twice more coke per unit surface area than the small pore diameter catalyst.

The coke analysis of the experimental Run ZBI presented some interesting results. Even at temperatures as low as 260°C, considerable coke was deposited on the catalyst (See Table X). An average of 16.2 wt% coke was deposited on the catalyst surface, which is comparable to the coke deposited on the same catalyst (KF-153 S, small pore) at 400°C. This experimental run was conducted for only 120 hours, compared to the 240 hour duration of the other experimental runs. No time effect, however, was determined on the catalyst coke content, signifying attainment of equilibrium coke content prior to 120 hours of oil-catalyst contact.

The nitrogen analysis of the product liquid samples revealed rapid deactivation during the first twenty-four hours of oil-catalyst contact. The rapid deactivation can be attributed to the initial carbonaceous build up on the catalyst surface, followed by gradual carbonaceous and metal deposition.

TABLE IX

COMPOSITE CATALYST BED COKE CONTENT
(RUN ZBH)

Sample Number		Total Loss in Catalyst Weight wt.%	wt.% C	wt.% N	wt.% H	wt.% S	Corrected Coke Content	Coke Per Unit Surface Area mg/m^2
Small Pore Catalyst								
(Top)	1	22.5	7.33	0.43	1.68	8.26	19.3	0.715
	2	18.4	7.84	0.40	1.59	8.26	15.3	0.565
	3	18.7	8.31	0.39	1.61	8.26	15.5	0.565
Large Pore Catalyst								
	4	18.7	9.01	0.38	1.26	8.75	15.4	1.233
	5	18.3	9.13	0.40	1.09	8.75	15.0	1.197
(Bottom)	6	20.2	9.60	0.44	1.27	8.75	16.9	1.344

TABLE X

TWO REACTOR BED COKE ANALYSIS
(RUN ZBI)

Sample Number		Total Loss in Catalyst Weight wt.%	wt.% C	wt.% N	wt.% H	wt.% S	Corrected Coke Content	Coke Per Unit Surface Area mg/m^2
Low Temperature Reactor								
(Top)	1	20.0	8.43	0.61	1.67	8.25	16.9	0.624
	2	18.0	8.04	0.67	1.70	8.26	14.8	0.549
(Bottom)	3	20.1	8.24	0.67	1.81	8.26	17.0	0.629
High Temperature Reactor								
(Top)	1	24.0	7.09	0.45	1.70	8.26	20.9	0.770
	2	24.5	8.70	0.51	1.77	8.26	21.4	0.791
(Bottom)	3	23.6	7.77	0.51	1.63	8.26	20.4	0.742

Chang (1982) reported rapid initial coke deposition on a Ni-Mo-Al_2O_3 catalyst while processing a coal-derived liquid. Figure 11 presents the coke data reported by Chang (1982); regression lines have been drawn to represent the deactivation trend. Note that the two regression lines intersect at approximately fifty to sixty hours of oil-catalyst contact, which may represent the rapid coke content deposition equilibrium attainment time.

The catalyst coke content did not show a strong dependence on process temperature; comparison of the coke content of the catalyst samples from the high temperature (400°C) and low temperature (260°C) reactors revealed the high temperature reactor catalyst to have only 4.7 wt.% more coke than the low temperature reactor catalyst. The coke deposited on the catalyst in the high temperature reactor (400°C) of Run ZBI was approximately equal to the coke deposited on the catalyst from Run ZBG, conducted under similar process conditions. These results point out that the catalyst coke content is not affected by mild hydrotreating of the feedstock prior to actual hydrotreating.

Literature regarding the dependence of coke content on temperature for hydrotreating and cracking catalysts is very scarce. Voorhies (1945) reported coke content on cracking catalyst to increase with increase in process temperature. Ternan et al. (1979) reported coke content on hydroliquefaction catalyst to generally increase with temperature, except in the temperature range of 375 to 440°C, where the coke content remained constant. The lack of coke data as a function of process temperature suggests a strong need for such a study.

Coke deposition on hydrotreating catalyst does not always result

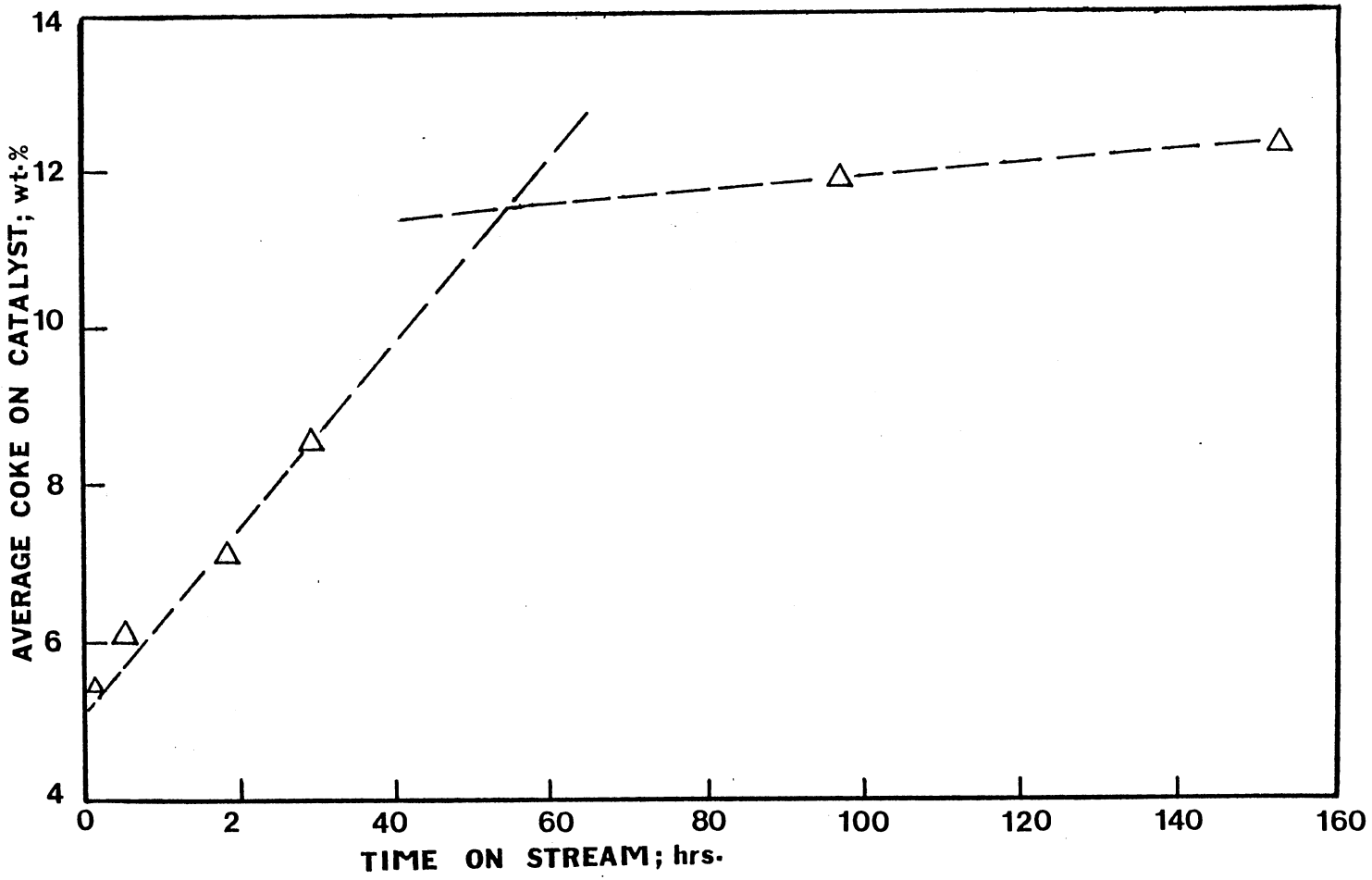

Figure 11. Average Reactor Coke Content vs. Time on Stream

in catalyst deactivation. Chang (1982) reported negligible catalyst deactivation while processing an Exxon Donor Solvent (EDS) Process liquid; 12.5 wt% coke was deposited on the catalyst. When an SRC liquid was used under similar conditions, substantial catalyst deactivation occurred(the catalyst coke content remained at approximately 12.3 wt%). For both these feedstocks, the catalyst suffered substantial decrease in pore volume and pore diameter. Bhan (1981) reported negligible HDN activity decay for a Ni-Mo-Al_2O_3 catalyst while processing an SRC Process Solvent; coke deposits as high as 30 wt% were reported. Both EDS liquid and SRC Process Solvent, used in the above studies contained high hydrogen content (>7.5 wt%), and negligible ash. The SRC Process Solvent contained 7.7 wt% n-pentane insoluble content, which is approximately one-third the n-pentane insoluble content of the feedstock used during the present study.

Coke deposits on hydrotreating catalysts, processing liquids (petroleum and coal liquids) with negligible asphaltene content have also been reported. Beuther and Schmid (1963) reported very little difference in coke content for catalysts processing vacuum reduced crudes and their deasphalted counterparts. Pazos et al. (1981), too, reported coke deposition to be independent of the asphaltene content of the feedstock (petroleum residua). Logically then, asphaltenes alone are not responsible for catalyst carbonaceous deposition, theoretically all hydrocarbons are susceptible to coke formation, however, some compounds (heterocyclic) are kinetically and thermodynamically more favored than others.

The section on catalyst coke deposition can be summarized as follows:

1. Substantial carbonaceous residues were deposited on the catalyst during hydrotreatment.

2. The coke content of the large pore diameter catalyst bed was observed to decrease from reactor inlet to outlet; the coke profile for the small pore diameter was exactly reverse.

3. Both on basis of catalyst mass and surface area, the large pore diameter catalyst deposited more coke; the coke deposited on the large pore catalyst (surface area basis) was twice as high as deposited on the small pore diameter catalyst.

4. No improvement in the amount of coke deposited on the catalyst in the composite bed was observed. The coke data were consistent with those observed for the single catalyst beds.

5. Even at temperatures as low as 260°C, considerable amount of coke was deposited on the catalyst (16.01 wt%).

6. The catalyst coke content did not show a strong dependence on the oil-catalyst contact time.

Catalyst Residue Elemental Analysis

All aged catalyst samples were analyzed in a Perkin-Elmer 240B elemental analyzer for nitrogen, carbon, and hydrogen content. The elemental analysis provided an insight into the nature of the residues deposited on catalysts. Nitrogen and carbon analyzed on the aged catalyst samples, had its origin in the residues deposited on the catalyst; hydrogen analyzed was contributed by the catalyst support (OH^- radical), and the catalyst residues.

Fresh small pore diameter catalyst (KF-153 S) contained approximately 1.3 wt% hydrogen; large pore catalyst (HT-115 E) contained

appreciably lower hydrogen content; 0.45 wt%. Fresh catalyst samples were calcined and evacuated prior to their elemental analysis; all the water adsorbed on the catalyst is removed during calcination, only water chemically bound to the catalyst support (OH^- radical) remains in the catalyst. The high combustion temperature of the Perkin-Elmer 240B analyzer (900°C) removes the chemically bound water, thereby contributing to the overall catalyst hydrogen signal strength. Correction for the hydrogen content of the fresh catalysts was made (see Appendix D) for all catalyst samples analyzed. Both the total, and the corrected hydrogen content, detected on the catalyst have been reported in this study.

The atomic ratios, as determined by the elemental analysis of the residues, have been invaluable in identifying the type of chemical species deposited on the catalyst. Table XI presents the used catalyst sample elemental analysis for all experimental runs conducted; catalyst samples from the top, middle, and the bottom sections of the reactor were analyzed.

For the experimental Run ZBF (large pore catalyst), the average nitrogen content of the aged catalyst was approximately 0.34 wt%. The elemental carbon content increased uniformly from 9.12 wt% in the top reactor section to 10.45 wt% in the bottom section. This corresponded to an average N/C atomic ratio of approximately 0.029.

Greater nitrogen concentration was noticed in the small pore diameter catalyst (0.41 wt%), compared to the large pore diameter catalyst. The carbon content of the aged small pore diameter catalyst (Run ZBG), decreased from 9.62 wt% in the top section to 7.82 wt% in the bottom section. The N/C atomic ratios on the small pore diameter catalysts

TABLE XI

AGED CATALYST SAMPLE ELEMENTAL ANALYSIS

Sample Number	Wt.% N	Wt.% C	Wt.% H	Total Wt.% H	N/C	H/C
Run ZBF						
Top	0.334	9.122	1.169	1.631	0.0320	0.988
Middle	0.340	9.697	1.274	1.770	0.0288	1.072
Bottom	0.347	10.450	1.035	1.519	0.0275	0.943
Run ZBG						
Top	0.425	9.616	0.775	2.031	0.0410	0.845
Middle	0.413	8.956	0.860	2.174	0.0411	0.940
Bottom	0.397	7.823	0.794	2.065	0.0439	0.943
Run ZBH - Top Reactor						
Top	0.425	7.328	0.374	1.676	0.0495	0.607
Middle	0.400	7.843	0.258	1.594	0.0431	0.494
Bottom	0.391	8.310	0.344	1.607	0.0450	0.594
Bottom Reactor						
Top	0.384	9.012	0.855	1.256	0.0367	1.033
Middle	0.398	9.125	0.641	1.091	0.0374	0.843
Bottom	0.441	9.601	0.735	1.266	0.0394	1.015
Run ZBI - Low Temperature Reactor						
Top	0.614	8.425	0.394	1.665	0.0643	0.575
Middle	0.672	8.041	0.369	1.697	0.0723	0.558
Bottom	0.667	8.239	0.529	1.807	0.0734	0.762
High Temperature Reactor						
Top	0.447	7.093	0.404	1.696	0.0540	0.674
Middle	0.511	8.696	0.480	1.770	0.0508	0.652
Bottom	0.513	7.774	0.334	1.633	0.0572	0.514

were consistently higher than for the large pore diameter catalyst, 0.042 atomic ratio for small pore diameter catalyst compared to 0.029 for the large pore diameter catalyst.

The larger deposition of nitrogen on the small pore diameter catalyst compared to the large pore diameter catalyst can be explained on the basis of the higher surface area of the small pore diameter catalysts. Larger surface area results in more active sites (acid sites) being present per unit weight of the catalyst. Assuming adsorption of basic nitrogen species to occur on catalyst active acid sites, the nitrogen deposition would increase with increase in catalyst surface area.

The total hydrogen signal from the large pore diameter catalyst (Run ZBF) corresponded to approximately 1.64 wt% hydrogen; after applying the correction for fresh catalyst hydrogen content, the hydrogen content of the residues was determined to be approximately 1.16 wt%. This corresponded to an H/C atomic ratio of slightly greater than one (1.01 H/C atomic ratio). For the small pore diameter catalyst (Run ZBG), the total hydrogen signal strength was considerably higher (2.1 wt%). Fresh small pore diameter catalyst contained approximately three times more hydrogen than the large pore diameter fresh catalyst. Upon correction for the fresh catalyst hydrogen content, the residue hydrogen content on the small pore diameter catalyst was determined to be only 0.8 wt%, which corresponded to an H/C atomic ratio of 0.91.

Several researchers have investigated the nature of deposits on hydrotreating catalysts. Furimsky (1982) reported deposition of polyaromatic structures containing high N and O content on the catalyst

surface. An N/C atomic ratio of 0.071 was reported for a pyridine washed, aged, coal liquid hydrotreating catalyst. Stiegel et al. (1983) reported the carbon content of a coal liquid hydrotreating catalyst (Ni-Mo-Al_2O_3) to increase with time on stream; H/C atomic ratios in the range of 1.42 to 0.99 were reported. Wukash and Rase (1982) identified the presence of N and H atoms in the carbonaceous residues deposited on a petroleum residua hydroprocessing catalyst. In a recent paper, Gutberlet and Bertolacini (1983) reported the adsorbtion of nitrogen containing heterocyclic compounds on hydrotreating catalysts to occur through the nitrogen heteroatom (pyridine). The adsorption was considerably inhibited for the compounds where the ring nitrogen was bound to a methyl group (alkylpyridines), implying the major role the heteroatoms play in catalyst deactivation. From the elemental analysis of catalyst residues, it can be concluded that catalyst residues are low in hydrogen and high in heteroatom content, the heteroatoms (N, C) form the link between the condensed molecules and the catalyst active sites.

The effect of temperature on the nature of the catalyst deposits can be observed from the analysis of the catalysts from Run ZBI. For a temperature increase from 260 to 400°C, the nitrogen content of the catalyst residues decreased on an average from 0.65 wt% to 0.49 wt%. A similar decrease in the average nitrogen content of the residues was reported by Bhan (1981) for a Ni-Mo-Al_2O_3 (HDN-30) catalyst. For a temperature increase from 325 to 435°C, the average nitrogen content of the residues was reported to decrease from 0.73 wt% to 0.35 wt%, a 50% decrease.

The higher nitrogen content of the catalyst residues at lower temperatures can be hypothesized to occur as follows: the polyaromatic species that deposit on the catalyst surface contain significant fractions of heteroatoms, the percentage of the heteroatoms increases with increase in the molecular weight of the fractions. At lower operating temperatures (260°C), only the lower molecular weight species can be expected to be hydrogenated by the catalyst active species, the higher molecular weight species containing the higher heteroatom content remain on the catalyst surface, and contribute to the higher nitrogen content. At higher operating temperatures (400°C), larger fractions of the heavy polyaromatics are removed from the catalyst surface due to the higher hydrogenation activity of the catalyst at that temperature, resulting in lesser nitrogen content.

During this study, an interesting experiment was conducted to investigate the phenomenon of catalyst residue deposition. Five grams each of the large, and the small pore diameter catalysts were separately mixed with the feedstock, equivalent to three times the pore volume of the catalyst. Four such samples were prepared, one pair (large and small pore catalyst) was maintained at 100°C, the other pair was held at room temperature. The samples were mixed every half-hour for the first two hours and subsequently allowed to stand for 24 hours.

The catalyst samples were extracted with n-pentane for a period of 24 hours. Some of the catalyst samples were removed and evacuated overnight at 125°C. The remaining catalyst pellets were Soxhlet extracted with THF for 24 hours and vacuum dried overnight. Both sets of catalysts samples were analyzed for their elemental content.

Surprisingly, even at room temperature, the catalysts deposited

residues, which could not be removed by THF extraction. The deposited species seem to adsorb irreversibly on the catalyst surface even at room temperatures.

Table XII presents the elemental analysis of the n-pentane and THF extracted samples. Note that the n-pentane extracted catalyst samples contained approximately 10-14 wt% carbon. The N/C and H/C ratio of the residues revealed their origin to be in the n-pentane insoluble fraction of the feedstock. Soxhlet extraction of catalyst samples with THF did not completely remove the deposited residues. The THF washed large pore diameter catalyst (100°C) contained approximately 7.6 wt% carbon, compared to only 3.4 wt% carbon determined on the same catalyst at room temperature.

The THF washed,small pore diameter catalyst deposited approximately half the amount of carbon as that on the large pore diameter catalyst. For both catalysts, the carbon content increased two-fold for a temperature increase from 27°C to 100°C. Greater carbon content on the large pore diameter catalyst can result due to the larger pore volume capacity (0.69 cm^3/gm vs. 0.48 cm^3/gm) of the large pore diameter catalyst. The higher deposition at higher temperatures can be attributed to the following:

1. Change in the liquid intermolecular forces at higher temperatures.

2. Higher temperature results in lower viscosity and higher diffusivity, leading to greater contact between the catalyst and the liquid. Note that the feedstock was highly viscous at room temperature.

From this non-reactive catalyst contact experiment, evidently carbonaceous deposits start forming on the catalyst the moment oil

TABLE XII

CATALYST ELEMENTAL ANALYSIS (24 HOURS OF CATALYST-FEEDSTOCK CONTACT)

Catalyst	Temp. °C	Total Residues	Wt.% N	Wt.% C	Corrected* Wt.% H	Total Wt.% H	N/C	H/C
n-Pentane Insolubles								
HT-115 E	27	13.76	0.52	12.43	0.81	1.26	0.035	0.751
HT-115 E	100	15.96	0.70	14.15	1.11	1.59	0.043	0.946
KF-153 S	27	10.95	0.46	10.26	0.23	1.50	0.039	0.274
KF-153 S	100	11.85	0.57	10.81	0.47	1.69	0.046	0.506
THF Insolubles								
HT-115 E	27	3.61	0.91	3.42	0.0	0.43	0.047	0.000
HT-115 E	100	8.26	0.30	7.58	0.38	0.84	0.034	0.600
KF-153 S	27	1.71	0.08	1.63	0.0	1.11	0.044	0.000
KF-153 S	100	3.96	0.19	3.77	0.0	1.11	0.043	0.000

* Corrected for hydrogen content of fresh catalyst.

contacts the catalyst. These deposits consist of polyaromatic compounds, high in heteroatom (N, O) content. At hydrotreatment process conditions (high temperature and high hydrogen partial pressure), the deposits are continuously hydrogenated. The hydrogenated deposits vaporize and new deposits form on the catalyst; this process occurs continuously on the catalyst surface. Those deposits, which cannot be easily hydrogenated, deposit on the catalyst permanently and deactivate the catalyst.

Nitrogen containing species identified in the coal-derived liquids are of two types, acidic and basic (Schultz, et al., 1977). Basic nitrogen species have a greater tendency to deposit on the catalyst active sites; this was experimentally confirmed by a simple experiment conducted during this study. Catalysts (small pore and large pore) were soaked in solutions of quinoline (basic), and carbazole (acidic) in benzene. A control sample was also soaked in pure benzene. The quinoline and carbazole solutions of approximately the same nitrogen strength as the feedstock were prepared; carbazole had to be dissolved in hot benzene. The catalysts and solutions were mixed thoroughly and allowed to equilibrate for 24 hours. The catalyst samples were Soxhlet extracted for 24 hours with THF, a blank catalyst sample was also extracted for comparison.

The extracted catalyst samples were evacuated overnight at 100°C. The elemental analysis of the catalyst samples provided some very interesting results. Nitrogen was detected only on the quinoline (basic) soaked catalyst sample. The quinoline soaked catalyst sample contained approximately 0.05 wt% N. Surprisingly, vacuum evacuation at 100°C could not remove the quinoline from the catalyst surface; the

quinoline seems to chemisorb on the catalyst surface. Furmisky (1982) reported considerable difficulty in removing pyridine, used for catalyst extraction, from the catalyst surface. Cable and Massoth (1981) reported adsorption of naphthalene on the catalyst acid sites, upon poisoning of the catalyst acid sites, no naphthalene adsorption occurred. Recently Fu and Schaffer (1983) reported strong poisoning of cracking catalysts by nitrogen containing compounds. Substitution of the nitrogen by a carbon in the aromatic ring (two or more rings) decreased the poisoning effect; it was also demonstrated that multi-ring nitrogen aromatic bases like quinoline are considerably more potent catalyst poisons than single ring heteroatoms (pyridine). Clearly the basic nitrogen compounds (nitrogen compounds being stronger bases compared to the other heteroatoms present in the feedstock) are preferentially adsorbed on the acid sites (metal sites MoS_2 and acid sites on the alumina base), and interact by transferring the unpaired electrons (the Bronsted acid site on the catalyst surface accepting the unpaired electrons in the bases).

The chemical route to species formation was first experimentally verified by Beguin and Setton (1972). They observed the formation of perylene, pyrene, and coronene to occur due to the coupling of the molecules at temperatures markedly lower than those used for commercial hydrotreating. Furimsky (1982) confirmed the presence of heavy polyaromatic molecules on coal liquid hydrotreating catalysts. Furimsky (1982) hypothesized the coupling reactions to be initiated by the Bronsted acid sites; aromatic structures being high in proton affinity dimerize after protonation to form deposits.

Flockhart et al. (1980) experimentally demonstrated the formation of perylene cations on catalytic alumina, the formation was prevented upon poisoning of the alumina surface by nitrogen bases. Phenol, too, has been reported to form polyaromatic structures at high temperatures and hydrogen deficient conditions (Cypres and Bettens; 1974, 1975). Catalyst deposits form from condensation of polyaromatic compounds present in the feedstock, the nitrogen and oxygen containing compounds being more susceptible to coke formation due to their polar nature.

Although the corrected hydrogen content of the carbonaceous residues is only approximate, still it demonstrates that the catalyst internal deposits contain relatively higher hydrogen content compared to analogous chemical species (same N and C content). The deposits are partially hydrogenated, hydrogenation makes the deposited species more volatile, and hence, cleans the catalyst surface. Furimsky (1982) reported partially hydrogenated rings in the catalyst residues by GC/MS techniques. Greater catalyst hydrogenation capacity would result in lower carbonaceous deposits due to greater cleaning activity. The carbonaceous deposition on the catalyst can be viewed as a dynamic process; multi-ring compounds deposit on the catalyst, are hydrogenated and subsequently vaporize from the surface, whereas new species are adsorbed on clean active sites. Loss in hydrogenation activity can result due to irreversible carbonaceous deposition, leading to the inaccessible active catalyst sites. The loss in catalyst activity can also occur due to metal deposition and sintering in addition to the refractory carbonaceous deposition.

This section on catalyst residue elemental analysis can be summarized as follows:

1. The elemental analysis of the carbonaceous catalyst deposits revealed the deposits to be composed of C, H, N and sulfur. The deposits contained high nitrogen concentration; the small pore diameter catalyst deposits contained higher nitrogen content than the large pore diameter catalyst. The hydrogen content of the residues was low, pointing to the polynuclear condensed molecular structure of the residues.

2. The nitrogen content of the catalyst residues decreased with the increase in process temperature.

3. The catalysts deposited residues even when contacted with the feedstock at low temperatures (27-100°C). These residues could not be removed even after Soxhlet extracting with THF after 24 hours.

4. Basic nitrogen containing species (quinoline) were irreversibly adsorbed on the fresh catalyst surface, and could not be removed even after extensive extraction with THF. No such adsorption was observed for the acidic nitrogen species (carbazole) and a reference aromatic, benzene.

Metal Deposition

Coked catalyst samples were analyzed for metal content by Energy Dispersive X-ray Analysis (EDAX) in a Scanning Electron Microscope (SEM). For all catalyst samples analyzed during this study, the catalyst surface was covered by a crust of residue matter high in metal content. Relatively low alumina count on the catalyst surface revealed the formation of this crust.

Atoms identified in the crust, according to their order of abundance were, Fe, S, Si, Ti, Al, Ca, K, Cr and Cu. The area fraction of

of sulfur and molybdenum could not be independently determined due to their close emission spectral energies, 2.321 keV.

Iron existed in the crust as a sulfide, and probably had its origin in the ash fraction. The external crust deposited on the catalyst pellet surface extended to a variable thickness (0-20 μm). The metals seemed to be embedded on the catalyst surface, polynuclear carbonaceous materials probably play the role of a gluing agent. The presence of Ni and Mo in the catalyst residue crust signified either the migration of the active metal species, which might have also occurred due to the extensive extraction of the catalyst samples with THF, or the presence of large fissures in the catalyst crust.

The surface deposits on the catalyst pellet were determined by taking overall scans at x1000 magnification. Although the EDAX analysis data are only semi-quantitative, still they are useful in determining the type of metals deposited. The concentration of surface metals by EDAX analysis is determined as area fraction of the metals present; the area fraction represents the count intensity of a particular element. Catalyst samples were selected at random from the top, middle, and the bottom reactor sections, and analyzed for deposited metals.

The deposits noticed on the catalyst periphery occurred in patches, the crust had grown to a thickness greater than 20 μm at some places, and hardly existed at others. Relatively low aluminum count on the catalyst surface revealed the crust to extend over the entire catalyst surface, its thickness varying from point to point. Figure 12 presents the SEM picture of the radial section of a catalyst pellet from Run ZBF (x1000 magnification). The crust extending on the catalyst surface

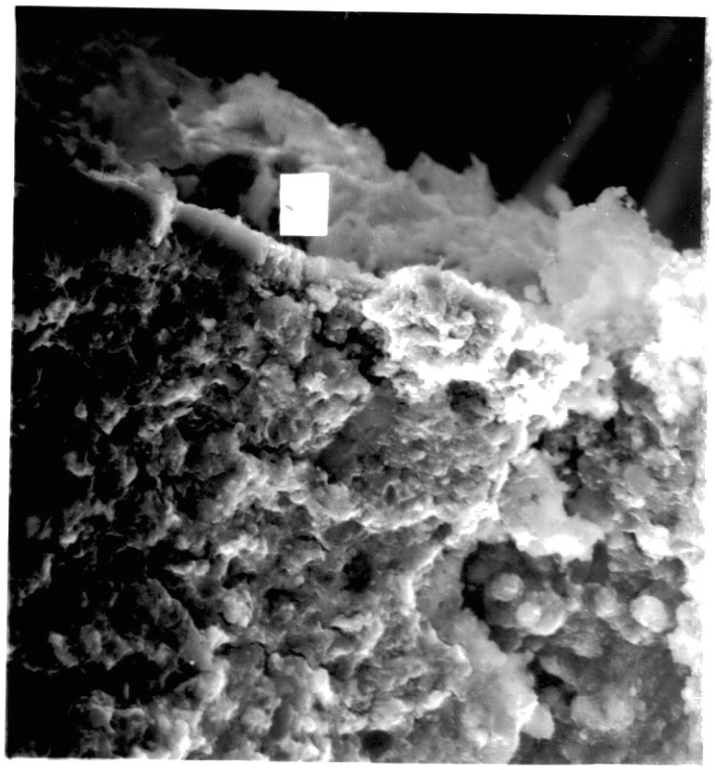

Figure 12. Scanning Electron Picture of Aged Catalyst Pellet at x1000 Magnification (Run ZBF).

can be clearly noticed, the white dot on the crust represents the area fraction on which EDAX scan was taken.

The surface EDAX analysis of the catalysts from experimental Runs ZBF, ZBG and ZBH revealed a low alumninum and high Fe, Si, and S count. Appreciable Ti content was noticed on the catalyst surface, signifying thermal dissociation and subsequent deposition of large organometallic complexes on the catalyst surface. No significant difference in the metal content of the crust was noticed along the reactor length for these experimental runs.

The catalyst pellets from the low temperature reactor (260°C, Run ZBI), too, were noticed to be covered by a metal crust, consisting primarily of Fe, S and Si. The surface of the high temperature catalyst from Run ZBI contained appreciably lower metal content. The Fe content in the catalyst crust decreased from an average of 24.1 area %, on the surface of the low temperature catalyst, to 5.4 area % on the high temperature catalyst; a reduction in the Si content was also noticed.

Formation of the iron crust over the catalyst surface can seriously impede the transport of large molecular species into the catalyst interior. The diffusional resistance offered by the crust will, however, depend on the porosity of the deposits, and also the extent of the fissures present in the catalyst crust. Sivasubramanian et al. (1980) noticed large cracks of 1-5 μm size present on the catalyst crust. Stanulonis et al. (1976) noticed a 0-90 μm thick inorganic crust deposited on a catalyst used for primary coal liquefaction; these deposits covered over 50 to 70% of the catalyst surface.

During this study, some selected catalyst samples were fractured radially, and analyzed for inside metal deposition by taking electron scans at different radial positions. For each catalyst pellet, four radial sections were analyzed: 10 μm, 60 μm, 120 μm inside the catalyst pellet, and the catalyst center. For each radial position, three scans were taken at different positions and the values averaged. The results were always analyzed for consistency before the next radial position was analyzed. The metal depositions inside the catalyst were very heterogeneous; titanium deposits usually occurred in clusters. Focusing of the electron beam on such deposits was avoided. Kang and Johnson (1976) also reported Ti to be present in clusters on a coal liquefaction catalyst.

For the large pore diameter catalyst (Run ZBF), the iron concentration decreased rapidly towards the pellet center for all positions along the reactor length. Negligible Ti and Fe concentration existed in the catalyst center. The metal deposition seemed to occur predominantly in the catalyst periphery. Even at radial distances as low as 60 μm, considerable decrease in metal concentration occurred. At approximately 200 μm inside the catalyst pellet, negligible metal deposition existed. The metals deposited in the catalyst periphery probably plug the catalyst pores, thereby, making the catalyst interior inaccessible to the metal-bearing molecules.

The metal concentration profiles for the small pore diameter catalysts were similar to the large pore diameter catalysts. Figure 13 and 14 present the Fe, Ti and Si profiles in the catalyst interior for the large and the small pore diameter catalysts, respectively.

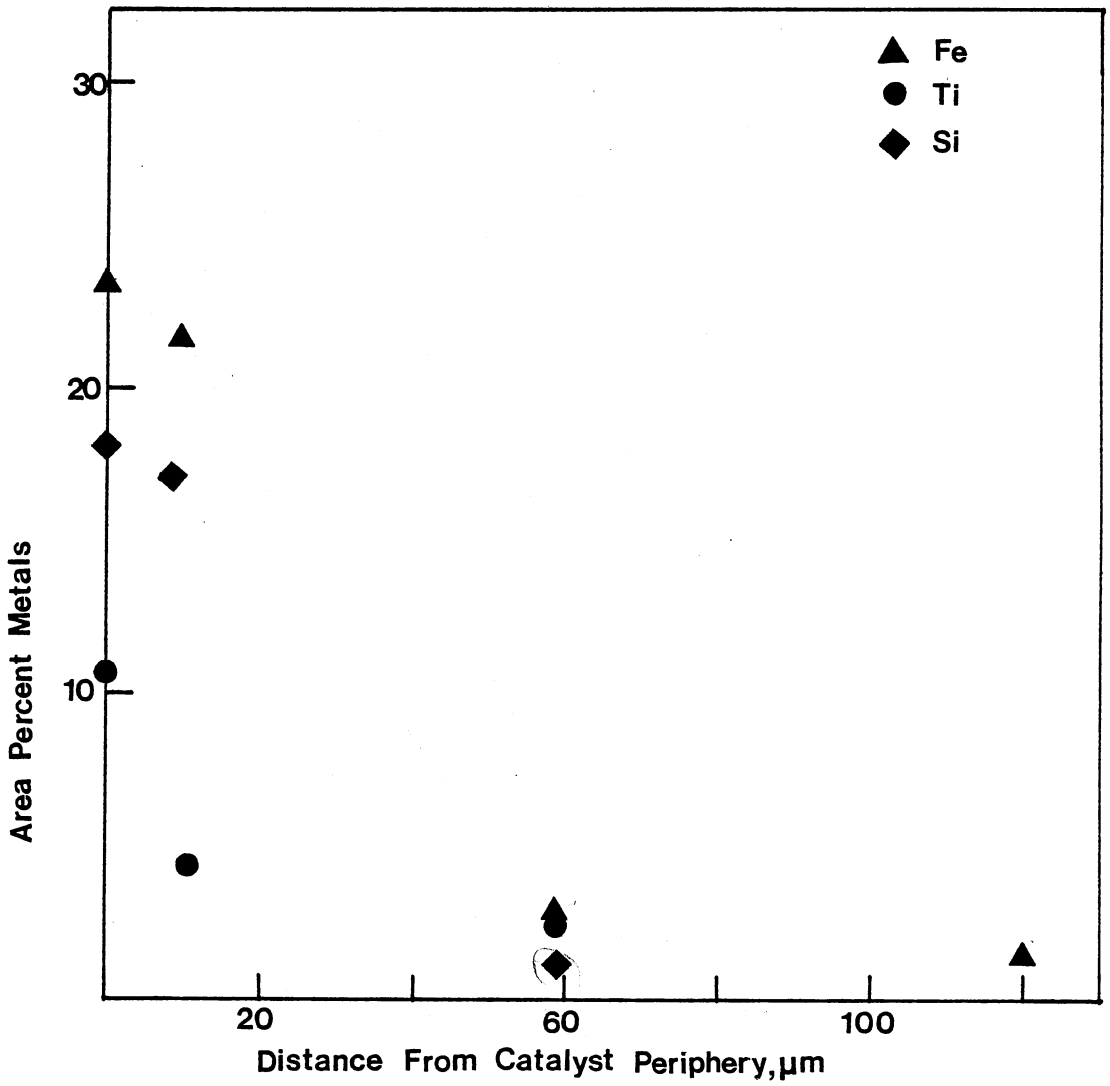

Figure 13. Fe, Ti, and Si Radial Profiles, Run ZBF

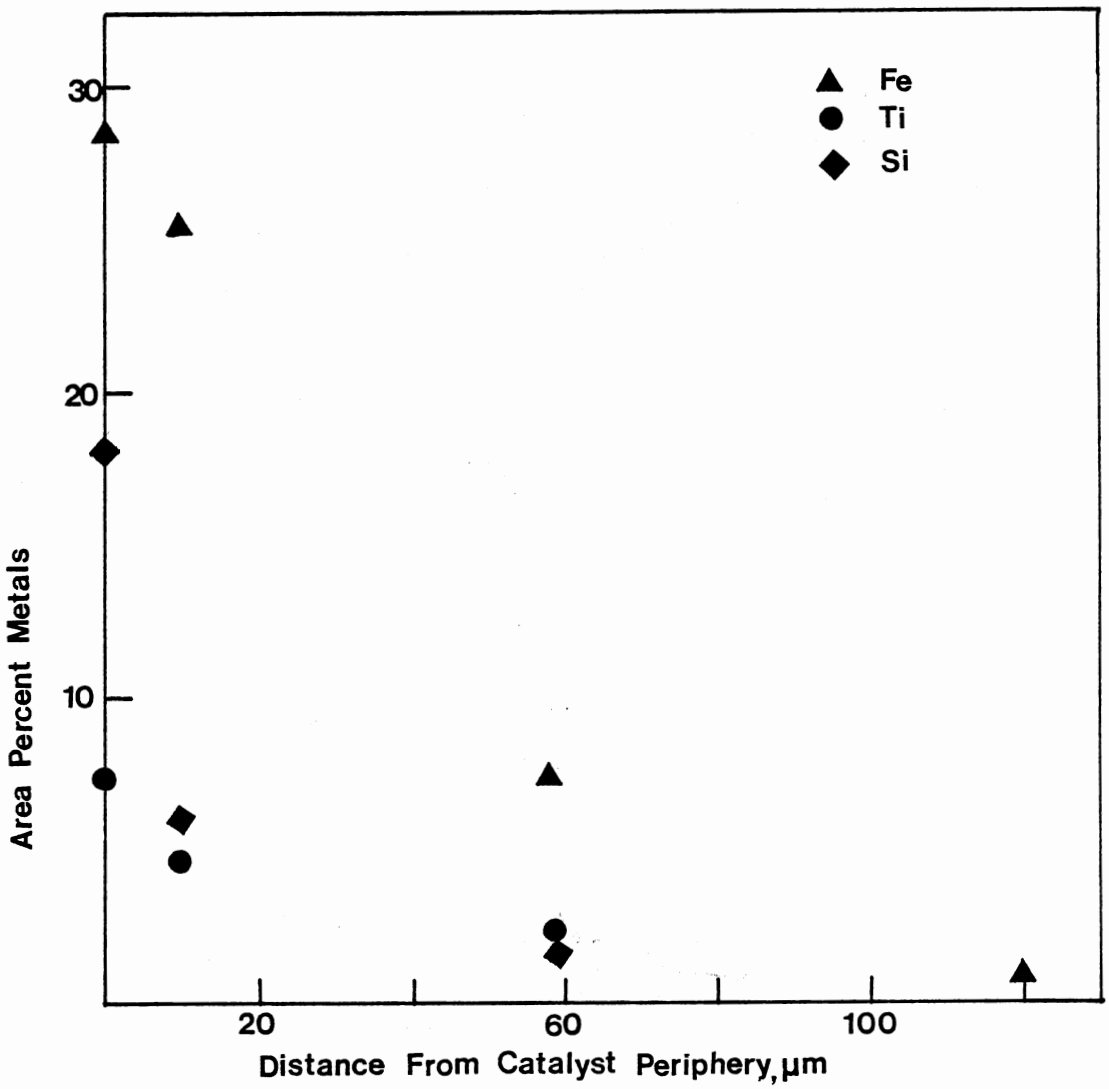

Figure 14. Fe, Ti, Si Radial Profiles, Run ZBG

No relationship, however, was noticed between the catalyst metal content and the catalyst axial reactor position. The catalysts from Run ZBH (composite bed) showed a similar trend for metal deposition. The tabulated results from the metal analysis of the catalysts from Run ZBF, ZBG and ZBH are presented in Appendix I.

For the catalyst samples from the low temperature reactor bed (Run ZBI), negligible Ti was noticed to be deposited in the catalyst interior. This might have occurred due to the organometallic origin of titanium present in coal-derived liquids; at the low operating temperature of the reactor, negligible hydrodemetallation reactions are expected to occur. Unlike Ti, Fe was noticed to be deposited in the pellet interior. Both Fe and Ti were noticed to be deposited inside the catalyst for the high temperature reactor, although to a much lower extent compared to the catalysts from Run ZBG. Figure 15 presents the Fe, Ti and Si profiles in the catalyst interior for the low and the high temperature catalyst pellets (Run ZBI).

No significant difference was observed in the metal deposition profiles for the small and large pore diameter catalysts. For both catalysts, only the catalyst periphery deposited metals (20% of the catalyst radius). The ash constituents were effectively screened and deposited on the catalyst crust for both the small, and large pore diameter catalysts. Surprisingly, even for a four-fold increase in catalyst pore diameter, no significant difference in the metal deposition profiles was noticed for the two catalysts. Various reasons can be attributed to this phenomenon: the EDAX data are only semi-quantitative and thus cannot be effectively used for comparing the metal deposition profiles; the organometallic

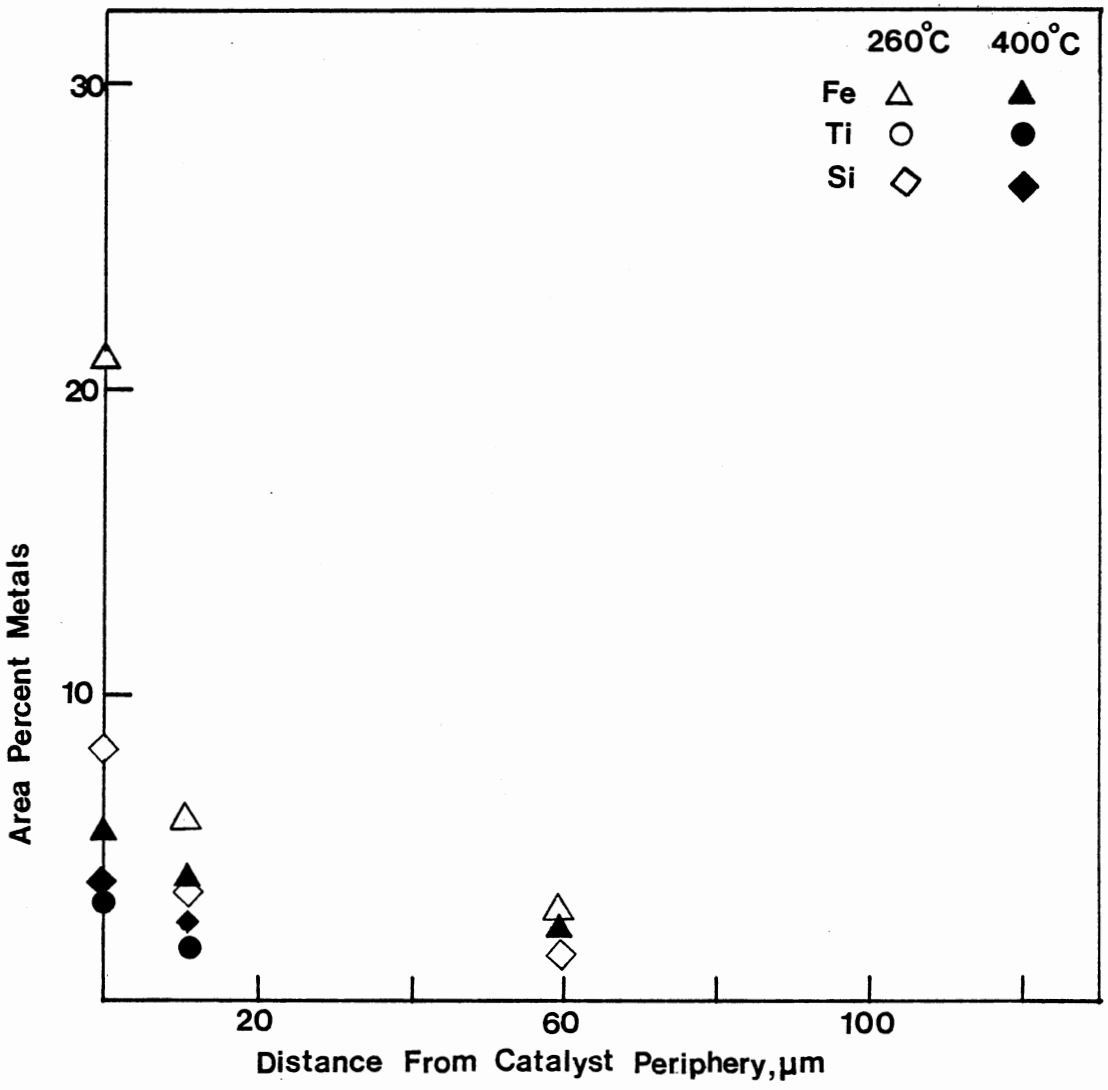

Figure 15. Fe, Ti, and Si Radial Profiles, Run ZBI

molecules depositing in the catalyst periphery may seriously impede the movement of the metal-bearing molecules into the catalyst interior for both catalysts.

Similar results for coal-derived liquids have been reported by Berry et al. (1977), metal deposition was reported to occur up to 300 μm inside the catalyst interior. Ash constituents were reported to be deposited on the catalyst periphery only. Cable and Massoth (1981) also reported metal deposition to occur within 100-200 μm of the catalyst surface for the H-Coal liquefaction catalyst.

This section on catalyst metal deposition can be summarized as follows:

1. All catalysts used in this study had a uniform crust deposited over their external surface. This crust was identified by energy dispersive X-ray analysis to consist primarily of Fe, Si and S. The crust thickness varied over the catalyst surface.

2. For the two temperature reactor zonal bed experiment, catalyst pellets from the low temperature reactor had a uniform inorganic crust deposited on them. This crust was absent for the catalysts from the high temperature reactor bed, which could have resulted due to complete removal of the inorganic constituents of the feedstock in the low temperature reactor zone.

3. The radial EDAX metal analysis within the catalyst pellet revealed gradation in metal deposition; the deposition occurred primarily in the catalyst periphery. Fe and Ti were the predominant metals deposited and had their origin in the oil-soluble and the particulate fraction of the feedstock.

4. No significant difference in the radial metal deposition profiles was observed between the large and the small pore diameter catalysts.

5. For the low temperature reactor experiment, negligible metals were noticed to the deposited inside the catalyst. Some Fe deposition occurred, but Ti metal was totally absent; indicating the hydrodemetallation reactions to occur at high process temperatures only.

Reactor Interstitial Deposits

Catalytic hydroprocessing of coal-derived liquids in fixed-bed reactors suffers from severe bed-plugging problems, which often cause premature reactor shutdown. A processing technique must be developed whereby catalyst bed-plugging in fixed-bed reactors is completely eliminated. One of the objectives of this study was to develop the concept of composite catalyst beds to reduce the incidence of catalyst bed-plugging.

For experimental Run ZBF (large pore catalyst), conducted for 240 hours, no bed-plugging problems were encountered during the first 210 hours of oil-catalyst contact, considerable pressure fluctuations, however, occurred in the last 20-40 hours of the experimental run. The shutdown was scheduled. The reactor was cooled under hydrogen pressure, and subsequently divided into six sections. The catalyst pellets in the top two sections were cemented together by a black residue, and had to be carefully chipped to remove the catalysts intact.

After Soxhlet extraction of the catalysts with tetrahydrofuran (THF), and subsequent vacuum drying, the residue fractions were removed by screening through a twenty-mesh size screen. The residues from each

section were weighed and analyzed for elemental content. The ash content of the residues was also determined. The metal constituents in ash were analyzed by energy dispersive X-ray analysis (EDAX) in a scanning electron microscope (SEM).

The amount of residues deposited, and the elemental analysis of the residues, for Run ZBF are presented in TableXIII. A total of 7.39 gms of residues were deposited in the interstices of the reactor. Note that the residues were washed with THF and were free of any adsorbed oil. The reactor interstitial deposit amount decreased from the top to the bottom section of the reactor; 1.96 gms of residues were deposited in the top glass bead section, compared to only 0.36 gms deposited in the bottom glass bead section.

High concentrations of Fe, S, Si and K existed in the interstitial deposits, traces of Ca, Al, and Cu were also present. The deposits consisted mostly of iron and silica. The iron in the residues existed in its sulfided form.

The EDAX analysis of the ash from the feedstock is presented in Chapter VI. Iron, silicon and pottasium present in the feedstock were preferentially deposited in the inlet reactor section. This may have occurred due to the inorganic origin of these elements. Titanium, a predominant metal species in the feedstock, did not deposit in the interstities. Titanium being present mostly in the oil-soluble organometallic complexes deposited inside, rather than outside, the catalyst pellet, signifying hydrodemetallation reactions to occur only in presence of catalysts.

Analysis of the residues revealed a high ash content; 72.9 wt% ash was deposited in the top section glass beads. The catalyst section

TABLE XIII

INTERSTITIAL DEPOSITS
(LARGE PORE CATALYST
RUN ZBF)

Sample Number	Weight of Deposits gms	Ash	N	C	H	N/C	H/C
		Wt.%				Atomic Ratio	
Top Glass Beads	1.96	72.9	0.75	28.22	1.41	0.023	0.60
(Top) 1	1.57	80.75	0.44	13.21	0.70	0.028	0.63
2	0.81	NA	0.30	12.76	0.93	0.021	0.87
3	0.26	NA	0.26	11.28	0.84	0.020	0.89
4	0.73	78.9	0.34	13.27	1.12	0.022	1.01
5	0.59	78.2	0.28	12.25	1.11	0.020	1.08
(Bottom) 6	1.13	NA	0.29	13.84	1.05	0.018	0.91
Bottom Glass Beads	0.36	NA	0.93	29.12	1.92	0.027	0.79
Total Residues	7.39						

interstitial residues contained higher ash content, approximately 78 to 80 wt% compared to 73 wt% in the glass beads section. The higher ash content of the interstitial residues in the catalyst bed occurs due to attrition during catalyst removal.

The elemental analysis of the interstitial residues revealed a low H/C atomic ratio. The H/C atomic ratio varied from 0.6 to 1.08; the H/C atomic ratio of the feedstock was approximately 1.0. The interstitial residue deposits can be hypothesized to have formed either due to the thermal cracking and subsequent condensation of the cracked species, or directly from the deposition of the THF insoluble fractions originally present in the feedstock. Examination of the H/C atomic ratio of the external residues revealed their H/C ratio to be lower than that of the THF insolubles present in the feed. During the 240 hours of oil-catalyst contact, an average of 75 grams of THF insolubles were processed. Analysis of the product liquid samples revealed negligible THF insoluble content. The THF insolubles get converted to preasphaltenes, asphaltenes, resins, and oils during hydrotreatment. The interstitial residues could have formed from the most refractory of the THF insoluble fractions contained in the feedstock. It is, however, difficult to say with certainty which of these two mechanisms is responsible for the interstitial deposition in the reactor bed.

The interstitial deposits contained high ash content. The feedstock contained approximately 0.1 wt% ash. For the 240 hours of oil-catalyst contact, a total of 7.2 gmsof ash is estimated to have passed through the reactor. Assuming 75 wt% ash content of the interstitial residues, 5.6 gms of ash contained in the feedstock can be accounted.

Some of the inorganics deposited on the glass-beads and the catalyst pellets may constitute the remaining fraction. Thus all the ash, contained in the feedstock, is removed and deposited in the catalytic reactor (product liquid samples contained no ash).

The glass beads in the top and the bottom sections of the reactor had a uniform layer of inorganic material deposited on their surface. Figure 16 is a picture of the glass beads from the top and the bottom sections of the reactor; a fresh, clean, glass bead is also shown for comparison. The top section glass beads suffered a two-fold increase in size due to the residue deposition. EDAX analysis of the glass beads revealed large quantities of iron, silica, and pottasium deposited on their surface. Table XIV presents the surface EDAX metal analysis of the top and the bottom section glass beads at x1000 magnification. Note that pottasium, iron and, silicon get preferentially deposited on the glass bead surface, and can be hypothesized to be glued to the surface of the glass beads by polynuclear aromatic compounds, which are either originally present in the oil, or are formed during hydrotreatment. The pottasium concentration on the glass beads was higher than the pottasium concentration in the interstitial residues (see Table XIV).

For the experimental Run ZBG, conducted with small pore diameter catalyst, similar results were obtained. Approximately 7.2 gms of interstitial residues were deposited in the reactor bed. The composition of the residues was similar to the residues from Run ZBF. The residues contained approximately 78 to 79 wt% ash. On an average, 5.7 gms of ash were deposited in the catalyst interstities. Change in the

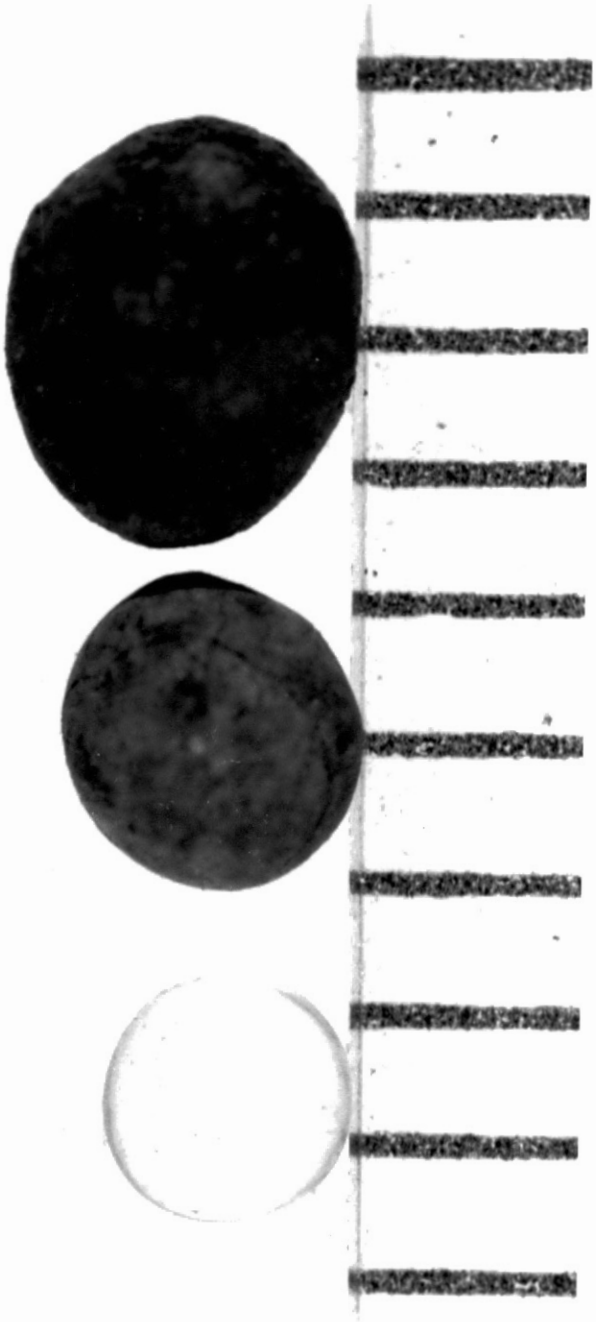

Figure 16. Comparison of Fresh and Aged Glass Beads

TABLE XIV

EDAX AREA SCAN DATA (GLASS BEAD SURFACE)

Metal	Top Glass Beads	Bottom Glass Beads	Interstitial Deposits (Ash)
K	33.1	27.5	18.7
Si	20.6	15.2	29.7
Fe	19.0	29.8	41.7
S	18.1	15.1	--
Cl	7.8	11.4	--
Al	1.4	3.6	3.5

catalyst pore diameter did not affect the quantity of the residues deposited. During this experimental run also, severe reactor plugging occurred during the last 40 hours of oil-catalyst contact. It seems that the top reactor sections (Run ZBF and ZBG) reach the maximum interstitial deposition capacity during the first two hundred hours of oil-catalyst contact; once the maximum capacity is reached, increased pressure drop develops.

The phenomenon of inorganics deposition on the glass bead surface was encountered during Run ZBG also. The glass beads increased in size uniformly; silica, iron, and pottasium being the predominant metal species deposited.

The interstitial residue elemental analysis for Run ZBG (small pore catalyst) is reported in Table XV. The residues contained low carbon and hydrogen concentrations; the H/C and the N/C atomic ratios were similar to the residues from experimental Run ZBF (large pore catalyst). The type of catalyst did not seem to affect the nature of the interstitial residues. This phenomenon can only occur if the interstitial deposits are formed non-catalytically: thermal cracking of the polyaromatics, or deposition of refractory THF insoluble fractions.

Experimental Run ZBH, conducted with two catalysts in combination, behaved exactly like the single catalyst bed (Run ZBF and ZBG). Table XVI presents the amount of deposits, and their elemental analysis. Note that the interstitial deposits decreased uniformly from the top to the bottom section of the reactor, consistent with the other experimental runs. The maximum interstitial deposition occurred in the top glass bead section, where no catalytic activity was present; further confirming our hypothesis of non-catalytic nature of interstitial deposits.

TABLE XV

INTERSTITIAL DEPOSITS
(SMALL PORE CATALYST
RUN ZBG)

Sample Number	Weight of Deposits gms	Ash	N	C	H	N/C	H/C
		Wt%				Atomic Ratio	
Top Glass Beads	1.87	76.3	0.76	23.18	1.64	0.028	0.85
(Top) 1	1.83	79.7	0.32	13.27	0.93	0.021	0.84
2	1.03	NA	0.36	13.38	1.15	0.023	1.03
3	0.53	NA	0.43	12.93	1.58	0.028	1.46
4	0.36	NA	0.49	16.67	1.37	0.025	0.98
5	0.23	NA	0.48	16.78	1.43	0.024	1.02
(Bottom) 6	0.16	NA	0.35	9.942	1.01	0.030	1.22
Bottom Glass Beads	0.27	NA	0.63	27.96	0.89	0.019	0.38
Total Residues	7.28						

TABLE XVI

INTERSTITIAL RESIDUES
(COMPOSITE CATALYST
BED RUN ZBH)

Sample Number	Weight of Deposits gms	Ash	N	C	H	N/C	H/C
		Wt.%				Atomic Ratio	
Top Glass Beads	2.48	76.3	--	--	--	--	--
(Top) 1	2.39	78.9	0.35	13.4	0.87	0.022	0.78
2	1.07	--	--	--	--	--	--
3	0.51	--	--	--	--	--	--
4	0.29	--	--	--	--	--	--
5	0.16	--	0.27	12.8	0.93	0.018	0.87
(Bottom) 6	0.11	--	--	--	--	--	--
Bottom Glass Beads	0.16	--	--	--	--	--	--
Total Residues	7.17						

Experimental Run ZBI provided some interesting results; this run was conducted with two catalytic reactor zones placed in series, each operated at a different temperature. Table XVII presents the amount of resiudes deposited in each reactor zone, and their elemental analysis. The top reactor zone contained essentially all the residues deposited, 3.19 gms,compared to 0.32 gms deposited in the bottom reactor section. Interestingly, the residue deposition occurred uniformly with the time on stream. Experimental Run ZBI was conducted for 120 hours, exactly half the duration of the other experimental runs, the residues deposited in Run ZBI (3.51 gms) were also approximately half of that deposited in the other experimental runs (7.3 gms).

Experimental Run ZBI revealed that guard bed reactors can be operated at substantially lower temperatures compared to the temperature of the hydrotreating reactor. The inorganic species tend to separate out at relatively low temperatures. Lower temperatures in the guard bed can result in substantial savings in the reactor vessel costs. Standard Oil Company of Ohio (Robinson and Evin, 1982) used two reactors in series for hydroprocessing shale-derived oils; the guard reactor was operated at a low temperature (216-271°C), and contained Shell-324 catalyst. Substantial interstitial residue deposition was reported in the guard reactor bed. The main hydrotreating reactor was residue free. These results are consistent with the observations made during this study.

Bed-plugging problems were encountered in the low temperature reactor all through the run duration (Run ZBI). The plugging was severe during the last 20 hours of operation. Even at temperatures as

TABLE XVII

INTERSTITIAL DEPOSITS (TWO REACTOR BEDS RUN ZBI)

Sample Number	Weight of Residues gms	Ash	N	C	H	N/C	H/C
		Wt.%				Atomic Ratio	
Top Reactor Bed (260°C)							
Top Glass Beads	2.05	50.1	1.33	47.32	2.65	0.024	0.672
Catalyst Top	0.83	--	0.88	21.02	1.89	0.035	1.079
Middle	0.15	--	--	---	--	---	---
Bottom	0.10	--	--	---	--	---	---
Bottom Glass Beads	0.06	--	--	---	--	---	---
Bottom Reactor Bed (400°C)							
Top Glass Beads	0.08	--	--	---	--	---	---
Catalyst Top / Middle / Bottom	0.24	--	0.32	17.41	0.813	0.0157	0.56
Bottom Glass Beads	0.20	--	--	---	--	---	---
Total Residues	3.51						

low as 260°C, some of the polyaromatics condensed to form deposits that plugged the reactor and disrupted the normal flow. Raising the temperature of the reactor by 5-10°C for a few minutes always resulted in the plug removal, and restoration of normal operation. This phenomenon of catalyst bed plugging can occur due to condensation and/or polymerization of some species present in the coal liquids. Beguin and Setton (1971) reported the reaction of polycondensed aromatics at relatively low temperatures, in presence of alkali metals, (K, Rb, and Cs), to yield a compound, which upon hydrolysis yielded either the original hydrocarbon or a mixture of dimers and polymers. For various polyaromatics, different temperatures were reported at which polymer formation occurred. The polymer formation temperatures for some of the compounds commonly found in the coal-derived liquids are as follows:

Perylene	> 250°C
Anthracene	> 250°C
Pyrene	> 200°C
Phenanthrene	> 200°C
Coronene	> 100°C

The presence of metals in the feed, thus play an important role in the residue formation and hence reactor bed-plugging.

The results from this section can be summarized as follows:

1. Organic and inorganic residue deposition occurred in the glass beads and catalyst interstices for all the experimental runs conducted.

2. The catalyst interstitial residues contained approximately 70 wt% ash, the remaining fraction being composed of C, N, H and S. The H/C atomic ratio of the residues was lower than the H/C atomic

ratio of the THF insolubles present in the feedstock.

3. The very low hydrogen content of the interstitial residues indicates their formation from highly condensed polyaromatic structures.

4. The interstitial deposition was the highest in the top reactor section and gradually decreased along the reactor length.

5. Both glass bead and catalyst sections accumulated interstitial deposits, indicating interstitial deposition reactions to occur non-catalytically (thermal reactions). The glass beads in the pre- and post-heat reactor sections had a uniform layer of inorganic material deposited on their surface. This material was identified to be composed of Fe, Si, and K.

6. For the two reactor bed experiment, the low temperature reactor accumulated substantial interstitial residues, negligible accumulation occurred in the high temperature reactor. This experiment indicated that the fraction in the feed, responsible for residue deposition, can be removed readily at relatively low temperatures.

7. The interstitial deposition occurs monotonically.

Catalyst Pore Volume, Surface Area and Pore Size Distribution

The aged catalyst samples from Run ZBF, ZBG, ZBH, and ZBI were analyzed for pore volume, pore size distribution, and surface area. Some of the catalyst samples were regenerated by controlled combustion in a muffle furnace; the regenerated catalyst samples were analyzed for pore volume, surface area, and pore size distribution. Extreme care was taken to avoid moisture adsorption on catalyst pellets.

All the catalysts used during this study lost considerable fraction of their pore volume and pore diameter; significant reduction in pore distribution was also noticed. Catalyst surface area loss showed a strong dependence on catalyst pore size, the small pore catalyst lost considerably more surface area compared to the large pore diameter catalyst. The catalysts did not regain their virgin pore volume, pore diameter, surface area, and pore distribution upon regeneration.

Figure 17 presents a comparison of the pore size distribution of the fresh, aged, and regenerated catalyst samples from Run ZBF (large pore catalyst). The most frequent pore diameter of the aged catalyst reduced from 177 Å to approximately 111 Å, a 37% reduction. The aged catalyst pore size distribution was also reduced; new pores were created in the size range of 35-100 Å. The distribution of the most frequent pore diameter was reduced considerably compared to the fresh catalyst. Catalyst pore sizes, greater than 150 Å suffered the maximum reduction in their distribution. The most frequent pore diameter of the regenerated catalyst samples was approximately 15% lower than of the fresh catalyst samples; the regenerated catalyst sample pore size distribution showed a shift towards the lower pore sizes (see Figure 17).

Figure 18 presents a comparison of the pore volumes of fresh, aged, and regenerated catalyst samples from Run ZBF (large pore catalyst). The aged catalyst pore volume decreased from 0.633 cm^3/gm, for the fresh catalyst to an average of 0.384 cm^3/gm, a 40% reduction. The regenerated catalyst samples regained only 88% of their pore volume upon regeneration (0.557 cm^3/gm). The pore size distributions of some of the aged and regenerated catalyst samples from Run ZBF are shown in

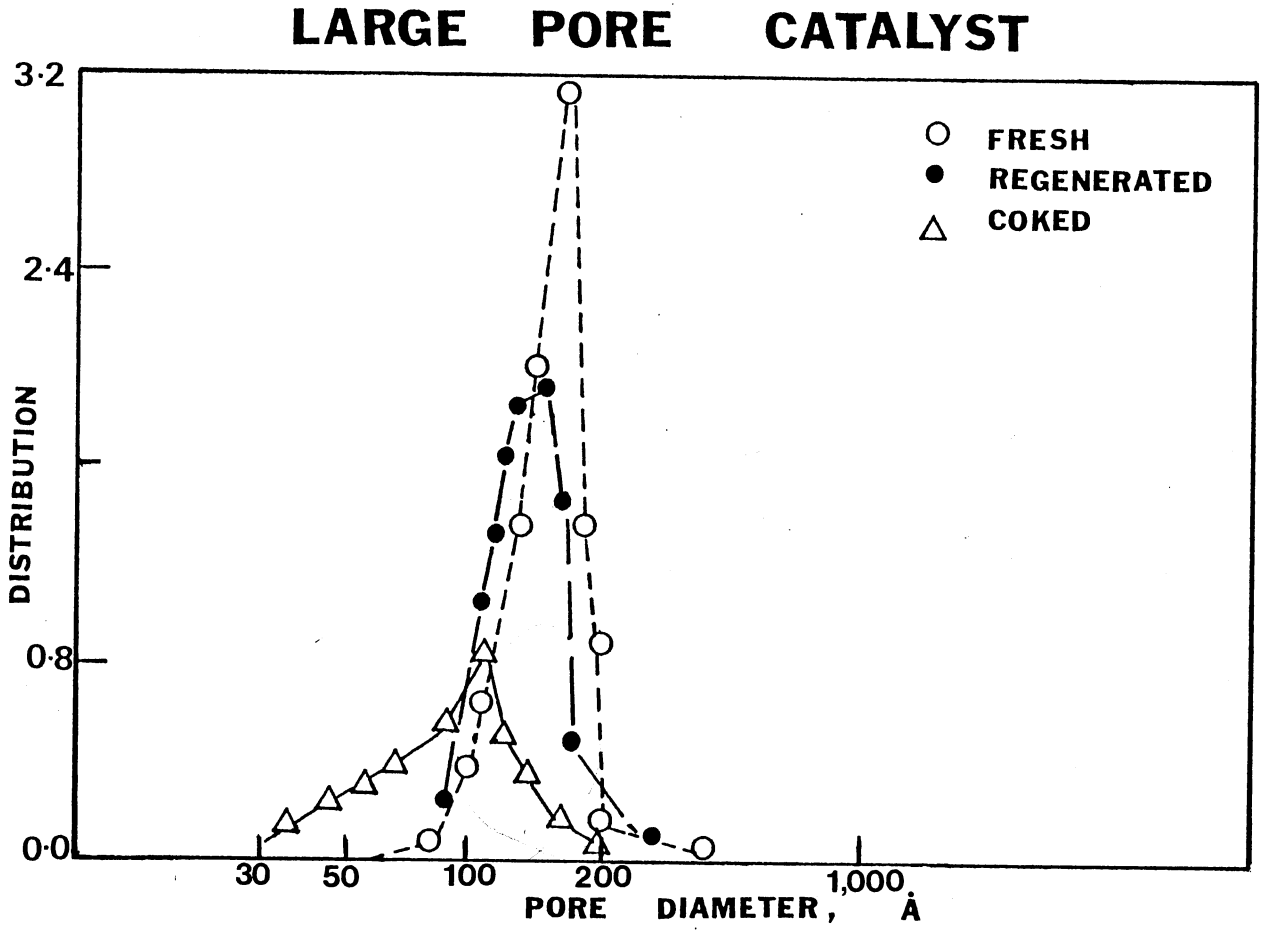

Figure 17. Comparison of Fresh, Aged and Regenerated Catalyst Pore Distribution (Run ZBF)

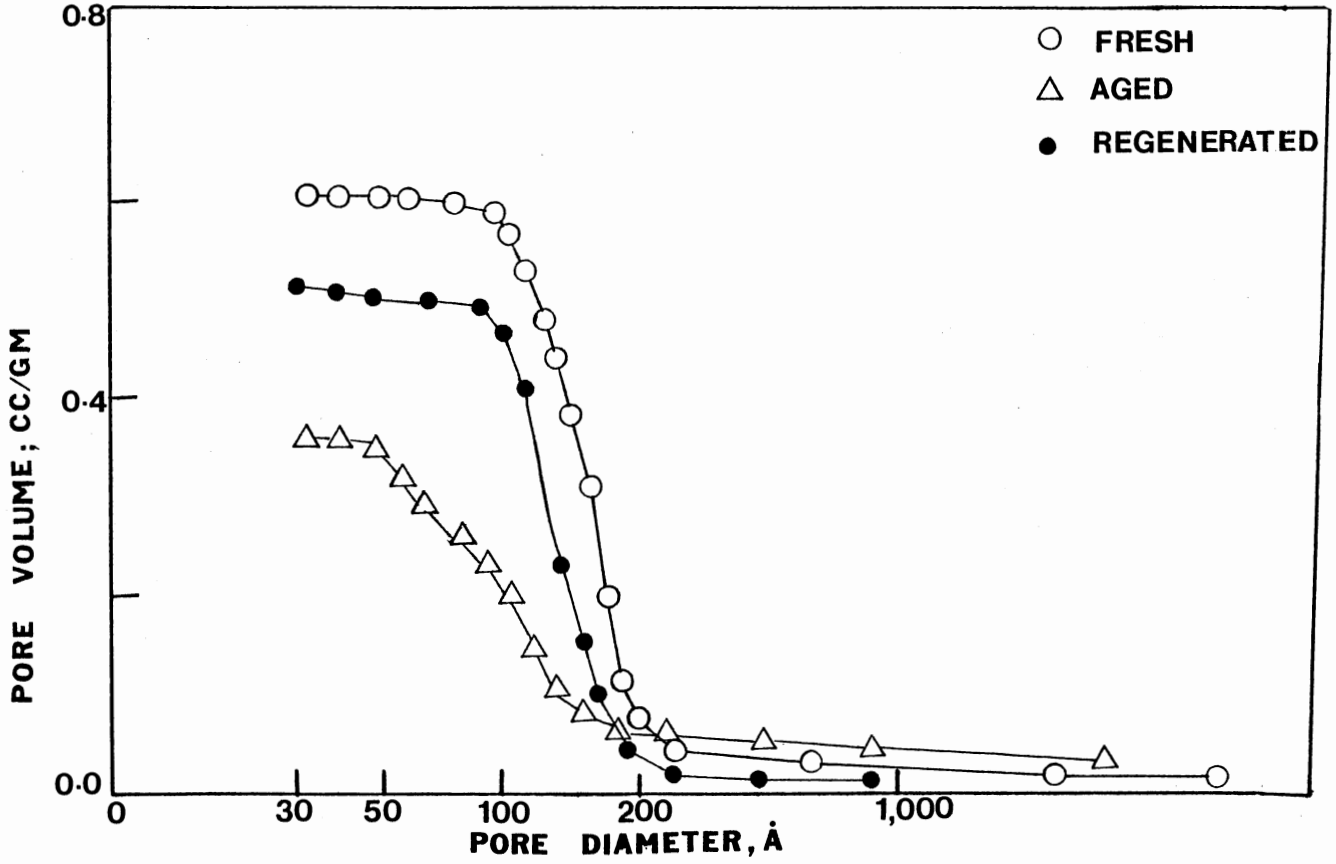

Figure 18. Comparison of Fresh, Aged, and Regenerated Catalyst Pore Volume (Run ZBF)

Appendix H.

Contrary to the considerable decrease in pore size, and pore volume upon aging of the large pore catalyst, their surface area decreased only slightly. On an average, the large pore catalyst surface area decreased from 125 m^2/gm (fresh catalyst) to 115 m^2/gm (aged catalyst), an 8% reduction. No definite relation was noticed between the catalyst coke content and the aged catalyst surface area, pore volume, and pore diameter for the large pore diameter catalysts. Table XVIII lists the aged catalyst physical properties as a function of coke content for Run ZBF. The regenerated catalyst physical properties of some samples are also shown.

Similar decreases in pore volumes, and pore distributions were noticed for the catalyst samples from Run ZBG (small pore catalyst). Figure 19 presents a comparison of the pore distribution of the fresh, aged, and regenerated catalyst samples from Run ZBG. The most frequent pore diameter of the aged catalyst reduced from 63 Å to approximately 48 Å, a 24% reduction. Unlike the substantial decrease in the pore size distribution of the large pore diameter catalyst, the small pore catalysts suffered only negligible decrease in their pore size distribution. The pore distribution curve shifted towards the lower pore sizes by 15-20 Å, the shape of the distribution curve remained essentially the same as for the fresh catalysts. The unaltered pore size distribution of the aged small pore catalyst samples represents uniform residue deposition inside the catalyst pores.

The pore volumes of the aged catalyst samples from Run ZBG decreased by 60% (0.49 to 0.20 cm^3/gm). A 23% decrease in the catalyst pore volume for the regenerated catalyst samples was also

TABLE XVIII

AGED CATALYST COKE CONTENT AND PHYSICAL PROPERTIES RUN ZBF (HT-115E)

Catalyst Position In Reactor	Wt. % Coke	Aged Catalyst			Regenerated Catalyst		
		Pore Volume cm^3/gm	Pore Diameter $\mathring{A}$	Surface Area m^2/gm	Pore Volume cm^3/gm	Pore Diameter $\mathring{A}$	Surface Area m^2/gm
Fresh Catalyst		0.63	177	125	0.63	177	125
1 (Top)	20.9	0.37	111	120	0.54	151	112
2	17.2	0.33	126	117	0.56	154	-
3	18.4	0.38	111	112	0.57	147	-
4	16.3	0.42	110	111	--	-	117
5	14.6	0.40	126	116	0.57	147	-
6 (Bottom)	15.7	0.41	111	112	NA	-	120

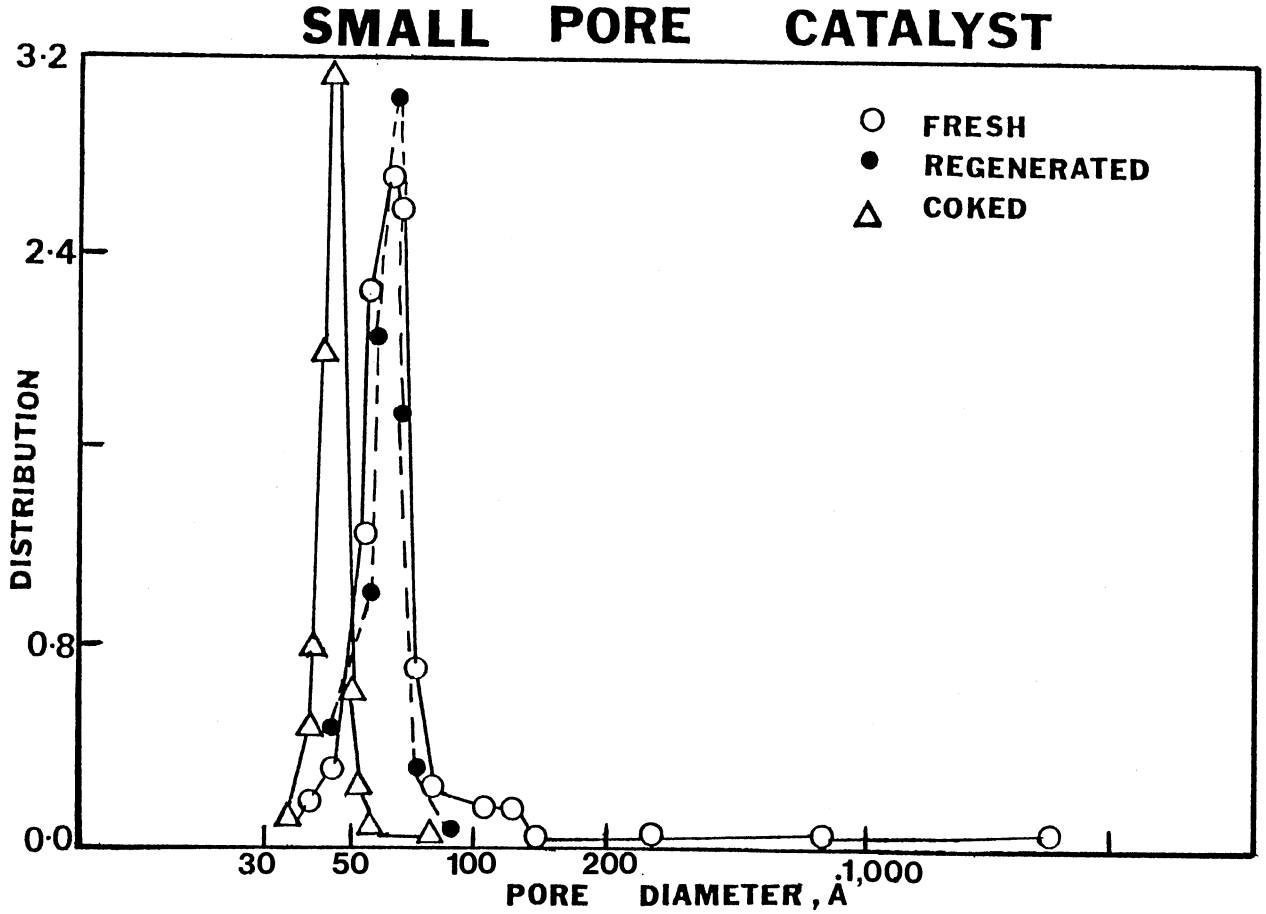

Figure 19. Comparison of Fresh, Aged, and Regenerated Catalyst Pore Distribution (Run ZBG)

observed. Figure 20 represents a comparison of the aged, regenerated, and fresh catalyst sample pore volume for the small pore diameter catalyst (Run ZBG). The pore size distributions of some of the aged and regenerated catalyst samples from Run ZBG are presented in Appendix H.

Contrary to the negligible decrease in the surface area of the large pore diameter aged catalysts (8%), the small pore diameter catalysts suffered a 35% decrease in their surface area. The surface area decreased from 270 m^2/gm, for the fresh catalyst to an average of 174 m^2/gm for the aged catalysts. The regenerated catalyst samples lost approximately 10% surface area. Here too, as for the large pore catalysts, no definite relation existed between the wt% coke deposited on the catalyst and the catalyst pore diameter, pore size, and surface area (see Table XIX). These results are contrary to the results obtained by Chang (1982), who while processing a 30 wt% SRC/Process Solvent blend over a Ni-Mo-Al_2O_3 catalyst observed a linear relationship between the catalyst pore diameter, pore volume, surface area and catalyst coke content. The data reported were obtained for oil-catalyst contact times of less than 153 hours.

The regenerated large pore diameter catalyst samples lost substantial fraction of their pore volume and pore diameter. This reduction in pore size can occur due to the metal and inorganic deposition on the catalyst surface. Contrary to the carbonaceous deposition, the inorganic and metal deposition cannot be removed upon combustion. The large pore diameter regenerated catalyst samples showed an 18% reduction in pore diameter, a 12% reduction in pore volume also occurred. The regenerated small pore catalysts did not show a reduction in their

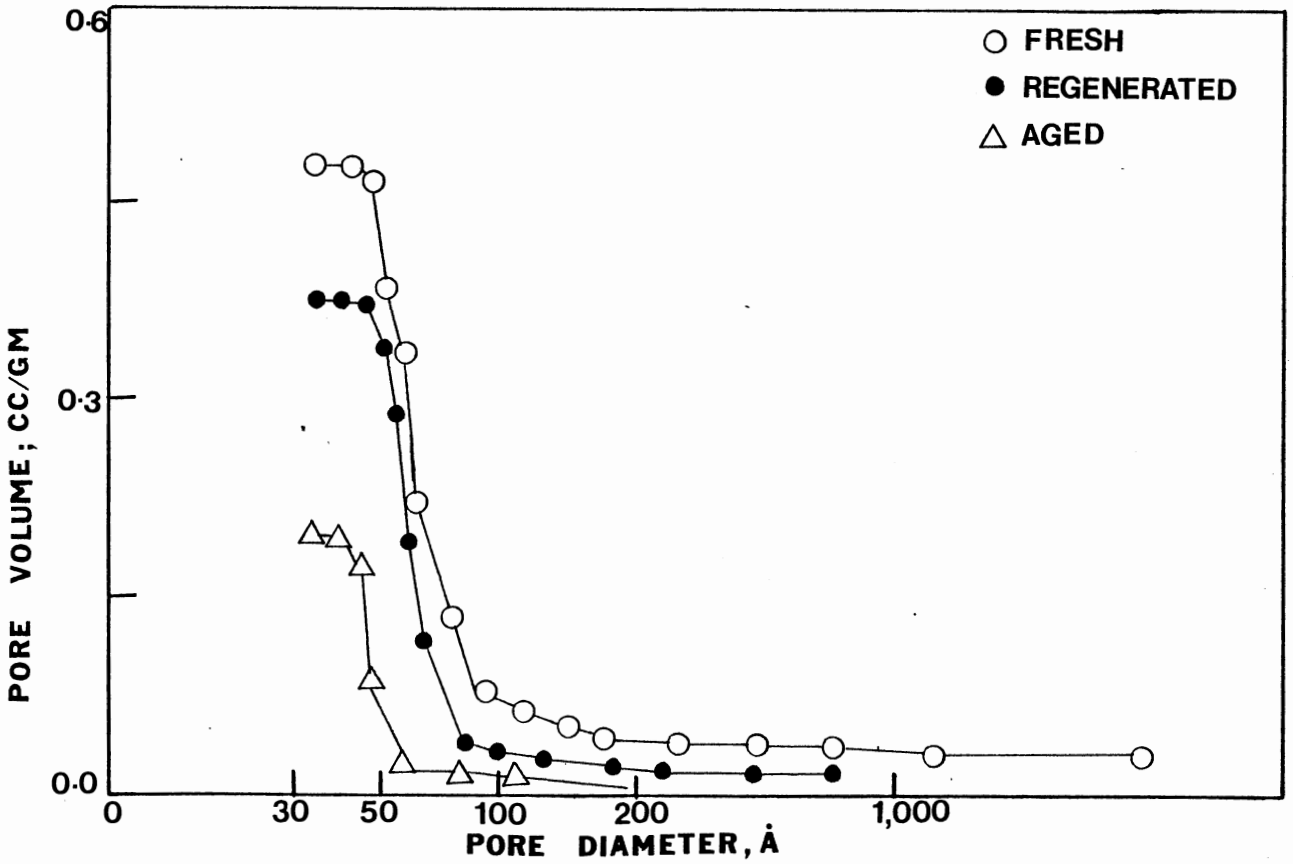

Figure 20. Comparison of Fresh, Aged, and Regenerated Catalyst Pore Volumes (Run ZBG)

TABLE XIX

AGED CATALYST COKE CONTENT AND PHYSICAL PROPERTIES RUN ZBG (KF-153S)

Catalyst Position In Reactor	Wt. % Coke	Aged Catalyst			Regenerated Catalyst		
		Pore Volume cm^3/gm	Pore Diameter $\mathring{A}$	Surface Area m^2/gm	Pore Volume cm^3/gm	Pore Diameter $\mathring{A}$	Surface Area m^2/gm
Fresh Catalyst		0.49	65	270	0.49	65	270
1 (Top)	16.8	0.19	47	165	0.39	65	245
2	18.2	0.21	47	189	--	--	-
3	17.9	0.20	47	179	--	--	-
4	18.4	0.18	46	172	0.39	63	240
5	18.7	0.21	52	171	--	--	-
6 (Bottom)	20.5	0.18	52	166	0.38	65	243

most frequent pore size, but a reduction of 23% in catalyst pore volume was observed. The surface area of the regenerated small pore catalyst samples decreased by 10% (see Tables XVIII to XIX). The decrease in surface area, and pore volume of the regenerated small pore catalyst, without a corresponding decrease in the most frequent pore diameter represents the loss of some of the small pores (<35 Å) to permanent pore blockage by inorganics and metals.

Figure 21 compares the pore size distribution of the catalysts from the top, and the bottom reactor zones for Run ZBH. Essentially, the composite aged catalyst bed contained catalysts with pore diameters ranging in size from 40 to 150 Å. As has been discussed previously, such a combination of pore sizes did not result in any improvement in the catalyst hydrotreatment activity. The pore size distribution of the composite catalyst bed was consistent with the analysis of the single catalyst beds. The most frequent pore size of the small pore diameter aged catalysts was 46 Å, which was comparable to the pore size of the aged catalyst from Run ZBG (47 Å). The most frequent pore size of the large pore catalyst, too, was comparable to the catalyst from Run ZBF. Both catalyst pore volume, and surface area behaved similarly. The regenerated catalyst analysis too revealed a similar trend. The catalyst pore size distributions of some aged, and regenerated catalyst samples from Run ZBH are shown in Appendix H. Table XX lists the physical properties of the catalysts from the composite catalyst bed as a function of the catalyst coke content. No relation between the coke content and the catalyst physical properties was noticed.

The analysis of catalyst samples from Run ZBI revealed some interesting results. Even at temperatures as low as 260°C, the small

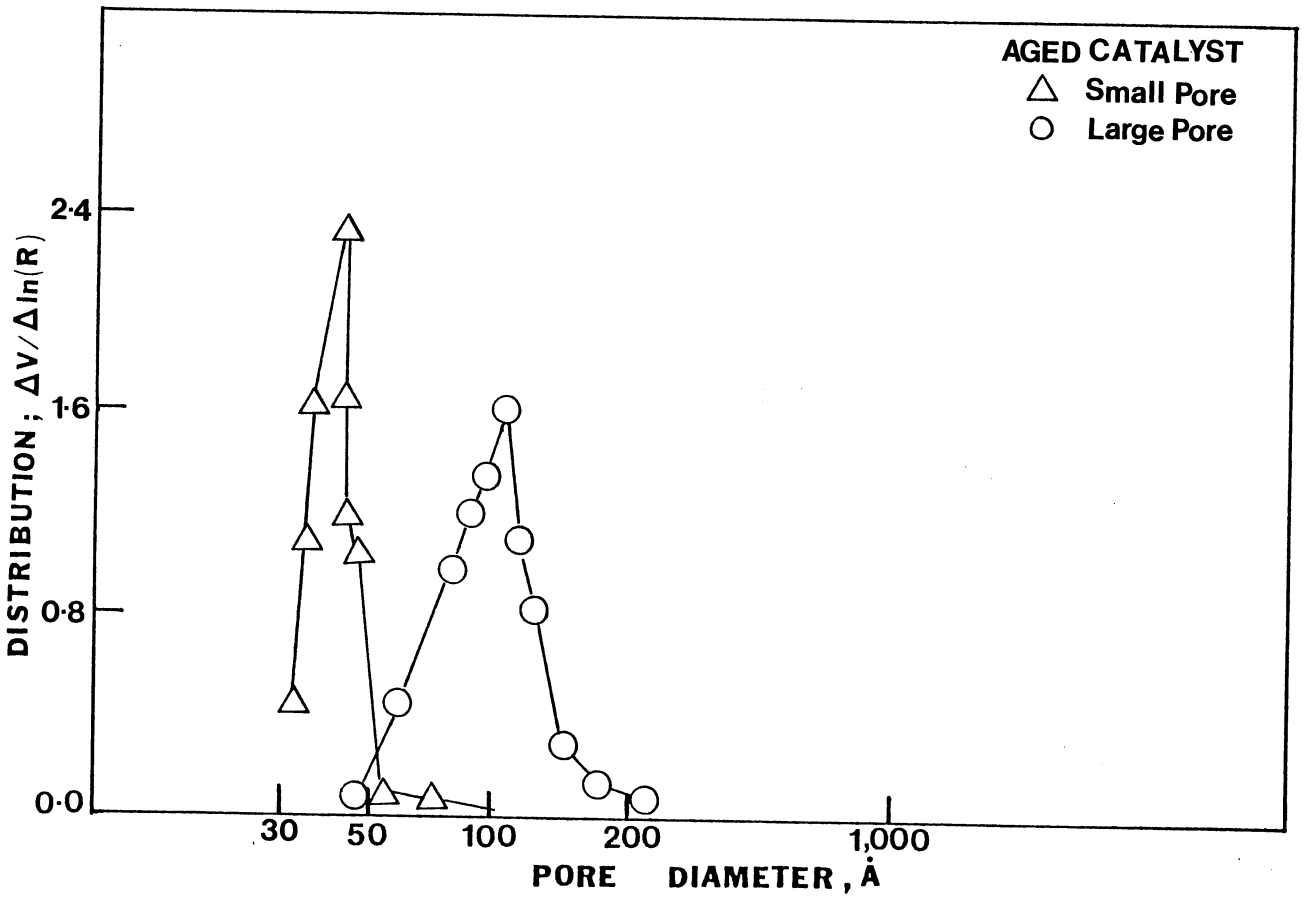

Figure 21. Comparison of Catalyst Pore Distribution (Run ZBH)

TABLE XX

AGED CATALYST COKE CONTENT AND PHYSICAL PROPERTIES
(COMPOSITE CATALYST BED)

Catalyst Position In Reactor	Wt. % Coke	Aged Catalyst			Regenerated Catalyst		
		Pore Volume cm^3/gm	Pore Diameter $\mathring{A}$	Surface Area m^2/gm	Pore Volume cm^3/gm	Pore Diameter $\mathring{A}$	Surface Area m^2/gm
Top Reactor Zone							
KF-153 S (Fresh)		0.49	65	270			
Top	19.3	0.18	45	171			
Middle	15.3	0.18	48	172			
Bottom	15.5	0.21	44	175	0.39	63	185
Bottom Reactor Zone							
HT-115 E		0.63	177	125			
Top	15.4	0.39	126	110			
Middle	15.0	0.38	126	118			
Bottom	16.9	0.32	118	115	0.65	147	118

pore catalyst most frequent pore diameter reduced to 47 Å, which was equal to the pore diameter of the catalyst aged at 400°C (Run ZBG). The regenerated catalysts from Run ZBI (260°C) regained slightly more surface area, pore volume, and pore diameter compared to catalysts from Run ZBG. This can be the result of greater metal penetration and deposition on the catalysts from Run ZBG (high temperature 400°C, and 240 hours of oil-catalyst contact) compared to the low temperature catalysts from Run ZBI.

Figure 22 presents the pore size distribution of the catalysts from the high temperature (400°C) and low temperature (260°) reactors for Run ZBI. The pore size of the catalyst samples from the high temperature and the low temperature reactor was essentially the same, 47 Å for low temperature catalyst and 44 Å for high temperature catalyst, however, the shape of the pore distribution curves was significantly different (see Figure 22).

The high temperature catalyst lost consistently higher surface area compared to the low temperature catalyst (155 m^2/gm vs. 177 m^2/gm). The catalysts from the high temperature (400°C) reactor section of Run ZBI lost more surface area and pore volume compared to the catalyst samples from Run ZBG, which was conducted at the same temperature. The high temperature catalyst samples from Run ZBI, however, regained consistently higher surface area and pore volume upon regeneration, compared to the catalyst samples from Run ZBG. This could have occurred due to the lower inorganic and metal deposition on the catalyst from Run ZBI; note that most of the inorganic deposits occurred in the low temperature catalyst bed. Table XXI lists the physical properties of the catalysts from the low and the high temperature reactor beds.

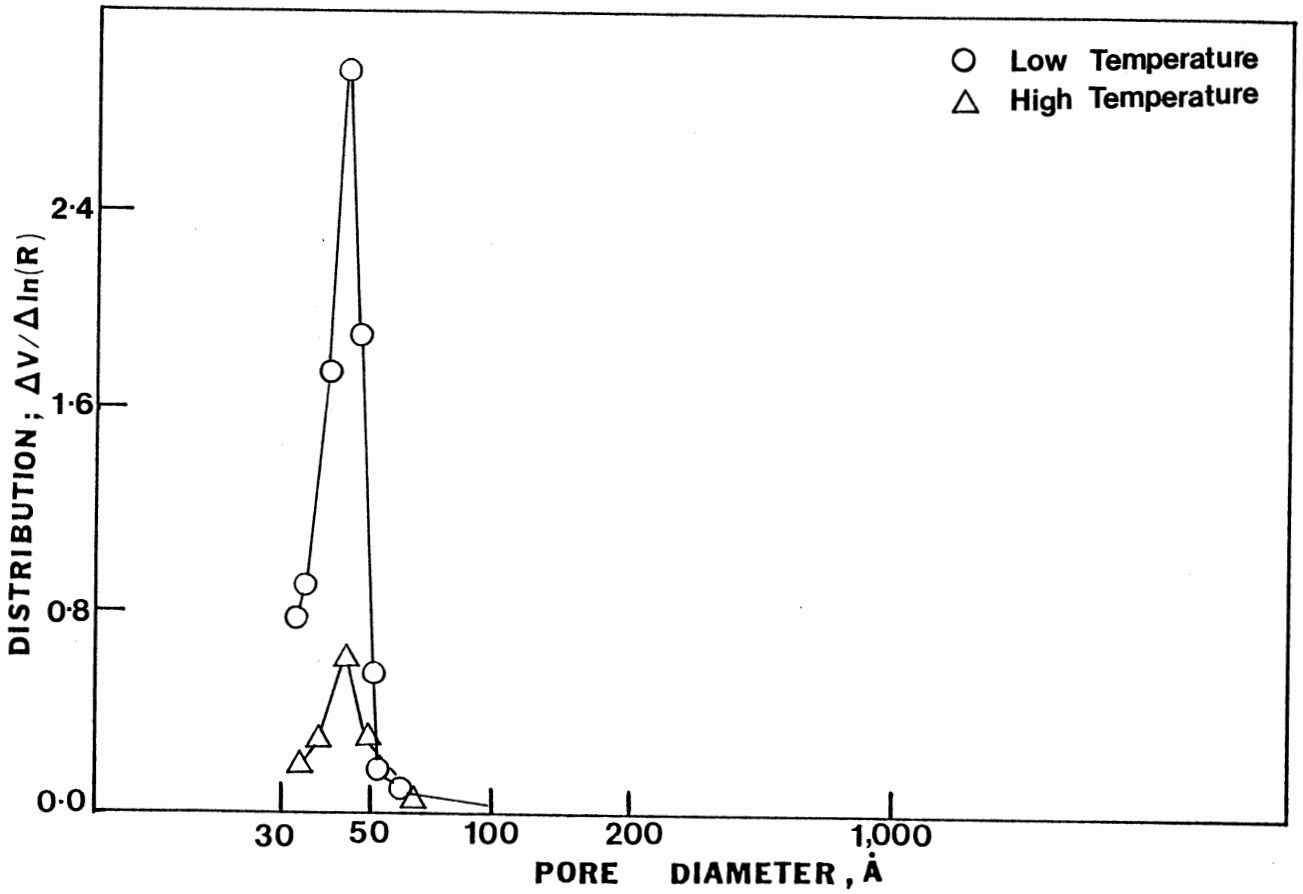

Figure 22. Comparison of Pore Distribution of High Temperature and Low Temperature Catalyst Samples (Run ZBI)

TABLE XXI

AGED CATALYST COKE CONTENT AND PHYSICAL PROPERTIES (TWO TEMPERATURE REACTOR ZONES)

Catalyst Position In Reactor	Wt. % Coke	Aged Catalyst			Regenerated Catalyst		
		Pore Volume cm^3/gm	Pore Diameter $\AA$	Surface Area m^2/gm	Pore Volume cm^3/gm	Pore Diameter $\AA$	Surface Area m^2/gm
Low Temperature Reactor (260°C)							
KF-153S (Fresh)		0.49	65	270			
Coked Catalyst							
Top	16.9	0.20	47	183	0.39	59	251
Middle	14.8	0.19	47	178			
Bottom	17.0	0.19	47	175			
High Temperature Reactor (400°C)							
KF-153S (Fresh)		0.49	65	270			
Coked Catalyst							
Top	20.9	0.14	44	151			
Middle	21.4	0.18	44	157			
Bottom	20.4	0.17	44	158	0.39	65	236

This section on catalyst pore volume, size and surface area can be summarized as follows:

1. The large pore diameter catalyst most frequent pore diameter decreased from 177 Å to approximately 111 Å over the 240 hours of oil-catalyst contact. The small pore diameter catalyst suffered a decrease from 63 Å to 48 Å. Contrary to the large decrease in the most frequent pore diameter of the large pore diameter catalysts, their surface area decreased only slightly. The surface area decrease for the small pore diameter catalyst was very significant (36% loss in surface area).

2. The large pore diameter catalysts suffered a significant decrease in their pore distribution, the distribution for the small pore catalysts changed only slightly. The unaltered pore size distribution of the small pore catalysts represents uniform pore deposition.

3. The large pore diameter, regenerated catalyst lost 12% pore volume, 7% surface area, and 13% of their original pore diameter; the small pore regenerated catalyst lost 9% surface area, and 23% pore volume, no loss in catalyst pore diameter occurred.

4. The catalysts from the composite bed, too, lost significant fraction of their pore volume, size, and surface area, over the 240 hours of oil-catalyst contact. The values were consistent with the results obtained for the single catalyst beds.

5. The catalysts from the low temperature reactor zone lost significant pore volume, size, and surface area upon aging. No significant difference in the pore volume and pore diameter of the catalysts from the low and high temperature reactors was noticed. The pore size distribution, and surface area of the high temperature reactor bed catalyst, however, was reduced considerably compared to the low

temperature reactor catalysts.

Liquid Sample Analysis

Elemental Analysis

All product liquid samples were analyzed for nitrogen, hydrogen, and carbon content. Sulfur analysis was conducted for only some liquid samples. The sulfur content of the product liquid samples was lower than the minimum detection limit of the analyzer (0.02 wt.% S); routine sulfur analysis of liquid samples was hence discontinued.

The elemental analysis of the product liquid samples provided some interesting results. Catalysts lost their hydrodenitrogenation (HDN) and hydrogenation activity rapidly. Significant activity loss occurred during the first 12 to 36 hours of oil-catalyst contact, a steady deactivation rate was observed during the remaining run duration. Similar loss in HDN activity was reported by Chang (1982), and Ahmed (1980) while hydroprocessing a coal-derived liquid.

One can hypothesize the initial catalyst activity loss to occur due to rapid carbonaceous deposition on the catalyst active sites. In general, the gradual catalyst decay, after the rapid initial deactivation, occurs due to the combined metal and carbonaceous deposition. The rate of carbonaceous deposition in the later periods being much slower than the initial rate.

The HDN activity of the catalysts showed a strong dependence on process temperature and LVHST. Precautions were taken against masking the catalyst activity at a certain temperature and space time by the past history of temperatures and space times. This was insured by cleaning the system for several hours; usually four reactor volumes,

passed through the reactor at the desired temperature and space time, were considered sufficient to stabilize the reactor system at the desired conditions. Intermediate liquid was always removed prior to collection of the desired liquid sample.

Figure 23 presents the total product liquid nitrogen and hydrogen content as a function of the time on stream (temperature of 400°C, and LVHST of 1.87 hours) for experimental Run ZBF (large pore catalyst). The product liquid nitrogen content increased from 0.31 wt% to 0.53 wt% during the first 12 to 36 hours of oil-catalyst contact (71% increase in product nitrogen content). During the 240 hours of oil-catalyst contact, the HDN activity of the catalyst reduced to 24 wt% nitrogen removal, compared to 72 wt% removal during the first twelve hours of oil-catalyst contact. Catalyst deactivation after 36 hours of oil-catalyst contact was very gradual; only 18 wt% loss in HDN activity was noticed.

The catalyst hydrogenation activity, too, decreased rapidly during the first thirty-six hours of oil-catalyst contact; product liquid hydrogen content decreased from 10.5 wt% to 9.4 wt% during this time. Product hydrogen content decreased gradually to 8.8 wt% during the rest of the experimental duration. The catalyst showed a very high hydrogenation activity for the first 12 hours of oil-catalyst contact, but lost activity severely thereafter.

The hydrogenation and hydrodenitrogenation (HDN) activity responses for Run ZBG (small pore catalyst) were similar to those of Run ZBF. The catalyst HDN activity decreased substantially during the first 12 to 36 hours of oil-catalyst contact. Gradual increase in product liquid nitrogen content occurred all through the experimetal

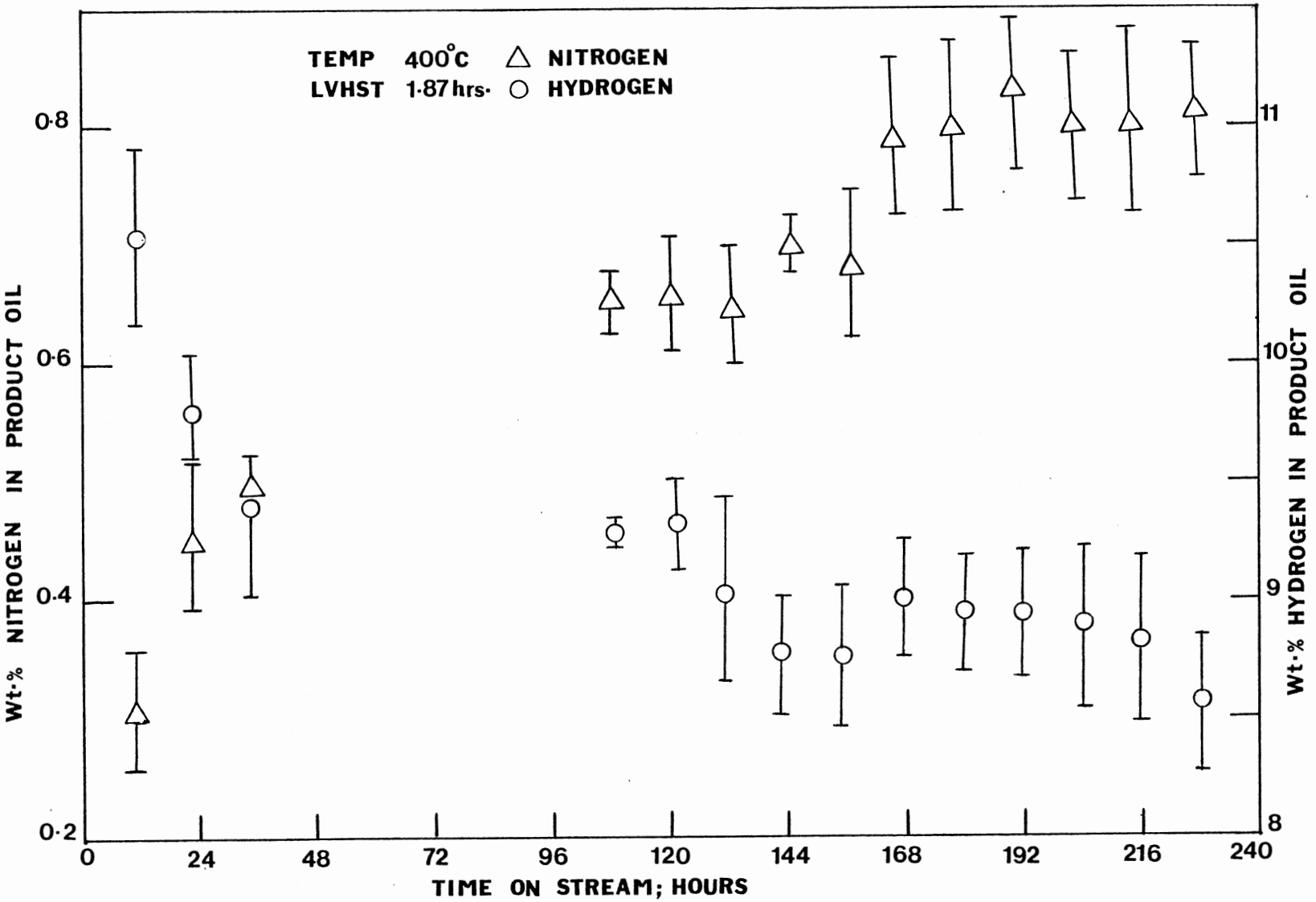

Figure 23: Product Liquid Nitrogen and Hydrogen Content as a Function Oil-Catalyst Contact Time (Run ZBF)

run duration. Figure 24 presents the product liquid nitrogen and hydrogen content as a function of the time on stream for a constant temperature of 400°C, and a LVHST of 1.87 hours.

The small pore diameter catalyst (Run ZBG) removed consistently more nitrogen from the feedstock compared to the large pore diameter catalyst (Run ZBF). The HDN activity of the large pore diameter catalyst decreased more rapidly than the small pore diameter catalyst. This lower deactivation rate and correspondingly higher activity of the small pore diameter catalyst can be attributed to several factors. The small pore diameter catalyst contains higher surface area (275 vs. 125 m^2/gm), hence more reactive sites per unit mass of the catalyst are available for the small pore diameter catalyst. More active sites result in higher activity of the small pore catalysts.

The feedstock used during this study contained 1.0 wt% THF insolubles, 6.4 wt% preasphaltenes, and 14.7 wt% asphaltenes, the balance being resins and oils. Approximately 44% nitrogen present in the feedstock is contained in the asphaltene, preasphaltene and THF insoluble fractions. The asphaltenes contain approximately 2.33 wt% nitrogen. At the reactor operating temperature (400°C), some of the asphaltenes can be considered to thermally crack to form lower molecular weight fragments. Approximately 50-60 wt% nitrogen present in the feedstock can be estimated to be contained in the oils and resins fraction. These molecular species, of size less that 15 Å, can enter both the small and the large catalyst pores freely, due to their comparatively smaller size (compared to the catalyst pore sizes). For the molecular species that enter the catalyst pores, the small pore catalyst will have a higher activity

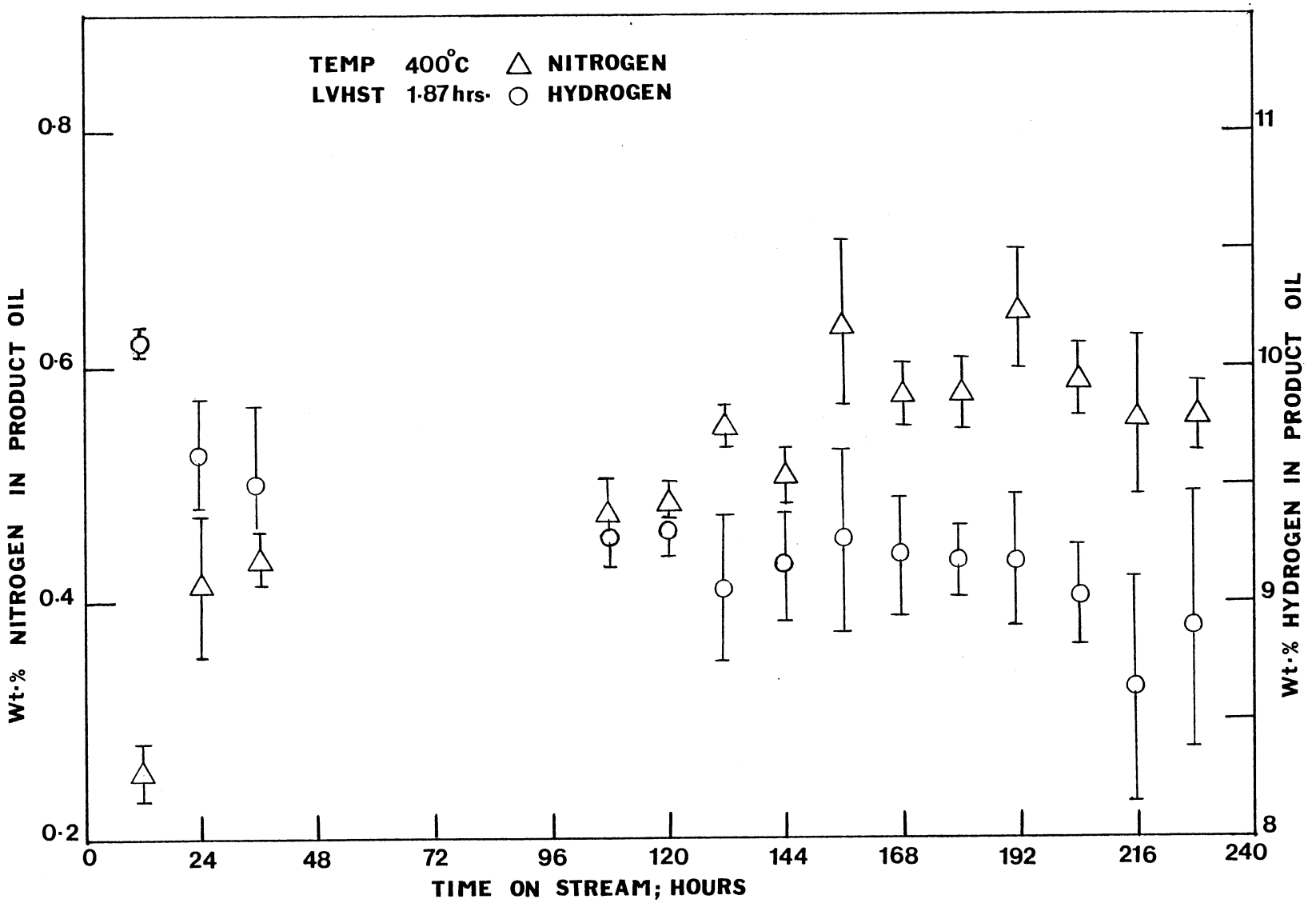

Figure 24. Product Liquid Nitrogen and Hydrogen Content as a Function of Oil-Catalyst Contact Time (Run ZBG)

due to its larger surface area.

The catalyst pore size and its distribution can have a strong effect on the catalyst activity decay (Richardson and Alley, 1975). The small pore diameter catalyst used during this study has a unique, narrow pore size distribution (90% decrease in distribution for 15 Å change in pore diameter), compared to the broad distribution of the large pore catalyst (90% decrease in distribution for 130 Å change in pore diameter). The narrow pore size distribution of the small pore catalyst can selectively exclude the very large molecular species (>30 Å) from entering the catalyst pore structure. These large molecular species are considered to be active coke precursors due to their large heteroatom and metal content. Elimination of these species from the catalyst interior results in lesser coke being deposited on the small pore catalyst, and hence higher activity maintenance.

Figure 25 presents Run ZBH (composite catalyst bed) product liquid nitrogen and hydrogen content as a function of the time on stream. Note that the composite catalyst bed combination, too, lost substantial HDN and hydrogenation activity over the run duration. The composite catalyst bed deactivated severely during the initial thirty-six hours of oil-catalyst contact; the deactivation was gradual during the remaining hours of the catalytic run.

Figure 26 presents a comparison of the HDN activity for Run ZBH with Run ZBF and Run ZBG. As has been explained earlier, small pore diameter catalyst showed greater HDN activity compared to the large pore diameter catalyst. The composite catalyst bed HDN activity varied intermediate to the response of the single catalyst beds. The deactivation response of the composite catalyst bed also followed

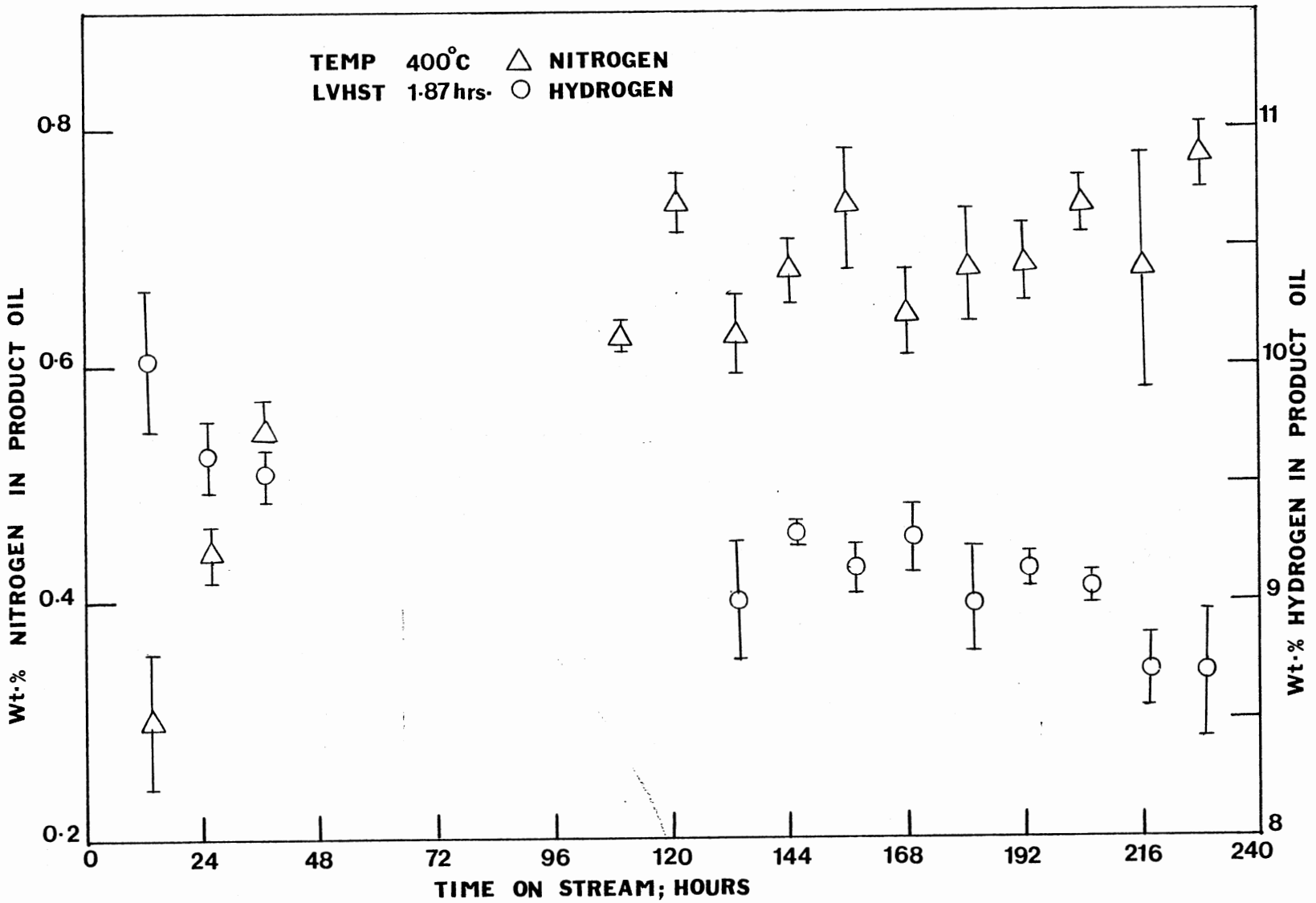

Figure 25. Product Liquid Nitrogen and Hydrogen Content as a Function of Oil-Catalyst Contact Time (Run ZBH)

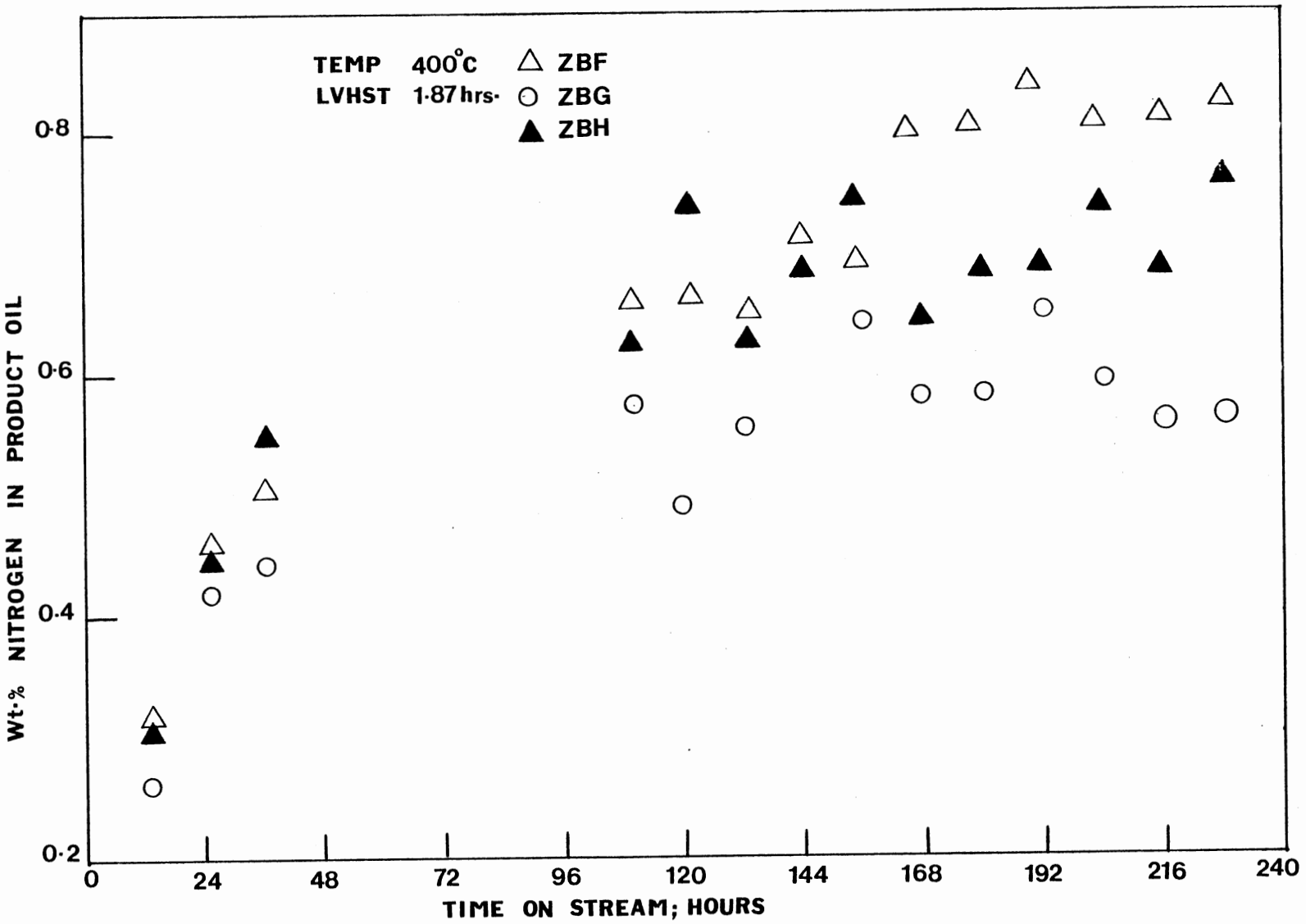

Figure 26. Comparison of HDN Activity for Run ZBF, ZBG and ZGH.

a similar trend. The large pore diameter catalyst deactivated the fastest, the small pore diameter catalyst deactivated the slowest, and the composite bed intermediate between the two. Clearly, the composite catalyst combination does not have a synergistic effect on the hydrodenitrogenation activity or deactivation response of the catalyst beds. The catalyst beds in the composite reactor combination tend to act independently, the past processing history of the liquid in the catalyst bed does not seem to affect the bed hydrodenitrogenation efficiency. Various factors can be attributed for the lack of response of composite catalyst bed combinations. The catalysts were observed to deactivate substantially in the initial hours of oil-catalyst contact. The first liquid sample was not collected until 12 hours of oil-catalyst contact time had elapsed. This early catalyst deactivation might have masked any response (HDN) the composite catalyst bed might have had. Further, at high process temperatures, the coal-derived liquid physical properties differ drastically from the coal liquid properties at room temperature. The large molecules disintegrate into smaller components (Ho and Briggs, 1981; Richardson and Alley, 1975), and thus, may not see the difference in the catalyst pore sizes.

Figure 27 presents the comparison of the product liquid nitrogen content as a function of space time for experimental Runs ZBF, ZBG and ZBH; all at a temperature of 400°C. Note that for all the experimental runs the process conditions: time on stream, temperature, LVHST, sampling sequence and schedule were held constant. The product liquid nitrogen content from Run ZBH (composite bed) was comparable to Run ZBF (large pore catalyst).

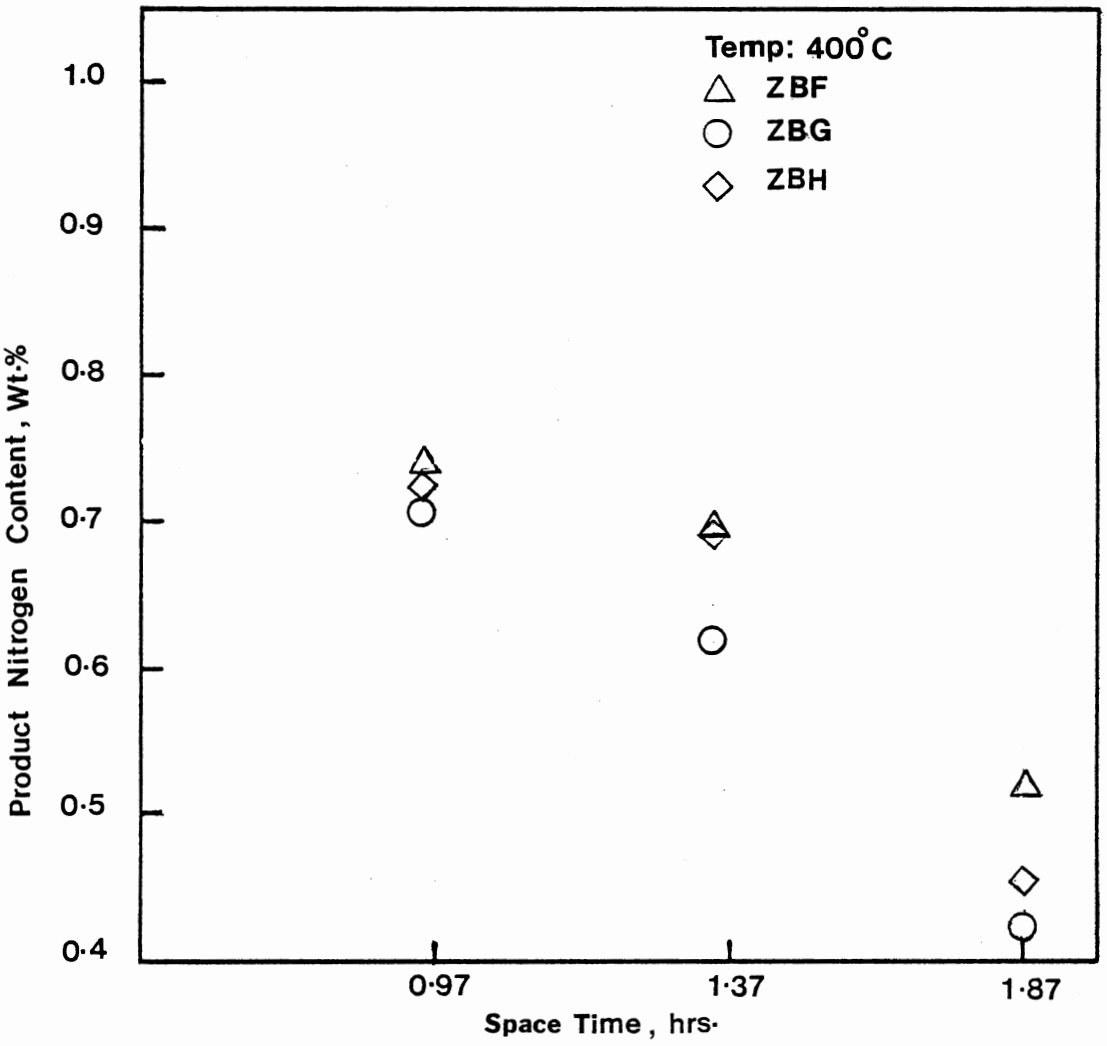

Figure 27. Comparison of the Product Liquid Nitrogen Content as a Function of Space Time for Runs ZBF, ZBG and ZBH at a Constant Temperature of 400°C

Figure 28 presents the product liquid nitrogen content as a function of the time on stream for experimental Run ZBI (low and high temperature reactor zones). The nitrogen content of the product liquids from the first reactor zone (intermediate samples) is also presented for comparison. As expected, essentially no hydrodenitrogenation of the liquid occurred at 260°C (see Table XXII).

The low temperature treatment of the feedstock prior to the high temperature processing seemed to have a beneficial effect on the catalyst hydrodenitrogenation activity. The product liquid nitrogen content for all four experimental runs at 48 hours of oil-catalyst contact time, and 0.94 hour space time are plotted in Figure 28. Note that at 48 hours of oil-catalyst contact time the process conditions were exactly the same for all experimental runs. Run ZBI nitrogen content was 15% lower than the nitrogen content of the other experimental runs. The liquid volume hourly space time (LVHST) for Run ZBI was defined on the basis of catalyst volume in the high temperature reactor.

Figure 29 presents the hydrogen content of the product liquids from experimental Run ZBI as a function of the time on stream. The hydrogenation activity of the catalyst decreased gradually over the 120 hours of oil-catalyst contact time. A slight increase in product hydrogen content occurred in the low temperature reactor. The product hydrogen content increased from 7.26 wt% to an average content of 7.61 wt%. This increase could have occurred due to the hydrogenation of olefins, diolefins, and naphthalenes present in the feedstock. No deactivation in the hydrogenation activity with the time on stream was

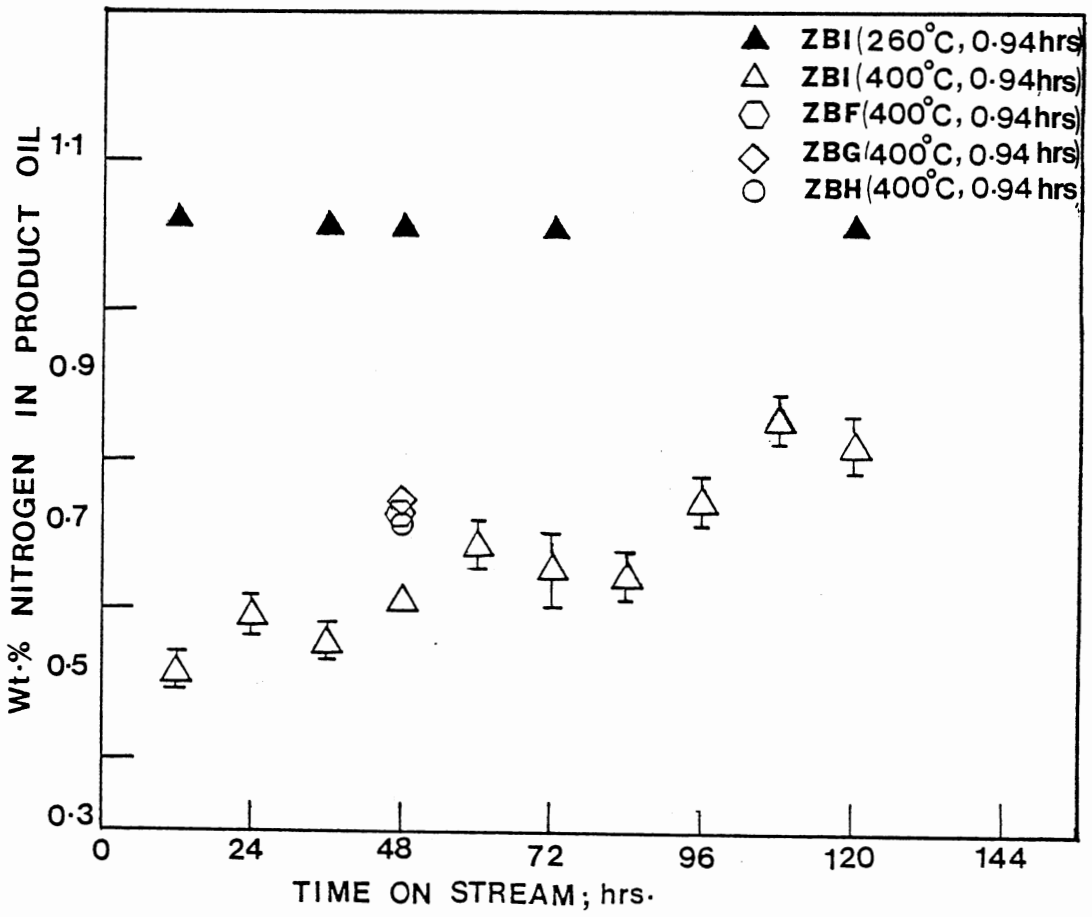

Figure 28. Product Liquid Nitrogen Content as a Function of the Time on Stream for Run ZBI

TABLE XXII

EXPERIMENTAL ANALYSES RESULTS FROM RUN ZBI
(TWO TEMPERATURE ZONES)

Catalyst: KF-153 S (Small Pore Catalyst)
LVHST: 0.94 hrs (Based on High Temperature Reactor Zone Catalyst Volume)

Intermediate Liquid Sample Analyses

Sample Number	Hours On Oil	Temperature °C	wt.% N	wt.% C	wt.% H
Feedstock			1.12	87.20	7.26
ZBI-Int.* #1	12	260	1.14	88.97	7.55
#2	36	260	1.17	87.53	7.64
#3	48	260	1.16	88.13	7.59
#4	72	260	1.12	87.63	7.73
#5	120	260	1.11	88.40	7.74
Final Liquid	Analyses				
ZBI #1	12	400	0.51	88.36	9.81
#2	24	400	0.59	88.20	9.73
#3	36	400	0.55	87.29	9.16
#4	48	400	0.61	88.32	8.82
#5	60	400	0.68	88.71	8.97
#6	72	400	0.65	88.38	9.30
#7	84	400	0.64	89.86	9.05
#8	96	400	0.74	89.34	9.06
#9	108	400	0.85	88.92	8.29
#10	120	400	0.82	88.18	8.62

* Intermediate sample taken after low temperature reactor zone.

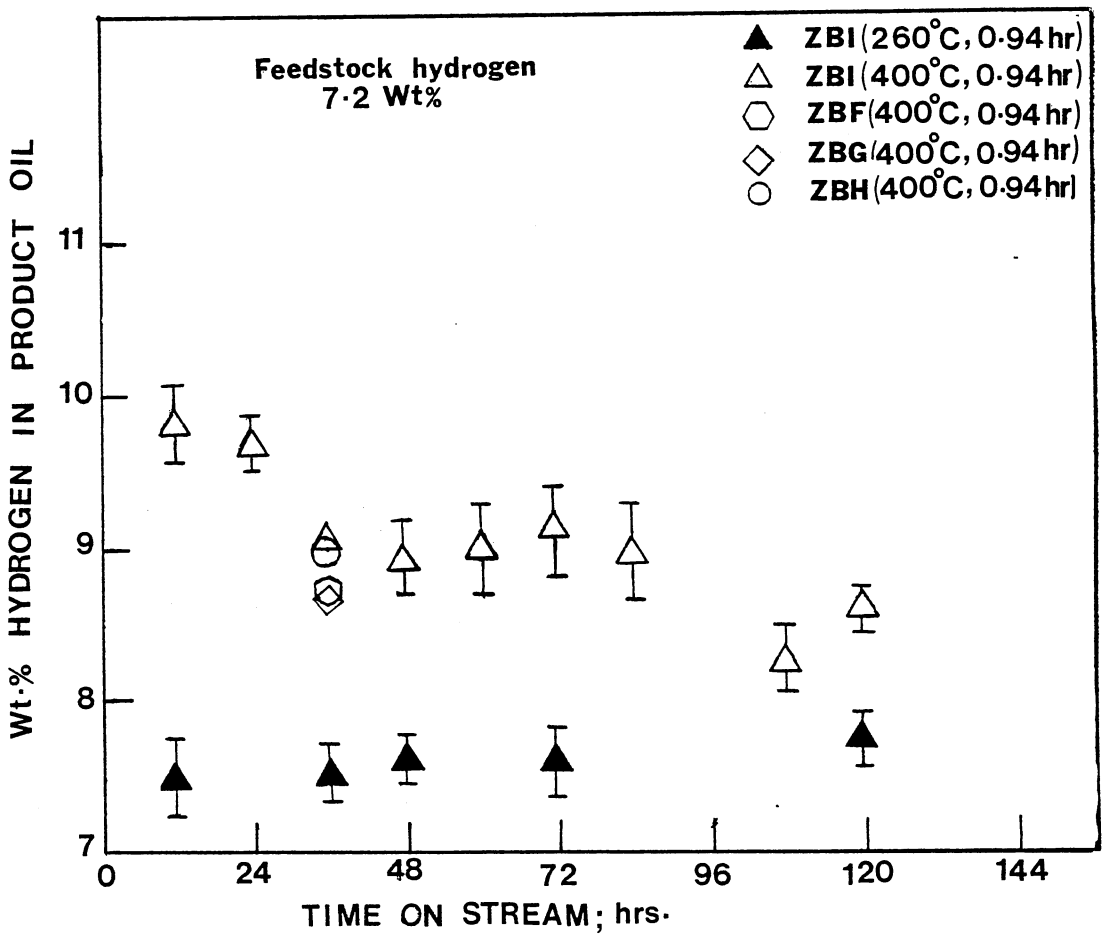

Figure 29. Product Liquid Hydrogen Content as a Function of Time on Stream for Run ZBI

observed for the low temperature product samples (see Figure 29).

The low temperature catalytic reactor was installed primarily to remove the inorganic constituents and coke precursors from the coal liquid. Olefins and diolefins are considered to be active coke precursors, their saturation would reduce the overall coke deposition. Lack of hydrogen present in liquid feedstock has also been cited to be responsible for excessive catalyst coke deposition. Increase in the saturation of naphthalene in the low temperature reactor would make more hydrogen available for saturation of the cracked molecules in the high temperature reactor (hydrogen donated by tetralin formed by naphthalene saturation). No decrease in the coke content of the catalyst in the high temperature reactor zone of Run ZBI was, however, noticed (see Table X). The hydrogen content of the product liquid samples from Run ZBI (overall sample) decreased with increase in time of oil-catalyst contact, signifying catalyst deactivation.

This section on liquid sample elemental analysis can be summarized as follows:

1. Both the small and the large pore diameter catalysts lost substantial hydrodenitrogenation and hydrogenation activity during the 240 hours of oil-catalyst contact. The catalyst lost activity rapidly during the first twelve to thirty-six hours of oil-catalyst contact; the activity loss was gradual over the remaining time. The initial catalyst activity was high during the first twelve hours of oil-catalyst contact for all catalysts and catalyst combinations tested.

2. The small pore diameter catalyst removed consistently more nitrogen from the feedstock compared to the large pore diameter catalyst. The larger surface area available to the reacting molecules in the small pore diameter catalyst may be responsible for their higher hydrotreating activity.

3. The small pore diameter catalyst maintained their hydrodenitrogenation activity longer than the large pore diameter catalyst. The unique, narrow pore size distribution of the small pore diameter catalysts may be responsible for its lower deactivation rate. The small pores selectively exclude the large molecular species and hence result in lower coke deposition and higher activity maintenance.

4. The composite catalyst bed did not show any improvement in the hydrodenitrogenation or the hydrogenation activity; the nitrogen content of the product liquid samples was intermediate between the responses of the single catalyst beds.

5. For the two temperature zones reactor bed experiment, no hydrodenitrogenation occurred in the low temperature reactor (260°C). The hydrogen content of the product liquid samples increased slightly from 7.26 wt% to 7.61 wt%. The overall bed HDN activity showed an improvement over the single catalyst beds operating under similar processes conditions. The catalysts in the high temperature reactor lost significant HDN and hydrogenation activity over the run duration.

Solvent and Distillation Residue Analysis

In this study, asphaltenes have been defined as the n-pentane insoluble and ethyl acetate soluble fractions. The n-pentane insoluble

fraction represents the asphaltenes, preasphaltenes, and tetrahydrofuran (THF) insolubles present in the coal liquid. During hydrotreatment, some of the n-pentane insolubles are converted to n-pentane soluble (resins and oils) fractions. The extent of hydrotreatment can be judged by the weight fraction of n-pentane insolubles remaining in the product liquid, also the change in the elemental content of these fractions reveals information about their hydrotreatment.

The forward sequential method discussed in Appendix F, where the liquid samples are separately treated with n-pentane, ethyl acetate, and THF, was used during this study. The residue fractions were analyzed for their elemental composition. Table XXIII presents the elemental composition of the various fractions precipitated from the feedstock used during the present study (15% SRC/Process Solvent). The hydrogen concentration in the precipitated residues decreased from 5.96 wt% in n-pentane insolubles to 4.40 wt% in THF insolubles; the nitrogen concentration decreased from 2.25 wt% in n-pentane insolubles, to 1.85 wt% in THF insolubles.

Only some of the product liquid samples were analyzed for ethyl acetate, and THF insoluble content. The concentration of the THF insolubles remaining in the product oils was very low. The ethyl acetate insoluble fractions represent the preasphaltene and the n-pentane insolubles present in the product liquid; the THF insolubles represent the ash and the undissolved coal fractions. Table XXIV presents a comparison of ethyl acetate insolubles in the product liquid samples from Run ZBF (large pore catalyst) and Run ZBG (small pore catalyst). The product liquid ethyl acetate insoluble content decreased from 6.4 wt% to 0.50 wt% for Run ZBF, and to 0.97 wt% for Run ZBG (12 hours

TABLE XXIII

FEEDSTOCK SOLVENT FRACTIONS* ELEMENTAL ANALYSIS
(15 Wt.% SRC/PROCESS SOLVENT)

	Wt. %		
	n-Pentane Insolubles	Ethyl Acetate Insolubles	THF Insolubles
Amount of Feed	22.1	6.4	1.0
Elemental Analysis			
C	81.30	80.10	64.55
H	5.96	4.84	4.40
N	2.25	2.15	1.85
S	0.56	0.61	0.60
O/Ash	Balance	Balance	Balance
H/C Atomic Ratio	0.88	0.72	0.82
N/C Atomic Ratio	0.024	0.023	0.025

*n-Pentane Insolubes = Asphaltenes + Preasphaltenes + THF Residues

Ethyl Acetate Insolubles = Preasphaltenes + THF Residues

THF Insolubles = Undissolved coal and ash

TABLE XXIV

COMPARISON OF ETHYL ACETATE INSOLUBLES FOR THE LARGE AND THE SMALL PORE CATALYSTS (RUN ZBF AND ZBG)

Sample Number	Space Time (Hours)	Hours on Oil	Temperature °C	Wt.% Ethyl Acetate Insolubles	
				Large Pore Catalyst (Run ZBF)	Small Pore Catalyst (Run ZBG)
Feedstock				6.39	6.39
#1	1.87	12	400	0.50	0.97
#3	1.87	36	400	0.45	0.87
#4	0.94	43	400	2.62	3.27
#5	1.34	50	400	2.11	2.31
#6	1.34	57	375	1.93	2.13
#7	1.87	67	375	1.74	1.94
#8	0.94	74	375	4.66	--
#9	0.94	81	350	6.20	6.29
#10	1.34	88	350	--	3.83
#11	1.34	96	350	--	2.76
#12	1.87	108	400	0.63	0.94
#14	1.87	132	400	--	--
#16	1.87	156	400	--	--
#18	1.87	180	400	--	--
#20	1.87	204	400	--	--
#22	1.87	228	400	--	--
#23	1.87	240	400	0.77	1.03

of oil-catalyst contact). The product liquid ethyl acetate insoluble content showed no significant variation during the subsequent run duration for Run ZBG (small pore catalyst). The ethyl acetate insoluble content of Run ZBF (large pore catalyst), however increased from 0.50 wt% to 0.77 wt% (54 % increase) during the 228 hours of oil-catalyst contact. The preasphaltene and the THF fractions(ethyl acetate insolubles) seem to be excluded from the small pore diameter catalyst interior (Run ZBG), the preasphaltene conversion probably occurs due to the thermal reactions outside the catalyst pores. The large pore diameter catalyst (Run ZBF) reduced the ethyl acetate insoluble consistently lower than the small pore catalyst (see Table XXIV) representing greater catalyst interaction between the large catalyst pores and the preasphaltene and THF insoluble fractions.

Table XXV presents the n-pentane insolube content of the product liquid samples from Run ZBF (large pore catalyst); the elemental content of the residues is also shown. No relation between the nitrogen content of the product liquid n-pentane insoluble residues and the process severity was noticed. The nitrogen content of the n-pentane insolubles in the feedstock constituted approximately 44% of the total nitrogen content. For the product liquid samples, the total nitrogen content in n-pentane insolubles constituted only 14 wt% of the total nitrogen present in the product liquid samples, the remaining nitrogen was contained in the oils and resins fraction (12 hour of oil-catalyst contact). During the 240 hours of oil-catalyst contact, the fraction of nitrogen contained in the n-pentane insolubles decreased to nine weight percent, indicating catalyst deactivation to affect the nitrogen removal

TABLE XXV

N-PENTANE INSOLUBLE ELEMENTAL ANALYSIS
(LARGE PORE CATALYST, RUN ZBF)

Sample Number	LVHST hrs.	Hours on Oil	Temperature °C	Wt. % n-Pentane Insolubles	Wt.% N	Wt.% C	Wt.% H
Feedstock				22.2	2.25	81.3	5.96
ZBF # 1	1.87	12	400	3.0	1.41	80.4	5.73
# 3	1.87	36	400	3.1	1.65	90.6	6.15
# 4	0.94	43	400	7.5	1.77	83.3	5.89
# 5	1.34	50	400	6.1	1.98	78.5	6.27
# 6	1.34	57	375	11.6	1.83	82.8	6.68
# 7	1.37	67	375	9.9	1.69	82.2	6.73
# 8	0.94	74	375	14.3	1.98	84.1	6.41
# 9	0.94	81	350	19.7	1.77	81.8	6.34
#10	1.34	88	350	15.8	N.A.	N.A.	N.A.
#11	1.87	96	350	15.3	N.A.	N.A.	N.A.
#12	1.87	108	400	4.6	1.65	84.8	6.21
#16	1.87	156	400	4.2	1.52	73.4	5.31
#20	1.87	204	400	4.04	1.53	81.1	5.71
#22	1.87	228	400	4.10	N.A.	N.A.	N.A.
#23	1.87	240	400	5.0	1.50	75.7	5.77

activity from the resins and oils fraction more severely. Ideally, all the nitrogen contained in the resins and oils should have been removed (small molecular size of resin and oil fraction). In actual practice, however, catalysts deactivation decreased the number of active sites available to the diffusing molecules, thereby, reducing the overall nitrogen removal activity.

Table XXVI presents the n-pentane insoluble residue content and elemental analysis of liquid samples from Run ZBG (small pore catalyst). The n-pentane insoluble content increases by 70 wt% during the 240 hours of oil-catalyst contact. The nitrogen content of the n-pentane insolubles decreased from 2.25 wt% in the feedstock to 1.58 wt% in the product liquid samples (400°C, 1.87 hrs LVHST, 12 hours). Here too, as in Run ZBF, no definite relation was observed between the elemental composition of the n-pentane insolubles and the hydrotreating severity. Only 13% of the product nitrogen content was contained within the n-pentane insoluble fractions (sample taken after 12 hours), the remaining fraction being contained in the oils and resins fraction. For the oil samples collected after 108 hours of oil-catalyst contact, only 10% of the product nitrogen was contained in the n-pentane insoluble fraction. This observation is consistent with the observation made for the large pore catalyst, where greater decrease in the activity of the catalyst occurred for removing nitrogen from the resins and oil fractions (n-pentane soluble fractions).

For the three experimental runs: ZBF, ZBG, and ZBH, Figure 30 presents the n-pentane insoluble content as a function of the hours of oil-catalyst contact. The small pore diameter catalyst (Run ZBG) consistently reduced the n-pentane insoluble content lower than the

TABLE XXVI

N-PENTANE INSOLUBLE ELEMENTAL ANALYSIS
(SMALL PORE CATALYST, RUN ZBG)

Sample Number	LVHST hrs.	Hours on Oil	Temperature °C	Wt.% n-Pentane Insolubles	Wt.% N	Wt.% C	Wt.% H
Feedstock				22.2	2.25	81.3	5.96
ZBG # 1	1.87	12	400	2.30	1.68	68.22	5.79
# 3	1.87	36	400	2.95	1.73	81.99	5.55
# 4	0.94	43	400	6.36	1.66	67.10	5.71
# 5	1.34	50	400	4.82	1.97	80.21	5.57
# 6	1.34	57	375	7.65	1.71	73.48	6.03
# 7	1.87	67	375	7.20	--	--	--
# 8	0.94	74	375	11.54	1.71	70.04	6.07
# 9	0.94	81	350	13.93	2.13	78.67	6.52
#10	1.34	88	350	12.14	1.99	77.04	6.22
#11	1.87	96	350	10.21	1.79	72.63	6.22
#12	1.87	108	400	3.24	1.70	73.05	5.61
#14	1.87	132	400	3.02	--	--	--
#16	1.87	156	400	3.67	--	--	--
#18	1.87	180	400	4.46	--	--	--
#20	1.87	204	400	3.85	1.42	75.72	6.05
#22	1.87	228	400	3.58	--	--	--
#23	1.87	240	400	3.88	1.66	69.91	6.60

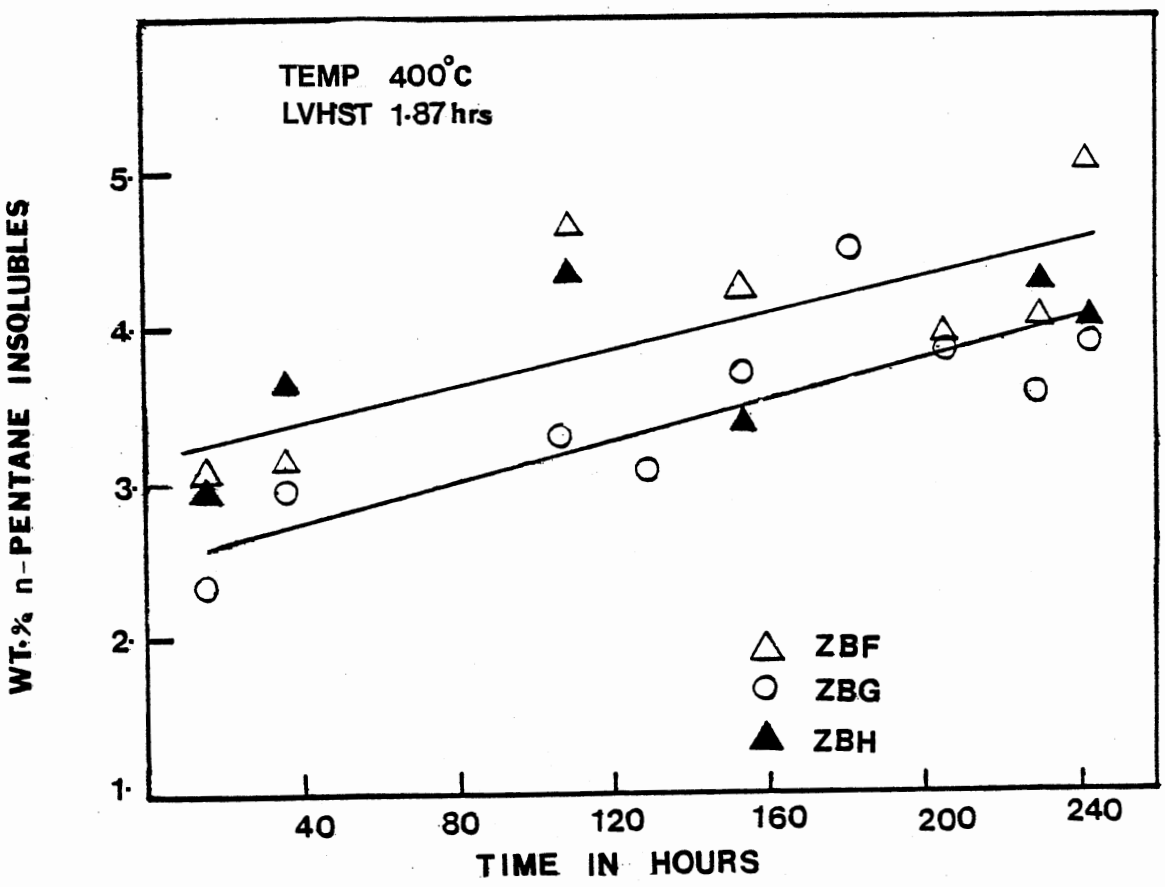

Figure 30. N-pentane Insoluble Activity Decay With Time on Stream for Run ZBF, ZBG, and ZBH

large pore diameter catalyst (Run ZBF). For both the small and the large pore catalysts, deactivation in the n-pentane insoluble reduction activity was noticed. Two linear regression lines have been drawn to represent the general deactivation trend. The composite catalyst bed (Run ZBH), too, lost significant n-pentane reduction activity during the run duration. The n-pentane insoluble content for the composite catalyst bed (Run ZBH) was intermediate between the responses of the large, and the small pore catalysts; no advantage in the removal of n-pentane insolubles was observed.

Figure 31 presents the n-pentane insoluble content of the product liquid samples from Run ZBI (two temperature zone experiment) as a function of the time on stream. The liquid volume hourly space time (LVHST) in each reactor was maintained at 0.94 hrs., the combined LVHST for the two reactors being 1.87 hrs. The n-pentane insoluble content increased from 4.7 wt% to 6.25 wt% during the 120 hours of oil-catalyst contact. The intermediate liquid samples from the top reactor could not be analyzed due to the very small liquid samples available. The n-pentane insoluble content for Run ZBF and ZBG at 400°C temperature, 0.94 hours LVHST, and 48 hours of oil-catalyst contact time, are also shown in Figure 31. The n-pentane insoluble content for Run ZBI (two temperature catalyst zones) was considerably lower than for both Run ZBF (large pore catalyst) and Run ZBG (small pore catalyst); 4.8 wt% n-pentane insoluble content for Run ZBI, compared to 6.3 and 6.1 wt% for Run ZBF and ZBG, respectively. This phenomenon is consistent with the observation made for the nitrogen content of the product liquid samples. It seems that pretreating the feed at 260°C in the guard bed has a beneficial effect on the

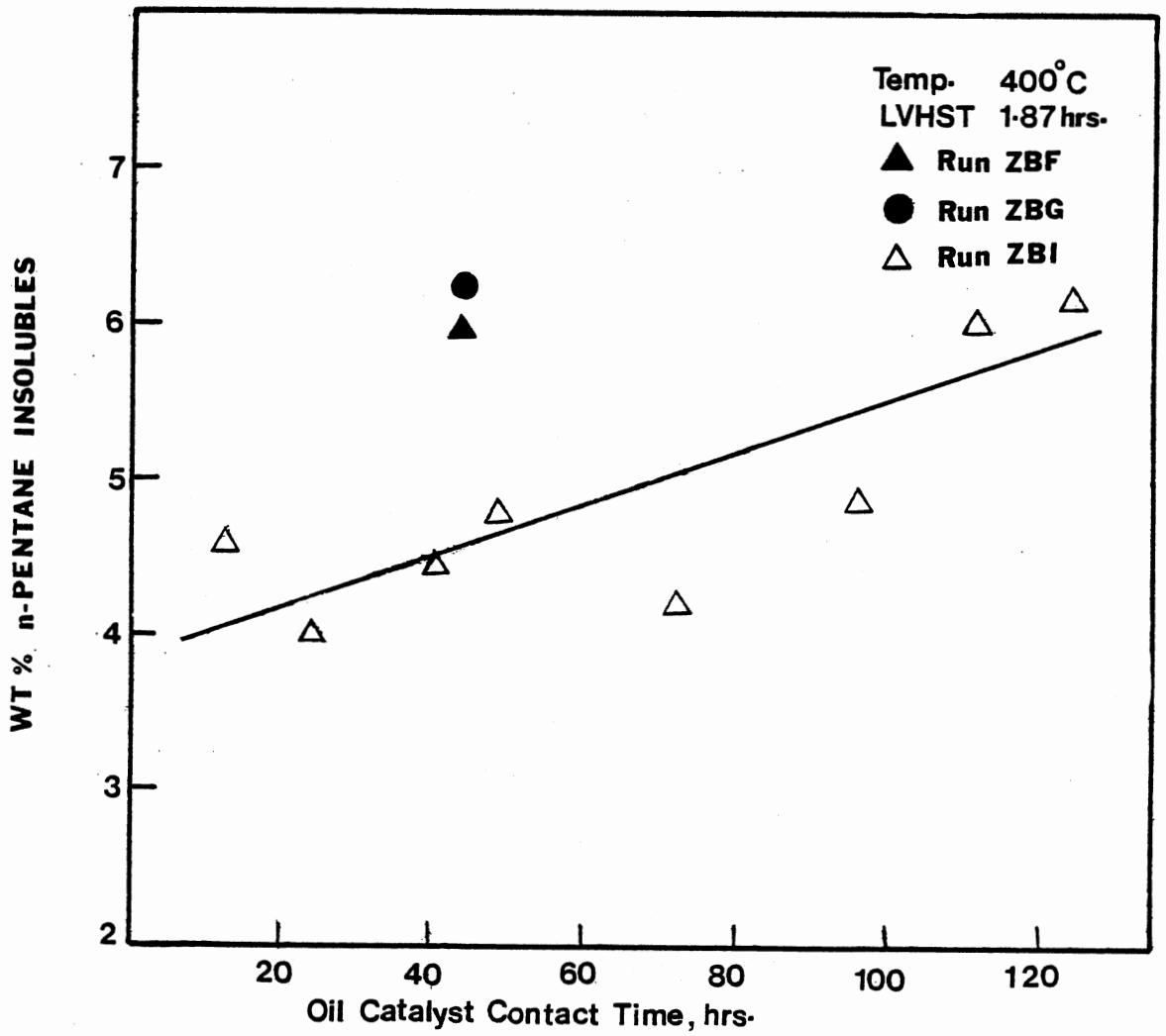

Figure 31. Product Liquid n-Pentane Insoluble Content as a Function of Time on Stream (Run ZBI)

hydrotreatment activity, however, no such advantage is observed in catalyst coking tendency for both the low temperature and high temperature reactor beds.

The product liquid n-pentane insoluble content (asphaltenes + preasphaltenes + THF insoluble) showed a strong dependence on the process temperature and LVHST. Figures 32, 33 and 34 present the dependence of the n-pentane insoluble content on temperature and LVHST for Runs ZBF, ZBG, and ZBH respectively. The higher temperatures and space times (higher process severity) favor higher conversion of n-pentane insolubles to oils and resins. At a LVHST of 1.87 hrs, the n-pentane insoluble content decreased from 15.5 wt% to 3.2 wt% (large pore catalyst, Run ZBF) for a temperature increase from 350 to 400°C Similarly, for Run ZBG (small pore catalyst), the n-pentane insoluble content decreased from 10.2 wt% to 3.1 wt% for a temperature increase from 350 to 400°C (LVHST of 1.87 hrs.).

In addition to the solvent residue determination, some liquid samples were vacuum distilled according to the ASTM D-1160 procedure. The liquid samples were separated into two fractions: liquids boiling below 454°C, and solids boiling above 454°C. The weight of the solid fraction was measured and referred to as "454 C^+ residue fraction". The solid residues are representative of the asphaltene, preasphaltene, and THF insoluble content of the liquid samples. The feedstock used during this study contained 20.4 wt% 454 C^+ residues. The distilled liquids and the residue solids were subjected to elemental analysis to determine the distribution of N, C and H in the two fractions.

Figure 35 presents the wt% 454 C^+ residues present in the product liquid samples as a function of the process temperature for Run ZBF

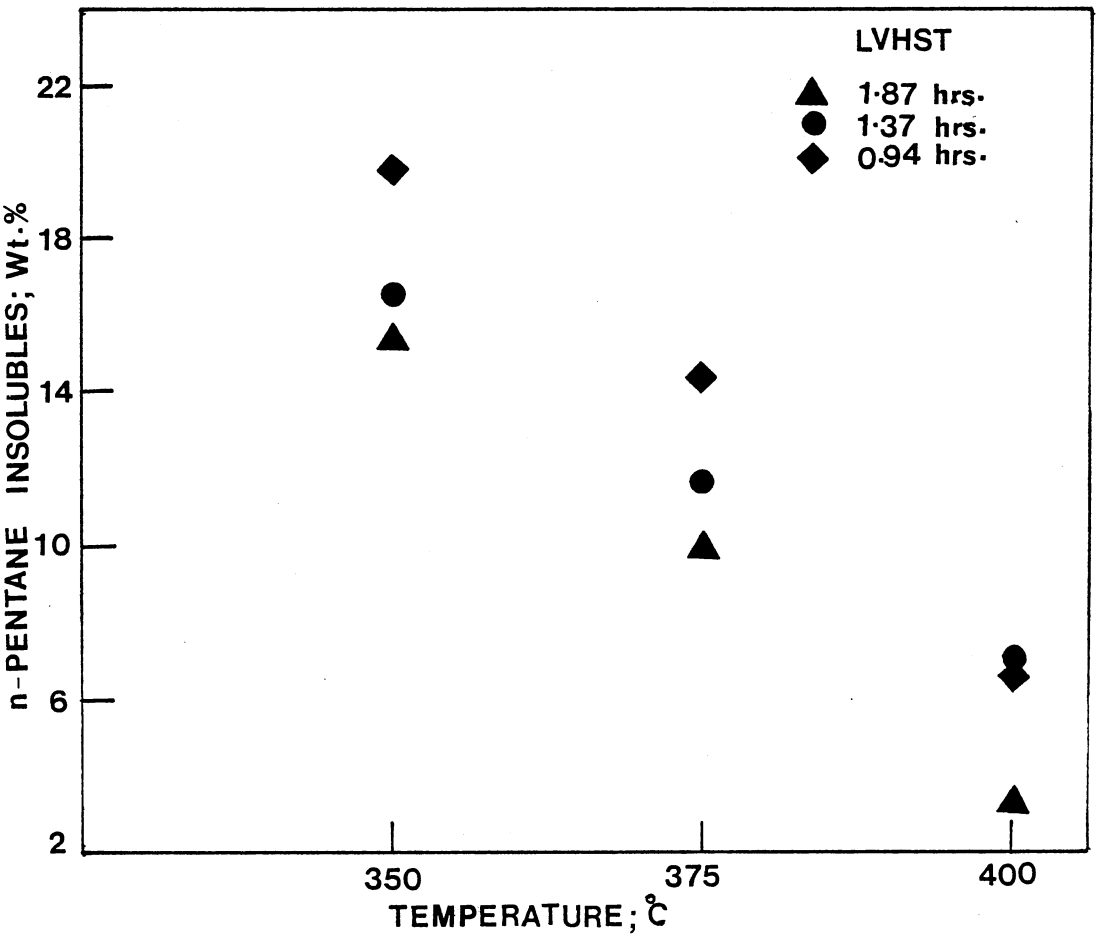

Figure 32. Effect of Process Temperature and LVHST on n-Pentane Insoluble Content for Run ZBF (Lare Pore Catalyst)

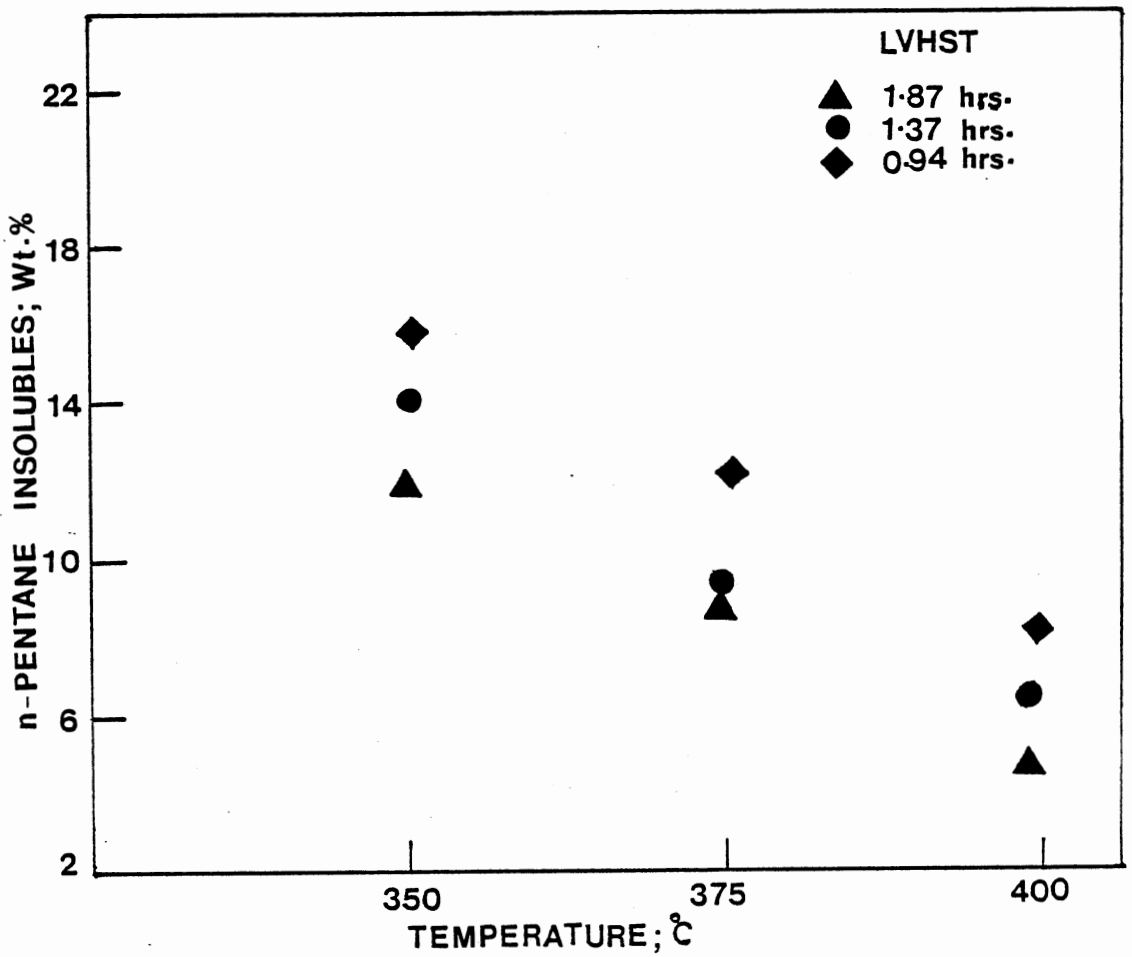

Figure 33. Effect of Process Temperature and LVHST on n-Pentane Insoluble Content for Run ZBG (Small Pore Catalyst)

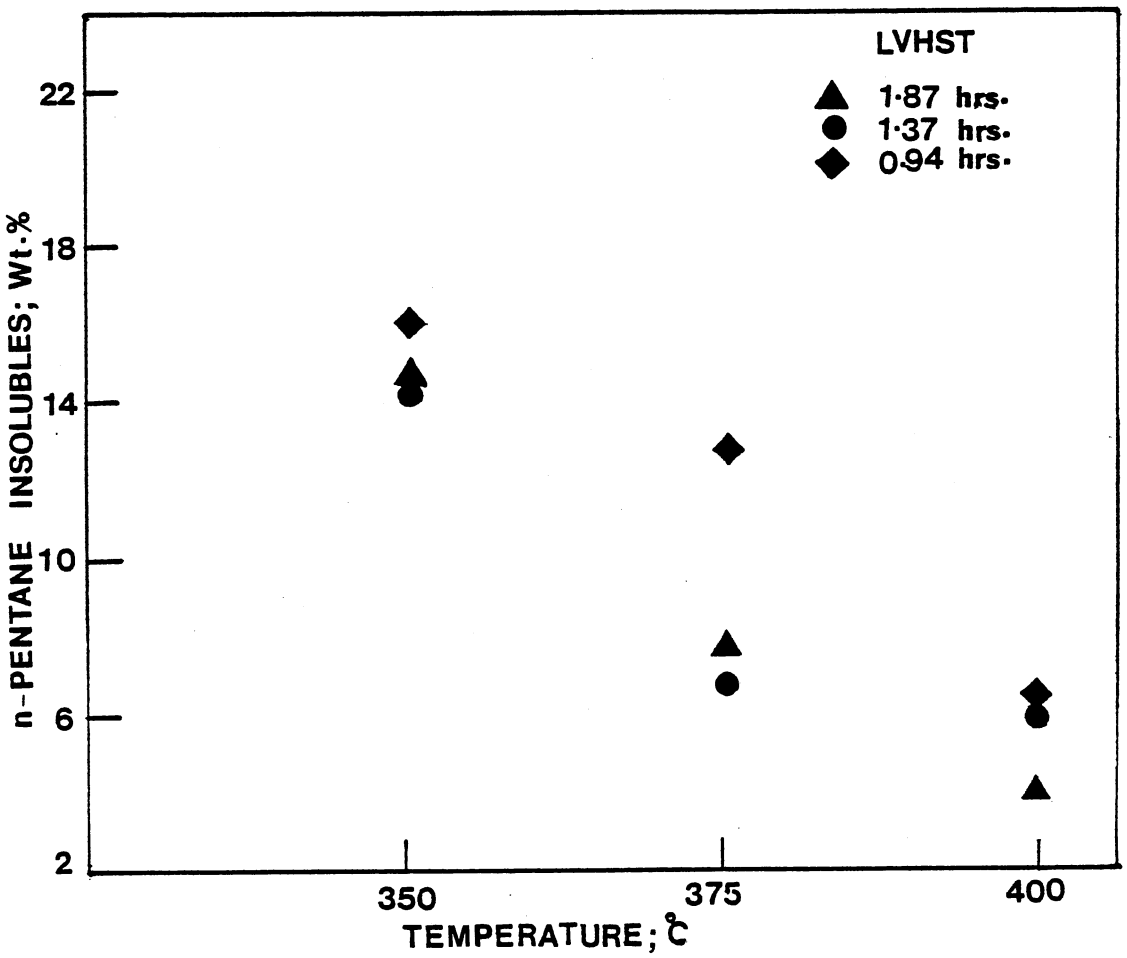

Figure 34. Effect of Process Temperature and LVHST on n-Pentane Insoluble Content for Run ZBH (Composite Catalyst Bed)

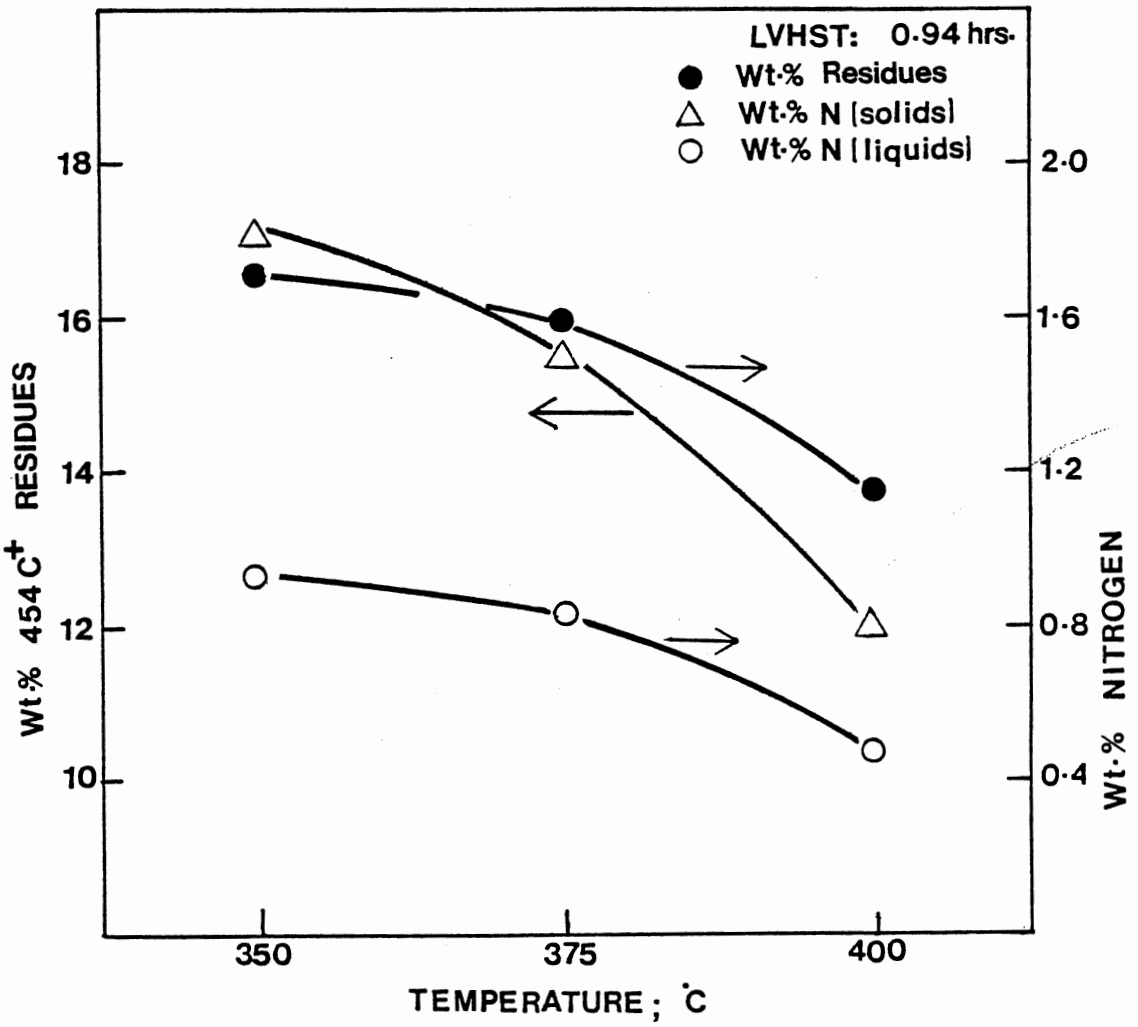

Figure 35. Effect of Process Temperature on 454 C^+ Residue Content for Run ZBF (Large Pore Catalyst)

(large pore catalyst). Greater reduction in 454 C^+ residues occurred when the temperature was increased from 375 to 400°C than for temperature increase from 350 to 375°C. This can be attributed to greater increase in cracking, hydrocracking, and hydrogenation activity for temperature increase from 375 to 400°C than for 350 to 375°C. The wt% N present in the 454 C^+ residues and the distilled liquids as a function of the process temperature is also present in Figure 35. The wt% nitrogen present both in the liquids and the 454 C^+ residues decreased with increase in the process temperature. The nitrogen content of the distilled liquids decreased by 43 wt% for an increase in temperature from 375 to 400°C (0.94 hr LVHST). Similarly, a 28 wt% reduction in the nitrogen content of the 454 C^+ residues was observed.

Figure 36 presents the effect of process temperature on the 454 C^+ residues for Run ZBG (small pore catalyst). The nitrogen content of the residues and the distilled liquid fractions is also presented. Consistent with the observation made for the large pore catalyst (Run ZBF), the 454 C^+ residue content for the small pore catalyst (Run ZBG) decreased more drastically for the temperature increase from 375 to 400°C, than for 350-375°C. The nitrogen content of the distilled liquids decreased gradually with increase in temperature, the nitrogen content of the 454C^+ residues also showed a decrease in nitrogen content with increase in process severity.

The composite catalyst bed (Run ZBH) showed a similar dependence on the process temperature as did the single catalyst beds (Runs ZBF and ZBG). The 454 C^+ residues decreased from 18.09 to 16.3 wt% for a temperature increase from 350 to 375°C, and to 13.23 wt% for temperature increase from 375 to 400°C. Consistent with the results of

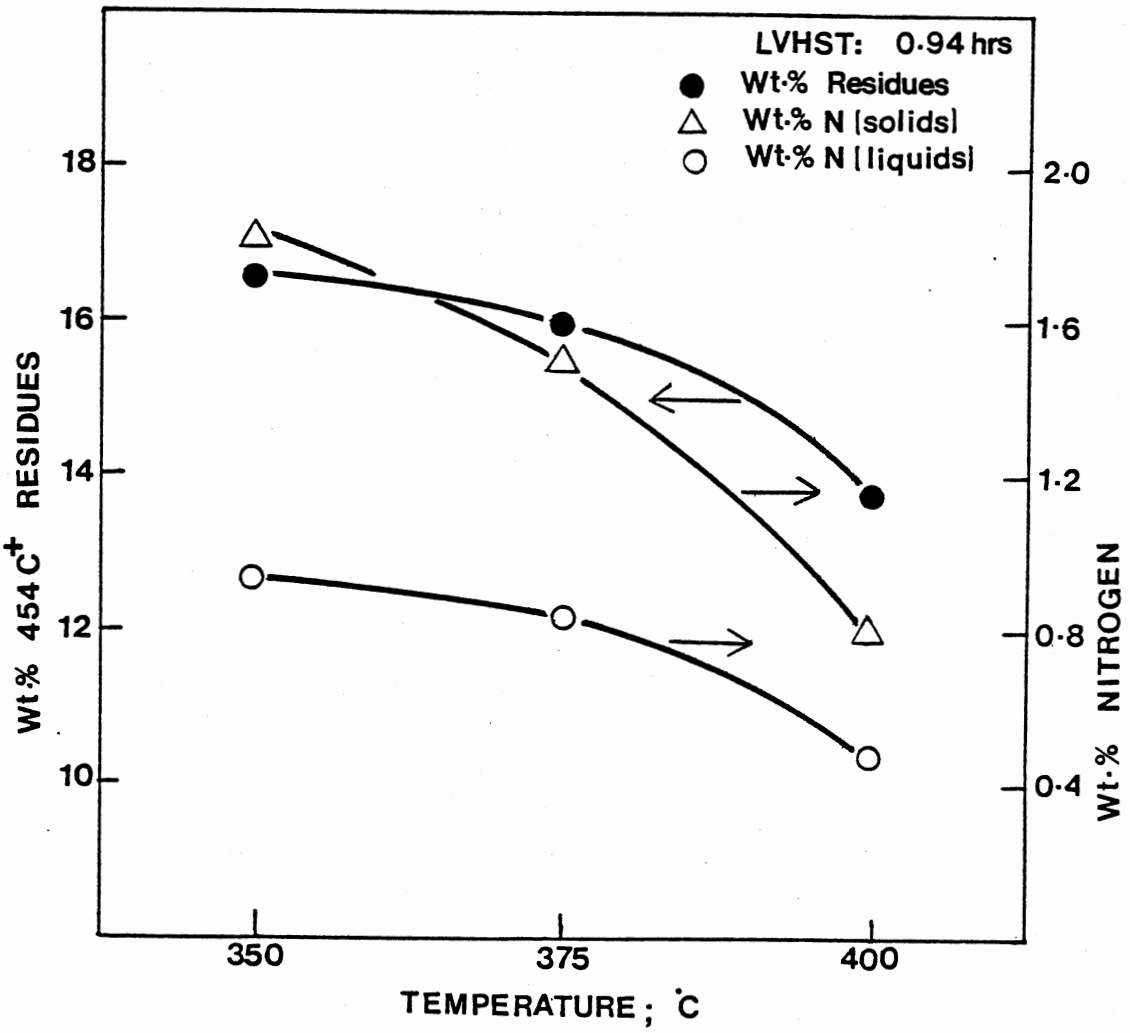

Figure 36. Effect of Process Temperature on 454 C^+ Residue Content for Run ZBG (Small Pore Catalyst)

experimental Run ZBF and ZBG, the N content of the residues from Run ZBH decreased with increase in temperature. Table XXVII summarizes the elemental analysis of the distilled liquids and 454 C^+ residues from Run ZBH. The nitrogen content of both the distilled liquids, and the 454 C^+ residues increased with catalyst age, this being consistent with the behavior of the single catalyst beds.

Figure 37 presents a comparison of the wt% 454 C^+ residues present as a function of time on stream for experimental Runs ZBF (large pore catalyst), ZBG (small pore catalyst) and ZBH (composite catalyst). Linear regression lines have been drawn to represent the deactivation trend. The catalyst deactivation increased the product liquid 454 C^+ residue content. For Run ZBF, the wt% 454 C^+ residue content increased from 9.05 wt%, at 12 hours of oil-catalyst contact time, to 12.52 wt% for 240 hours. The gradual increase in the 454 C^+ residues with catalyst age represents the catalytic nature of the 454 C^+ residue conversion. As can be seen from the two linear regression lines, the small pore diameter catalyst reduced the 454 C^+ residues consistently lower than the large pore diameter catalyst. It is also observed that the rate of deactivation of the 454 C^+ residue removal activity is higher for large pore catalyst compared to the small pore catalyst. This is consistent with the coke data presented in the earlier sections. The response of the composite catalyst beds for 454 C^+ residue reduction was consistent with the observations made for the n-pentane insoluble content for Runs ZBF, ZBG, and ZBH.

Figure 38 presents a comparison of the nitrogen content of the

TABLE XXVII

ELEMENTAL ANALYSIS OF DISTILLATION PRODUCTS FROM RUN ZBH (COMPOSITE CATALYST BED)

Sample Number	Distilled Liquid Wt.%			454 C^+ Residues Wt.%		
	N	C	H	N	C	H
ZBH #1	0.124	88.34	10.78	0.930	85.97	7.31
ZBH #2	0.366	88.79	9.55	1.075	75.28	6.87
ZBH #4	0.561	88.79	9.34	1.102	74.43	7.09
ZBH #8	0.709	88.69	8.89	1.310	71.21	6.37
ZBH #9	0.747	89.25	8.59	1.339	71.86	6.48
ZBH #13	0.461	89.69	9.09	1.010	70.17	6.64
ZBH #16	0.605	88.89	9.05	1.053	75.07	7.15
ZBH #23	0.657	88.16	9.12	1.085	72.46	6.57

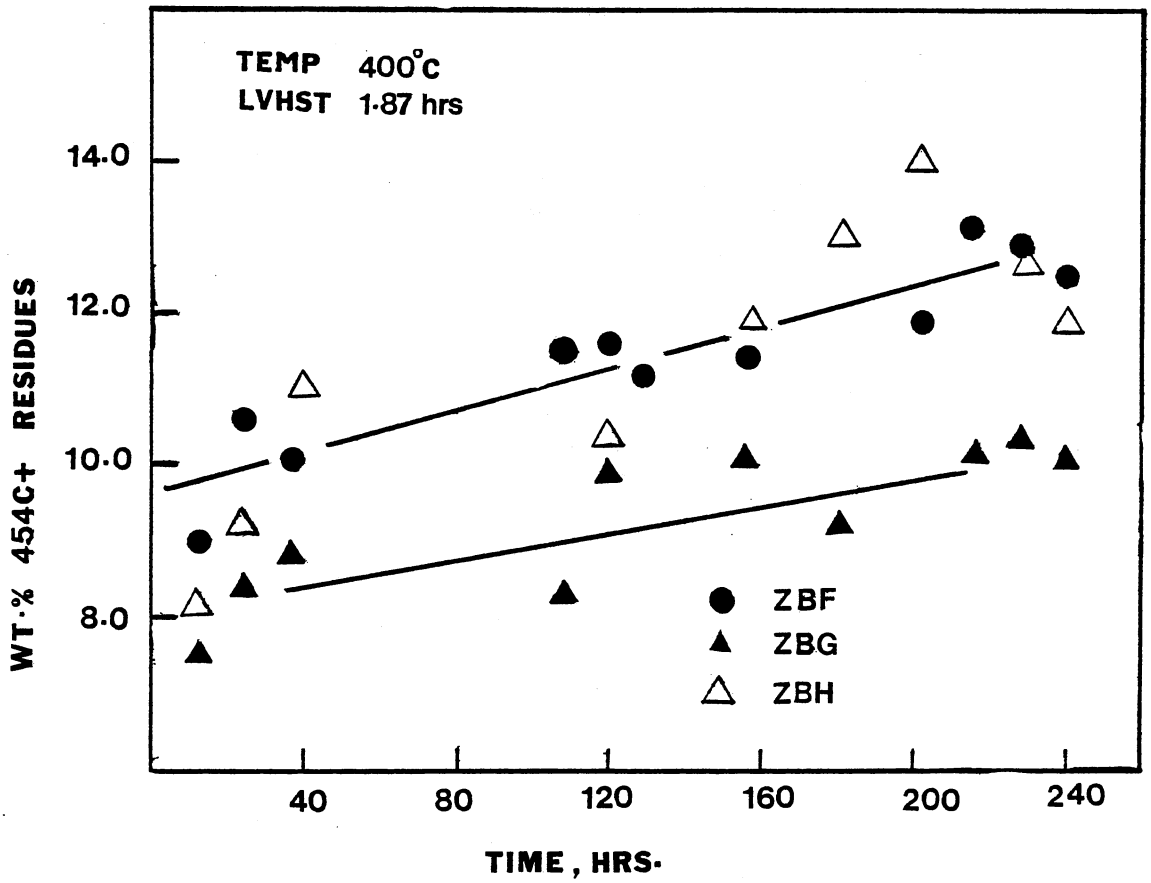

Figure 37. Comparison of 454 C^{+} Residues from Run ZBF, ZBG and ZBH as a Function of Time on Stream

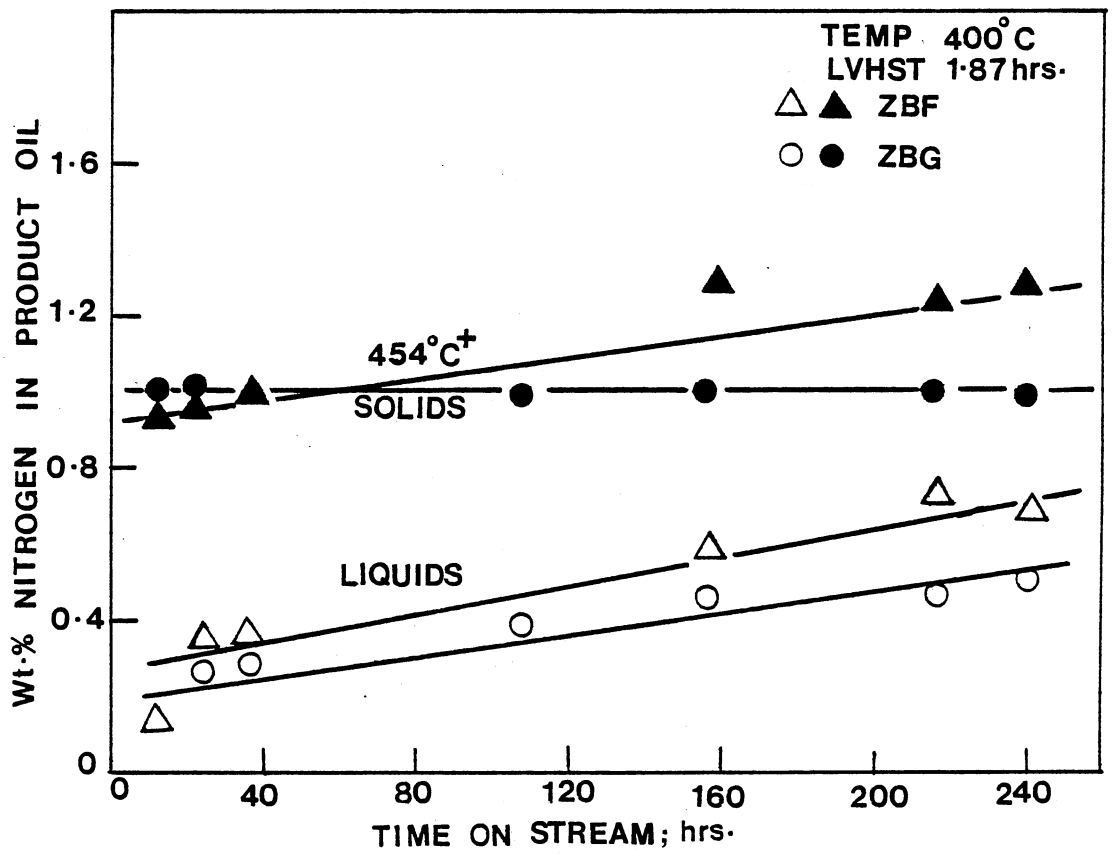

Figure 38. Effect of Process Temperature on 454 C^+ Residue Content for Run ZBF and ZBG

product distilled liquids and 454 C^+ residues from Runs ZBF and ZBG as a function of the time on stream. Note that the nitrogen content of the 454 C^+ residues from Run ZBG (small pore catalyst) did not show a significant change with the catalyst age. In comparison, the nitrogen content of the 454 C^+ residues for Run ZBF (large pore catalyst) increased with the catalyst age. The distilled liquid fraction from Run ZBG showed consistently lower nitrogen content compared to Run ZBF. This further strengthens our assumption of higher activity of the small pore catalysts. For the fraction of feedstock that diffuses into the catalyst interior, the small pore catalyst has a higher activity due to its larger surface area. For the small pore catalyst, the catalyst exclusion of the large molecular species is apparent due to negligible dependence of the residue nitrogen content on the catalyst age. For the large pore catalyst, the large sized molecules seem to enter the catalyst pore structure, and may be responsible for relatively higher coke deposition.

Figure 39 compares the wt% 454 C^+ residues content determined at 48 hours of oil-catalyst time, 400°C and 0.94 hours LVHST, for all the experimental runs. The residue content did not vary significantly, which is contrary to the observations made for the elemental and the solvent residue analyses. This lack of response may be due to the low precision of the 454 C^+ residue determination (8.5% deviation). The intermediate liquid samples from Run ZBI could not be subjected to ASTM D-1160 distillation because of insufficient quantities of liquid available. Figure 39 also shows the 454 C^+ residue content for Run ZBI (two temperature catalyst zones) as a function of the

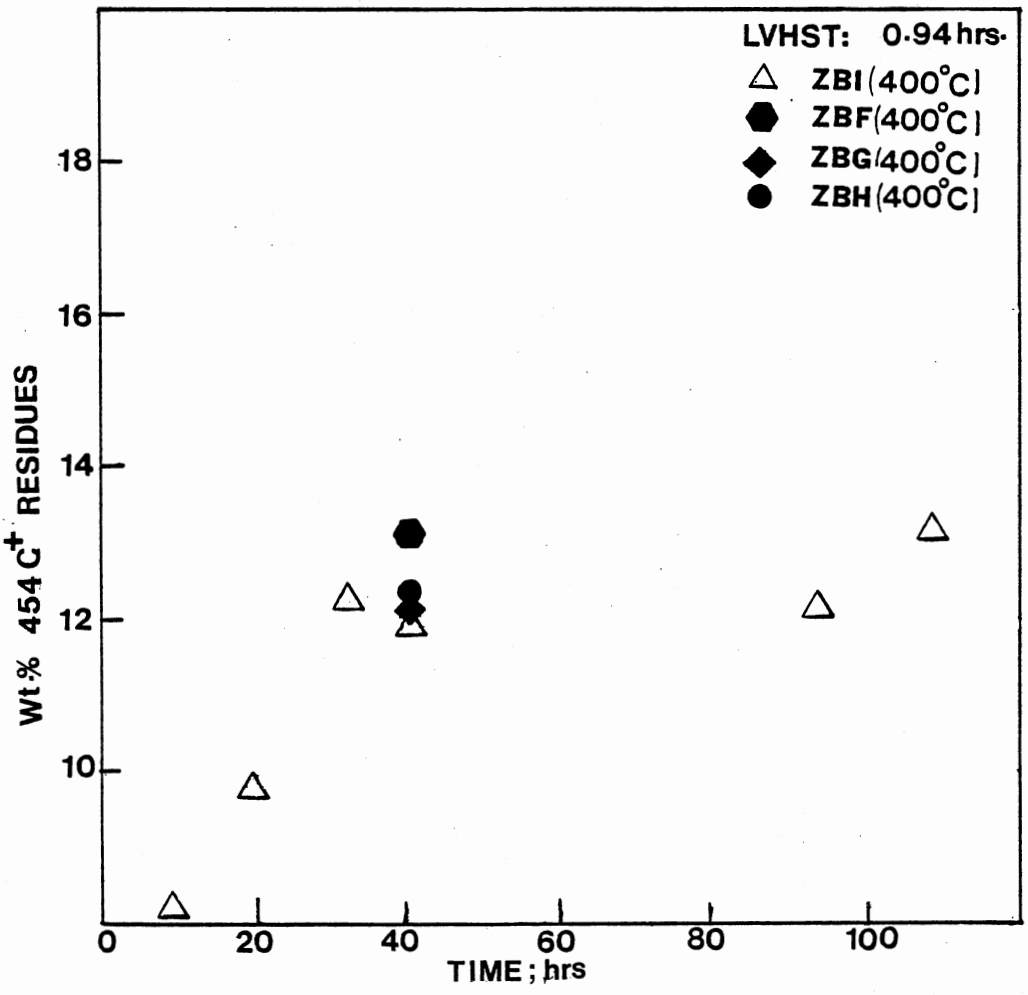

Figure 39. Wt.% 454 C^{+} Residues as a Function of Time on Stream for Run ZBI (Two Temperature Reactor Zones)

time on stream. The 454 C^+ residues showed a strong dependence on catalyst age. The wt% residues increased from 7.76 to 13.23 wt% during the 108 hours of oil-catalyst contact.

The 454 C^+ residues represent the high boiling fractions present in the feedstock. Approximately 40 wt% reduction in the 454 C^+ residue content occurred due to hydrotreating at 400°C. The large molecular species, which mainly compose the 454 C^+ residues hydrogenate, hydrocrack, and crack under the combined thermal and catalytic action; hydrotreating reduces the feedstock residue content according to the following general scheme (not meant to be suggestive of any mechanism).

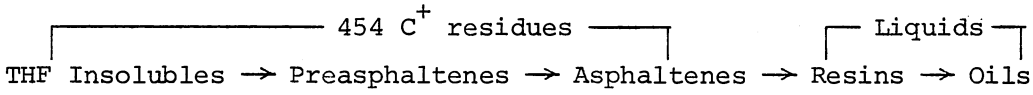

The 454 C^+ residues are mainly composed of the THF insolubles, preasphaltenes, and asphaltenes; the liquid fraction being composed of the oils and resins. For the small pore catalyst, the ethyl acetate insolubles, which represent 6.4 wt% of the feedstock, are selectively excluded from the catalyst interior. This fraction represents the preasphaltene and the THF insoluble fraction. The resins and oils, which compose the other 74 wt% of the feed, can freely enter the catalyst interior. For the large pore catalyst, all the fractions (THF insolubles, preasphaltenes, asphaltenes, resins and oils) can enter the catalyst interior. The small pore catalyst has a higher activity due to its larger surface area, thus larger conversion of the resins and asphaltenes to oils occurs. Some of the preasphaltene fractions crack external to the catalyst, thereby augmenting the activity of the small pore catalysts.

One can conclude that the selection of a hydrotreating catalyst

should depend mainly on the feedstock characteristics (solvent residue and heteroatom content). The surface area of the catalyst must be maximized keeping the catalyst pore diameter large enough to allow unhindered diffusion of the asphaltenes, resins and oils. Stronger pore diffusion resistance to the movement of the large molecular species (organometallic, THF insolubles, preasphaltenes) is highly desirable. Considerable study needs to be conducted to determine the size of the various molecular species present in the coal liquid at process conditions to arrive at the most optimum catalyst pore size. The concept of composite catalysts is a step in the right direction, it allows different catalyst pore sizes in a single catlaytic bed, thereby, improving the bed versatility. Removal of the THF insolubles, and organometallic in the top reactor section, with very large catalyst pores (>300 Å), and subsequent hydrotreatment over a small pore diameter, high surface area catalyst is highly recommended.

This section on product liquid asphaltene and 454 C^+ residue analysis can be summarized as follows:

1. The ethyl acetate insoluble fraction, representing the preasphaltene and the THF insoluble fractions present in the product liquid , increased with catalyst age for the large pore diameter catalyst. For the small pore diameter catalyst, the preasphaltene content remained constant. The large pore diameter catalyst reduced the preasphaltene content of the product liquid samples consistently lower than the small pore diameter catalyst.

2. The product liquid n-pentane insoluble content (asphaltene, preasphaltene and THF insoluble fraction) showed a strong dependence on catalyst age, process temperature, and LVHST for both the small and large pore diameter catalyst.

3. The small pore diameter catalyst reduced the n-pentane insoluble content consistently lower than the large pore diameter catalyst. Both catalysts lost significant n-pentane reduction activity over the run duration.

4. No advantage in the reduction of the n-pentane insolubles was noticed for the composite catalyst bed.

5. Deactivation in the n-pentane removal activity was also noticed for the two temperature reactor zone bed experiment. This reactor bed combination exhibited higher n-pentane insoluble reduction capacity compared to the other experimental runs conducted under similar conditions.

6. The 454 C^+ residues showed a strong dependence on the catalyst age, process temperature and LVHST. The small pore diameter catalyst reduced the residue content consistently lower than the large pore diameter catalyst.

7. The nitrogen content of the 454 C^+ residues decreased with process severity. The most refractory of the 454 C^+ residue fractions remained in the product liquid samples. The nitrogen content of these fractions remained constant with the increase in catalyst age for the small pore diameter catalysts. For the large pore diameter catalysts, the nitrogen content of the 454 C^+ residues showed a strong dependence on the catalyst age, signifying that the most refractory of the 454 C^+ residues do not enter the small pore catalyst pore structure.

8. The two temperature reactor zone experiment did not show any improvement in the 454 C^+ residue reduction activity.

CHAPTER IX

MATHEMATICAL MODELING

In the literature, hydrodenitrogenation (HDN) kinetics has been modeled using both the power-law model and complicated intrinsic kinetic models. The power law model represents the overall kinetics and not the intrinsic catalyst activity. The effect of the mass transfer resistances on the chemical reaction rate is lumped into an overall reaction rate constant. The simplicity of the global models makes them highly useful for design and scale-up of heterogenous catalytic reactors. The intrinsic reaction rate models, on the contrary, are complicated and usually suffer from the disadvantage of high uncertainty involved in the experimental determination of the liquid viscosity, bulk diffusivity, molecular weight, and tortuosity factor.

Global Kinetics

In this study, both the first and second order global reaction models were fitted to the nitrogen data. The nitrogen content data were determined for samples taken after 36 to 108 hours of oil-catalyst contact. The catalyst lost activity rapidly during the first 36 hours of oil-catalyst contact, but levelled off during the remaining run. The catalyst deactivation was represented by a catalyst decay constant, τ which was defined on the basis of the reaction rate

constant:

$$k = k_o e^{-t/\tau}$$

where k = actual reaction rate constant

k_o = reaction rate in absence of catalyst deactivation

τ = catalyst decay constant; hours

t = time of oil-catalyst contact; hours

Using a non-linear regression technique (Marquardt), the kinetic parameters: activation energy, frequency factor, catalyst decay constant were determined.

First-order Model:

$$C_i = C_{io} \cdot \exp.(-A_o \cdot \exp.(-E/RT) \cdot LVHST + t/\tau)$$

Second-order Model:

$$C_i = C_{io} \cdot \exp.(t/\tau)/(1 + A_o \cdot \exp.(-E/RT) \cdot LVHST)$$

where C_i = exit liquid concentration, i = nitrogen

C_{io} = inlet liquid concentration

E = activation energy; Kcals/kg-mole

R = gas constant; 1.9857 Kcal/kg-mole/°K

T = absolute temperature; °K

t = time of oil-catalyst contact; hours

τ = catalyst decay constant; hours

A_o = frequency factor

LVHST = liquid volume hourly space time; hours

The reaction rate constants based on reactor volume, catalyst surface area, and catalyst mass were determined as follows:

k_v (volume basis) = $A_o e^{-E/RT}$

k_s (surface area basis) = $k_v / S_i / \rho_B$

k_m (catalyst mass basis) = k_v / ρ_B

where S_i = catalyst surface area, cm^2/gm

ρ_B = bulk reactor catalyst density, gm/cm^3

k_v = reaction rate constant based on reactor volume

k_s = reaction rate constant based on catalyst surface area

k_m = reaction rate constant based on catalyst mass

The HDN data fit was excellent for the first-order model ($\pm$ 0.036 standard error), but considerable lack of fit existed for the second-order model ($\pm$ 0.108 standard error). Table XXVIII presents the activation energy, frequency factor, deactivation constants determined for the small and large pore diameter catalysts used during this study. The values of the reaction rate constants (reactor volume, surface area, and catalyst mass basis) are also presented. The deactivation constants (τ) for the large pore and the small pore diameter catalyst were determined to be 364 and 548 hours, respectively. The smaller catalyst deactivation constant for the large pore catalyst represents shorter active catalyst life.

The small pore diameter catalyst showed higher temperature dependency for HDN activity compared to the large pore diameter catalyst. The activation energy for the large pore diameter catalyst was determined to be 14,830 Kcals/kg-mole, the small pore activation energy was determined to be 23,502 Kcals/kg-mole. Activation energies for coal liquid HDN in the range of 10,000-35,000 Kcal/kg-mole have been reported for Ni-Mo-Al_2O_3 catalysts. Angevine (1979) reported the activation energy for HDN of 70% SRC over Mobil HCl-2 catalyst to be

TABLE XXVIII

RESULTS OF FIRST-ORDER MODEL FIT FOR HDN DATA

Model: $C_i = C_{io} \cdot \exp.(-A_o \cdot \exp.(-E/RT) \cdot LVHST + t/\tau)$

Run Series	Catalyst	Model Parameters			Temp.	First-Order Rate Constants		
		A_o	E (Kcal/kgmole)	τ (hr)	°K	k_v (hr^{-1})	k_s (cm/sec)	k_m ($gm/cm^3/sec$)
ZBF	HT-115 E (Large Pore)	3.0376×10^4	14,823.4	364	673	0.463	1.902×10^{-10}	2.378×10^{-4}
					648	0.297	1.221×10^{-10}	1.526×10^{-4}
					623	0.1903	0.7821×10^{-10}	0.978×10^{-4}
ZBG	KF-153 S (Small Pore)	2.540×10^7	23,502.3	548	673	0.562	0.923×10^{-10}	2.492×10^{-4}
					648	0.316	0.519×10^{-10}	1.402×10^{-4}
					623	0.137	0.226×10^{-10}	0.608×10^{-4}

19,152 Kcal/kg-mole.

Comparison of the first order reaction rate constants for the small and the large pore diameter catalysts revealed some interesting results. On the reactor volume basis, the small pore catalyst was more active than the large pore catalysts. When the catalyst were compared on the mass basis, the activity was almost equal. On the surface area basis, the large pore diameter catalyst was twice as active as the small pore catalyst.

Tables XXIX and XXX present the experimental and model predicted HDN data. The mean error in the model prediction ranged from $\pm$ 0.036 to $\pm$ 0.053 , the experimental error was in the range of $\pm$ 0.042 to $\pm$ 0.053 . Figure 40 through 42 present the comparison of the model predicted and experimental HDN data.

As explained in the experimental results section, the composite catalyst bed behaved similar (additive) to the single catalyst beds in its HDN activity, no synergistic effect of catalyst grading was noticed. The experimental data for the composite catalyst bed were predicted with the following model, which is a combination of the first-order models for the small and the large pore diameter catalysts:

$$C_i = C_{io} \cdot \exp.(-LVHST \cdot (1.27 \times 10^7 \cdot e^{-11,825/T} + 1.519 \times 10^4 \cdot e^{-7,458/T}) + t/438)$$

Table XXXI presents comparison of the experimental and predicted HDN data. The model predicts the product liquid nitrogen content with a mean error of 0.037 wt%.

TABLE XXIX

PREDICTED AND EXPERIMENTAL HYDRODENITROGENATION ACTIVITY RESULTS FOR RUN ZBF (LARGE PORE CATALYST)

Model: $C_i = C_{io} \cdot \exp.(-3.0376 \times 10^4 \cdot \exp.(-14{,}823.4/RT) \cdot LVHST + t/364)$

Sample Number	C_i Experimental	Experimental Error	C_i Calculated	$(C_{ical.} - C_{iexp.})$
ZBF#1	0.310	± 0.050	0.492	+ 0.182
#3	0.474	± 0.029	0.518	+ 0.044
#4	0.743	± 0.064	0.810	+ 0.008
#5	0.697	± 0.091	0.686	- 0.006
#6	0.877	± 0.055	0.872	- 0.005
#7	0.768	± 0.056	0.761	- 0.007
#8	1.032	± 0.045	1.027	- 0.005
#9	1.152	± 0.065	1.160	- 0.008
#10	1.049	± 0.061	1.094	+ 0.045
#11	1.000	± 0.047	1.104	+ 0.104
#12	0.641	± 0.026	0.634	- 0.007
#14	0.639	± 0.056	0.675	+ 0.036
#15	0.689	± 0.054	0.698	+ 0.009
#17	0.781	± 0.070	0.746	- 0.035
#19	0.816	± 0.063	0.796	- 0.020
#21	0.796	± 0.067	0.851	+ 0.055
#23	0.837	± 0.055	0.901	± 0.064
	Mean Standard Error	0.055		Mean Error 0.036

TABLE XXX

PREDICTED AND EXPERIMENTAL HYDRODENITROGENATION ACTIVITY RESULTS FOR RUN ZBG (SMALL PORE CATALYST)

Model: $C_i = C_{io}.\exp.(-2.54 \times 10^7.\exp.(-23{,}502.3/RT) \cdot LVHST + t/548)$

Sample Number	C_i Experimental	Experimental Error	C_i Calculated	$(C_{ical.} - C_{iexp.})$
ZBG #1	0.249	± 0.037	0.383	+0.134
#3	0.428	± 0.021	0.400	-0.028
#4	0.728	± 0.051	0.696	-0.032
#5	0.624	± 0.031	0.570	-0.054
#6	0.794	± 0.063	0.833	+0.039
#7	0.711	± 0.024	0.720	+0.009
#8	0.974	± 0.084	0.965	-0.009
#9	1.010	± 0.011	1.136	+0.126
#10	0.893	± 0.079	1.081	+0.188
#11	0.912	± 0.029	1.001	+0.089
#12	0.471	± 0.033	0.467	-0.004
#15	0.499	± 0.027	0.487	-0.012
#18	0.568	± 0.028	0.521	-0.047
#21	0.547	± 0.076	0.556	+0.009
#23	0.612	± 0.044	0.581	-0.031
	Mean Standard Error	± 0.043		Mean Error ± 0.053

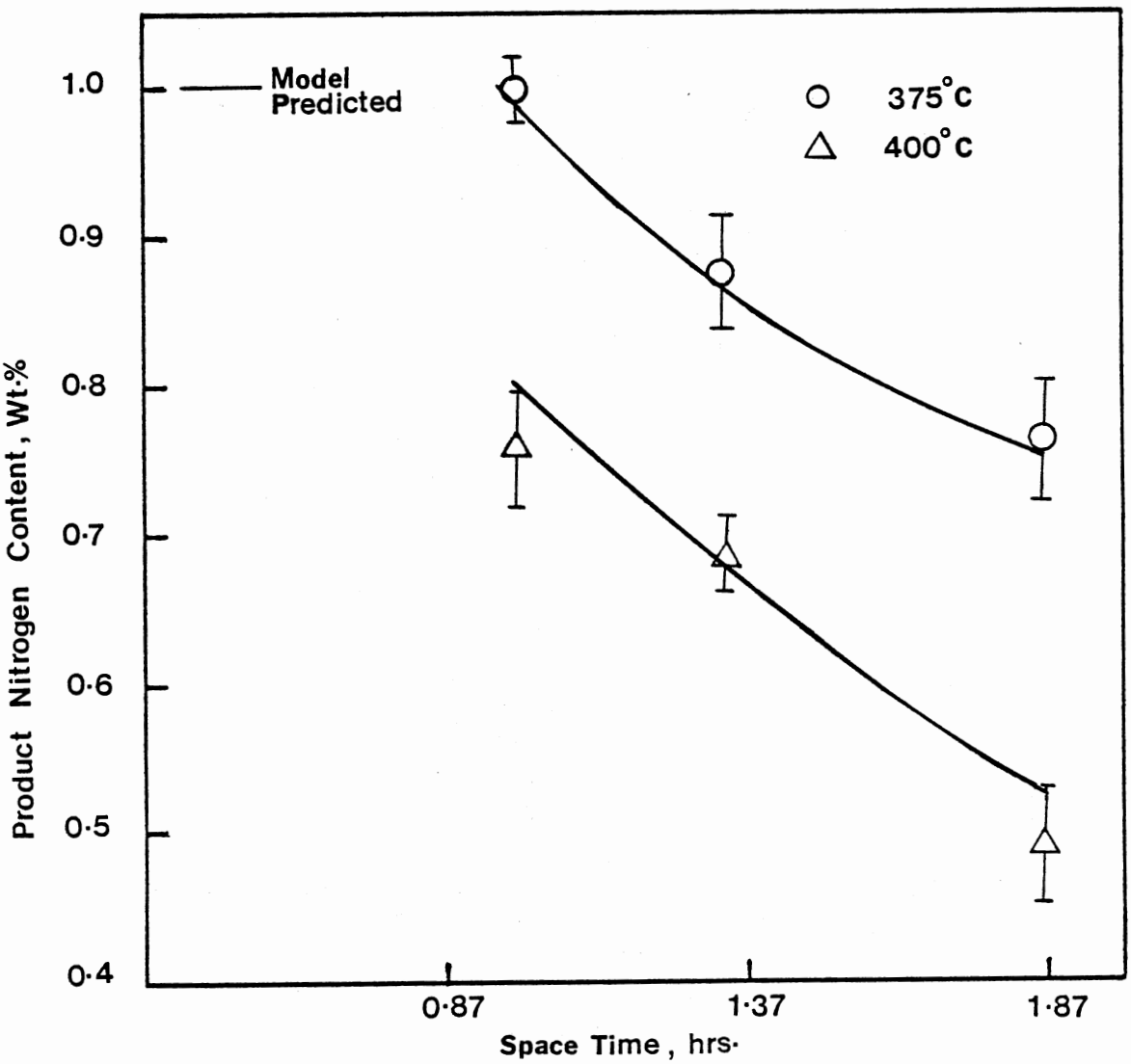

Figure 40. Effect of Space Time on Product Liquid Nitrogen Content (Run ZBF)

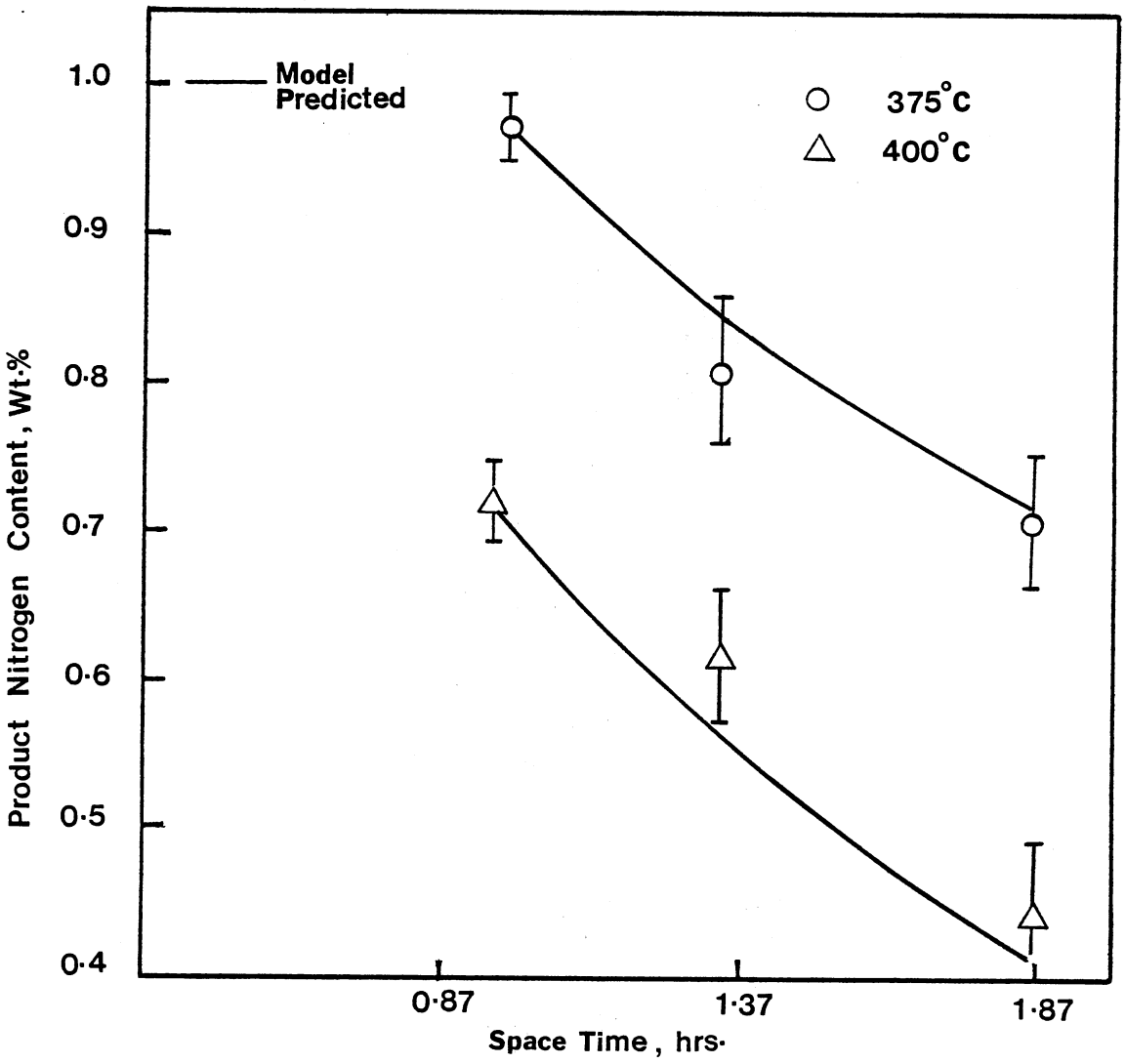

Figure 41. Effect of Space Time on Product Liquid Nitrogen Content (Run ZBG)

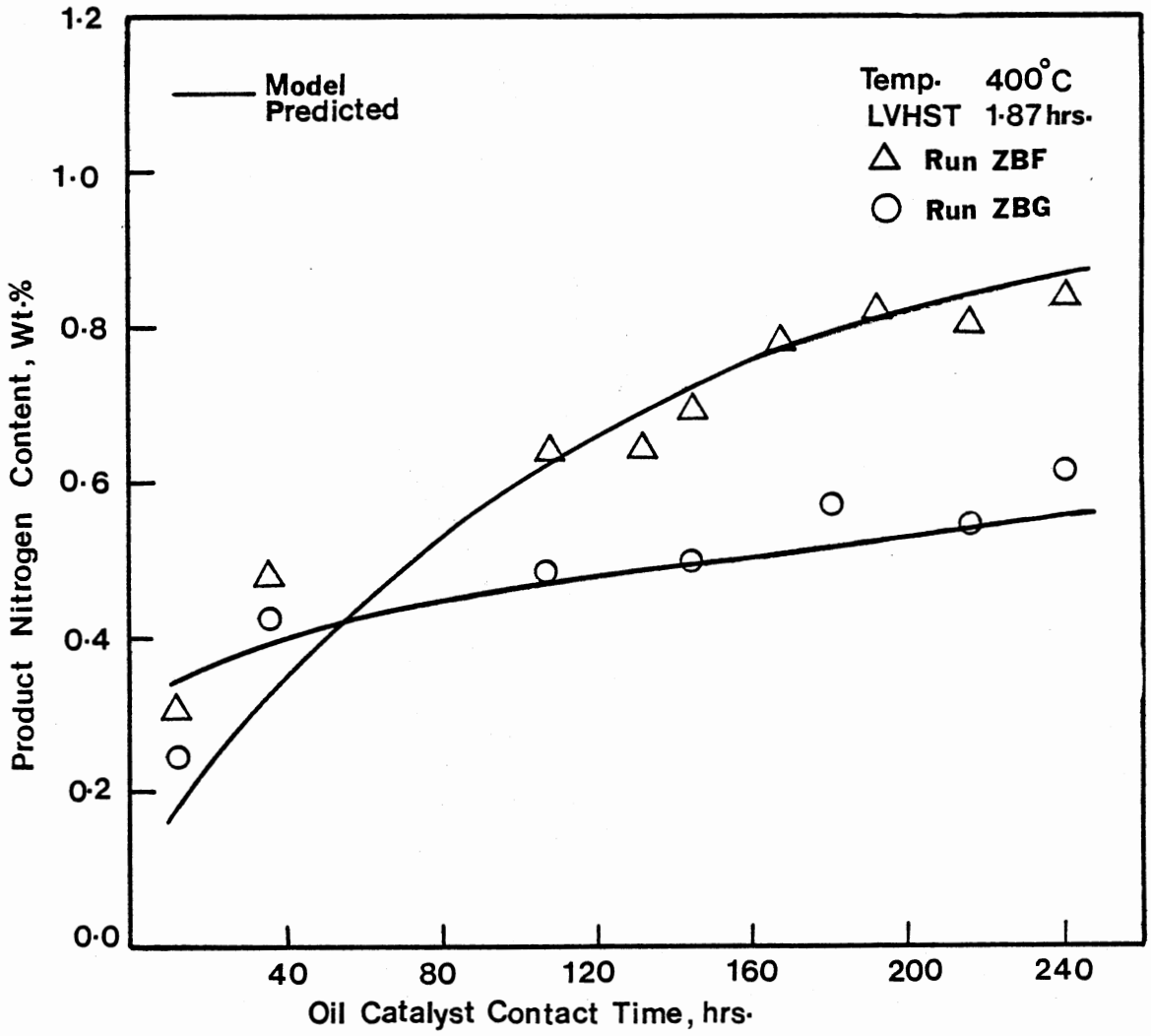

Figure 42. Effect of Oil Catalyst Contact Time on Product Liquid Nitrogen Content

TABLE XXXI

PREDICTED AND EXPERIMENTAL HYDRODENITROGENATION ACTIVITY RESULTS FOR RUN ZBH (COMPOSITE BED)

Model: $C_i = C_{io} \cdot \exp.(-LVHST \cdot (1.27 \times 10^7 \cdot e^{-11,825/T} + 1.519 \times 10^4 \cdot e^{-7,458/T}) + t/438)$

Sample Number	C_i Experimental	Experimental Error	C_i Calculated	$(C_{ical.} - C_{iexp.})$
ZBH #1	0.299	± 0.060	0.423	+ 0.124
#3	0.548	± 0.025	0.447	- 0.101
#4	0.711	± 0.022	0.745	+ 0.034
#5	0.698	± 0.005	0.612	- 0.086
#6	0.813	± 0.007	0.843	- 0.030
#7	0.829	± 0.019	0.734	- 0.095
#8	0.951	± 0.037	0.990	+ 0.039
#9	1.025	± 0.011	1.140	+ 0.115
#10	0.982	± 0.004	1.084	+ 0.104
#11	1.001	NA	1.010	+ 0.009
#12	0.628	± 0.004	0.527	- 0.101
#15	0.666	± 0.043	0.573	- 0.093
#18	0.680	± 0.053	0.621	- 0.059
#20	0.727	± 0.013	0.656	- 0.071
#23	0.756	± 0.018	0.712	- 0.044
	Mean Standard Error	± 0.019	Mean Error	± 0.037

Intrinsic Kinetic Modeling

In heterogenously catalyzed reactions, where diffusion and chemical reaction occur simultaneously on the catalyst surface, concentration gradients of the reactants and products are established. If the diffusion process is rapid compared to the chemical reaction rate, the reaction will occur on the entire catalyst surface. In such a case, the true intrinsic kinetics can be measured. On the other hand, if the catalyst is very active, and the diffusion of the reactive species is comparatively slow, the molecules will react before they have diffused very far into the catalyst particle. There will be a deep concentration gradient within the pellet. In such a case, the entire catalyst pellet surface is not utilized, and thus one does not measure the true intrinsic kinetics.

The global kinetic model cannot account for the difference in catalyst activity due to the difference in catalyst physical properties. An intrinsic kinetic model, capable of predicting catalyst hydrotreatment activity and deactivation rate, based on catalyst internal pore structure, catalyst pellet dimension, and diffusing species molecular size has been developed in this section. Knowing the approximate molecular size of the diffusing species, experimentally determined catalyst pore diameter and catalyst pellet size, the hydrotreatment activity and deactivation rate can be predicted for Ni-Mo-Al_2O_3 catalysts containing approximately 3% NiO and 15% MoO_3 active metal loading.

For modeling purposes the conditions in the reactor during the hydrotreatment operation can be assumed to be as follows:

1. Catalyst pores are filled with coal-derived liquid.

Ketkar (1977) in his study with FMC oil observed complete pore filling of alumina support at atmospheric pressure and 138°C. Under the reaction conditions applied during the present study, 11.7 MPa (1700 psig) pressure and 400°C temperature, the coal liquid will encounter lesser resistance due to viscous and surface tension forces and hence can be assumed to completely fill the pores.

2. The catalyst pellet is completely surrounded by a liquid film.

3. The liquid phase is in equilibrium with hydrogen, thereby implying that no mass transfer limitations exist between the gas and the liquid phase. Soni (1977), and Sooter (1974) observed that hydrogen pressure has a small effect on the catalyst hydrotreatment activity above the pressure of 6.9 MPa (1000 psig) for various coal liquids. In this study, the pressure was held constant at 11.7 MPa (1700 psig), hence it can be assumed that an excesses of hydrogen was present in the liquid phase and no bulk mass transfer resistances existed.

4. The HDN reactions occur on the catalyst active sites, the molecules must diffuse into the catalyst interior to avail the internal surface area.

With the above assumptions, the generalized approach in the catalyst activity development model consisted of the following:

1. The trickle-bed reactor is in ideal plug-flow, with negligible axial dispersion.

2. The intrinsic reaction rate expression for HDN is assumed to follow first-order kinetics.

3. The trickle-bed reactor is considered to be isothermal.

Mass Balance Over Catalyst Pellet

Species mass balance over a cylindrical pore can be represented by a second order differential equation:

$$D_{eff} \cdot \frac{d^2C_i}{dx^2} = \frac{k_s \cdot C_i}{r} \qquad (1)$$

where k_s = intrinsic reaction rate constant based on catalyst surface area

C_i = i th species concentration

D_{eff} = effective diffusivity

r = average pore radius, $2V_i/S_i$

V_i = catalyst internal volume

S_i = catalyst internal surface area

Solving Equation 1 (details in Appendix G) we have

$$\eta = \frac{1}{\phi} \qquad (2)$$

where η = effectiveness factor

ϕ = Thiele modulus

$$= \frac{V_e}{A_e} \cdot \left(\frac{\rho_p \cdot S_i \cdot C_i^{n-1} k_s}{D_{eff}}\right)^{1/2} \qquad (3)$$

ρ_p = catalyst pellet density

V_e = external pellet volume

S_e = external pellet surface area

n = order of the reaction

The effective diffusivity in case of restricted diffusion can be determined by the Spry and Sawyer's (1975) correlation:

$$D_{eff} = \frac{D_B \cdot \varepsilon_p}{\tau} \cdot f(\lambda) \qquad (4)$$

where D_B = bulk diffusivity

ε_p = catalyst pellet porosity

τ = tortuosity factor, dimensionless

$f(\lambda)$ = partition coefficient function

λ = ratio of molecular diameter to the pore diameter

= MD/PD

MD = molecular diameter, $\mathring{A}$

PD = pore diameter, $\mathring{A}$

Substituting Equations 3 and 4 in 2 we have

$$\eta = \frac{1}{R_e} \cdot \left(\frac{D_B \cdot \varepsilon_p}{\tau \rho_p S_i k_s}\right)^{1/2} \cdot (1 - \lambda)^2 \tag{5}$$

By definition

$$V_i = \varepsilon_p / \rho_p \tag{6}$$

$$\eta = \frac{1}{R_e} \cdot \left(\frac{D_B \cdot V_i}{\tau S_i k_s}\right)^{1/2} \cdot (1 - \lambda)^2 \tag{7}$$

where R_e = effective catalyst pellet radius.

Chemical Reaction Occurring Inside Catalyst Pore

For a first-order, irreversible reactionoccurring on the catalyst active sites, the reaction rate based on catalyst mass is represented as follows:

$$-r_m = k_s \cdot C_i \cdot \eta \cdot S_i \tag{8}$$

Substituting for η from Eq. 7 we have

$$-r_m = \frac{C_i}{R_e} \cdot \left(\frac{D_B \cdot V_i k_s S_i}{\tau}\right)^{1/2} \cdot (1 - \lambda)^2 \tag{9}$$

Calculation of Optimum Catalyst Pore Size

For cylindrical catalyst pores, the specific surface area and pore diameter vary according to the following relation

$$S_i = \frac{4V_i}{PD} \tag{10}$$

An increase in PD results in a corresponding decrease in surface area and vice versa. An optimum pore diameter thus exists, for which the catalyst surface area is maximized without subsequent increase in catalyst diffusional resistance. From Eq. 9 we have

$$-r_m = \frac{C_i}{R_e} \cdot \left(\frac{D_B V_i k_s S_i}{\tau}\right)^{1/2} \cdot (1 - \lambda)^2$$

By definition

$$V_i k_s S_i = \frac{\varepsilon_p k_s S_i}{\rho_p} = \frac{\varepsilon_p k_s S_i V_e}{W}$$

$$= \frac{4V_i}{PD} \cdot \frac{\varepsilon_p k_s V_e}{W} \cdot \frac{\lambda}{MD} \; PD$$

$$= \frac{4V_i V_e \varepsilon_p k_s}{W \cdot MD} \cdot \lambda \equiv \alpha\lambda \tag{11}$$

Where W = catalyst pellet mass

V_e = catalyst external pellet volume

$$\alpha \equiv \text{constant} \equiv \frac{4V_i V_e \varepsilon_p k_s}{W \cdot MD}$$

MD = molecular diameter

ε_p = catalyst pellet porosity

Substituting Eq. 11 in Eq. 9, one obtains

$$-r_m = \frac{C_i}{R_e} \left(D_B \frac{\alpha \cdot \lambda}{\tau}\right)^{1/2} (1 - \lambda)^2 \qquad (12)$$

For constant molecular diameter of the diffusing species, $(D_B \alpha/\tau)^{1/2} \cdot C_i/R_e$ can be represented by a constant, K.

Hence,

$$-r_m = K(\lambda)^{1/2}(1 - \lambda)^2 \qquad (13)$$

Differentiating with respect to λ, one obtains for the optimum pore size:

$$\lambda_{opt} = 0.20$$

This analysis represents that for optimum catalyst activity, the catalyst pore size must be approximately 5 times the size of the diffusing molecule. Thus, knowing the diffusing molecular species diameter, the optimum catalyst pore size can be determined. Assuming the average molecular size of the diffusing species to be 24 Å, the catalyst pore size from this analysis is determined to be 120 Å.

Various researchers have developed theoretical models to determine the most optimum catalyst pore diameter for hydroprocessing coal-derived liquids and petroleum feedstock. Ruckenstein and Tsia (1981) determined for a partition coefficient of one, the optimum pore size to be about twice the size of the diffusing molecule. Rajagopalan and Luss (1979) determined from theoretical analysis the catalyst pore diameter for optimum initial activity to be never larger than five times the diameter of the diffusing species. Spry and Sawyer (1975) recommended catalyst pore size ten times larger than the size of the diffusing molecules.

Analysis for Plug-Flow Reactor

For plug-flow reactor

$$LVHST = -\int_{C_{io}}^{C_i} \frac{dC_i}{(-r_v)} = \int_{C_{io}}^{C_i} \frac{dC_i}{(-r_m \rho_B)} \qquad (14)$$

where LVHST = liquid volume hourly space time, hrs.

ρ_B = bulk catalyst reactor density, gm/cm^3

C_{io} = inlet species concentration

Substituting Eqn. 9 in Eqn. 14 and integrating, we have

$$\ln \frac{C_{io}}{C_i} = \frac{LVHST\ \rho_B}{R_e} \cdot \left(\frac{D_B\ k_s\ S_i\ V_i}{\tau}\right)^{1/2} \cdot (1-\lambda)^2 \qquad (15)$$

The bulk species diffusivity is determined by the Stokes-Einstein Eqn. (Bird et al., 1960).

$$D_B = \frac{kT}{3\pi \cdot MD \cdot \mu} \qquad (16)$$

where μ = solvent viscosity, gm/cm/sec

k = Boltzmann's Constant

= 1.3805×10^{-16} $gm \cdot cm^2/sec^2/°K$

T = absolute temperature, °K

Viscosity is determined by the following equation (Reid, et al., 1978).

$$\mu = Ae^{B/T} \qquad (17)$$

Substituting Eqns. 16 and 17 in Eqn. 15 and rearranging

$$\ln \frac{C_{io}}{C_i} = \frac{LVHST \cdot \rho_B}{R_e} \cdot \left(\frac{k}{3\pi A}\right)^{1/2} \cdot \left(\frac{T}{e^{B/T}}\right)^{1/2} \cdot \left(\frac{k_s\ S_i\ V_i}{MD \cdot \tau}\right)^{1/2} \cdot \left(1-\frac{MD}{PD}\right)^2 \qquad (18)$$

Coking Reactions

During this study, the hydrotreating catalysts deposited carbonaceous residues. These residues reduced the catalyst activity due to the reduction in catalyst pore size and also due to the coverage of catalyst active sites. The coking reactions were observed to occur independent of the main hydrotreating reactions. The coke formation on the catalystoccurred the very moment the oil contacted the catalyst. The purpose of this study was not to investigate the catalyst coke deposition. Coke deposition data from a previous study (Chang, 1982) were used to model the coking reactions.

The following simplified assumptions were made to develop the coking mathematical model:

1. The coking reaction is slow compared to the main hydrotreating reactions; pseudo steady-state assumption.

2. Coking reaction occurs according to the independent fouling mechanism. The coke can be formed directly from the feedstock, from the intermediates, and also from the reaction products. Coke deposition on the catalyst at a temperature of 260°C, when no heteroatom removal reactions occur, justifies this reaction.

3. Coking reactions have a second-order dependence on the fraction of catalyst uncoked. This assumption implies that coke deposits only on the uncoked catalyst surface. This assumption is based on the experimental results obtained by Chang (1982).

The coking reaction rate is represented as:

$$\frac{dC}{dt} = k_c\left(1 - \frac{C}{C_{max}}\right)^2$$

where C = coke content per unit catalyst mass, gms of coke/gm of catalyst

C_{max} = maximum catalyst coke capacity

$= V_{io}\rho_c$

k_c = coking reaction rate, gm of coke/gm of catalyst/hr

V_{io} = fresh catalyst pore volume, cm^3/gm

ρ_c = coke density, gms of cm^3/m

t = time of oil-catalyst contact, hrs.

Solving Eqn. 18 we have

$$C = \frac{k_c \cdot C_{max} \cdot t}{(C_{max} + k_c \cdot t)} \tag{19}$$

4. Loss in catalyst activity occurs due to the reduction in catalyst pore size and pore volume due to coke deposition. The reduction occurs according to the following relations:

$$V_i = V_{io} - C/\rho_c \tag{20}$$

$$PD = PD_o(V_i/V_{io}) \tag{21}$$

where V_{io} = fresh catalyst pore volume, cm^3/gm

V_i = catalyst pore volume at any time, t

PD_o = fresh catalyst pore diameter

PD = catalyst pore diameter at any time, t

C = catalyst coke content

Substituting Eqn. 19 in Eqns. 20 and 21, we have

$$V_i = V_{io}\left(1 - \frac{k_c \cdot t}{V_{io}\rho_c + k_c t}\right) \tag{22}$$

$$PD = PD_o \left(1 - \frac{k_c t}{V_{io}\rho_c + k_c t}\right)^{1/2} \tag{23}$$

Eqns. 22 and 23 describe the change in catalyst physical properties due to carbonaceous deposition.

Substituting Eqns. 22 and 23 in Eqn. 18 and simplifying:

$$\ln \frac{C_{io}}{C_i} = \frac{LVHST \cdot \rho_B}{R_e} \cdot \left(\frac{k}{3\pi A}\right)^{1/2} \cdot \left(\frac{T}{e^{B/T}}\right)^{1/2} \cdot \left(\frac{k_s S_i}{MD \cdot \tau}\right)^{1/2}$$

$$\cdot V_{io}^{1/2} \cdot \left(1 - \frac{k_c t}{(V_{io}\rho_c + k_c t)}\right)^{1/2}$$

$$\cdot \left(1 - \frac{MD}{\left(1 - \frac{k_c t}{(V_{io}\rho_c + k_c t)}\right)^{1/2}}\right)^2 \tag{24}$$

Substituting Arrhenius' relation for specific reaction rate constant

$$k_s = k_o \cdot e^{-E/RT}$$

we have

$$\ln \frac{C_{io}}{C_i} = \frac{LVHST\ \rho_B}{R_e} \cdot \left(\frac{k}{3\pi A}\right)^{1/2} \cdot \left(\frac{T}{e^{B/T}}\right)^{1/2} \cdot \left(\frac{k_o \cdot e^{-E/RT} \cdot S_i}{MD \cdot \tau}\right)^{1/2}$$

$$\cdot V_{io}^{1/2} \left(1 - \frac{k_c t}{(V_{io}\rho_c + k_c t)}\right)^{1/2}$$

$$\cdot \left(1 - \frac{MD}{PD_o \left(1 - \frac{k_c t}{(V_{io}\rho_c + k_c t)}\right)^{1/2}}\right)^2 \tag{25}$$

where C_{io} = inlet species concentration, wt%

C_i = exit liquid species concentration, wt%

LVHST = liquid volume hourly space time, hrs.

ρ_B = bulk reactor density, gm/cm^3

R_e = effective catalyst pellet radius, cm

k = Boltzmann's constant

= 1.3805×10^{-16} $gm.cm^2/sec^2/°K$

A = viscosity equation constant, gm/cm/sec

B = viscosity equation constant, °K

T = absolute temperature, °K

k_s = intrinsic surface reaction rate constant, cm/sec

= $k_o \cdot e^{-E/RT}$

k_o = frequency factor

E = activation energy, Kcal/Kmole

S_i = internal catalyst surface area, cm^2/gm

MD = molecular diameter, Å

τ = tortuosity factor, constant

V_{io} = fresh catalyst pore volume, cm^3/gm

k_c = coking reaction rate, gm of coke/gm of catalyst/hr

ρ_c = coke density, gm/cm^3

PD_o = fresh catalyst pore diameter, Å

Model Fit

The HDN data from the experimental Runs ZBF and ZBG were fitted to Equation 25, using Marquardt's non-linear regression procedure. Attempts were made to develop a generalized model for HDN activity of

Ni-Mo-Al_2O_3 catalysts. This model was based on the assumption that the intrinsic reaction rate constants of the Ni-Mo-Al_2O_3 catalysts, of approximately similar metal loading, are the same. Table XXXII lists the constants used in the model calculation. Three parameters were determined from the non-linear fitting of HDN data: molecular diameter, MD; coking reaction rate constant, k_c; and intrinsic reaction rate constant, k_s, at different temperatures. The activation energies and frequency factors were determined by fitting the Arrhenius temperature dependence equation. The variables fitted in the model were: product liquid nitrogen content, C_i; liquid volume hourly space time, LVHST; and temperature, T.

The values of the constants present in Table XXXII were either experimentally determined or values supplied by the vendor used. The values for the coke density and catalyst tortuosity were estimated from similar studies involving hydrotreating catalysts and coal-derived liquids. The maximum coke content of the hydrotreating catalysts was considered to be the maximal coke capacity the catalyst pore structure would tolerate, which is equal to the product of catalyst pore volume and coke density.

The tortuosity factor, τ, used for the effective diffusivity calculation is defined as a measure of the ratio of the distance which a diffusing molecule must travel on an average, compared to the geometric distance. Tortuosity factor takes into consideration the non-linearity of the catalyst pores. The experimental data on the tortuosity factor for alumnia hydrotreating catalysts are very rare, usually values in the range of 1.4 to 5 have been used. As recommended

TABLE XXXII

CONSTANTS USED IN MODEL CALCULATIONS

	Large Pore Catalyst	Small Pore Catalyst
Catalyst bulk density, ρ_B, gm/cm^3	0.547	0.626
Fresh catalyst pore volume, V_{io}, cm^3/gm	0.632	0.488
Fresh catalyst surface area S_i, cm^2/gm	125×10^4	270×10^4
Catalyst pellet radius R_e, cm	0.108	0.108
Catalyst tortuosity, τ	2.3	2.3
Inlet feed nitrogen content, C_{io}	1.112	1.112
Fresh catalyst pore diameter, PD_o, Å	177	67

by Satterfield (1973), a tortuosity factor of 2.3 has been used.

The bulk diffusivity of the diffusing species is determined using the Stokes-Einstein equation; this equation was developed for large molecules (Satterfield and Sherwood, 1963).

$$D_B = 1.05 \times 10^{-9} \frac{T}{\mu . V_b^{1/3}}$$

where D_B = bulk diffusivity, cm^2/sec

T = absolute temperature, °K

μ = viscosity of the solution, gm/cm/sec

V_b = molar volume of the diffusing solute, cm^3/gm mole

In order to determine the bulk diffusivity; the viscosity, molecular weight, and molar volume of the oil at the process conditions must be known. Whitehurst (1979) has reported the average molecular size of the SRC liquids to be between 20 to 40 Å. Angevine et al. (1981) reported the average molecular size of the short contact time SRC coal liquid to be approximately 28 Å. The reader is referred to the section on literature review for further information on coal liquid molecular size. In this study, the molecular diameter was varied between 15-40 Å, and the best fit molecular diameter determined.

For pure compounds, the molecular diameter can be calculated from published values of bond lengths, bond angles, and Van der Waals' radia. Satterfield et al. (1973) calculated molecular diameter of several compounds using such correlations, some of the published molecular diameters were: water, 2.8 Å; toluene, 6.3 Å; triethyl benzene, 9.2 Å; triphenyl benzene, 12.2 Å. An estimate of the molar volume and hence molecular diameter can also be made using the Kopp's law of additive atomic volumes (Satterfield and Sherwood, 1963).

No viscosity data of the coal liquids at high temperatures are available, however, values can be extrapolated from lower temperature data. Stein et al. (1978) developed the following correlation for viscosity of a mixture of SRC in Recycle Solvent at various temperatures (204°C maximum temperature).

$$\ln(KV) = X_{sol}[A_{sol} + E_{sol}/(T + B_{sol})] + X_{src}[A_{src} + E_{src}/(T + B_{src})]$$

where KV = kinematic viscosity

T = temperature in °F

X = weight fraction SRC or solvent

Assuming average molecular weights of SRC and Recycle Solvent to be 750 and 250, respectively, the constants for the above equations were determined.

For the present study, the viscosity of 15% SRC in Process Solvent was determined at various temperatures using the above equation. The viscosity data were regressed using the following viscosity equation:

$$\mu = Ae^{B/T}$$

The constants determined were:

$A = 1.754 \times 10^{-3}$ gm/cm/sec

B = 820.15

Using this correlation, the viscosity of the feedstock, used during this study, was determined to be 0.593×10^{-2} gm/cm/sec.

From the above available viscosity and molecular size data, the bulk diffusivity of the 15% SRC/Process Solvent feedstock was determined to be 5.941×10^{-6} cm^2/sec (average molecular diameter, 28 Å; temperature, 400°C; viscosity 0.593×10^{-2} gm/cm/sec). For a 30% SRC/Process

Solvent mixture, Chang (1982) determined the diffusivity to range between 4.5×10^{-6} to 5.0×10^{-6} cm^2/sec.

Convergence of Solution

The generalized HDN activity model for the Ni-Mo-Al_2O_3 catalysts failed to converge even after 20 iterations, the lack of convergence of the generalized HDN activity model signifies:

1. The intrinsic HDN activity for the two catalysts used in this study (KF-153S and HT-115E) is different.

2. The two catalysts decay at different rates.

The HDN data from the Runs ZBF and ZBG were separately fitted and the intrinsic reaction rates and coke deactivation constants for each catalyst determined. The HDN data from Run ZBG were fitted with unrestricted constraints for all three parameters (molecular size, coking reaction rate and surface reaction rate); approximate values of the parameters were thus determined. The intrinsic reaction rate constant and catalyst deactivation constant were next fixed and the solute molar diameter allowed to vary unconstrained; this procedure was repeated for each parameter.

The program usually converged in less than seven iterations. The convergence for the small pore diameter catalysts was much faster compared to the large pore diameter catalysts.

Results of Regression

The resulting parameters of the non-linear regression model are presented in Table XXXIII for both the small and the large pore diameter catalysts. The intrinsic reaction rate constants at 400°C were

TABLE XXXIII

RESULTING PARAMETERS FROM DATA FITTING

Variables	Description	Small Pore Catalyst (Run ZBG)	Large Pore Catalyst (Run ZBF)
k_s	Intrinsic surface reaction rate constant, HDN reactions, cm/sec		
	400°C	8.829×10^{-10}	5.5079×10^{-10}
	375°C	2.734×10^{-10}	9.975×10^{-11}
	350°C	4.623×10^{-11}	1.575×10^{-11}
k_o	Frequency factor, HDN reactions	8.073×10^{6}	9.4146×10^{9}
E	Activation energy, Kcal/Kgmole	48,849.6	58,862.9
k_c	Coking reaction rate constant, gm of coke/gm of catalyst/hr	0.1035×10^{-2}	0.3862×10^{-2}
MD	Solute molecular diameter, Å	24	24

determined to be 8.829×10^{-10} cm/sec and 5.5079×10^{-10} cm/sec for the small and the large pore diameter catalysts, respectively. The intrinsic reaction rate constants for the small pore diameter catalyst was consistently higher than the large pore diameter catalyst, signifying higher activity of the small pore catalysts. The large pore diameter catalyst, however, showed a higher temperature dependence compared to the small pore catalyst.

The two catalysts deactivated at different rates, the deactivation rate, as determined by the coking reaction rate constant, was approximately three times higher for the small pore catalyst compared to the large pore catalyst. The molecular diameter determined by fitting the HDN data from Run ZBG (small pore catalyst) was approximately 24 Å, the solute molecular diameter was not varied for subsequent regression runs.

Table XXXIV shows a comparison of the experimental and calculated product liquid nitrogen content for Runs ZBF and ZBG. The standard deviation for the large pore diameter catalyst was $\pm$ 0.045, compared to $\pm$ 0.036, for the small pore catalyst. Figure 43 presents a comparison of the model predicted catalyst loss in activity and the actual loss in catalyst HDN activity. Note that the experimental data for the large pore diameter catalyst deviate significantly from the model prediction ($\pm$ 0.045 std. error). This signifies deactivation in large pore diameter catalysts to occur differently from the simplified approach used in this model.

The catalyst deactivation was modeled to occur due to geometric pore size reduction upon carbonaceous deposition, no consideration was given to the poisoning of catalyst active sites by other phenomena, such as: basic

TABLE XXXIV

COMPARISON OF EXPERIMENTAL AND CALCULATED VALUES

Model: $$\ln \frac{C_{io}}{C_i} = \frac{LVHST \cdot \rho_B}{R_e} \cdot \left(\frac{k}{3\pi A}\right)^{1/2} \cdot \left(\frac{T}{e^{B/T}}\right)^{1/2} \cdot \left(\frac{k_o e^{-E/RT} S_i}{MD \cdot \tau}\right)^{1/2} \cdot V_{io}^{1/2} \cdot \left(1 - \frac{k_c t}{(V_{io}\rho_c + k_c t)}\right)^{1/2} \cdot \left(1 - \frac{MD}{PD_o\left(1 - \frac{k_c t}{(V_{io}\rho_c + k_c t)}\right)^{1/2}}\right)^2$$

Temp. °K	LVHST hrs	Time hrs	Large Pore Catalyst (Run ZBF)			Small Pore Catalyst (Run ZBG)		
			$C_{i_{exp}}$	$C_{i_{cal}}$	$(C_{i_{cal}} - C_{i_{exp}})$	$(C_{i_{exp}}$	$C_{i_{cal}})$	$(C_{i_{cal}} - C_{i_{exp}})$
673	1.87	12	0.310	0.442	0.130	0.249	0.392	0.143
673	1.87	24	0.449	0.463	0.013	0.414	0.405	0.009
673	1.87	36	0.529	0.484	0.045	0.428	0.418	0.010
673	0.94	43	0.743	0.066	0.077	0.728	0.686	0.042
673	1.34	50	0.697	0.570	0.125	0.624	0.575	0.049
648	1.34	57	0.877	0.889	0.012	0.794	0.812	0.018
648	1.87	67	0.768	0.740	0.028	0.711	0.725	0.014
648	0.94	74	0.932	0.959	0.027	0.974	0.904	0.070
623	0.94	81	1.152	1.052	0.100	1.010	1.014	0.004

TABLE (Continued)

Temp °K	LVHST hrs	Time hrs	Large Pore Catalyst (Run ZBF) $C_{i_{exp}}$	$C_{i_{cal}}$	$(C_{i_{cal}} - C_{i_{exp}})$	Small Pore Catalyst (Run ZBG) $C_{i_{exp}}$	$C_{i_{cal}}$	$(C_{i_{cal}} - C_{i_{exp}})$
623	1.34	88	1.049	0.926	0.123	0.893	0.977	0.084
623	1.87	95	1.000	0.901	0.100	0.912	0.928	0.016
673	1.87	108	0.641	0.583	0.060	0.471	0.489	0.018
673	1.87	120	0.689	0.598	0.080	0.476	0.501	0.025
673	1.87	168	0.781	0.646	0.140	0.568	0.544	0.024
673	1.87	192	0.794	0.665	0.130	0.573	0.562	0.013
673	1.87	204	0.796	0.679	0.120	0.581	0.573	0.008
673	1.87	240	0.837	0.706	0.130	0.012	0.602	0.010
			Mean Error		± 0.045	Mean Error		± 0.036

species absorption, catalyst structural changes (austetic formation), and metal deposition. For the small pore diameter catalyst, the model predicts the catalyst deactivation within the range of experimental variance ($\pm$ 0.036 std. error). The coking model developed in this study is thus more akin to the small pore diameter catalyst than the large pore diameter catalyst.

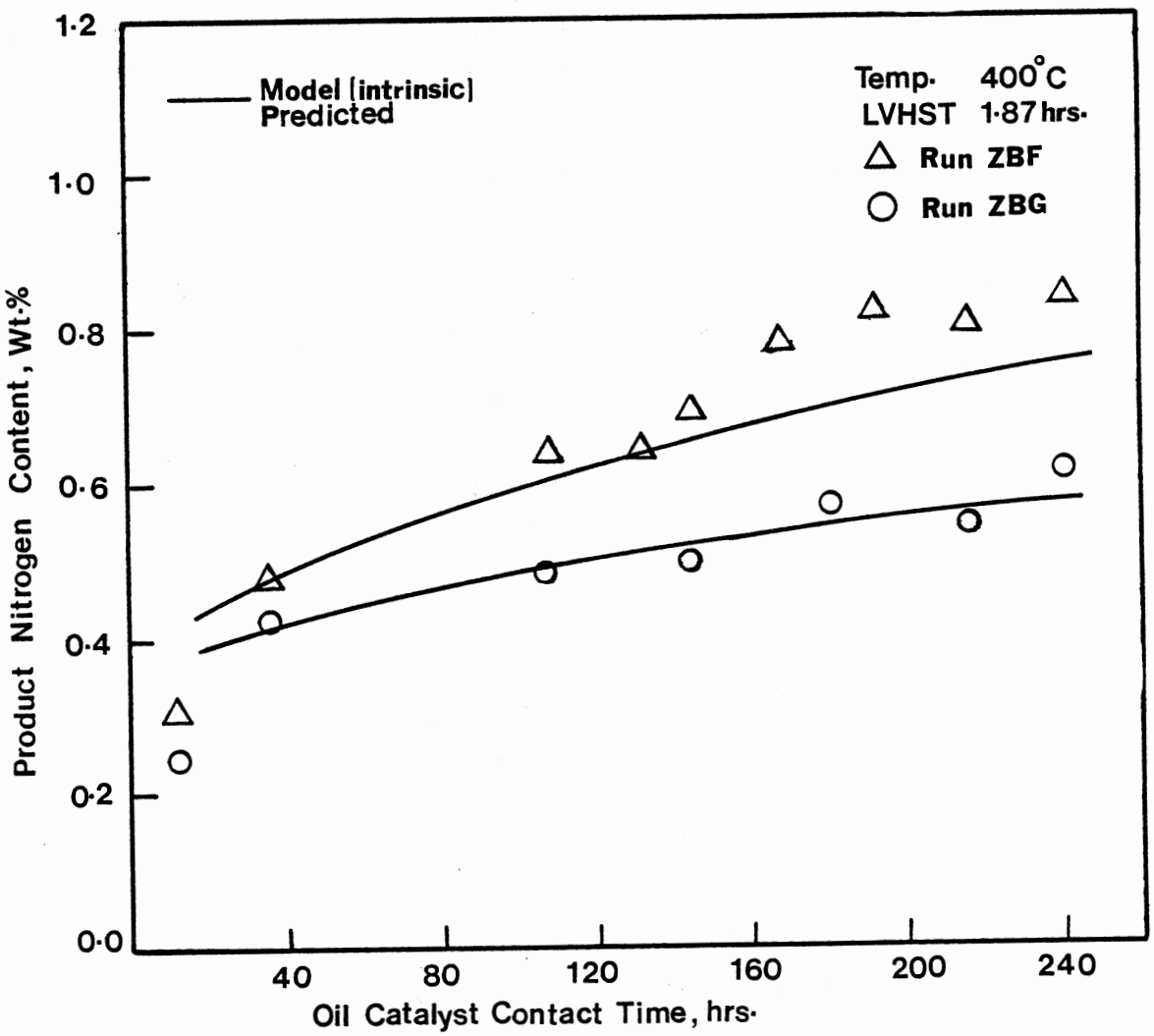

Figure 43. Comparison of the Model Predicted and Experimental Product Liquid Nitrogen Concentrations

REFERENCES

Aczel, T., R. B. Williams, N. F. Chamberlain, and H. E. Lumpkin; ACS, Advances in Chem. Ser., 195, 237 (1979).

Adam, C. E., and H. T. Williams; U. S. Patent No. 3,531,398, September 29 (1970).

Ahmed, M. M., and B. L. Crynes; Symp. on Effect of Pore Size on Catalyst Behavior, Presented Before Div. of Pet. Chem., ACS, Miami Beach Meeting, Sept. 10-15 (1978).

Ahmed, M. M.; Ph.D. Dissertation, Oklahoma State University, Stillwater, Oklahoma (1979).

Anderson, R. P.; Proc. of 15th Inter-Society Energy Conversion Engineering Conference, Seattle, Aug. 18-22 (1980).

Angevine, P. J., M. Becker, R. B. Callen, M. J. Dabkowski, M. P. Granchi, L. A. Green, R. H. Heck, C. A. Simpson, S. S. Shih, T. R. Stein; EPRI Report No. AF-1253 (1979).

Angevine, P. J., R. H. Heck, S. S. Shih, T. R. Stein; Mobil Research and Development Company; EPRI Contractor's Conference, Palo Alto, California (1981).

_____, Armak Chemical Company, KF-153S Catalyst Properties Bulletin, Pasadena, Texas (1981).

Appleby, W. G., J. W. Gibson, and G. M. Good; Ind. Eng. Chem. Process Des. Dev., 1, 102 (1962).

Arey, W. F., R. B. Mason, D. Springs, and R. C. Paule; U. S. Patent No. 3,254,017; May 31 (1966).

ASTM Standards, Part 23, D-482 (1979).

ASTM Standards, Part 23, D-1160 (1979).

Baker, A., and A. Relthaar, Ind. Eng. Chem. Prod. Res. Dev., 21, 590 (1982).

Beeckman, J. W., and G. F. Froment; Chem. Eng. Sci., 35, 805 (1980).

Beeckman, J. W., and G. F. Froment; Ind. Eng. Chem. Fund., 18, 245 (1979).

Beguin, F., and R. Setton; Carbon, 10, 539 (1972).

Berg, L., and F. P. McCandless; U.S. DOE Report No. FE-2034-20, June 13 (1980).

Berry, D. A., L. J. Hillenbrand, H. M. Grotta, D. H. Stewart, W. R. Alcron, and G. E. Elliott; U.S. DOE Report No. FE-2321-25, November (1977).

Bertolacini, R. J., L. C. Gutberlet, D. K. Kim, K. K. Robinson; EPRI Report No. AF-574, November (1977).

Bertolacini, R. J., L. C. Gutberlet, D. K. Kim, K. K. Robinson; EPRI Report No. AF-1084, June (1979).

Beuther, H., and B. K. Schmid; Sixth World Petroleum Congress, Section III, PD 7, Paper 20, 297 (1964).

Beuther, H., O. A. Larson, and A. J. Peratta; "Catalyst Deactivation"; Editors: B. Delmon and G. F. Froment, E'lsevier Publishing (1980).

Bhan, O. K.; M. S. Thesis, Oklahoma State University, Stillwater, Oklahoma (1981).

Bhan, O. K.; Unpublished results

Bird, R. B., W. E. Stewart, and E. N. Lightfoot; "Transport Phenomena", John Wiley and Sons, New York (1960).

Bockrath, B. C., C. L. Delle Donne, F. K. Schweighardt; Fuel, 57, 4 (1978).

Bockrath, B. C., K. T. Schroeder, and F. W. Steffgen; Anal. Chem., 51, 8, 1164 (1979).

Bockrath, B. C., and F. K. Schweighardt; Adv. in Chem. Ser., ACS, 195, 29 (1979).

Bowman, R. M., B. J. Jody, and G. Jarvi; U.S. DOE Report No. DOE/SF/10760-2 (1980).

Brito , J., R. Golding, F. Severino, and J. Laine; Div. of Pet. Chem.; ACS, Kansas City Meeting, September 14-17 (1982).

Brooks, J. A., R. J. Bertolacini, L. C. Gutberlet, and D. K. Kim; EPRI Report No. AF-190, Palo Alto (1976).

Brunn, L. W., A. A. Montagna, and J. A. Paraskos, Progress in Processing Synthetic Crudes and Resids, Div. of Pet. Chem.; ACS, Chicago Meeting, August 24-29 (1975).

Cable, T. L., F. E. Massoth, and M. S. Thomas; 74th Annual AIChE Meeting, New Orleans, November (1981).

Cable, K., and K. B. McCaskill; U.S. DOE Report No. METC/RI/79/1, February (1979).

Chandler, J., Personal Communication, Computer Sciences Department, Oklahoma State University, Stillwater (1982).

Chang, C. D., and A. J. Silvestri; Ind. Eng. Chem. Process Des. Dev., 13, 3, 315 (1974).

Chang, H. J.; Ph.D. Dissertation, Oklahoma State University, Stillwater (1982).

Chiou, M. J., and J. H. Olson; Preprints Div. Pet. Chem., ACS, 23, 1421 (1978).

Chirakaparambil, F. G.; M. S. Thesis, Oklahoma State University, Stillwater (1974).

Christ, M. A., G. N. Shah, L. G. Sherman; Oil and Gas Journal, May 28, 95 (1979).

Crynes, B. L.; U.S. DOE Report No. DE-14876-6, Quarterly Report, April (1981).

Crynes, B. L.; "Chemistry of Coal Utilization," Editor: M. A. Elliott, John Wiley and Sons, Inc. (1981).

Cypres, R., and B. Bettens; Tetrahedron, 31, 359 (1975).

Cypres, R., and B. Bettens; Tetrahedron, 30, 1253 (1974).

Dautzenberg, F. M., J. V. Klinken, K. M. A. Pronk, S. T. Sie, and J. B. Wiffels; ACS, Symp. Ser., 65, 254 (1978).

de Roset, A. J., G. Tan; Adv. Chem. Ser., 179, 109 (1979).

Drushel, H. V.; Symp. Adv. Analysis of Petr. Prod.; Div. of Pet. Chem., ACS, New York Meeting, August 27 (1972).

Drushel, H. V.; Paper Presented Before Div. of Pet. Chem., ACS, Chicago Meeting, August 24-29 (1975).

Eberby, P. E., Jr., C. N. Kimberlin, Jr., W. H. Miller, and H. V. Drushel; Ind. Eng. Chem. Process Des. Dev., 5, 193 (1966).

El'bert, E. I., Y. R. Katsobashvilli, V. K. Smirov, G. I. Barino, and and E. V. Spiglazova; Pererab. Tverd. Topl., 2, 99 (1970). Cited from Janardanrao (1980).

El'bert, E. I., Y. R. Katabashvilli; U.S.S.R. Patent No. 189, 405, Nov. 30, 1966, Chem. Abstr., 72, 123745 (1970).

Farragher, A. L., and P. Cossee; Proc. Fifth Int. Congr. Catalysis, Amsterdam, 1301 (1973).

Ferry, J. D.; J. Gen. Physiol., 20, 95 (1936).

Flockhart, B. D., I. M. Sesay, and R. C. Pink; J. Chem. Soc. Chem. Comm., 439 (1980).

Froment, G. F., and K. B. Bischoff; Chem. Eng. Sci., 16, 189 (1961).

Fu, Y. C., B. F. Rand, J. C. Winslow; Preprints Div. of Fuel Chem., 23, 1, 81 (1978).

Furimsky, E.; Fuel Processing Tech., 6, 1 (1982).

Furimsky, E.; Ind. Eng. Chem. Prod. Res. Dev., 17, 329 (1978).

Gates, B. C., J. R. Katzer, C. G. A. Schuit; "Chemistry of Catalytic Processes," McGraw Hill Book Company (1979a).

Gates, B. C., et al.; U.S. DOE Report No. FE-2028-15 (1979b).

Gibson, K. R., and D. C. Green; CEP, May, 93 (1983).

Giddings, J. C., E. Eucera, C. P. Russell, and M. N. Meyers; J. Phy. Chem., 72, 4397 (1968).

Green, D. C., and D. H. Broderick; CEP, December, 33 (1981).

Greskovich, E. J., E. N. Givens, and M. A. Collura; U.S. DOE Report No. 20003-21 (1977).

Gutberlet, L. C. and R. J. Bertolacini, Ind. Eng. Chem. Prod. Res. Dev., 22, 246 (1983).

_____, Harshaw Chemical Company, HT-115E Catalyst Properties Bulletin, Beachwood, Ohio (1981).

Halderman, R. G., and M. C. Botty; J. Phy. Chem., 63, 489 (1959).

Hall, G., and S. P. Herron; Adv. in Chem. Ser., ACS, 195, 137 (1979).

Hardin, A. H., R. H. Packwood, and M. Ternan; Symposium on Effect of Pore Size on Catalytic Behavior, ACS, Miami Beach Meeting, September 10-15 (1978).

Hensley, A. L., and L. M. Quick; AIChE Fuels and Petrochemicals Div., Reprints, 1, 728 (1980).

Ho, P. O., and S. W. Weller; Fuel Processing Technology, 4, 21 (1981).

Ho, B., and E. Briggs; AIChE New Orleans Meeting, November 10 (1981).

Holloway, P. H., and G. C. Nelson; ACS, Div. Pet. Chem. Preprints, 22, 4, 1352 (1977).

Huang, W. J., N. L. Smith, J. A. Guinn, C. W. Curtis, and A. R. Tarrer; 74th Annual AIChE Meeting, New Orleans, November 18 (1981).

Hughes, C. C., and R. Mann, ACS Symp. Ser., 65, 201 (1978).

Inoguchi, M.; Shokubai, 18, 7, 78 (1976), Cited from Ohtsuka (1977).

Jacob, H. E., J. F. Jones, and R. T. Eddinger; Ind. Eng. Chem. Proc. Des. Dev., 10, 558 (1971).

Janardanrao, M.; Ind. Eng. Chem. Prod. Res. Dev., 21, 375 (1982).

Jankowski, A., W. Doehler, and U. Graeser; Paper presented at International Workshop on the "Science of Coal Liquefaction," Lorre, Victoria, Australia, Published by Butterworth and Co. Ltd., May 24-28 (1982).

Jones, J. F., N. J. Bunsvold, H. D. Terzian, L. J. Scotti, F. H. Schoemann, R. C. Merrill, J. D. Alcantrara, D. J. Dumina, S. J. Romelczyk, and L. Ford; F.M.C. Corporation, U.S. DOE Report No. FE-1212-T-9, September (1975).

Kang, C., J. Gendler, EPA Report No. EPA - 60/7-78-159 (1978).

Kang, C., and E. Johnson, ACS Division Fuel Chemistry, 21 (5), 32 (1976).

Kovach, S. M., L. J. Castle, and J. V. Bennett; Ind. Eng. Chem. Prod. Res. Dev., 17, 1, 62 (1978).

Kwan, T., and M. Sato; Nippon Kagaku Kaishi, 91, 12, 1103, 1970, Cited from Ohtsuka (1975).

Laine, J., K. C. Pratt, L. T. David; Ind. Eng. Chem. Prod. Res. Dev., 18, 4, 329 (1979).

Langhout, W. C. V. Z., C. Ouwerkerk, and K. M. A. Pronk; Oil and Gas Journal, 78, 48, 120 (1980).

LeNobel, J. W., and J. H. Choufoer; Proc. Fifth World Petrol. Congr., Section III, Paper 18 (1959).

_____, Leco Automatic Sulfur Determinator, Instruction Manual, Laboratory Equipment Corporation, Michigan.

Lee, H. C., and J. B. Butt; J. Catalysis, 49, 320 (1977).

Liebenberg, B., and H. G. Potgieter; Fuel, 52, 130 (1973).

Lipsch, J. M. J. G., and C. G. A. Schuit; J. Catalysis, 15, 163 (1969).

Long, R. B.; Adv. in Chem. Ser., 195, ACS (1979).

Madison, J. J., and R. M. Roberts; Ind. Eng. Chem., 50, 237 (1958).

Malone, D. M., J. L. Anderson; 83rd AIChE National Meeting, Houston, TX, March (1977).

Masumune, S., and J. M. Smith; AIChE Journal, 12, 304 (1966).

Mears, D. E.; Chem. Eng. Sci., 26, 1361 (1971).

Mehta, D. C.; Ph.D. Dissertation, Oklahoma State University, Stillwater (1978).

Misserov, K. G., J. of Catalysis, 13, 169 (1969).

Mosby, J. F., and G. B. Hoekstra, T. A. Kleinheng, and J. M. Sroka; Hydrocarbon Processing, May, 93 (1973).

Moschopedis, S. E., S. Parkash, and J. G. Speight; Fuel, 57, 431 (1978).

Moschopedis, S. E., and J. G. Speight; Fuel, 55, 187 (1976).

Moschopedis, S., E., J. F. Fryer, and J. G. Speight; Fuel, 55, 227 (1976).

Montagona, A. A., S. W. Chun, J. A. Fryer; Ninth World Petroleum Congress, Tokyo, PD 18(1), 1 (1975).

Muchida, I., S. Inone, K. Moedor, K. Takeshita; Carbon, 15, 1, 9 (1977).

Mullendore, A. W., and M. L. Lieberman; "Chemical Studies On Synthoil Process," Sandia Laboratories Reports; Cited from Holloway et al. (1977).

Murakami, Y., T. Kobayashi, T. Hattori, and J. Masuda; Ind. Eng. Chem. Fund., 7, 599 (1968).

Murphy, J. R., S. A. Treese; Proceedings American Pet. Inst. Refin., 44th Midyear Meet., San Fransisco, CA, May 14-17, 1979. Published by API, 58, 343 (1979).

Newson, E. J.; Preprints, Div. of Fuel Chem., ACS, New York Meeting, 17, 2, 49 (1972).

Newson, E. J.; Ind. Eng. Chem. Proc. Des. Dev., 14, 1, 27 (1975).

Nielson, A., B. H. Cooper, A. C. Jacobsen; Symp. On Residuum Upgrading and Coking, Div. of Pet. Chem., ACS, Atlanta Meeting, March 29 - April 3 (1981).

Ohtsuka, T., Y. Hasengana, and N. Takanari; Bull. Jpn. Petrol. Inst., 10, 14, 1968, Cited from Ohtsuka (1977).

Ohtsuka, T.; Cat. Rev. Sci. Engr., 16, 271 (1977).

Otto R. D.; Akzo Catalyst Company, Pasadena, TX, Personal Communication (1982).

Panfilov, I. A., E. I. El'bert, V. A. Titushkin, L. B. Kostyok, V. K. Smirnov; Nauki Khim. Prom., 58, 1973; Chemical Abstracts, 81, 80037C (1974).

Pazos, J. M., L. Aguino, and J. Pachano; ACS Atlanta Meeting, March, 456 (1981).

_____, Perkin Elmer Corporation, Instruction Manual for 240 B Elemental Analyzer, Norwalk, Conn. (1981).

Petersen, E. E.; "Chemical Reaction Analysis," Prentice Hall Inc., Englewood Cliffs, NJ (1966).

Pfeiffer, J. P., and R. N. Saal; Phys. Chem., 44, 139 (1940).

Polinski, L. M., G. J. Steigel, and R. E. Tischer; U.S. DOE Report No. DOE/PETC/TR-81/2 (1981).

Potts, J. D., K. E. Hastings, R. S. Chillingworth, H. Unger; U.S. DOE Report No. FE-2038-39 (1980).

Rajagopalan, K., and D. Luss; Ind. Eng. Chem. Process Des. Dev., 18, 3, 459 (1979).

Ramifrez de Agudelo, M. M., P. Gajardo, and L. Gonzalez Reyes; ACS, Div. of Pet. Chem., Kansas City Meeting, September 12-17 (1982).

Reid, R. C., J. M. Prausnitz, T. K. Sherwood; "The Properties of Gases and Liquids," Third Edition, McGraw Hill Book Co., N.Y. (1977).

Richardson, R. L., and S. K. Alley; Symp. on Hydrocracking and Hydrotreating, Div. of Pet. Chem., ACS, Philadelphia Meeting, March 12 (1978).

Richardson, R. L., and M. Ishikawa; Oil and Gas Journal, May 28, 80 (1979).

Riley, K. L.; Paper Presented Before Div. of Pet. Chem., ACS, Anaheim Meeting, March 12 (1978).

Roberto, R. G., D. C. Cronaver, and L. G. Gabya; Fuel Processing Tech., 5, 103 (1981).

Robinson, E. T., and C. G. Evin; Symposium On Shale Oil Upgrading and Refining, AIChE Annual Meeting, Los Angeles, Nov. (1982).

Ruckenstein, E., and M. C. Tsia; AIChE Journal, 27, 4, 697 (1981).

_____, Ruska Proportioning Pumps, Instruction Manual, Ruska Instrument Corporation, Houston, TX.

Satchell, D. P.; Ph.D. Dissertation, Oklahoma State University, Stillwater (1974).

Satterfield, C. N.; AIChE Journal, 21, 2, 209 (1976).

Satterfield, C. N., C. K. Colton, and W. H. Pitcher, Jr.; AIChE J., 19, 628 (1973).

Satterfield, C. N., and T. K. Sherwood; "The Role of Diffusion in Catalysis," Chapter I, Addison-Wesley Publishing Co. (1963).

Schmid, B. K., and H. Beuther; Ind. Eng. Chem. Proc. Des. Dev., 6, 2, April, 207 (1967).

Schultz, H., and M. J. Mima; Dept. of Energy, PETC/TR-80/3, May (1980).

Schwager, I., J. T. Kwan, W. C. Lee, S. Meng, T. F. Yen; Anal. Chem., 51, 11, September, 1803 (1979).

Schwager, I., T. F. Yen; Fuel, 58, March, 219 (1979).

Schwager, I., W. C. Lee, T. F. Yen; Anal. Chem., 49, 14, December, 2364 (1977).

Schweighardt, F. K., C. M. White, S. Friedman, and J. L. Schultz; Preprints Div. of Fuel Chem., ACS, 22 (1977).

Schweighardt, F. K., H. L. Retcofsky, and R. Raymond; ACS, Div. of Fuel Chem., Preprints, 21 (1976).

Seapan, M., et al.; U.S. DOE Report No. DOE/BC/10306-22, Interim Report, April (1983).

Shah, Y. T., and J. A. Paraskos; Ind. Eng. Chem. Process Des. Dev., 14, 4, 368 (1975).

Shultz, J. L., G. M. White, F. K. Schweighardt, A. C. Sharkey; DOE Report No. PERC/RI/77/7 (1977).

Sivasubramanian, R.; Ph.D. Dissertation, Oklahoma State University, Stillwater (1977).

Sivasubramanian, R., J. H. Olson, J. R. Katzer; ACS, Preprints Div. of Fuel Chem., 25, 84 (1980).

Soni, D. S.; M. S. Thesis, Oklahoma State University, Stillwater (1974).

Sooter, M. G.; Ph.D. Dissertation, Oklahoma State University, Stillwater (1974).

Speight, J. G., ACS, Div. Pet. Chem.; New York Meeting, August (1981).

Speight, J. G., and S. E. Moschopedis; "Chemistry of Asphaltenes," Adv. in Chem. Series, ACS, 1 (1979).

Spry, J. C., and W. H. Sawyer; AIChE 68th Annual Meeting, Los Angeles, California, November 16 (1975).

Stanulonis, J. J., B. C. Gates, and J. H. Olson; AIChE Journal, 22, 3, May, 576 (1976).

Steigel, G. J., R. E. Tischer, and L. M. Polinski; Ind. Eng. Chem. Proc. Res. Dev., 22, 411(1983).

Stein, T. R., A. V. Cabal, R. B. Callen, M. J. Dabkowski, R. H. Heck, C. A. Simpson, S. S. Shih; EPRI Annual Report No. AF-873, December (1978).

Steffgen, F. W., K. T. Shroeder, and B. C. Bockrath; Analytical Chemistry, 51, 8, 1164 (1979).

Sternberg, H. W., R. Raymond, and S. Akhtar; ACS Symp. Ser., Div. of Pet. Chem., Philadelphia Meeting, April 6-11 (1975).

Sternberg, H. W., R. Raymond, and F. K. Schweighardt; Science, 188, 49 (1975).

Sternberg, H. W.; ACS, Div. of Fuel Chem., Preprints, 21, 1 (1976).

Stern, E. W.; J. Catalysis, 57, 370 (1979).

Sullivan, R. F., C. E. Rudy, D. C. Green, H. C. Chen; U.S. DOE Report No. FE-2315-45 (1981).

Ternan, M., and J. R. Brown; Fuel, 61, November (1982).

Tamm, P. W., H. F. Harnsberger, and A. L. Bridge; Ind. Eng. Chem. Proc. Des. Dev., 20, 262 (1981).

Ternan, M., E. Furimsky, and B. I. Parson , Fuel Processing Technology, 2, 45 (1979).

Ternan, M., and J. R. Brown; Fuel, 61, November (1982).

Tekeuchi, C. and Y. Shirota, ACS Sym. Ser., Div. of Pet. Chem., Honolulu Meeting, April (1979).

Thakkar, V. P., R. M. Baldwin, and B. L. Bain; Fuel Processing Technology, 4, 235 (1981).

Tischer, R. E.; U.S. DOE Pittsburgh Energy Technology Center, Personal Communications (1982).

Utz, B. P., N. K. Narain, R. A. Herbert, and B. D. Blaustein; Chapter in "Advances in Coal Characterization and Allied Topics," E. L. Fuller, Jr., editor, ACS, Symp. Ser., No. 205 (1982).

van Glinneken, A. J. J., M. M. van Kessel, G. Renstrom; Oil and Gas J., 28, April, 59 (1975).

van Zoonen, D.; Proc. of the 3rd. Int. Congress on Catalysis, 1320 (1965).

Veluswamy, L. R.; Ph.D. Thesis, University of Utah, Salt Lake City (1977).

Voorhies, A. Jr.; Ind. Eng. Chem., 37, 318 (1945).

Well, J. W.; M. S. Thesis, Oklahoma State University, Stillwater (1977).

Weller, S., M. G. Petipetz, and S. Freidmann; Ind. Eng. Chem., 43, 1575 (1951).

Wheeler, A.; Adv. Catal., 3, 249 (1951).

Wheeler, A.; Catalysis, 2, 105 (1955).

White, P. J., J. F. Jones, and R. T. Eddinger; Hydrocarbon Processing, 47, 12, 97 (1968).

Whitehurst, D. D., et al.; EPRI Report No. AF-1255 (1979).

Wukash, J. E., and H. F. Rase; Ind. Eng. Chem. Prod. Res. Dev., 21, 558 (1982).

Yen, T. F.; "Chemistry of Asphaltenes," Adv. Chem. Series, ACS, 195, 39 (1979).

Yen, T. F.; U.S. DOE Report No. FE-2031-14 (1980).

APPENDIX A

DETAILS OF HYDROTREATMENT EQUIPMENT

A schematic diagram of the experimental setup employed in this study is given in Figure 44. Hydrogen enters the top of the reactor through a check-valve; a Ruska feed pump feeds oil at a predetermined rate to the top of the reactor. The oil and hydrogen gas flow cocurrently down the reactor packed with catalyst. The hydrogen pressure is maintained by a pressure regulator upstream of the reactor, the flow rate is fine adjusted by a micrometering valve and metered through a flow or a bubble meter installed in the off-gas line. The oil and gas coming of the reactor are separated in high pressure sample bombs. Liquid samples are collected after purging with nitrogen gas at atmospheric pressure. The pressure of the system is monitored on a Heise gauge; temperature along the length of the catalyst bed is measured by means of thermocouples and indicated on a digital read out. A detailed description of the system is given below.

Oil and Hydrogen Feed System

Oil Feed

The oil feed system consisted of a stainless steel feed tank, a Ruska positive displacement pump, oil feed and relief lines. The feed tank was specially designed for handling highly viscous liquids. The liquid in the feed tank was stirred prior to its being transferred to

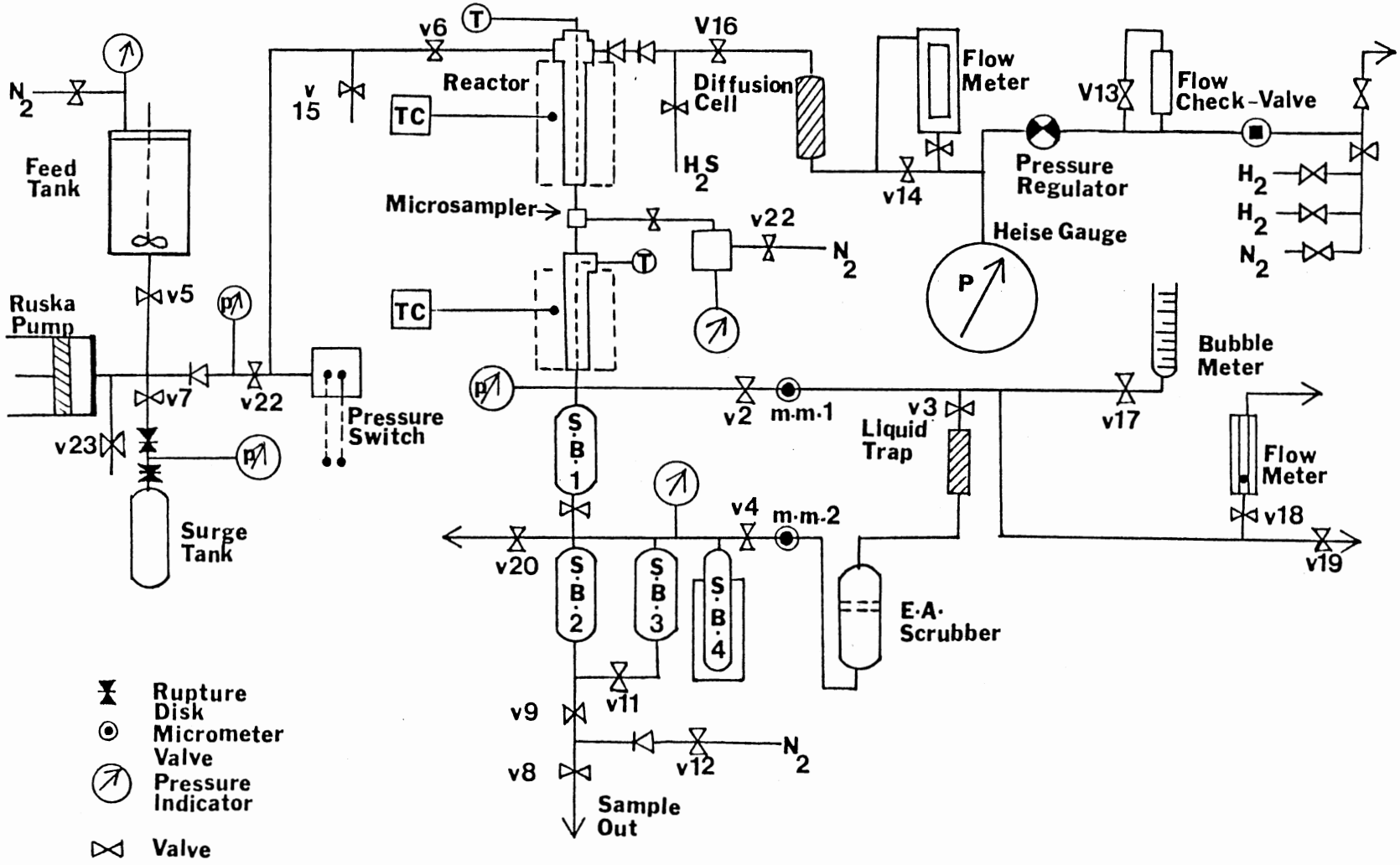

Figure 44. Detailed Experimental System

the Ruska pump; a set of baffles fitted inside the tank facilitated mixing. The feed tank could be sealed to 205 kPa (30 psig) pressure. Two 300 watt heating bands, wrapped on the outside, were used to heat the liquid prior to its being transferred to the Ruska pump. The temperature in the feed tank was monitored by a thermocouple fitted in a thermowell. A fifty-mesh size screen was placed at the exit of the liquid feed tank to avoid any solid lumps (undissolved coal) from entering the reactor system. Figure 45 presents the internal details of the pressure feed tank.

The oil was fed to the reactor with a Ruska positive displacement pump, capable of delivering liquids at pressures up to 74.8 MPa (11,000 psig). The possible pressure build up in the system, while pumping liquid with a constant displacement pump as in case of clogging of the reactor or a portion of the oil lines, was avoided by installing pressure relief devices in the oil feed lines. Two rupture disks, rated at 17.9 MPa (2600 psig) and 22.1 MPa (3200 psig), respectively, were installed close to the pump exit and connected to a 2400 ml. sample bomb by means of a 1/4 - inch pipe. A pressure gauge was connected between the two rupture disks; in case of a rupture in the first disk, the pressure would be indicated on the pressure gauge. A pressure switch was also installed in the system . The pressure switch would activate in case the system pressure exceeded 17.2 MPa (2500 psig), an alarm would sound and the power to the pump automatically shut-off. Thus, two types of safety devices (pressure switch and rupture disks) were installed in the system to take care of any oversight by the operator.

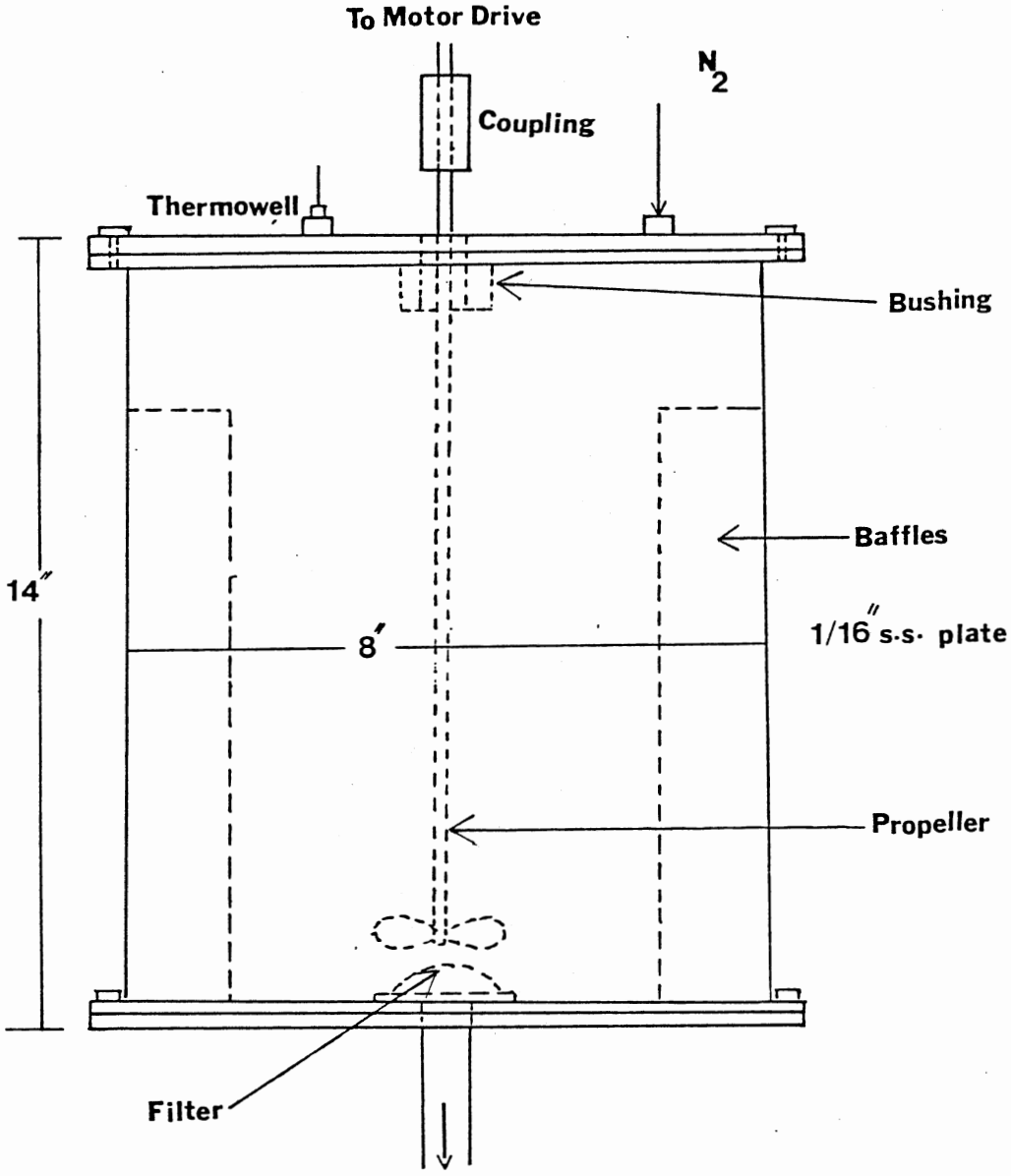

Figure 45. Details of the Oil Feed Tank

The oil feed lines were all wrapped with flexible heating tape and insulated with fiberglass. The oil cylinder of the Ruska pump was heated and insulated in a similar manner. The temperature of the oil lines and Ruska pump cylinder was manually controlled by means of powerstats; care was taken not to overheat any section. The temperature along the entire length of the feed lines was monitored by means of thermocouples connected to a multipoint selector, which could be used to select any one of the various points for display on an Omega digital read out.

Hydrogen Feed

Hydrogen was directly fed from the gas bottles through a manifold, this allowed the changing of the hydrogen bottles without interrupting the normal run. The hydrogen gas was metered through a high pressure flow-meter capable of being operated at pressures up to 34 MPa (5000 psig). A "Mity-Mite" pressure regulator was used to regulate upstream hydrogen pressure. The pressure regulator was loaded to the desired operating pressure with nitrogen gas.

An excess gas flow-check valve was provided close to the manifold to shut-off the hydrogen gas supply in case of a flow surge, as during a line rupture. A quarter-turn valve was installed upstream to the excess flow valve, thus providing for rapid manual cut-off of the hydrogen supply to the system in case of emergency.

Two check-valves were installed immediately prior to the oil entrance into the reactor; they were to avoid the flow of oil in the reverse direction. An oil trap, consisting of a high pressure sample bomb containing high surface area alumnia balls (4 mm diameter), was

installed to avoid any oil vapors from diffusing into the hydrogen gas feed system.

Reactor System

The reactor system principally consisted of one, or two trickle-bed reactors connected in series, with an assortment of temperature control accessories.

Reactor

The reactor (single reactor system) conisted of a 81.3 cm (32 inches) long, 1.27 cm (1/2 inch) O.D., and 0.175 cm (0.069 inch) thick, 316 stainless steel tube, fitted with half-inch Swagelok cross and union at the top and bottom, respectively. For the system with two reactors in series, each reactor was 40.6 cm (16 inches) long, the other dimensions being the same as for the single reactor. The effective reactor length was 38.1 cm (15 inches) for the two reactor system and 76.2 cm (30 inches) for the single reactor.

A thermowell made of 0.317 cm. (1/8 - inch) O.D., 316 stainless steel tubing, with one end welded shut was secured at the top of the reactor by means of a 1/4 - inch to 1/2 - inch reducing union, which was drilled for easy sliding on the thermowell tubing. For the two reactor system, two separate thermowells were used. For the bottom reactor, of the two reactor system, the thermowell entered through a 1/2 - inch "tee" fitting; the exit oil from the top reactor entered the second reactor vertically.

Inside the reactor, the thermowell was centered by means of 0.64 cm (1/4 - inch) stainless steel disks, with 1 mm holes along the

entire periphery; in addition to centering the thermowell, these disks also improved the solid-liquid contacting efficiency. Stainless steel screens of 50 mesh-size were used at both reactor ends to hold the catalyst and the inerts in the reactor. The reactor tubing was rated to 75.8 MPa (11,000 psi) maximum pressure at room temperature.

Reactor Temperature Controls

The heating blocks consisted of two monolithic aluminum blocks 76.2 cm (30 inches) long, with grooves of reactor diameter running across the entire length. These blocks were secured and bolted together around the reactor tube. For the two reactor system, the blocks were of 40.6 cm (16 inches) and 35.7 cm (14 inches) length, respectively. These blocks were machined for 4 inch heating bands to fit precisely around the assembled block Six heating bands, 15.24 cm (5 inches) long, each rated at 300 watts were secured around the reactor; for the two reactor system, three heating bands were used for each reactor. The power was supplied to the band heaters from two temperature controllers, each rated at 1500 and 2000 watts, respectively. For the two reactor system, each reactor was separately controlled by a temperature controller. Two platinum resistance thermometers were placed in holes drilled in the aluminum blocks and the output fed to the temperature controllers for precise temperature control. Figure 46 shows deatils of the reactor heating system.

Five iron-constantan thermocouples (J-type), of 1/4 - inch diameter, were placed over a 12.7 cm (5 inch) interval over the entire aluminum block length, and connected to the temperature indicator through a 40 point temperature selector for temperature monitoring.

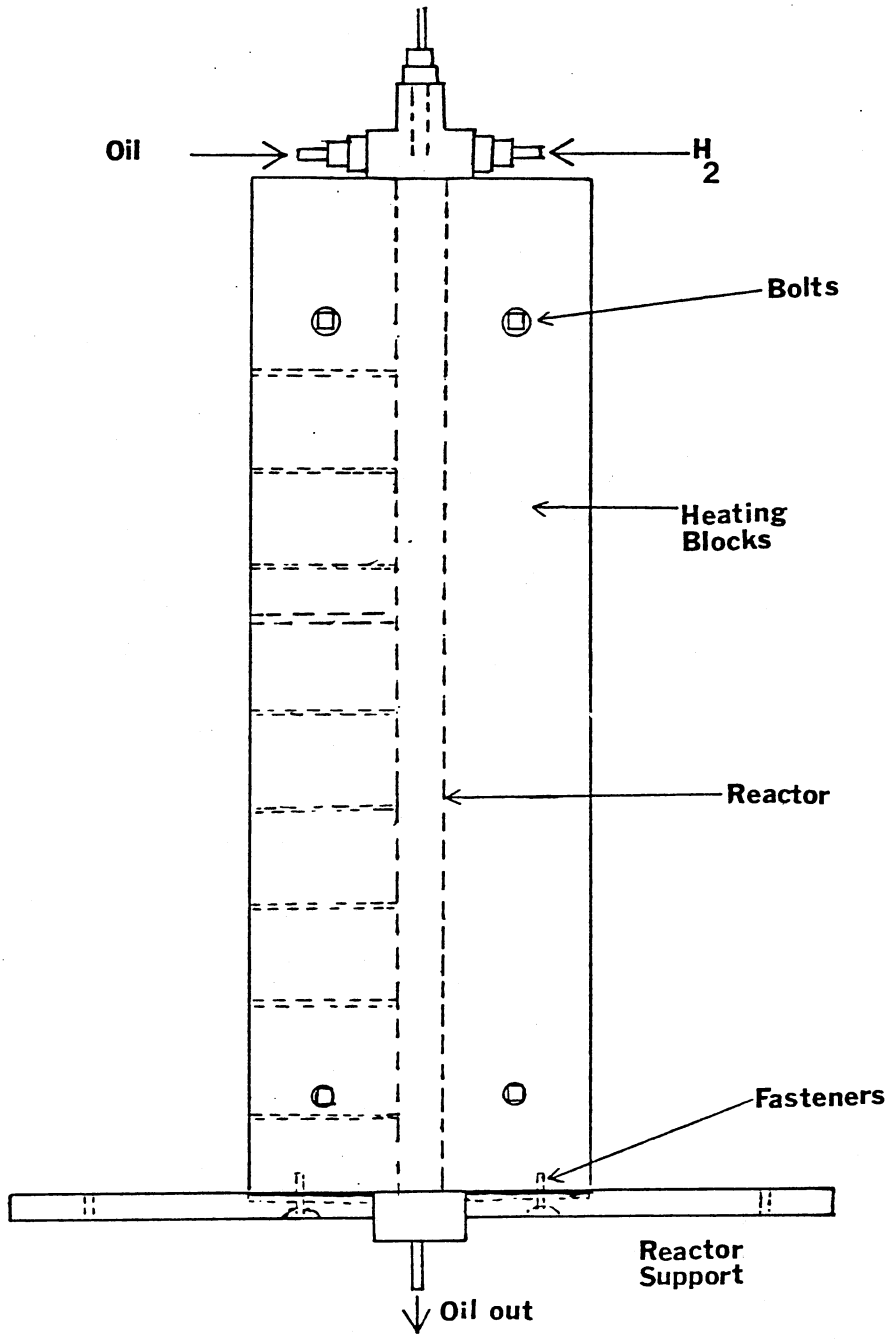

Figure 46. Details of Reactor Heating System

Slight adjustment in the set-point of the temperature controllers always resulted in establishment of a flat temperature profile along the entire reactor length.

Felt insulation in the form of cylinders, split in the middle, were used for insulating the reactor. In addition to the felt insulation, fiberglass insulation was wrapped around the reactor and held in place by means of asbestos tape. Care was taken to fill any gaps in the insulation with fiberglass. Electrical connections for the heaters were made through breaks in the insulation.

The reactor inside temperature was measured with twelve, 0.0254 mm (0.001 inch) thermocouples, which were placed at 5 cm (2 inch) intervals along the entire catalyst bed length. Extreme caution was exercised in installing these thermocouples in the thermowell, usually a few drops of silicone oil were used to facilitate installation. The output from the thermocouples was fed to an Omega digital read out through a multipoint temperature selector switch. The temperature inside the reactor could be read in sequence, with just the flick of a switch. For the two reactor system, six thermocouples were installed in each reactor bed.

Sampling System

Normal Liquid Sampling

The sampling system was designed to obtain samples without causing interruption in the normal operation. The system consisted of four sample bombs, two bombs were used for the liquid sampling, the other two mainly for avoiding liquid entrainment into the gas exit lines.

The bottom end of the reactor was connected to a 180 ml, 34.0 MPa (5000 psig) maximum pressure bomb, which was maintained at approximately 200°C to prevent heavy product separation. The length of the 1/4 - inch tubing connecting the sample bomb and the reactor bottom was minimized to avoid plugging by heavy products. The entry of the 1/4 - inch stainless steel tubing into the bomb was made possible by drilling a hole in the 1/2 - inch tube-to-pipe connector, the seal on the tube was made by a Swagelok fitting. The tubing was maintained at a temperature of 200°C by heating with a heating tape.

The liquid and gas products from the first sample bomb flowed into the second sample bomb, which was maintained at ambient temperature. The vapor-liquid separation occurred in the second sample bomb, the vapors and gases exiting through the third sample bomb. A 1/2 - inch, extended stem, high temperature valve connected sample bombs 1 and 2. During sampling, this valve was closed and the gas flow rerouted through micro-meter valve 1 (see Figure 44).

The gases from the sample bomb 3 passed into sample bomb 4, where any entrained liquid was removed by passing the gases through a bed of alumina pellets, sample bomb 4 was maintained at 0°C by surrounding in an ice bath. Two Bourdon-type pressure gauges monitored the pressure in sample bombs 1 and 2.

Microsampling System

The microsampling system was designed to collect 3-5 mls of liquid samples without disturbing the normal system operation. The system principally consisted of a three-way valve, a pressure gauge, and a high pressure liquid sample holder.

The gases and liquids from the first reactor would normally flow through the three-way valve into the top of the second reactor. During sampling the flow was diverted into the microsampling unit, which was prior pressurized to approximately 340 kPa (50 psi) less than the system operating pressure with nitrogen gas. The liquid was allowed to collect in the microsampler for approximately 3-5 minutes, depending on the liquid flow rate. The sample holder was depressurized after rerouting the flow through the normal path. The liquid sample was collected in sample vials placed inside the high pressure sample holder. Figure 47 shows the details of the microsampling system.

The three-way valve, and the tubing connecting the two reactors was maintained at approximately 200°C by heating with a heating tape. The valve and the piping were completely insulated with fiberglass insulation. Thermocouples connected to the multipoint selector were used to monitor the temperature along the liquid flow path. The three-way valve was rated for temperature up to 400°C.

Pressure and Flow Control System

Pressure Control

The system pressure was controlled by means of a "Mity-Mite" pressure regulator, and monitored on a 0-3000 psig Heise gauge. Pressure upstream of the regulator was maintained by a manifold pressure regulator, a pressure differential of 80-100 psig was maintained between the manifold pressure and the outlet regulator pressure.

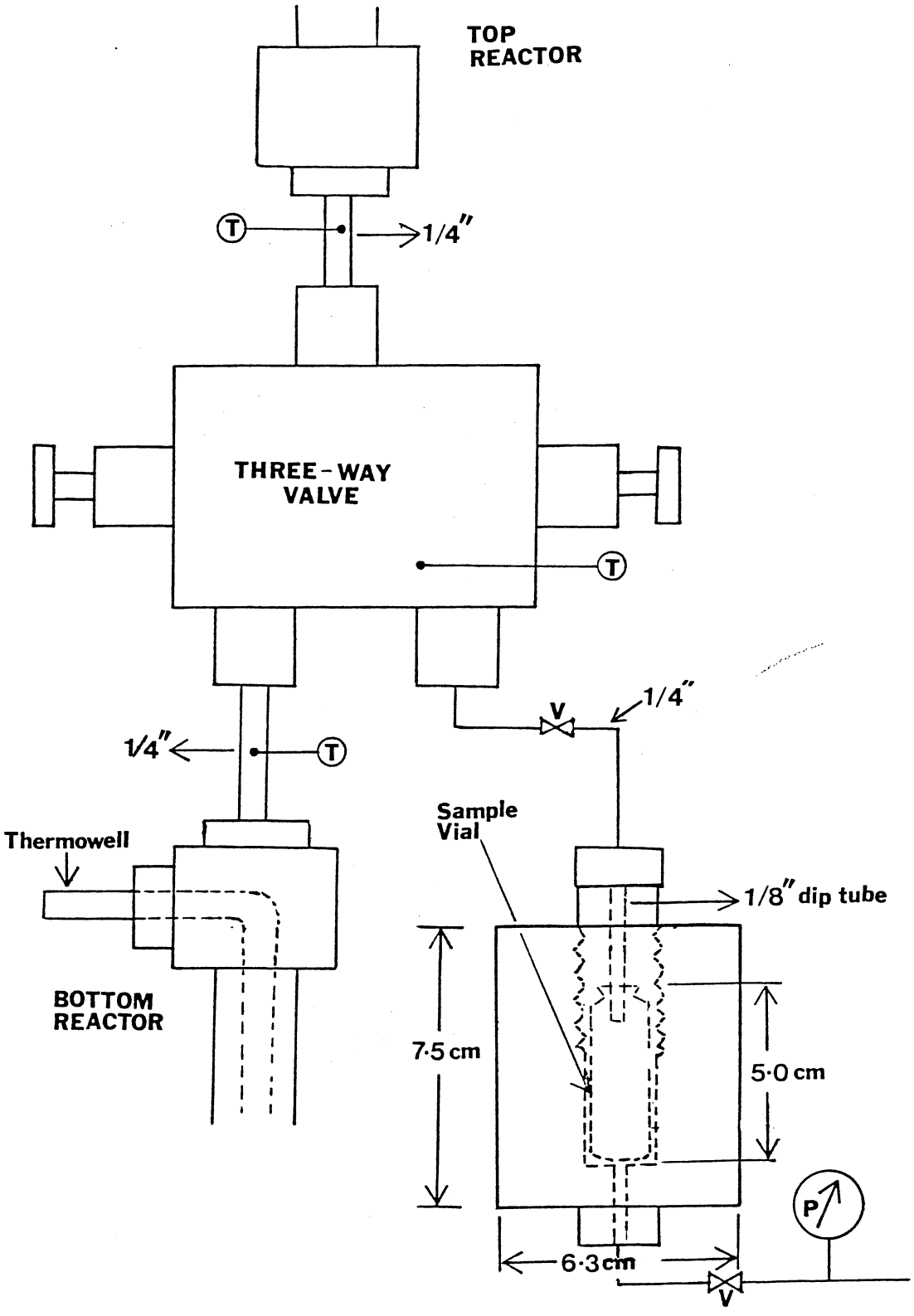

Figure 47. Details of the Microsampling System

Gas Flow Control

The gas flow rate was maintained by means of micrometer valve 1 (see Figure 44). The gas flow was monitored downstream from the micrometer valve by means of a 0-500 ml bubble flow meter. Prior to metering, the exit gases were scrubbed in a 50 vol% ethanolamine solution. A liquid trap, containing alumina spheres, was used to avoid entrainment of the scrubbing liquid into the gas measuring devices. In order to avoid continuous gas flow through the bubble meter, a bypass line was connected between the bubble meter and the low-pressure rotameter. Gas flow would normally occur through the low-pressure rotameter, the bubble meter being connected only when the gas was to be metered accurately.

Inert Gas Purging Facility

The liquid product samples were purged with nitrogen gas in the sample bombs 2 and 3 to remove any ammonia and hydrogen sulfide dissolved in the liquid sample. Nitrogen gas was supplied to the bottom of sample bomb 2 directly from supply cylinders. Nitrogen gas entered the reactor bomb through a flow-check valve and escaped through a separate line connected to the top of sample bomb 2 (see Figure 44). This separate line was connected to avoid the flow of purging gases through the metering valves. The pressure in the nitrogen gas cylinders was always maintained higher than the system operating pressure to facilitate use of nitrogen gas for repressuring the system after sample collection.

Gas Detectors

A combustible gas detector, MSA Model 501, was installed with two detector heads, located over the hydrogen bottles and the reactor system, respectively. A red light and an audible alarm would come on in case the hydrogen concentration in the room exceeded 40% of the lower explosive limit for hydrogen gas. The system was always tested prior to starting an experiment by releasing controlled amounts of hydrogen gas near the sensing head and observing the detector response.

A portable hydrogen sulfide detector was kept handy during catalyst presulfidation and also while taking liquid samples. It provided a digital output of the instantaneous, average, and maximum hydrogen sulfide concentration during a time interval. This detector was set to sound an alarm at 17-20 ppm concentration of hydrogen sulfide, the alarm frequency increased with the increase in concentration.

APPENDIX B

LIST OF MAJOR EQUIPMENTS

Following is a list of the major equipments used in this study.

Oil Feed System

1. Ruska Positive Displacement Pump - 1000 cc barrel capacity, 2.5 - 260 cc/hr feed rate; Model 2336 S II; Ruska Instrument Corporation, Houston, TX.

2. Storage Tank - 12 liter capacity, 30 psig maximum pressure; fabricated at the Department of Physics Workshop, Oklahoma State University, Stillwater.

3. Pressure Gauges - Crosby Engineering, 5000 psig maximum pressure.

4. Rupture Disks - 1/4 - inch, bursting pressure: 2600, and 3200 psig at 72°F; Autoclave Engineering Company.

5. Pressure Switch - 500-3000 psig pressure range, on/off type, 120 volts; SOR Inc., Olathe, Kansas, Model No. INN-K5-M4.

6. Storage Tank Heater - 120 volts, 300 watts band heaters; Model No: 500-8-3; Thermal Corporation, Richardson, TX.

7. Valves - 1/2 - inch Parker Hannifan, maximum operating temperature: 316°F, CPI Model No. V6LJ.

- 1/4 - inch Autoclave Engineering, 316 stainless steel Model No: 10V-4071.

Hydrogen Feed System

1. Gas Supply Manifold - 3600 psig maximum pressure; Matheson Equipment Corporation.

2. Pressure Regulator - Mity-Mite type, internally loaded, inlet pressure: 5000 psig, outlet pressure: 3000 psig, 1/4 - inch inlet and outlet connections; Grove Valve Co., Oakland, California.

3. High Pressure Flow Meter - 5000 psig maximum pressure; Brooks Instrument Company, Hatfield, PA, Model No. 1482-02D1R1A; Tube Model No. R2-15-A.

4. Heise Gauge - Heise-Bourdon tube gauge, 3000 psig maximum pressure; Heise Bourdon Tube Company, Newton, Connecticut.

5. Quarter-Turn Valve - 303 stainless steel; Hoke valve Model No. PS490.

6. Excess Flow-Check Valve - 1/4 - inch, ball check type; Autoclave Enginering Model No. SK-4402.

7. Diffusion Trap - 300 cc capacity, 5000 psig maximum pressure, Hoke Model No. 80H1365.

8. Check Valves - 1/8 inch, 316 stainless steel, maximum pressure: 6000 psig; Autoclave Engineering Model No. OB2200.

Reactor System

1. Reactor - 316 stainless steel, seamless, 1/2 inch diameter, 0.069 inch wall thickness, heat treated.

2. Aluminum Heating Blocks - fabricated at Oklahoma State University, Mechanical Engineering Laboratory, 4 inch diameter, 30 inch long.

3. Heaters - 400 watts, 120 volts, band heaters, stainless steel clading, 4 inch diameter; Thermal Corporation Model No. 502-4-5.

4. Temperature Programmers - Valley Forge Instrument Co., Phoenixville, PA; a) 115V, 20 A max., Model No. 3359 b) 120 V, 10 A max., Model No. 3274.

5. Powerstats - 120 volts input, 0-140 volts output, 10 A, 1.4 KVA; Superior Electric Co. Model No. 116.

6. Temperature Indicator - Omega trendicator, °C; Omega Engineering, Stamford, Connecticut, Model No. 475A-C.

7. External Thermocouples - Iron-constantan, J-type, stainless steel sheath; Omega Engineering Model No. TJ36-1CSS-18U-12.

8. Internal Thermocouples - 1/1000 - inch, stainless steel sheath, 18, 24 ,36 inches, Omega Engineering Model No. SICSS-O1OU-36, 24, 18.

9. Thermowell - 1/8 - inch OD, 316 stainless steel tubing, 38 inches, one end welded.

Microsampling Unit

1. Three-way Separation Valve - 316 stainless steel, high temperature service, 400°C maximum temperature, 11,500 psi maximum operating pressure; Autoclave Engineering Model No. 10V-4075.

2. Micro-sample Holder - fabricated at the Mechanical Engineering Laboratory, Oklahoma State University, Stillwater, Oklahoma.

3. Sample Vials - 5 cc, serum vials, Sargent Welch Company.

4. Pressure Gauge - maximum pressure 3000 psig, Ashcroft.

5. Valve - regulating type, Whitey Model No. 3124.

Product Oil Separation and Sampling System

1. Pressure Gauges - 5000 psi maximum pressure; Matheson Model No. 63-5633.

2. Sample Bombs - 180,300,500 cc capacity, 5000 psig maximum pressure; Hoke Model No. 80-HT36.

3. Scrubber Bomb - 300 cc capacity, 1800 psig maximum pressure; Matheson Model No. 6-645-232.

4. Extended Stem Valve - 1/2 - inch, high temperature (400°C), extended stem, 316 stainless steel; Whitey Model No. 6VS4.

5. Flowmeter - Rotameter; Matheson Model No. R2-15D.

6. Micrometer Valve - 1/4 - inch, 316 stainless steel, Whitey Model No. 22RS4.

7. Valves - 1/4 - inch, 316 stainless steel, 11,000 psig maximum pressure; Autoclave Engineering Model No. 10V-4071.

8. Check-Valve - 1/4 - inch, 5000 psig operating pressure, Nupra Valve Company.

Miscellaneous

1. Hydrogen Gas Detector - combustible gas alarm, MSA Instrument Corporation, Model No. I-501.

2. Hydrogen Sulfide Detector - concentration range, 0-50 ppm, audible alarm; Sierra Labs Inc., Model No. 10HS.

3. Multipoint Temperature Selector - 40 point temperature selector; Omega Engineering, Norwalk, Connecticut.

4. Felt Insulation - ceramic fiber insulation, maximum temperature, 1260°C; Thermal Corporation, Houston, Texas.

5. Fiberglass Insulation - McMaster Carr.

6. Insulating Tape - 1 - inch width, Sargent Welch Company.

Microfiltration Unit

1. Filtration Cell - 100 mls capacity, stainless steel, Millipore Corporation.

2. Pressure Bomb - 1800 psig, stainless steel, Whitey.

3. Pressue Gauge - 60 psig maximum pressure, Crosby Engineering.

4. Valves - CPI valves, Parker Hannifan Company, Model No. 116F.

5. Burette - 500 mls capacity, pyrex, Sargent Welch Company.

6. Ultrasonic Bath - 125 watts, Branson Equipment Company, Shelton, Connecticut.

7. Teflon Filters - 10 mm, L C filter type, Millipore Corporation, Catalog No. LCWP-O-4700.

APPENDIX C

DETAILS OF EXPERIMENTAL PROCEDURE

In this appendix, detailed experimental procedure is described. The sequence of the steps involved in the actual experiment were the same as given here. The experimental procedure consisted of catalyst preparation and loading, catalyst presulfidation, normal operation, sampling and shutdown.

Catalyst Preparation and Loading

Catalyst Preparation

Two commercially available catalysts, HT-115E and KF-153S, were used in the present study. Both catalysts were 1/16 - inch extrudates. These catalysts were calcined in a muffle-furnace at a temperature of 475°C $\pm$ 10°C, for a period of 6 hours. This step was meant to remove any adsorbed water from the catalyst support. The catalysts were cooled to room temperature and stored in desiccators until further use.

Catalyst Loading

The reactor was packed at the two ends with 2 mm glass beads, the catalyst was packed in the middle to minimize the end effects. The packing procedures were similar for the single and the multiple reactor system. The reactor was packed according to the following general procedure.

1. The reactor tubing was cut to the required length and the cut edges smoothed with 200 grain sandpaper. A 1/4 - inch thick, perforated stainless steel disk, with 1/8 - inch hole in the middle for the thermowell, was snugly fitted into the reactor bottom.

2. A fifty-mesh size screen was wedged in between the bottom of the reactor and a 1/2 - inch stainless steel union.

3. A 1/8 - inch thermowell was held centrally inside the reactor with one end inside the middle hole of the perforated disk.

4. 2 mm glass beads were poured into the reactor while vigorously tapping the reactor for uniform packing around the thermowell. For the single reactor system, the reactor bottom was packed with fresh glass beads to a height of 6.4 cms (2.5 inches); for the two reactor sysem the reactor bottom was packed to a height of 3.8 cms (1.5 inches).

5. A 1/4 - inch perforated disk was next slipped into the reactor and firmly set on top of the glass beads.

6. The amount of catalyst was determined by weight before packing.

7. The catalyst was then poured into the reactor by following the procedure described earlier. The reactor was packed to a height equal to one-half of the desired catalyst bed height; a 1/4 - inch perforated disk was placed on top of the catalyst bed and the remaining catalyst bed height filled. Another perforated disk was slipped on top of the catalyst bed. The perforated disks served the dual purpose of improving the liquid distribution over the catalyst bed, and also facilitating catalyst separation upon run completion. (See Figure 48.)

8. The rest of the reactor length was packed with 2 mm glass beads, making sure to distribute them evenly.

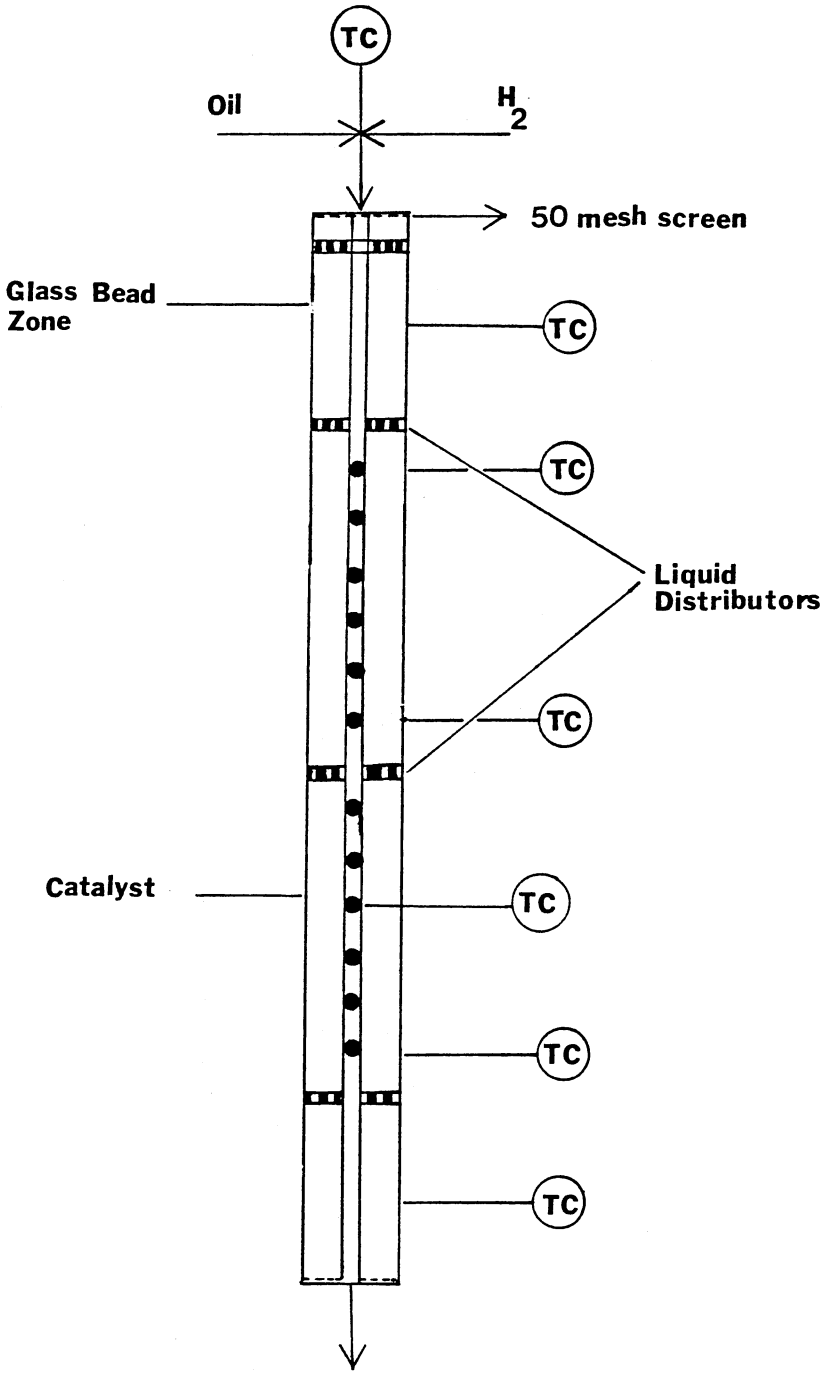

Figure 48. Reactor Internal Details

9. Another perforated disk was fitted on top of the glass beads. A 50-mesh screen, with a hole in the middle for the thermowell, was slipped on top of the glass beads.

10. The packed reactor was next fitted with a 1/2 - inch stainless steel cross/ tee. The thermowell was centered and secured by means of a 1/8 - inch Swagelok fitting. For the two reactor system, the thermowell entered the bottom reactor through the side rather than from the top, as in the single reactor. The thermowell had to be bent to facilitate its entry into the "tee" fitting.

11. The reactor was pressure tested before installing in the reactor system. The reactor was pressurized with nitrogen gas to a pressure approximately 689 kPa (100 psig) higher than the system operating pressure and each fitting tested for leaks. The system was kept under pressure for one hour, in case the pressure drop was higher than 138 kPa (20 psig), the system was depressurized and all suspect fittings tightened. The reactor was next placed inside the reactor system and the above stated procedure repeated. The system was considered leak free provided the system pressure decreased by less than 138 kPa (20 psig) in one hour. Details of the reactor interior are shown in Figure 48.

The aluminum blocks were next secured around the reactor and firmly bolted together. The band heaters were slipped over the aluminum blocks and secured in position. The electrical connection were checked for electrical continuity with a volt-ohm meter. The hydrogen and oil feed lines were next connected. The electrical wires were connected to the controllers and electrical connections insulated by glass tape. The outside thermocouples were slipped into appropriate holes in the aluminum blocks and the reactor insulated by

first fitting blocks of felt insulation over the heating bands and then insulating with fiberglass. The insulation was held together with glass tape bands.

The heating system was tested by turning on the temperature controllers and raising the reactor temperature by about 25°C above the ambient temperature. Twelve 0.0254 mm (1/1000 - inch) thermocouples were next inserted into the thermowell. This was done with extreme care - by first lubricating the thermowell hole with silicone oil and then carefully inserting the thermocouples, one at a time.

The procedure for the two reactor system was slightly different. The bottom reactor was first fixed in position, the microsampling unit was next attached to the top of the bottom reactor. After the microsampler was installed, the second reactor was secured in position. The bottom of the top reactor being fixed to the microsampling unit input. The rest of the procedure was similar to the one reactor system.

Catalyst Sulfidation

After the reactor set up and pressure testing, the reactor pressure was released. The reactor temperature was gradually raised to 400°C and stabilized while maintaining a nitrogen gas flow rate of 200 cc/min through the system. After the temperature in the reactor was stabilized, the system was ready for sulfidation to begin.

The nitrogen gas supply was cutoff, all the valves except valves 2 and 3, and micrometer valve 1 were closed (Figure 44). A mixture of 5.14% H_2S in H_2 was passed through the reactor at a pressure of 551.7 kPa (80 psig) by opening value 1 completely. The gas flow rate was maintained at 500 cc/min for a period of 3 hours; the total amount of

hydrogen sulfide passed through the system was three times the stichometric amount required for complete sulfidation of all the nickel and molybdenum present in the catalyst.

Startup Procedure

After presulfiding, the H_2S/H_2 gas stream was cutoff. Nitrogen gas, at a flow rate of 200 cc/min, was allowed to flow through the system to purge it of any residual hydrogen sulfide. In the meantime, the feed tank was filled with the oil and the Ruska pump feed rate set at the operating liquid flow rate. The oil in the feed tank was heated to approximately 100°C, and thoroughly mixed by turning on the motor attached to the stirrer. A nitrogen gas pressure of approximately 138 kPa (20 psig) was maintained in the feed tank. The Ruska pump was filled by closing all valves around the pump and opening valve 5, connecting the oil feed tank and the Ruska pump. The Ruska pump was equipped with a rapid traverse motor for rapid filling of the pump cylinder with oil.

The temperature controllers were next shut-off, and the temperature inside the reactor allowed to fall by approximately 10°C of the operating sulfidation temperature. The system was pressurized to the desired operating pressure by gently turning the Matheson pressure regulator (connected to the hydrogen gas manifold) in the clockwise direction and monitoring the pressure increase on the Heise gauge. During this time, valves 13 and 14 were left fully open to avoid the flow of gases through the excess flow check valve and the high pressure flow meter.

The Ruska pump was pressurized by closing all valves around the pump and traversing the pump in the forward direction till the pressure

indicated on the pressure gauge 4 was approximately 13.8 MPa (2000 psig). The Ruska pump gear was shifted to the feed position and valve 22 opened. Valve 15 was opened and the pump flow cutoff upon the first drop of oil coming out of the line; valve 15 was closed and the pump traversed till the pressure indicated by pressure gauge 4 was approximately 12.4 mPa (1800 psig). The Ruska pump gear was shifted to the feed position and the pump cutoff. Valve 7 was completely opened to connect the rupture disks to the high pressure system.

The desired gas flow rate was attained by fine adjusting micrometer valve 2; valves 16, 10 and 4 were all left fully open during this period. The Ruska pump was turned on and valve 6 opened. The temperature rise in the catalyst bed was carefully monitored; after the first wave of temperature rise had passed through the system (which usually took 1 hour), the system temperature was raised to the desired operating temperature by adjusting the set-point temperature on the controllers.

Normal Operation

The system was considered to be operating normally when the pressure and temperature had stabilized. A pressure variation of $\pm$ 138 kPa and a temperature variation of $\pm$ 3°C along the reactor length was considered normal. During normal operation, the temperature profile, pressure gauge reading, gas flow rate, pump reading, and hydrogen gas bottle pressure were noted every hour. The temperature profile inside the reactor bed was measured from top to the bottom of the catalyst bed by thermocouples placed inside the thermowell.

During normal operation, hydrogen gas entered the reactor top through valve 16; oil entered through valve 6 and flowed co-currently down the packed bed (Figure 44). The unreacted hydrogen, product oil, and the gaseous products flowed into sample bomb 1, which was placed immediately below the reactor. The liquids and gases flowed into sample bomb 2 through valve 10. Gas-liquid separation occurred in sample bomb 2, the gases escaping through valve 4 and micrometer valve 2. During normal operation, valve 2 was kept closed. The gases from sample bomb 2 escaped into the sample bombs 3 and 4, where any liquid entrained by the gases was removed. The gases were metered through a flow meter after scrubbing in an ethanolamine scrubber. The hydrogen gas flow rate was fixed at the desired rate by fine adjusting micrometer valve 2.

During normal operation,valves 13 and 14 were closed to allow hydrogen gas to flow through the high pressure flow meter and the excess flow-check valve. The high pressure flow meter proved invaluable in the system operation, it indicated the condition of no flow in the reactor.

Whenever the gas flow was to be metered carefully, the flow was diverted into the bubble meter by closing valves 18 and 19. For the remaining period, the flow was metered through a rotameter, by closing valves 17 and 19 and opening valve 18.

The pump liquid level was always checked by noting the distance traversed by the cylinder. Anytime the pump traversed a distance greater than 900 mls, it was refilled. This was accomplished by closing valve 22 and depressurizing the pump by traversing the pump in the reverse direction.

Valve 5 was completely opened when zero pressure was indicated by the pressure gauge 4. The liquid in the feed tank was prior heated and mixed; the pump was traversed in the reverse direction and the liquid sucked into the pump cylinder. Upon complete filling of the pump cylinder, valve 5 was closed and the pump traversed in forward direction till a pressure of 12.4 MPa (1800 psig) was indicated, valve 22 was then opened. The pump gear was shifted to the feed position and normal operation restored.

Sampling Procedure

Liquid Sampling

The system was designed with the objective of removing the product liquid samples without disturbing the normal operation. The reactor section beyond valve 10 (Figure 44) was isolated from the system by closing valves 3, 4, and 10. Sample bombs 2, 3 and 4 were depressurized by slightly opening valve 20; the pressure inside the sample bombs was monitored on pressure gauge 2. When the pressure in the bombs was released completely, the liquid was purged with nitrogen gas at 689.6 kPa (100 psig) for a period of 10-15 minutes. The nitrogen gas entered pressure bomb 2 through valve 12 and exited through valve 20; valve 4 was closed during sampling to avoid gas flow into the scrubber. After 10-15 minutes of nitrogen purging, the gas supply was cutoff and the pressure inside the bombs allowed to drop to 344.8 kPa (50 psig), valve 20 was then closed. Valves 8 and 9 were opened and closed alternately to collect the liquid sample in the sample bottle, valve 11 was kept open for the entrained liquid to flow into the sample

bottle. Valves 8 and 9 were closed when the pressure gauge 2 indicated zero pressure.

During the sampling procedure, the gases and liquids from the reactor flowed into the sample bomb 1, where gas-liquid separation occurred. The gases flowed out through valve 2 and micrometer valve 1, valve 3 was kept closed to avoid gases from entering the scrubbing system.

The sample bombs were repressurized by nitrogen gas to a pressure of approximately 344.8 kPa (50 psig) less than the system operation pressure. Pressure bomb 1 was next connected to the system by fully opening valve 10; valve 2 was closed and normal hydrogen gas flow restored by opening valves 4 and 3.

Microsampling Procedure

The microsampling procedure was designed to remove 3-5 mls of liquid sample inbetween the reactors placed in series. The liquid and gas flow from the bottom of the first reactor was diverted into the microsampling bomb through a three-way valve. Valve 22, connecting the nitrogen gas bottle and the microsampling bomb, was opened and the system pressurized to approximately 50-100 psig less than the system operating pressure. Valve 21 was kept closed for 3-5 minutes (depending upon the flow rate), after the three-way valve had been opened to collect the liquid in the line joining valve 21 and the three-way valve. Valve 21 was then momentarily opened, upon pressure increase in pressure gauge 3, this valve was closed. The three-way valve was readjusted for normal operation after valve 21 was closed. The

microsampling system was depressurized by opening valve 22, and the sample vial containing the liquid sample removed. Valve 4 was also closed during microsampling to avoid the pressure in the sample bomb to drop considerably from the operating pressure.

Shutdown Procedure

The pump was first switched off and valve 6 closed. The reactor heaters were turned off and the reactor allowed to cool. The reactor pressure was maintained at normal operating valve and the hydrogen flow rate quadrupled to accelerate the reactor quenching. Part of the reactor insulation was taken off to accelerate the cooling. When the reactor reached the ambient temperature, the system was depressurized by closing the hydrogen inlet valve 16.

The reactor heating bands were next removed followed by the removal of the aluminum blocks. The reactor was removed and cut into sections, the catalysts and the glass beads from each section were removed for further analysis.

The pump was traversed in the reverse direction to allow all the liquid in the feed lines to collect in the pump cylinder. The pump liquid was discharged by closing valve 22 and opening valve 23. In case some liquid was left in the feed tank, it was drained by opening valve 5 and 23. The system was thoroughly cleaned with acetone by first filling the feed tank with acetone and then pumping it through the entire reactor sysem, valve 16 was closed during this operation to avoid acetone from entering the gas feed system.

APPENDIX D

ANALYTICAL PROCEDURE

The experimental procedure for the analysis of the liquid and the catalyst samples is described in this Appendix.

Product Liquid Sample Analyses

The feedstock and the product liquid samples were characterized in terms of the nitrogen, hydrogen, sulfur content; n-pentane, ethyl acetate, tetrahydorfuran insoluble content; and ASTM distillation 454 C^+ residue content. Details of the hydrogen, nitrogen, and sulfur determination procedure are given by Bhan (1981). The procedures for determining the n-pentane, ethyl acetate, and tetrahydrofuran insoluble content, 454 C^+ residue content, and ash content are described here.

n-Pentane, Ethyl Acetate, and Tetrahydrofuran Insoluble Content

The routine procedure consists of the following steps:

1. Thoroughly clean a 100 ml beaker with acetone.

2. Weigh approximately five grams of the sample to be analyzed in the beaker.

3. Partially assemble the Millipore apparatus by placing a preweighed 10 μm filter in the filter cell.

4. Dilute the sample in the beaker with approximately 20 mls of the designated solvent (n-pentane, ethyl acetate, tetrahydrofuran). Stir with a glass rod. For the feedstock samples, it is advisable to add 2 mls of toluene prior to adding the solvent. This avoids the formation of gum deposits in the precipitate. This procedure is not necessary for the product liquid samples.

5. Add approximately 60 mls of the designated solvent to the solution in the beaker. Place the beaker in an ultrasonic bath for approximately 3 minutes; sonicate all samples for the same period of time.

6. Pour the contents of the beaker into the filtration cell. Clean the beaker by rinsing with the particular solvent being used, making sure no residue is sticking to the beaker. Add the residual solution to the contents of the filtration cell.

7. Attach the apparatus as shown in Figure 49. Add approximately 400 mls of the designated solvent to the solvent reservoir.

8. Open valves 2 and 3 (Figure 49), and allow the solvent to flow from the solvent reservoir into the pressure bomb. Close valves 2 and 3 and open valve 1. Adjust the pressure on the gas manifold to approximately 40 psig.

9. Open valve 4, the solvent from the pressure bomb flows into the filter cell under pressure. There will be a pressure surge when all the solvent has passed through the filter cell. Allow nitrogen gas to pass through the cake for 5 minutes.

10. Close valves 4 and 1, and vent the system by opening valve 2.

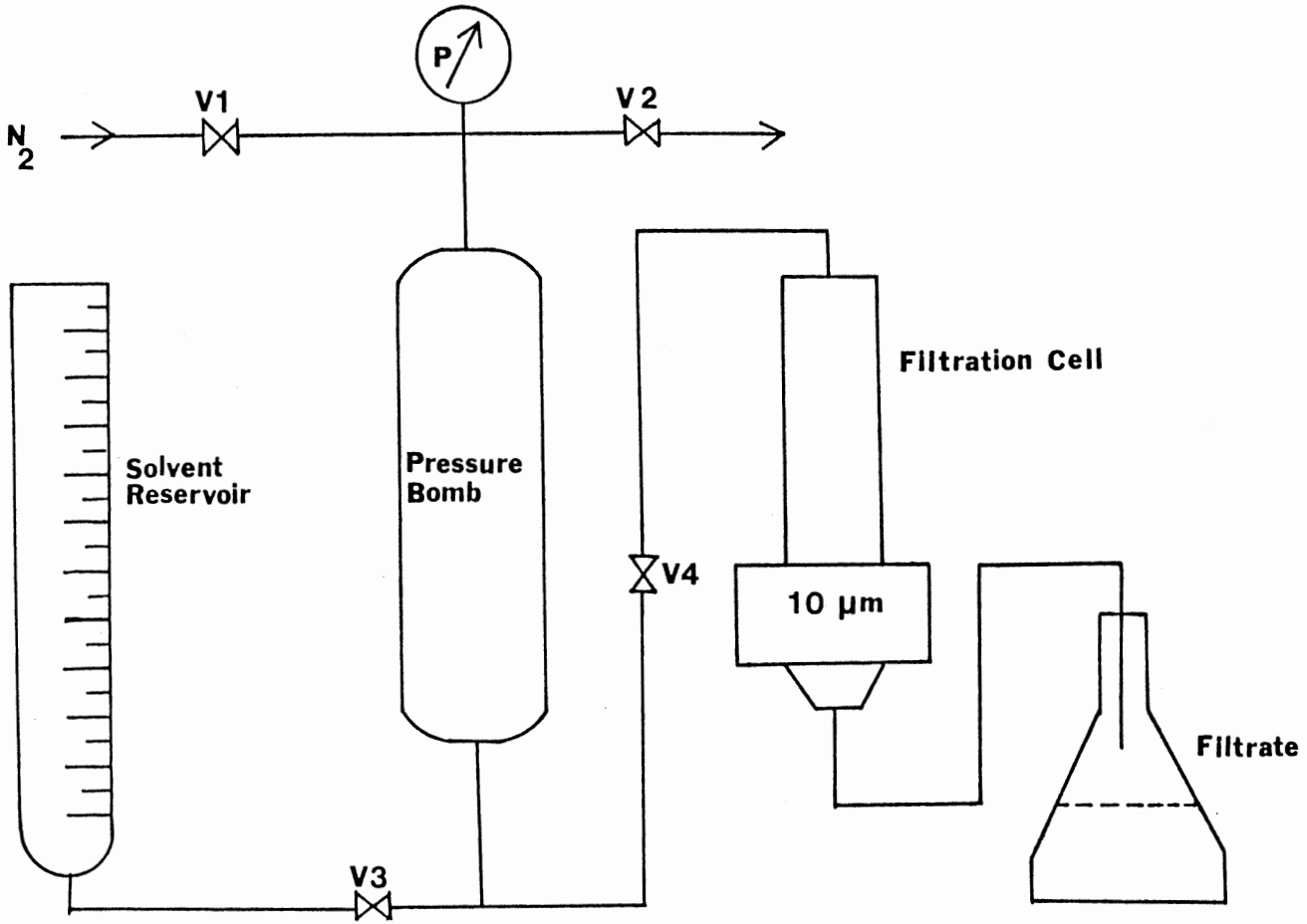

Figure 49. Microfiltration Apparatus

11. Disassemble the filter cell and carefully remove the teflon filter paper. Place the filter-cake on pre-weighed wax-paper. Scrape any residues from the walls of the filter cell and add to the filter-cake.

12. Dry the residues in an oven at 100°C for a period of one hour.

13. Remove the residues and weigh immediately. Reject any sample which does not give a friable filter cake or shows evidence of tarry residues.

14. The weight percent residues is determined as:

$$\text{wt\% residues} = \frac{W_1}{W_2} \times 100$$

W_1 = net weight of residues

W_2 = weight of oil

ASTM Distillation and 454 C^+ Residues

The procedure is based on the ASTM D-1160 standard. It consists of the following steps:

1. Take 100 mls of liquid sample in a 500 ml flask. Make sure to add weighed boiling chips to the liquid before clamping the flask to the unit.

2. Load the cold trap with dry ice and acetone. Turn water heater on and connect temperature recorder to the thermocouple.

3. Turn on the hot water pump.

4. Turn on the vacuum pump and adjust the pressure to 20 mm of Hg by adjusting the valve on the vacuum line.

5. Turn on the powerstat; initial setting of the powerstat is determined by operator (recommended 60 or higher).

6. Record the vapor temperature when the first drop of vapor condenses; record it as the initial boiling point. Record the temperature when 10, 20,..., volume percent is distilled. Powerstat settings are increased to give a uniform distillation rate.

7. When the vapor temperature of 310°C is indicated, turn off the powerstat and the vacuum pump.

8. Let the system cool to approximately 100°C, repressurize slowly by opening the by-pass valve.

9. Allow the residues in the flask to cool to room temperature. Remove and weigh the residues, subtract the weight of the boiling chips, the remaining fraction represents the fraction of 454 C^+ residues.

10. Clean the flask by boiling acetone in it. Cleanup is best accomplished by atmospheric distillation of 20-30 mls of acetone.

Oil Ash Content

The routine procedure consisted of the following steps:

1. Thoroughly clean a ceramic crucible and its lid with acetone. Heat the crucible and the lid in a furnace overnight at 500°C $\pm$ 20°C.

2. Remove the n-pentane insoluble fractions from 10 gms of oil following the procedure described earlier.

3. Weigh the crucible and the lid at temperature slightly higher than the ambient.

4. Pour the n-pentane insoluble residues into the crucible and cover with the lid. Heat in furnace at 500°C for a period of 24 hours.

5. Allow the crucible to cool to room temperature, make sure

not to remove the lid until the weighing is done.

6. The weight fraction ash is determined as:

$$\text{wt\% ash} = 10 \cdot (W_1 - W_2)$$

W_1 = weight of crucible, lid and residues before combustion.

W_2 = weight of crucible, lid and residues after combustion.

Catalyst Characterization

The used catalyst samples from each experimental run were separated into six sections, the glass beads in the pre- and post-reactor section were also separated. The catalysts and glass bead samples were extensively extracted with tetrahydrofuran in a Soxhlet apparatus to remove any soluble material. The extraction was conducted at room temperature for a period of 24 hours; the solvent generally became clear within 6-8 hours. The catalysts were dried overnight at 100°C under vacuum. The washed and dried samples were screened through a 20 mesh-size screen and the residues collected and weighed. The catalyst were characterized in terms of coke content, elemental content, surface area, pore volume, pore diameter and distribution, surface metal deposition and metal penetration.

Surface Area Analysis

The reader is referred to the operator's manual of the Micromeritics Model 2100 D ORR Surface Area-Pore Volume Analyzer for details of catalyst surface area analysis.

Pore Volume and Pore Size Distribution

The reader is referred to the operator's manual of the Micromeritics Model 900 Mercury Penetration Porosimeter for details of the pore volume and pore size distribution.

Coke Content

The routine procedure for determining the coke content consists of the following steps:

1. Place approximately 2 gms of dried and evacuated catalyst sample in the sample holder of the Micromeritics Model 2100D ORR analyzer and evacuate for a period of 6 hours at a temperature of 100°C.

2. Allow the sample to cool to room temperature while still in the sample holder.

3. Fill the sample holder with dry helium gas to a pressure of approximately 780 mm of Hg. This procedure is conducted to avoid moisture adsorption from air. Weigh the sample holder and the catalyst.

4. Carefully pour the catalyst into a clean ceramic crucible and heat in a furnace at a temperature of 475°C $\pm$ 10°C for a period of 24 hours.

5. Cool the crucible to room temperature and repeat steps 1, 2 and 3.

6. The weight percent coke is determined as:

$$\text{wt\% coke} = \frac{W_1 - W_2}{W_2} \times 100$$

W_1 = weight of coked catalyst

W_2 = weight of regenerated catalyst

Catalyst Elemental Analysis

The catalyst elemental analysis was conducted to determine the nature of the carbonaceous deposits on the catalyst. The following is the general procedure for determining the catalyst elemental content:

1. Evacuate catalyst samples (fresh and aged) at a temperature of 100°C.

2. Analyze a fresh catalyst pellet of 10 mgs approximate weight in the Perkin-Elmer 240B Elemental Analyzer. Determine the hydrogen peak output in microvolts.

3. Weigh the calcined pellet from the analyzer. Hydrogen content of fresh pellet is determined as:

$$\text{Hydrogen content of fresh pellet} = \frac{\text{Hydrogen Signal in } \mu V}{\text{Weight of the fresh calcined pellet, mg}}$$

4. Analyze aged catalyst pellet of approximately 10 mgs weight in the elemental analyzer. Accurately weigh the calcined pellet. Determine the correction for hydrogen content as follows:

$$\text{Correction for Hydrogen Content of Catalyst Pellet} = \left(\text{Hydrogen content of fresh catalyst}\right) \times \left(\text{weight of the calcined pellet}\right)$$

5. The N, C, H content of the carbonaceous residues is determined as follows:

$$\text{wt\%N} = \frac{\text{Signal strength - Blank - Zero}}{K_N \times \text{Weight of the calcined pellet}}$$

$$\text{wt\%C} = \frac{\text{Signal strength - Blank - Zero}}{K_C \times \text{Weight of the calcined pellet}}$$

$$\text{wt\%H} = \frac{\text{Signal strength - Correction factor - Blank - Zero}}{K_H \times \text{Weight of the calcined pellet}}$$

where

K_N, K_C, K_H = Sensitivity factor for N, C, and H, respectively.

Surface Metal Deposition and Penetration

Catalyst metal analysis was conducted using a JEOL Model JFM-35 Electron Scanning Microscope equipped with an Energy Dispersive X-ray Analyzer. This apparatus is located in the Microbiology department of Oklahoma State University. The reader should consult Ms. Denise at (405)624-6765 for details of the analytical procedure.

APPENDIX E

GASES AND CHEMICALS USED

The gases and chemicals used in the hydrotreatment system, elemental analyzer, solvent residue analysis and catalyst analyses are listed in this Appendix.

Hydrotreatment System

Hydrogen	99.5% purity, 2300 psig (Sooner Supplies)
Nitrogen	99.5% purity, 2300 psig (Sooner Supplies)
Hydrogen Sulfide	5.14% mixture in H_2, 2000 psig (Matheson)
Inert Packing	2 mm borosilicate glass beads, Prooper Mfg. Co., Long Island City, NY.

Elemental Analysis

Oxygen	Ultra high purity (99.99%), 2700 psig, Linde
Helium	Chromatographic (99.995%), 2500 psig, Linde
Aluminum capsules	Perkin-Elmer, part #240-0642
Nickel capsules	Perkin-Elmer, part #240-0643
Platinum gauge	Perkin-Elmer, part #240-1147
Silver gauge	Perkin-Elmer, part #240-0092
Magnesium perchlorate	Reagent grade, Fischer Scientific Company
Silver vanadate	Reagent grade, Perkin-Elmer, part #240-1117
Tungstic anhydride	Perkin-Elmer, part #240-1238

Quartz wool	Perkin-Elmer, part #240-1118
Colocarb	Perkin-Elmer, part # 240-0115
Copper	60-100 mesh size, Perkin-Elmer, part # 240-0017
Silver oxide - silver tungstate on chromosorb	Perkin-Elmer, part #240-0113
Silver tungstate-magnesium oxide	Perkin-Elmer, part #240-1344
Acetanilide	BDH Chemicals
Quartz combustion tube (9mm ID x 11.2mm OD)	Thermal American Quartz
Quartz reduction tube	Perkin-Elmer

Catalyst Extraction

Tetrahydrofuran	Reagent grade, Fischer Scientific
Extraction Thimbles	Cellulose, Single thickness, 35 mm x 80 mm, Whatman

Catalyst Analysis

Nitrogen	Chromatographic, 99.995% purity, 2500 psig, Air Products Co.
Helium	Chromatographic, 99.995% purity, 2500 psig, Air Products Co.

n-Pentane, Ethyl Acetate, Tetrahydrofuran Insoluble Analyses

n-Pentane	Reagent grade, Fischer Scientific
Ethyl Acetate	Reagent grade, Fischer Scientific

Tetrahydrofuran	Reagent grade, Fischer Scientific

APPENDIX F

METHODS USED FOR ASPHALTENE SEPARATION

Various methods have emerged for quantitative separation of the coal- and petroleum-derived preasphaltenes, asphaltenes, resins, and oils. Different procedures produce different results, however, each procedure is completely reproducible.

The methods used for coal liquid fractionation vary from solvent precipitation to chromatographic separation. For the solvent separation methods, the amount of asphaltenes is strongly dependent upon the choice of solvent, extraction method, time of extraction, and the sequence of extraction. The petroleum asphaltenes, on the other hand, are insensitive to the solvent sequence and the extraction time.

For the coal-derived liquids, three general extraction sequences have been used: direct extraction, forward sequential extraction, and reverse sequential extraction. For the direct technique, individual samples are separately extracted with pentane, benzene, and pyridine. The insoluble portions are dried in a vacuum oven and weighed separately to determine each fraction weight percent. For the forward sequential method , the feed sample is first extracted with n-pentane, the residues are dried, weighed and subsequently treated with benzene, and pyridine to determine the benzene and pyridine insoluble content.

The reverse sequential method is similar to the forward method with the exception that pyridine is used first. The pyridine insolubles are vacuum dried and weighed; pyridine is stripped from the pyridine solubles, and the residues extracted with benzene. The benzene insolubles are dried and weighed, and the benzene stripped from the benzene solubles. Finally the benzene solubles are extracted with n-pentane. The insoluble fractions are separated, dried, and weighed.

Various techniques have been used for extracting asphaltenes from coal-derived liquids. Soxhlet extraction method has been developed and used extensively at Pittsburgh Energy Technology Center (PETC). In this method, the sample is continuously extracted with fresh solvent in a Soxhlet apparatus at elevated temperatures. Repeated centrifuging has also been used for asphaltene separation. An excellent review of the various methods used for asphaltene separation has been presented by Schultz and Mima (1980).

The choice of a particular method for asphaltene separation cannot be based on the criterion of accuracy, because there is no independent measure of the purity of a fraction. A method may, however, be preferred on the basis of the time needed for the complete analysis, and the consistency and reproducibility of the results.

The Soxhlet extraction method is extremely laborious and time consuming, each sample may take more than 24 hours for complete analysis. Centrifuging too, is a cumbersome procedure and requires constant attention. A shortcut procedure for asphaltene separation was developed at Amoco Petroleum Company by Bertolacini et al. (1977). This procedure was later modified at PETC (Utz et al., 1982). This method involves pressure filtration of the precipitated mixture

at room temperature. This method of analysis reduces the sample determination time to approximately half an hour and gives equally reliable results.

Steffgen et al. (1979) examined the differences in the amount of aspahltenes determined depending upon the solvent and method used. This work demonstrated that certain differences in the procedure have a large affect on the asphaltenes determined; the amount of toluene used during slurry formation being very critical. (During the precipitation of asphaltenes from the coal liquids, a slurry is first prepared with a small amount of toluene, before the large excess of pentane is added.) With no or inadequate amount of toluene added during slurry formation, gum deposits were reported in the precipitated asphaltenes. A ratio of 3 ml/gm of toluene was recommended for slurry formation. The authors further reported no difference in the amount of asphaltenes determined, when benzene was replaced by toluene for separation of benzene soluble fraction.

Bockrath et al. (1979), too, reported a strong dependence of the asphaltenes separated upon the quantity of toluene used for slurry preparation. These authors reported an increase in molecular weight of the coal-derived asphaltenes with decrease in the asphaltene yield; the molecular weights were reported to increase from 516 to 958, for a decrease in the yield of asphaltenes from 21.7 to 11.8%. It can be concluded that heavier molecular fractions precipitate out first from the solvent - coal liquid mixture.

Yen (1980) separated coal liquids into five fractions, using benzene and CS_2 instead of benzene and pyridine. Pentane soluble fractions were further treated with liquid propane, the insoluble

fraction was reported to constitute the resinous fraction and the soluble, the oil fraction. The benzene insolubles were further treated with CS_2, the soluble fractions were called carbenes (pre-asphaltenes), and the insoluble fractions carboids (THF insoluble).

Schweighart et al. (1977) substituted tetrahydrofuran (THF) for pyridine to separate the benzene insoluble fraction of Synthiol coal liquid into THF soluble (pre-asphaltene) and THF insoluble fractions (coal, coal-ash). The THF insoluble fraction contained approximately 80% ash. Pyridine was reported to be more effective for reducing pyridine insoluble content than THF.

Mitchell and Speight (1981) reported asphaltene yields using different precipitating solvents. Liquid propane was reported to precipitate 50% of Athabasca bitumens as asphaltenes, the yield using n-pentane, n-heptane, and n-decane was 7, 11, and 9%, respectively. Lower asphaltene precipitation was also reported to occur when less than the required amount of hydrocarbons were added for precipitation, a minimum of 40 volumes of the hydrocarbon were recommended for complete precipitation.

Coal-derived asphaltenes (CDA) have been divided into acidic, basic and neutral fractions. Sternberg (1976) separated CDA into acid/base complexes by bubbling dry HCl gas through a mixture of coal-derived liquids and toluene. The basic components precipitated, whereas, the acid and the neutral fraction remained in solution and were separated by solvent evaporation.

Schwager et al. (1979) fractionated Synthoil coal liquid samples by chromatography on styrene-divinyl benzene packing. Five fractions were eluted in the molecular weight range of 359 to 1280. Aromatic

molecules with large saturated substituents eluted before the smaller and more aromatic molecules. Schwager and Yen (1979) using rapid chromatographic procedures separated asphaltenes derived from five major coal liquefaction processes (Synthoil, HRI H-Coal, FMC-COED PAMCO-SRC, Catalytic Inc. - SRC), into acid, basic and neutral fractions.

APPENDIX G

DETAILS OF THE EFFECTIVENESS FACTOR DETERMINATION

Assume that the catalyst pellet consists of cylindrical pores parallel to each other. Species mass balance over the cylindrical pore can be written as:

$$\pi r^2 D_{eff} \frac{d^2 C_i}{dx^2} = 2\pi r \cdot k_s \cdot C_i \qquad (1)$$

where k_s = intrinsic reaction rate constant based on catalyst surface area

C_i = i th species concentration

D_{eff} = effective diffusivity

r = average pore radius

$= 2 V_i/S_i$

V_i = catalyst internal volume

S_i = catalyst internal surface area

The equation is solved with the following boundary conditions:

$$C_i = C_{io} \qquad \text{at } x = 0$$

$$\frac{dC_i}{dx} = 0 \qquad \text{at } x = L$$

The solution of this equation is

$$C_i = \frac{C_{io} \text{ Cosh } (\phi \ (1 - x/L))}{\text{Cosh } \phi} \tag{2}$$

where $\phi = R_e \left(\frac{\rho_p S_i k_s}{D_{eff}}\right)^{1/2}$ (Thiele Modulus) (3)

R_e = effective catalyst radius

$= V_e/S_e$

V_e = external pellet volume

S_e = external pellet surface area

ρ_p = pellet density; gm/cm^3

C_{io} = bulk species concentration

Define catalyst effectiveness as:

$$\eta = \frac{r_{pore}}{r_{ideal}} \tag{4}$$

where r_{pore} = reaction rate inside catalyst pore

r_{ideal} = reaction rate in the absence of diffusional resistance

Substituting Eqn. 2 in Eqn. 4 and solving we have

$$\eta = \frac{\tanh \phi}{\phi} \tag{5}$$

for high $\phi (\phi > 3)$

$$\eta \equiv \frac{1}{\phi} \quad \text{(Petersen, 1966)} \tag{6}$$

APPENDIX H

PORE SIZE DISTRIBUTION OF SPENT CATALYSTS

Figures 50 - 66 present the pore size distribution of aged, and regenerated catalayst samples from Run ZBF, ZBG, ZBH and ZBI.

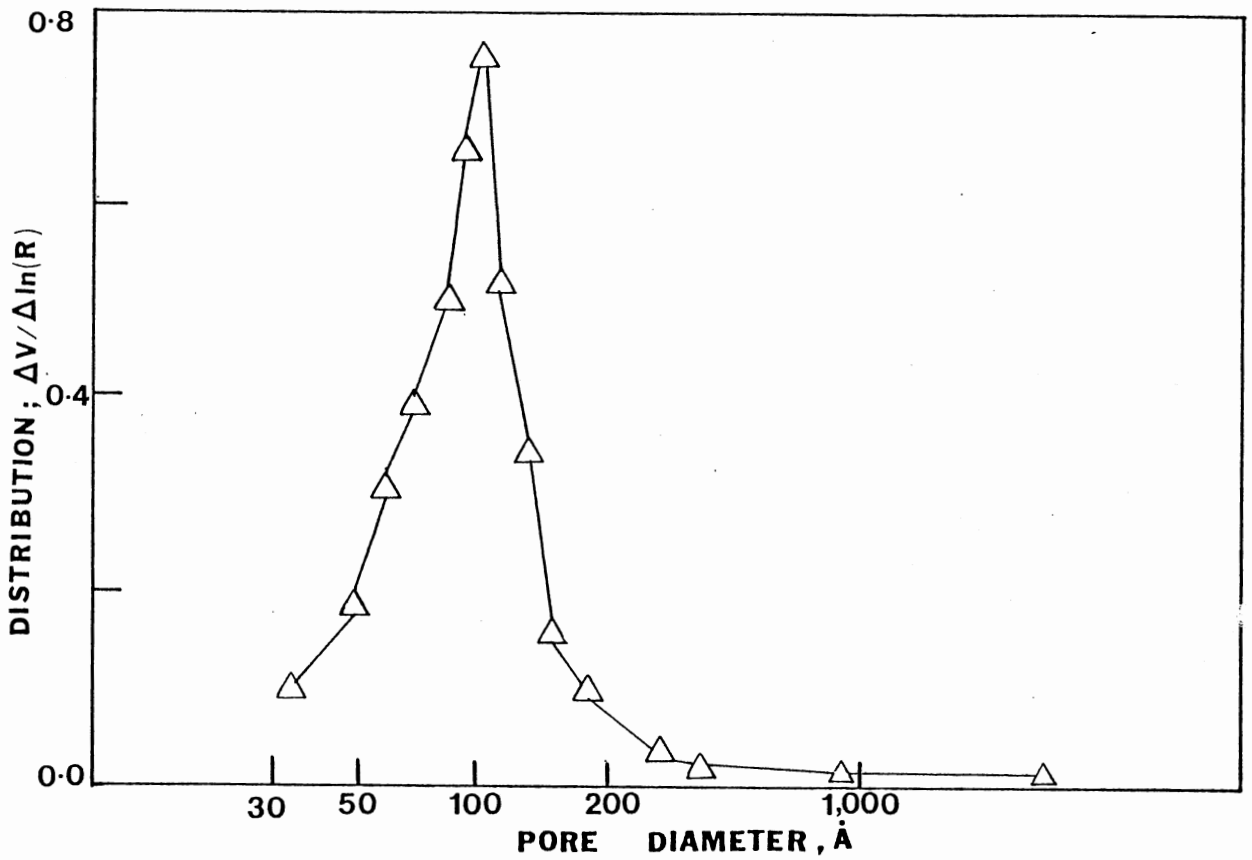

Figure 50. Pore Size Distribution of Aged Catalyst From Reactor Top (Run ZBF)

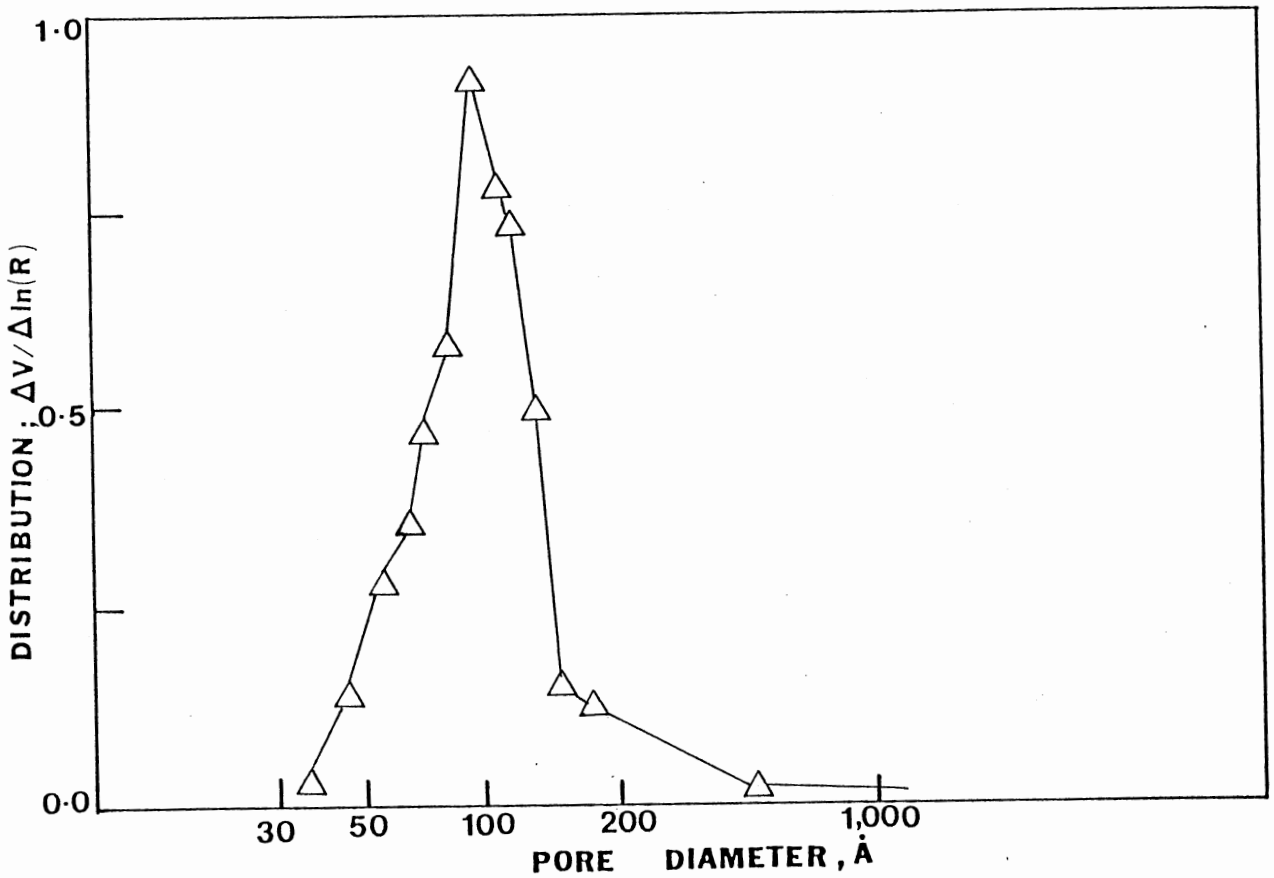

Figure 51. Pore Size Distribution of Aged Catalyst from Reactor Middle (Run ZBF)

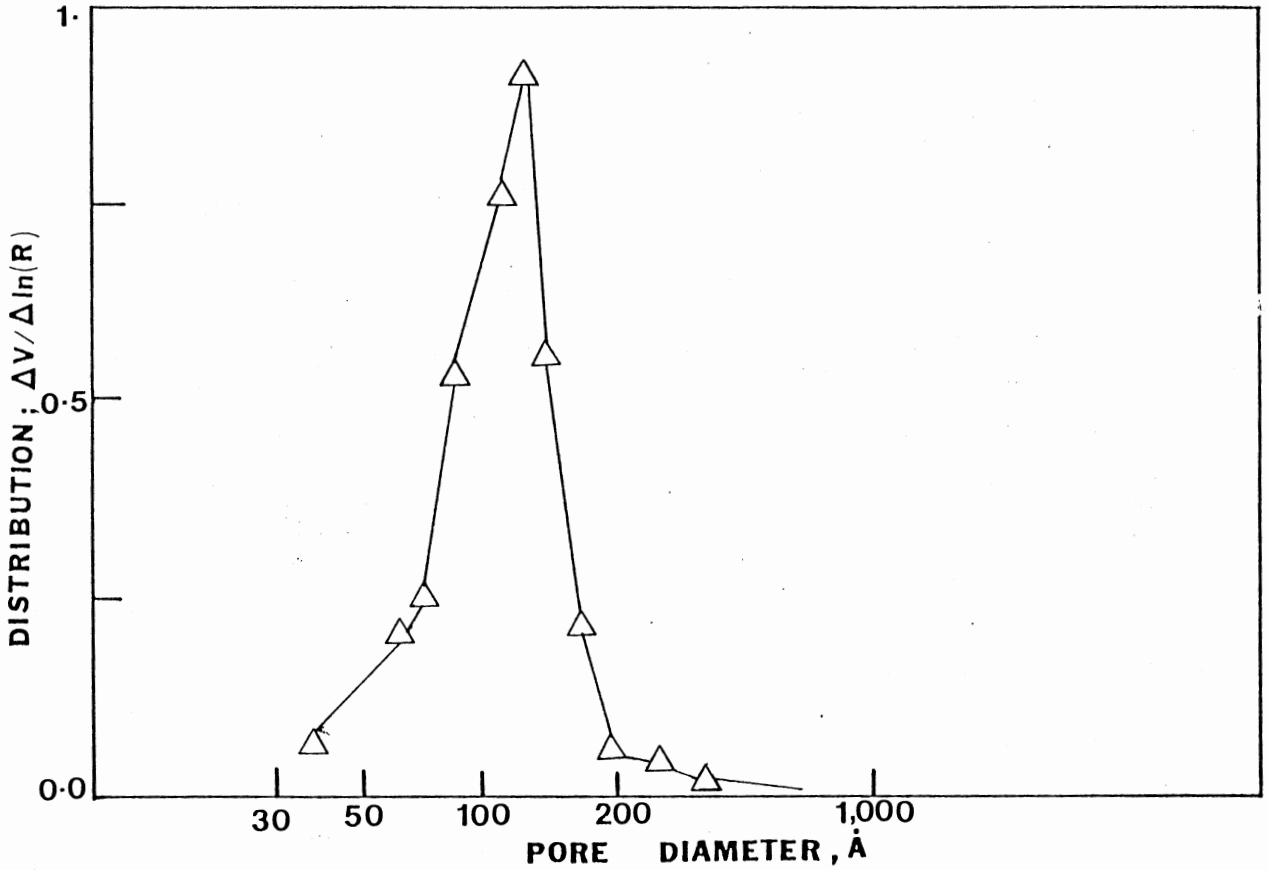

Figure 52. Pore Size Distribution of Aged Catalyst from Reactor Bottom (Run ZBF)

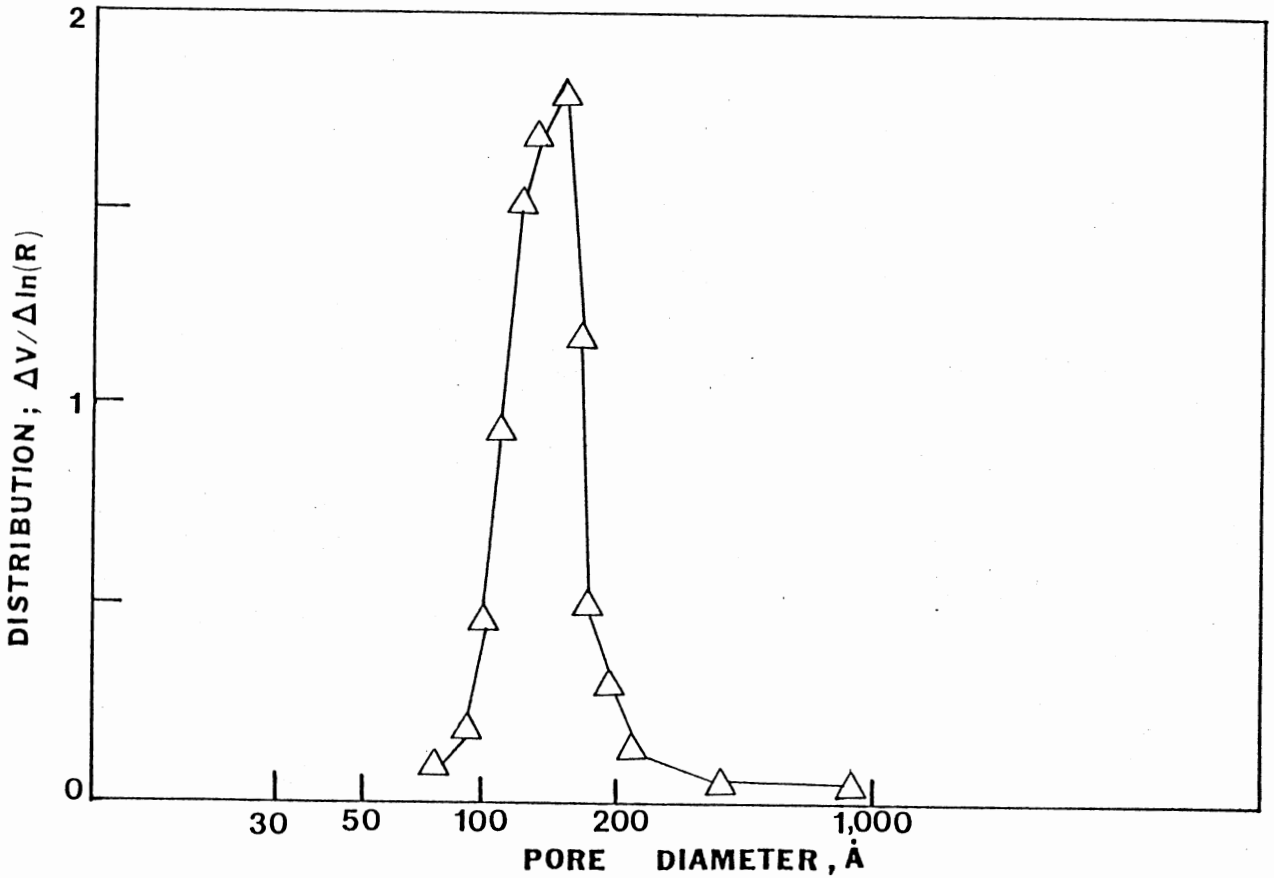

Figure 53. Pore Size Distribution of Regenerated Catalyst from Reactor Top (Run ZBF)

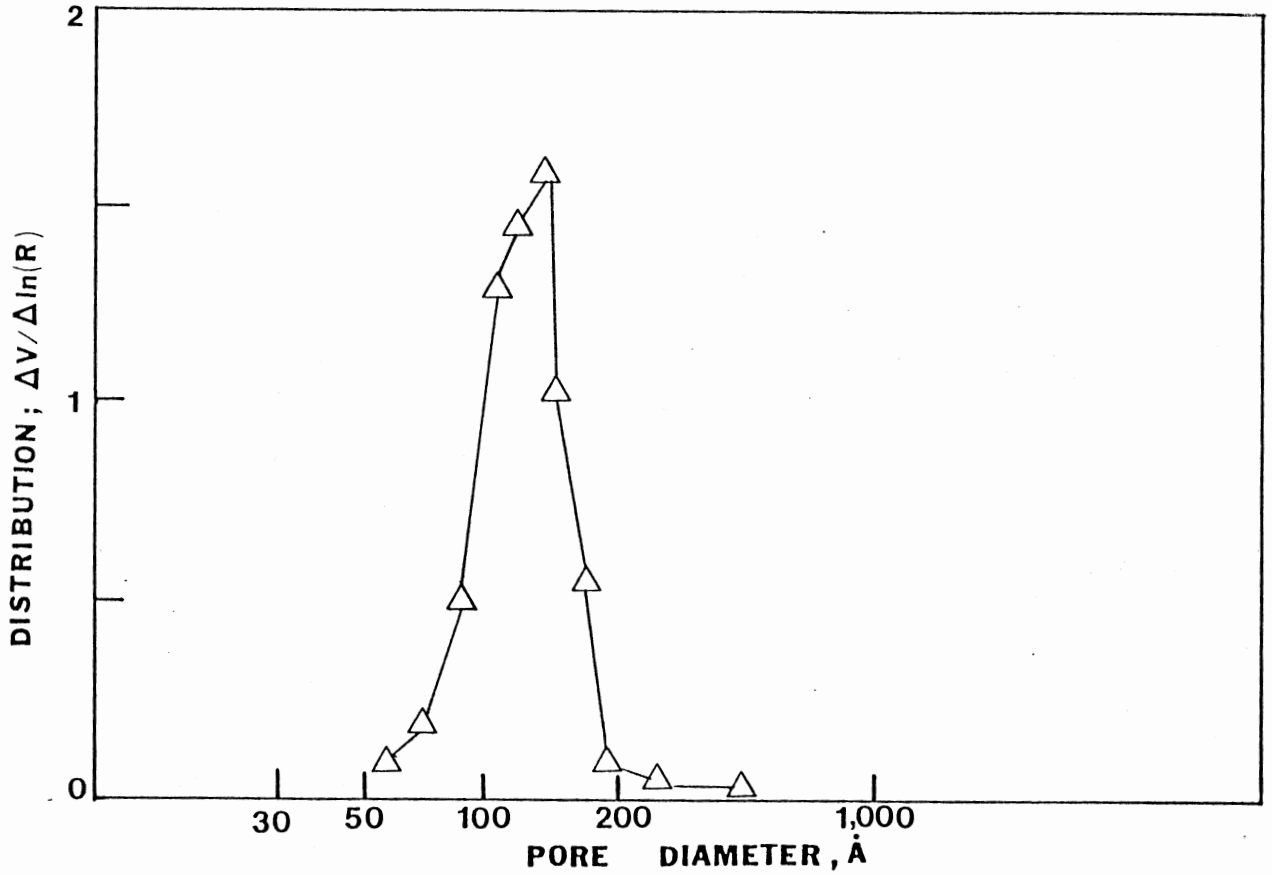

Figure 54. Pore Size Distribution of Regenerated Catalyst from Reactor Bottom (Run ZBF)

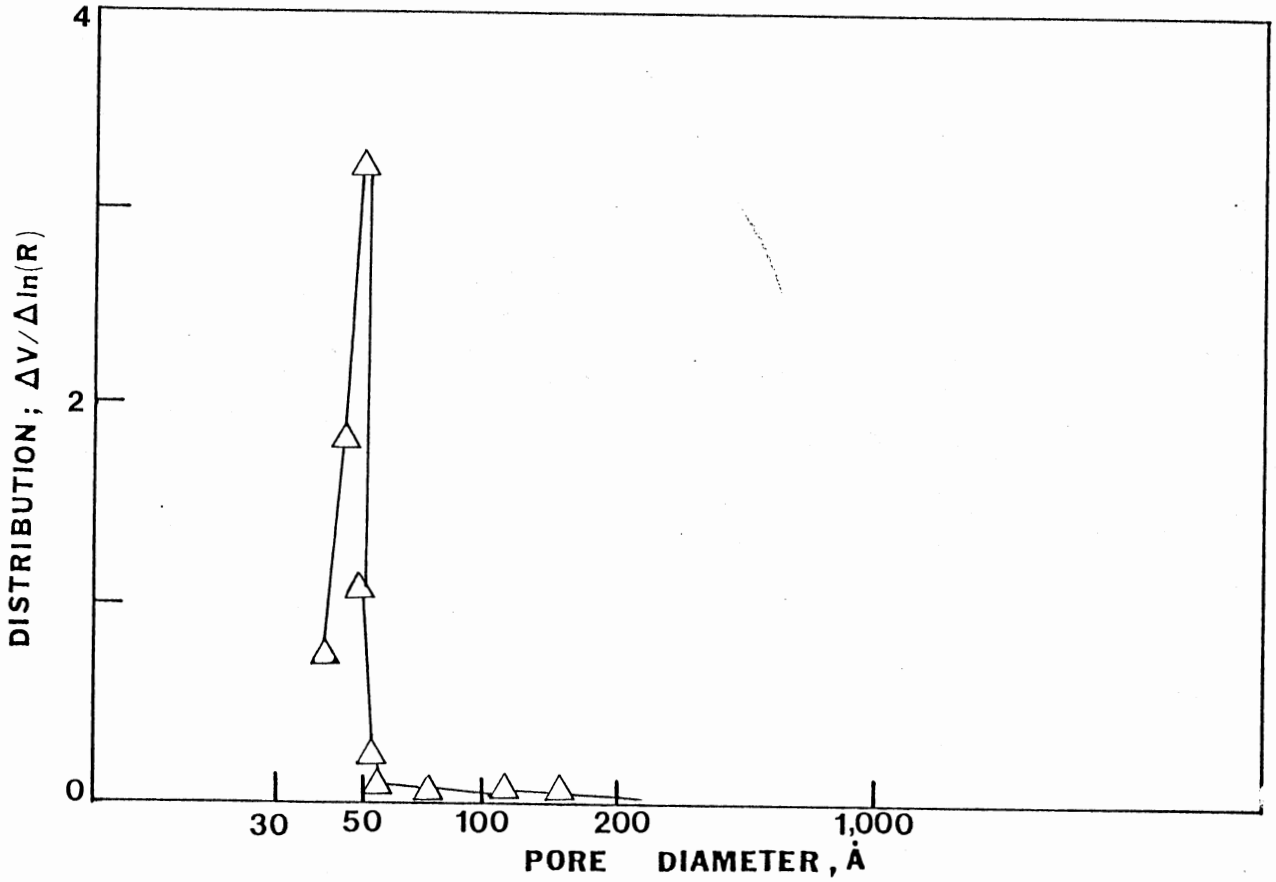

Figure 55. Pore Size Distribution of Coked Catalyst from Reactor Top (Run ZBG)

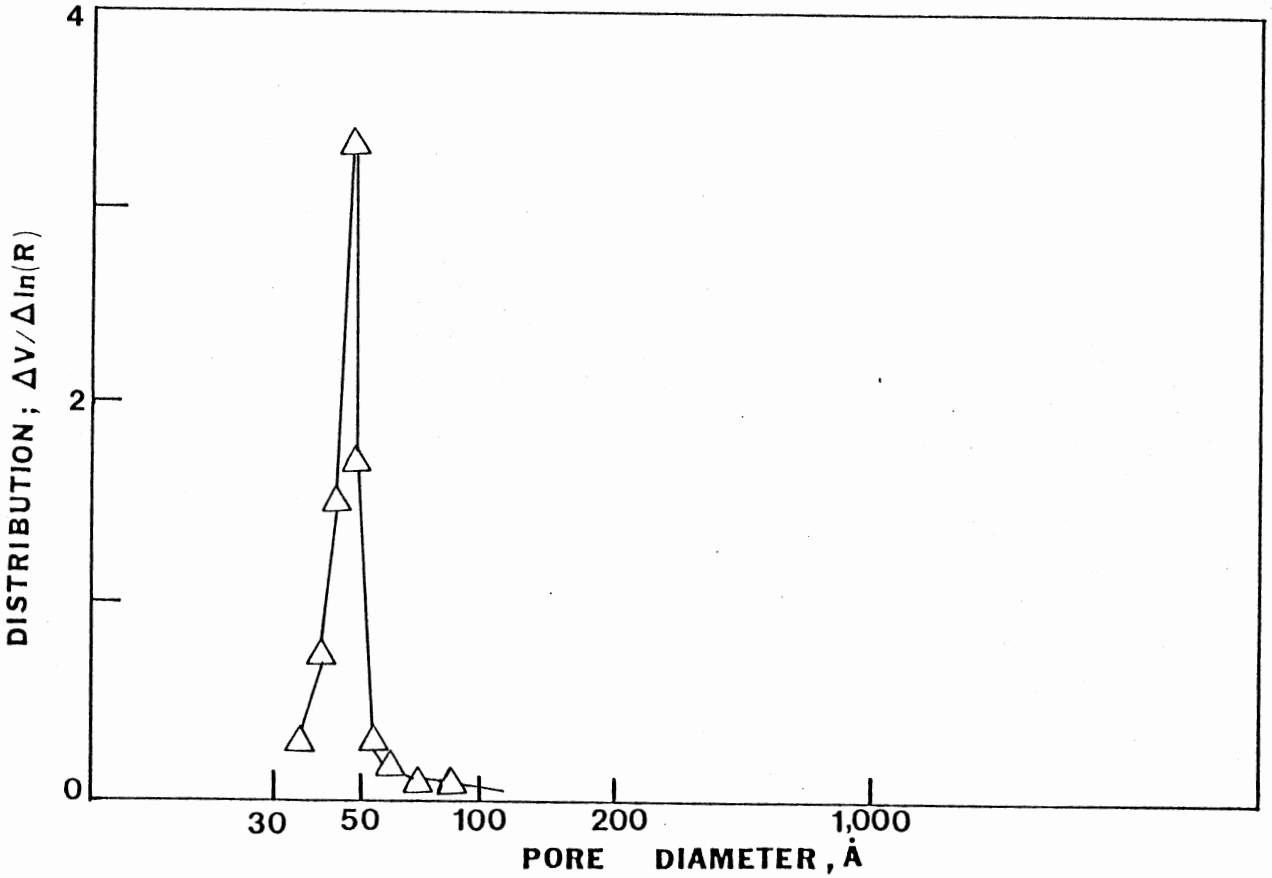

Figure 56. Pore Size Distribution of Coked Catalyst from Reactor Middle (Run ZBG)

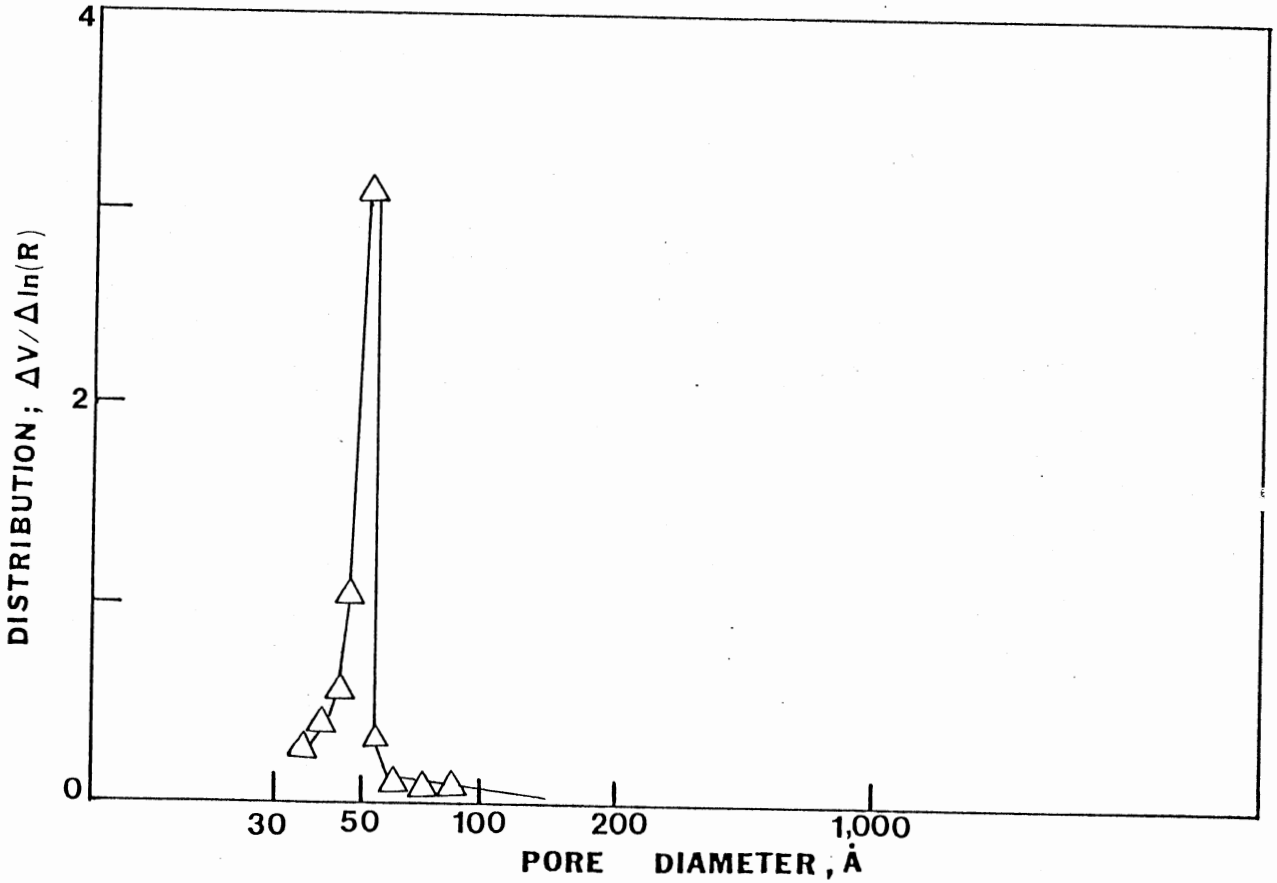

Figure 57. Pore Size Distribution of Coked Catalyst from Reactor Bottom (Run ZBG)

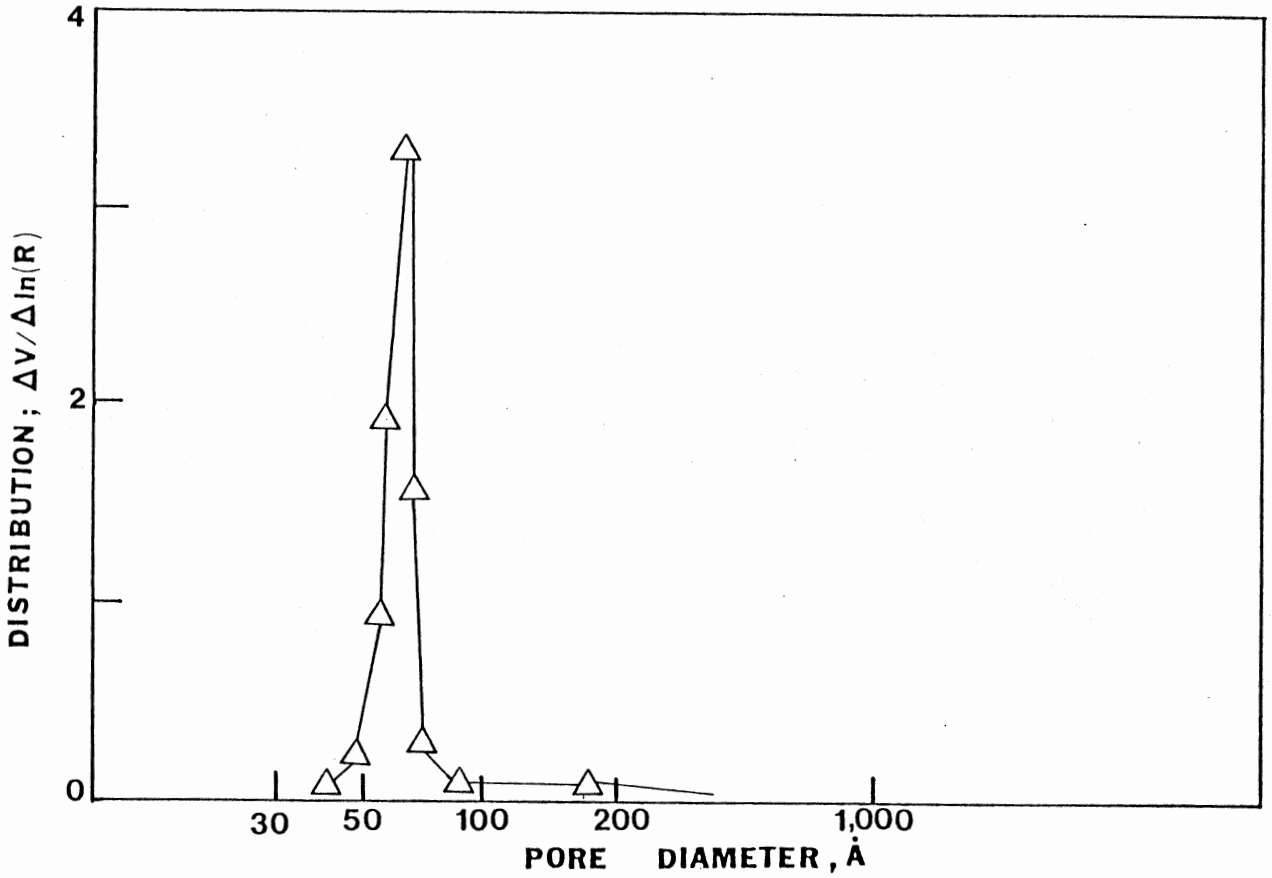

Figure 58. Pore Size Distribution of Regenerated Catalyst from Reactor Top (Run ZBG)

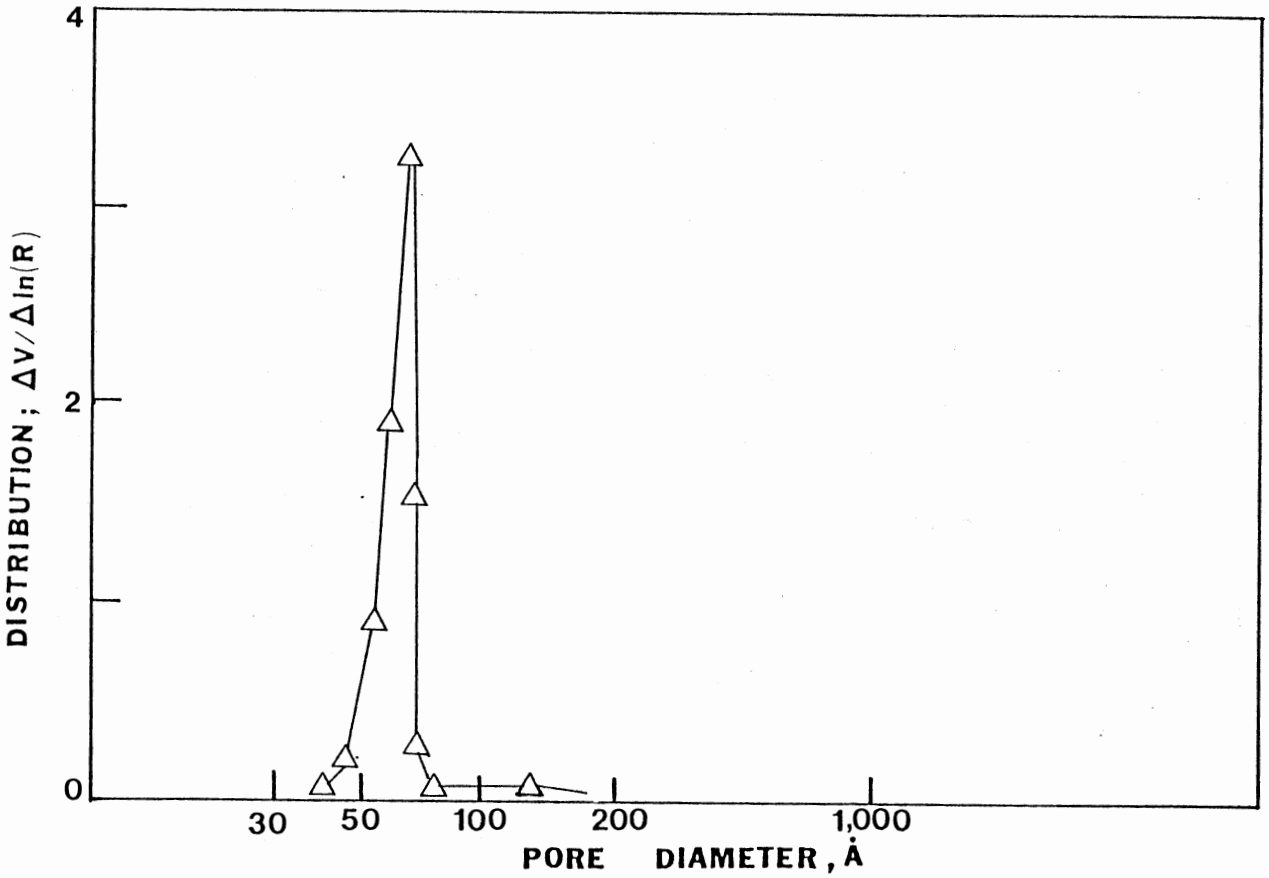

Figure 59. Pore Size Distribution of Regenerated Catalyst from Reactor Bottom (Run ZBG)

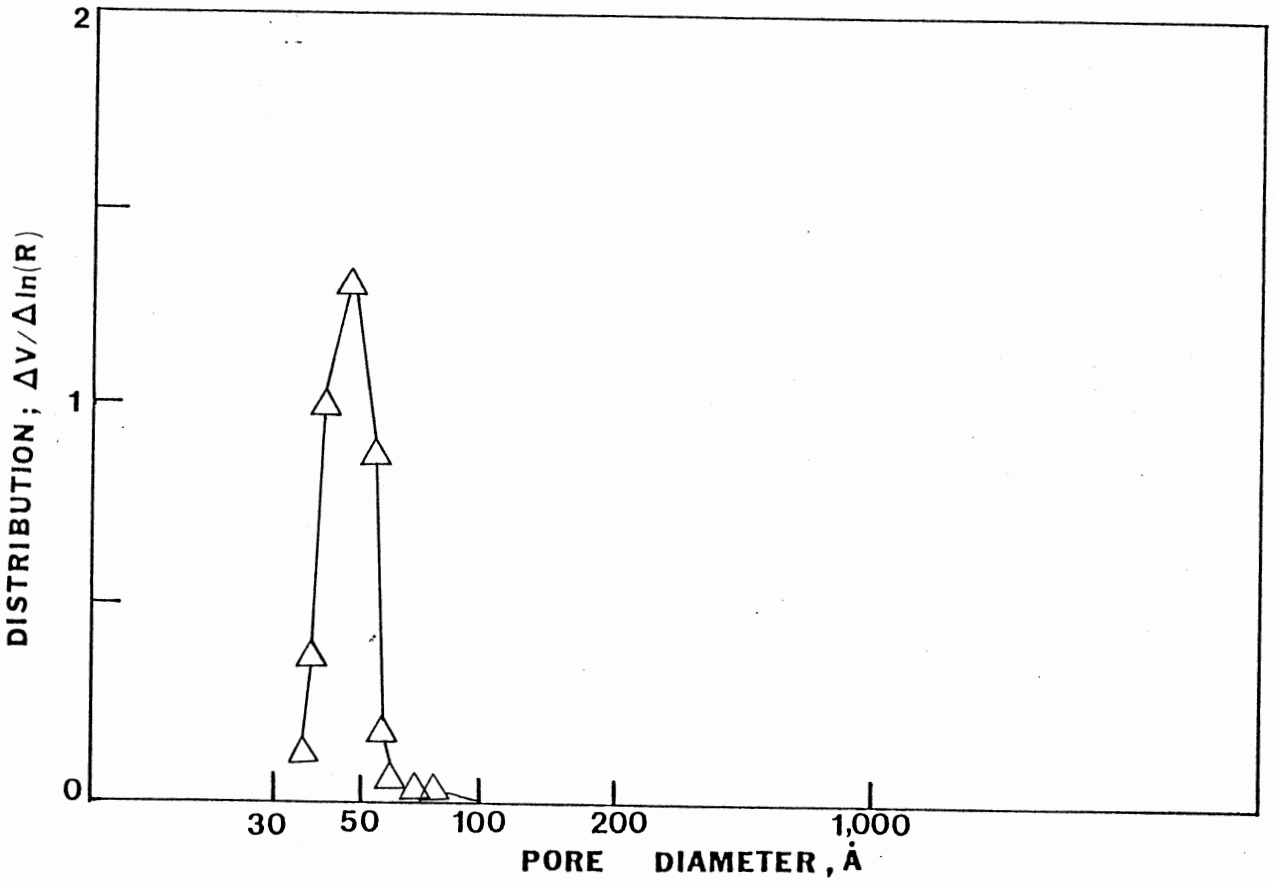

Figure 60. Pore Distribution of Coked Catalyst from Top Reactor (Run ZBH)

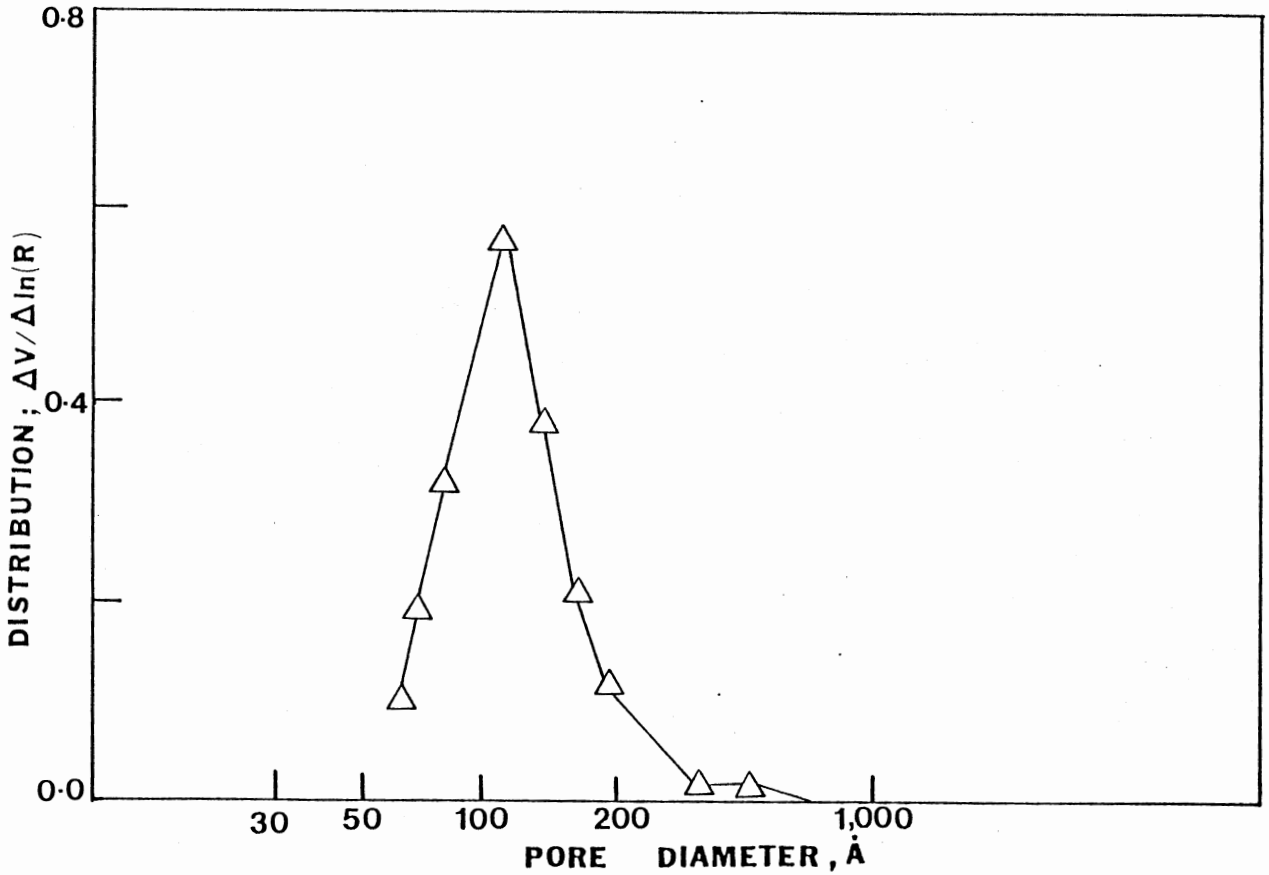

Figure 61. Pore Distribution of Coked Catalyst from Bottom Reactor (Run ZBH)

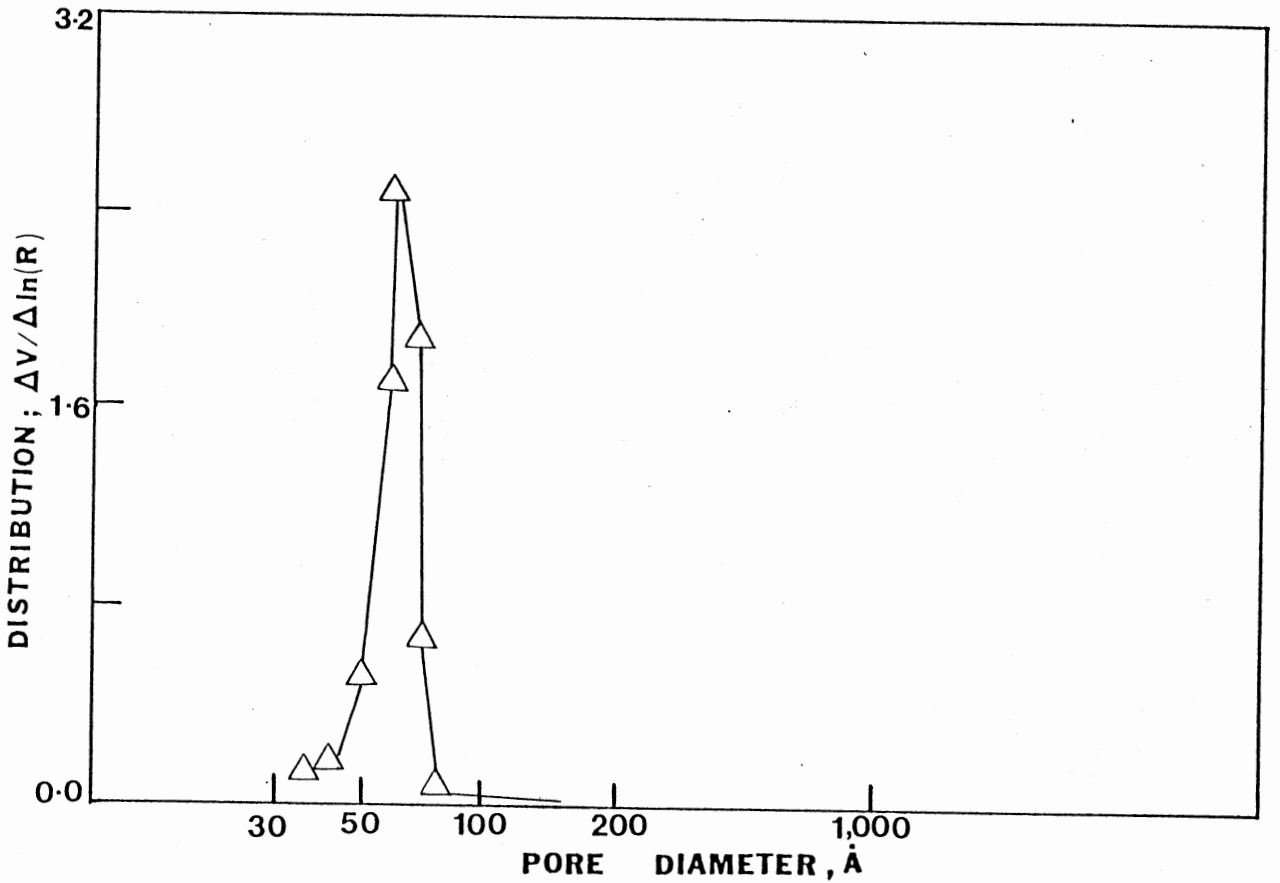

Figure 62. Pore Distribution of Regenerated Catalyst from Top Reactor (Run ZBH)

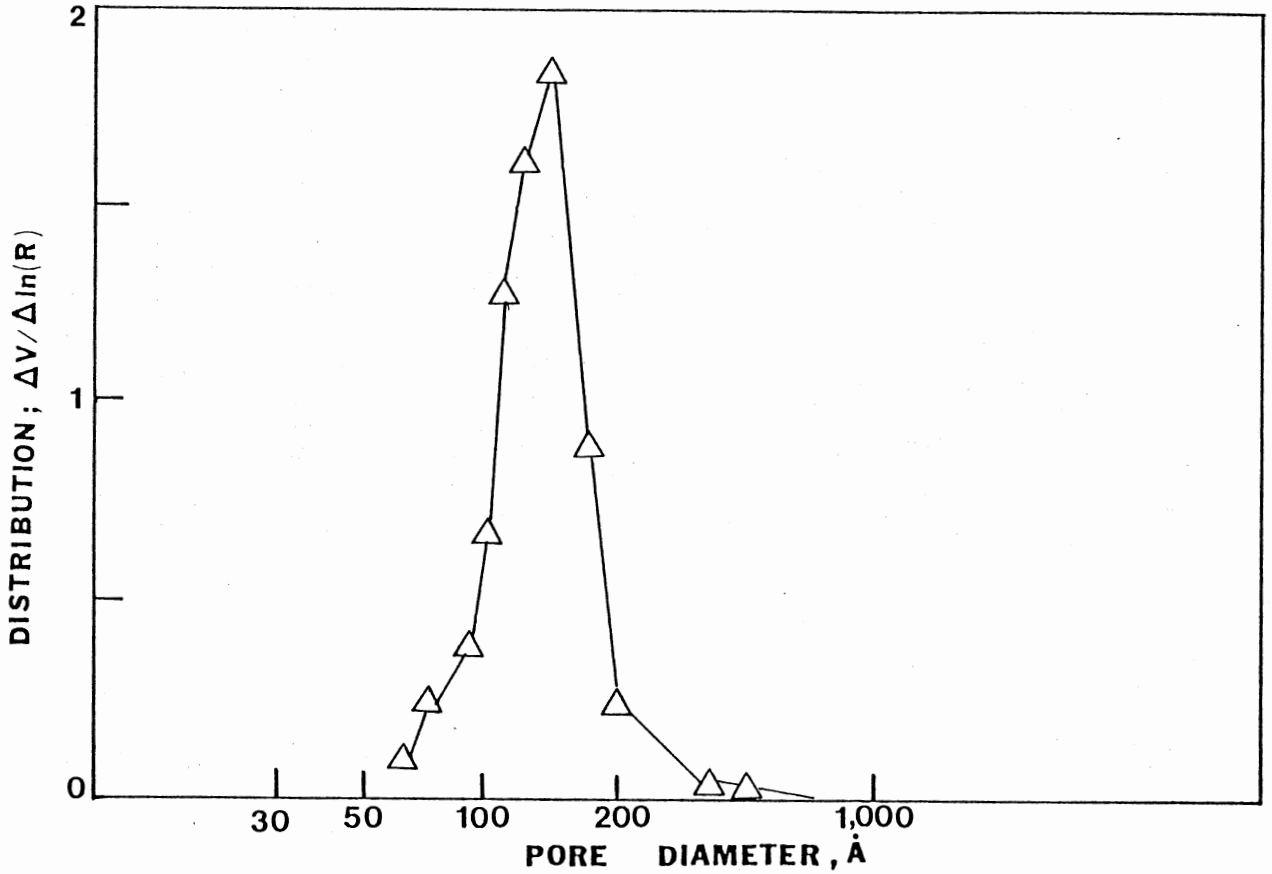

Figure 63. Pore Distribution of Regenerated Catalyst from Bottom Reactor (Run ZBH)

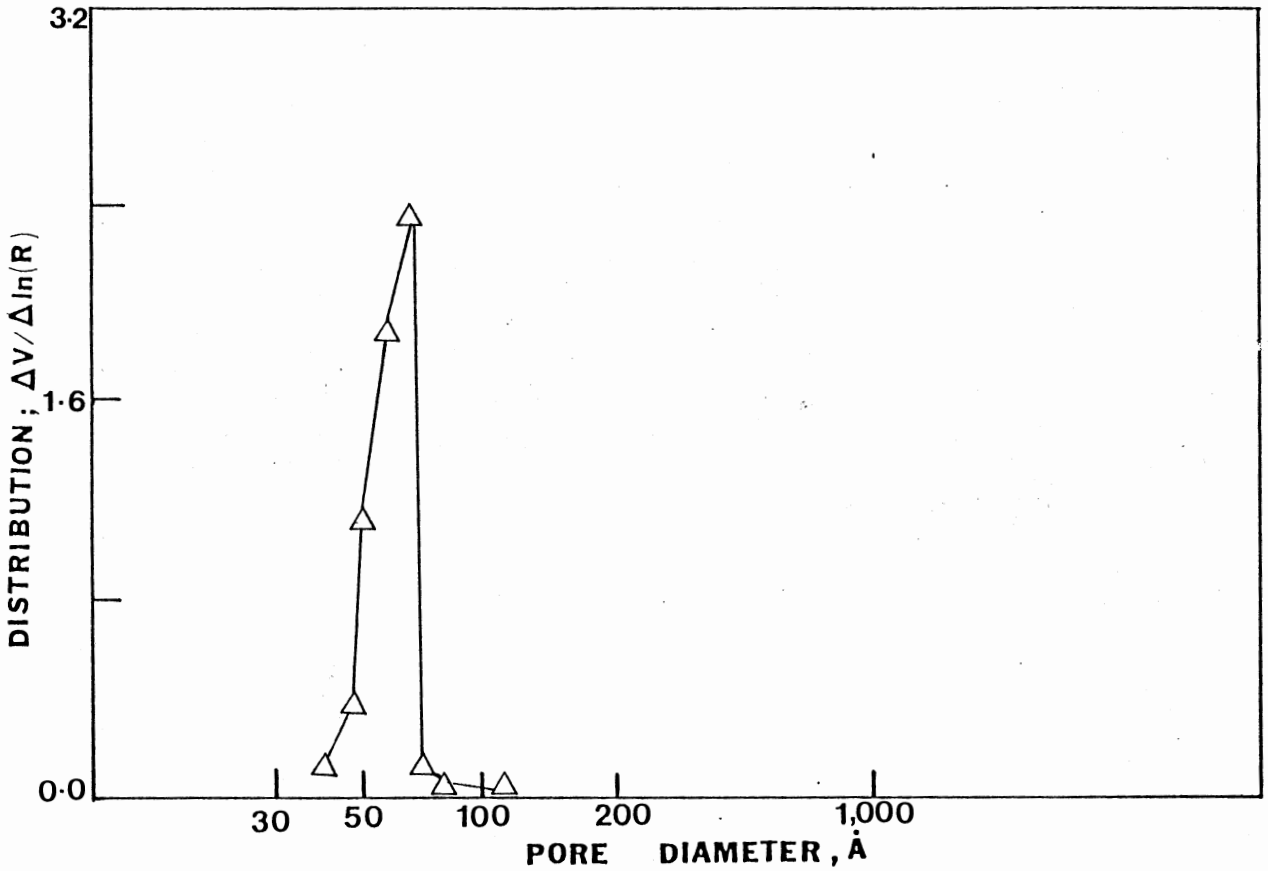

Figure 64. Pore Distribution of Coked Catalyst from High Temperature Reactor (Run ZBI)

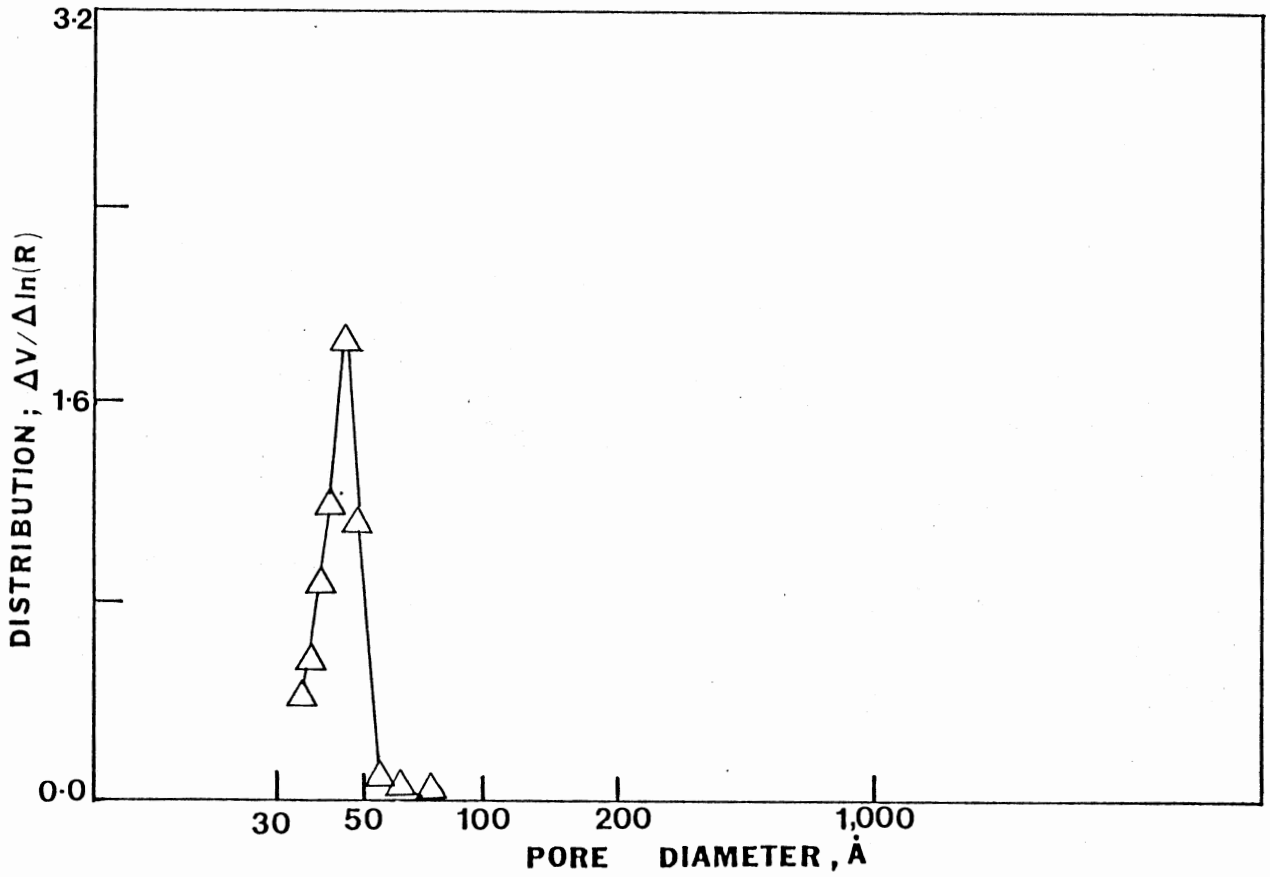

Figure 65. Pore Distribution of Coked Catalyst from Low Temperature Reactor (Run ZBI)

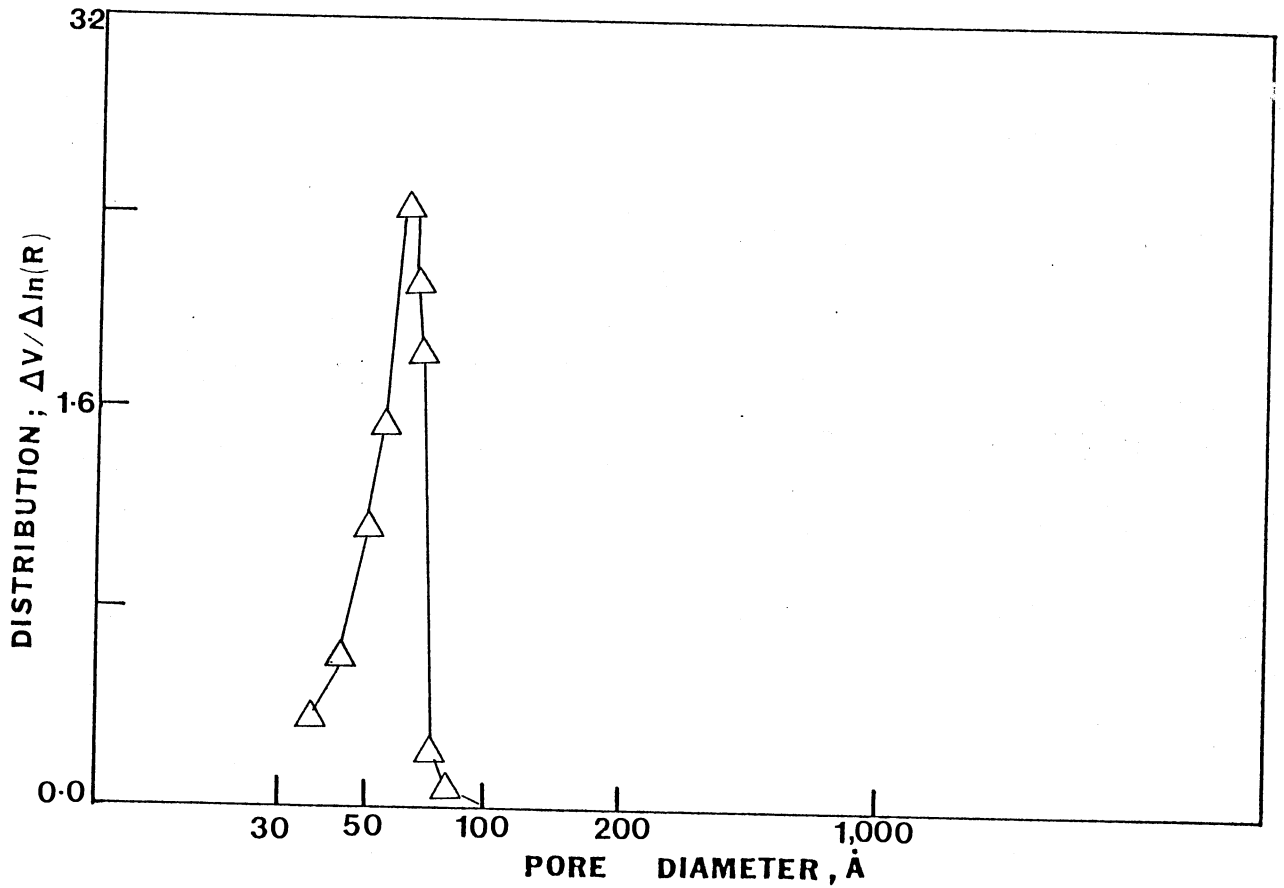

Figure 66. Pore Distribution of Regenerated Catalyst Sample from High Temperature Reactor (Run ZBI)

APPENDIX I

EXPERIMENTAL DATA

Two commercial Ni-Mo-Al_2O_3 catalysts were used to hydrotreat a 15 wt% SRC/Process Solvent mixture. Temperatures in the range of 350 to 400°C, and liquid volume hourly space times (LVHST) of 0.94 through 1.87 hours were employed at a constant reactor pressure of 11.7 MPa (1700 psig). The product liquid samples were analyzed for their elemental, solvent residues and 454 C^+ residue content. The aged catalyst samples were analyzed for their physical properties, metal deposition and coke deposits.

TABLE XXXV

ELEMENTAL ANALYSES RESULTS FEEDSTOCK:
15 WT.% SRC/PROCESS SOLVENT

Run/Sample Number	LVHST hrs.	Hours on Oil	Temperature °C	Wt.% N	Wt.% C	Wt.% H
Feedstock	--	--	--	1.12	87.20	7.26
ZBF # 1	1.87	12	400	0.31	89.38	10.50
ZBF # 2	1.87	24	400	0.45	90.06	9.55
ZBF # 3	1.87	36	400	0.48	89.09	9.43
ZBF # 4	0.94	43	400	0.74	88.86	8.74
ZBF # 5	1.34	50	400	0.70	86.89	8.55
ZBF # 6	1.34	57	375	0.88	89.52	8.66
ZBF # 7	1.87	67	375	0.77	89.88	8.70
ZBF # 8	0.94	74	375	0.93	90.27	8.37
ZBF # 9	0.94	81	350	1.15	90.35	8.02
ZBF #10	1.34	88	350	1.05	89.86	8.18
ZBF #11	1.87	96	350	1.00	89.52	9.19
ZBF #12	1.87	108	400	0.64	89.97	9.26
ZBF #13	1.87	120	400	0.65	89.31	9.31
ZBF #14	1.87	132	400	0.64	89.63	8.99
ZBF #15	1.87	144	400	0.69	90.25	8.71
ZBF #16	1.87	156	400	0.67	90.55	8.76
ZBF #17	1.87	168	400	0.78	90.56	9.00
ZBF #18	1.87	180	400	0.79	90.38	8.91
ZBF #19	1.87	192	400	0.82	89.40	8.89
ZBF #20	1.87	204	400	0.79	89.48	8.81
ZBF #21	1.87	216	400	0.79	90.21	8.67
ZBF #22	1.87	228	400	0.86	89.62	8.58
ZBF #23	1.87	240	400	0.84	87.80	8.83
ZBG # 1	1.87	12	400	0.25	89.65	10.10
ZBG # 2	1.87	24	400	0.41	87.69	9.68
ZBG # 3	1.87	36	400	0.43	87.74	9.48
ZBG # 4	1.87	43	400	0.73	89.78	8.77

TABLE XXXV (Continued)

Run/Sample Number	LVHST hrs.	Hours on Oil	Temperature °C	Wt.% N	Wt.% C	Wt.% H
ZBG # 5	1.34	50	400	0.62	86.15	8.88
ZBG # 6	1.34	57	375	0.79	89.42	8.92
ZBG # 7	1.87	67	375	0.71	89.01	9.11
ZBG # 8	0.94	74	375	0.97	89.05	8.49
ZBG # 9	0.94	81	350	1.01	89.17	8.22
ZBG #10	1.34	88	350	0.95	89.07	8.32
ZBG #11	1.87	95	350	0.91	89.34	8.35
ZBG #12	1.87	108	400	0.47	88.41	9.33
ZBG #13	1.87	120	400	0.48	89.42	9.57
ZBG #14	1.87	132	400	0.54	87.73	9.08
ZBG #15	1.87	144	400	0.50	88.40	9.34
ZBG #16	1.87	156	400	0.63	90.25	9.53
ZBG #17	1.87	168	400	0.57	87.88	9.22
ZBG #18	1.87	180	400	0.57	86.98	9.16
ZBG #19	1.87	192	400	0.64	90.51	9.19
ZBG #20	1.87	204	400	0.58	86.96	9.02
ZBG #21	1.87	216	400	0.55	86.50	8.67
ZBG #22	1.87	228	400	0.55	84.59	8.91
ZBG #23	1.87	240	400	0.61	91.33	9.10
ZBH # 1	1.87	12	400	0.30	90.97	10.03
ZBH # 2	1.87	24	400	0.44	89.20	9.66
ZBH # 3	1.87	36	400	0.55	89.06	9.57
ZBH # 4	0.94	43	400	0.71	89.44	8.82
ZBH # 5	1.34	50	400	0.70	89.75	8.93
ZBH # 6	1.34	57	375	0.81	89.36	8.78
ZBH # 7	1.87	67	375	0.83	89.90	8.82
ZBH # 8	0.94	74	375	0.95	89.19	8.31
ZBH # 9	0.94	81	350	1.02	88.19	7.73
ZBH #10	1.34	88	350	0.98	88.98	8.29
ZBH #11	1.87	96	350	1.00	89.01	8.34
ZBH #12	1.87	108	400	0.63	89.42	8.98

TABLE XXXV (Continued)

Run/Sample Number	LVHST hrs.	Hours on Oil	Temperature °C	Wt.%		
				N	C	H
ZBH #13	1.87	120	400	0.74	88.46	9.21
ZBH #14	1.87	132	400	0.63	88.85	8.99
ZBH #15	1.87	144	400	0.67	88.47	9.32
ZBH #16	1.87	156	400	0.73	88.57	9.16
ZBH #17	1.87	168	400	0.64	88.26	9.28
ZBH #18	1.87	180	400	0.68	89.13	9.01
ZBH #19	1.87	192	400	0.68	88.63	9.17
ZBH #20	1.87	204	400	0.73	87.72	9.08
ZBH #21	1.87	216	400	0.68	90.82	8.70
ZBH #22	1.87	228	400	0.77	90.64	8.67
ZBH #23	1.87	240	400	0.78	90.53	8.74

TABLE XXXVI

N-PENTANE INSOLUBLE CONTENT

Run/Sample Number	LVHST hrs.	Hours on Oil	Temperature °C	Wt.% n-Pentane Insolubles
ZBH # 1	1.87	12	400	2.93
ZBH # 2	1.87	24	400	2.91
ZBH # 3	1.87	36	400	3.69
ZBH # 4	0.94	43	400	6.06
ZBH # 5	1.34	50	375	6.33
ZBH # 6	1.34	57	375	7.77
ZBH # 7	1.87	67	375	8.45
ZBH # 8	0.94	74	375	12.52
ZBH # 9	0.94	81	350	16.26
ZBH #10	1.34	88	350	14.83
ZBH #11	1.87	96	350	14.92
ZBH #12	1.87	108	400	4.36
ZBH #13	1.87	120	400	3.88
ZBH #16	1.87	156	400	3.42
ZBH #20	1.87	204	400	3.83
ZBH #21	1.87	216	400	4.39
ZBH #22	1.87	228	400	4.24
ZBH #23	1.87	240	400	3.98
ZBI # 1	0.94	12	260/400	4.70
ZBI # 2	0.94	24	260/400	4.06
ZBI # 3	0.94	36	260/400	4.51
ZBI # 4	0.94	48	260/400	4.86
ZBI # 6	0.94	72	260/400	4.23
ZBI # 8	0.94	96	260/400	4.98
ZBI # 9	0.94	108	260/400	6.44
ZBI #10	0.94	126	260/400	6.26

TABLE XXXVII

ASTM-D1160* VACUUM DISTILLATION RESULTS

Run/Sample Number	LVHST hrs.	Hours On Oil	Temperature °C	Volume % Distilled			Wt. % 454C+
				10	50	80	
ZBF # 1	1.87	12	400	228	291	387	9.05
ZBF # 2	1.87	24	400	230	297	386	10.65
ZBF # 3	1.87	36	400	228	295	380	10.12
ZBF # 4	0.94	43	400	237	307	380	11.75
ZBF # 8	0.94	74	375	257	318	410	15.53
ZBF # 9	0.94	81	350	261	324	423	17.13
ZBF #12	1.87	108	400	249	320	389	11.47
ZBF #13	1.87	120	400	237	306	383	11.63
ZBF #14	1.87	132	400	249	319	384	11.16
ZBF #16	1.87	156	400	248	314	386	11.37
ZBF #18	1.87	180	400	258	326	406	12.93
ZBF #20	1.87	204	400	254	318	392	11.85
ZBF #22	1.87	228	400	258	321	398	12.91
ZBF #23	1.87	240	400	256	324	397	12.52
ZBG # 1	1.87	12	400	228	296	360	7.54
ZBG # 2	1.87	24	400	232	303	377	8.36
ZBG # 3	1.87	36	400	236	301	376	8.82
ZBG # 4	0.94	43	400	240	308	380	12.25
ZBG # 8	0.94	74	375	255	320	414	15.94
ZBG # 9	0.94	81	350	257	326	391	16.89
ZBG #12	1.87	108	400	242	308	383	8.46
ZBG #13	1.87	120	400	227	296	360	9.81
ZBG #16	1.87	156	400	243	308	380	10.04
ZBG #18	1.87	180	400	239	304	376	9.37
ZBG #21	1.87	216	400	240	312	383	10.43
ZBG #22	1.87	228	400	243	326	384	10.73
ZBG #23	1.87	240	400	237	315	383	10.12
ZBH # 1	1.87	12	400	224	299	357	8.22

TABLE XXXVII (Continued)

Run/Sample Number	LVHST hrs.	Hours On Oil	Temperature °C	Volume % Distilled 10	50	80	Wt. % 454C+
ZBH # 2	1.87	24	400	232	314	366	10.23
ZBH # 3	1.87	36	400	243	316	377	11.06
ZBH # 4	0.94	43	400	249	323	394	13.23
ZBH # 8	0.94	74	375	263	326	406	16.30
ZBH # 9	0.94	81	350	267	336	425	18.09
ZBH #13	1.87	120	400	234	303	368	10.81
ZBH #16	1.87	156	400	240	318	383	11.90
ZBH #20	1.87	216	400	251	323	392	12.89
ZBH #23	1.87	240	400	251	317	382	11.93
ZBI # 1	1.87	12	400	214	290	389	7.76
ZBI # 2	1.87	24	400	224	293	373	9.67
ZBI # 3	1.87	36	400	219	318	402	12.40
ZBI # 8	1.87	96	400	236	304	384	11.86
ZBI # 9	1.87	108	400	251	311	404	13.23
ZBI #10	1.87	120	400	--	--	--	--

* Normal boiling point determined from 20 mm Hg boiling point data.

TABLE XXXVIII

ELEMENTAL ANALYSIS OF DISTILLATION PRODUCTS*

Sample/Run Number	Distilled Liquids Wt. %			454 C^+ Residues Wt. %		
	N	C	H	N	C	H
ZBF # 1	0.135	88.24	10.80	0.935	87.96	7.62
ZBF # 2	0.347	90.34	10.08	0.951	85.45	7.43
ZBF # 3	0.380	89.63	9.38	1.055	90.49	7.25
ZBF # 4	0.483	90.10	8.83	1.164	90.03	6.88
ZBF # 8	0.853	90.40	8.91	1.603	76.26	6.34
ZBF # 9	0.918	89.99	8.84	1.707	77.99	6.21
ZBF #16	0.582	88.90	9.26	1.286	95.49	7.81
ZBF #20	0.706	91.30	9.82	1.238	84.75	7.27
ZBF #23	0.679	88.85	8.88	1.276	83.01	6.99
ZBG # 1	0.122	87.31	10.87	0.949	79.56	7.11
ZBG # 2	0.262	92.39	10.09	1.042	84.74	7.36
ZBG # 3	0.277	90.77	9.87	1.019	80.67	7.09
ZBG # 4	0.521	90.76	9.19	1.195	75.79	6.56
ZBG # 8	0.653	89.83	8.30	1.449	72.22	6.18
ZBG # 9	0.729	90.69	8.74	1.396	75.35	5.99
ZBG #12	0.398	86.45	9.48	0.983	80.93	7.22
ZBG #16	0.468	87.60	9.31	1.050	80.32	8.03
ZBG #20	0.548	88.81	9.52	1.014	84.99	7.68
ZBG #23	0.495	88.84	9.54	0.977	78.00	6.87
ZBI # 1	0.373	87.90	9.77	1.098	67.87	6.38
ZBI # 4	0.463	89.39	9.26	1.0902	70.98	5.57
ZBI # 8	0.598	89.38	8.99	1.1830	70.92	6.85
ZBI # 9	0.691	90.314	8.88	1.216	67.11	6.35

*Vacuum distillation, 20 mm of mercury.

TABLE XXXIX

EDAX CATALYST ANALYSIS

Cursor Position	Catalyst Position	Area Percent							
		Al	S+Mo	Fe	Ti	Si	Ni	Ca	K
Run ZBF (Large Pore Catalyst)									
Overall	Top	13.8	26.9	21.5	--	18.9	4.7	2.1	1.9
Surface	Middle	14.5	24.1	25.2	11.6	15.9	1.3	3.8	3.1
Scan	Bottom	16.1	26.7	24.5	9.6	20.0	3.2	3.7	4.1
10μm	Top	19.7	22.3	22.5	3.9	19.5	1.7	3.1	3.5
Inside	Middle	19.1	21.6	23.8	3.2	15.6	0.9	2.9	4.6
Catalyst Surface	Bottom	20.3	24.2	21.7	6.4	17.5	1.4	3.9	3.8
60μm	Top	44.0	41.3	3.0	6.9	--	4.7	-	-
Inside	Middle	54.9	36.0	1.7	2.2	--	3.6	-	-
Catalyst Surface	Bottom	30.0	50.0	4.3	3.2	--	9.8	1.4	-
Catalyst	Top	81.4	12.9	2.6	1.1	--	1.7	-	-
Center	Middle	82.6	12.3	0.9	-	--	1.7	-	-
	Bottom	84.6	12.5	-	-	--	1.6	-	-
Run ZBG (Small Pore Catalyst)									
Overall	Top	8.3	31.2	26.1	5.6	18.9	1.5	2.3	1.4
Surface	Middle	9.8	27.4	30.3	6.5	20.1	-	2.7	3.1
Scan	Bottom	7.6	28.7	30.3	5.2	17.4	-	2.6	2.9
10μm	Top	16.8	32.4	16.8	4.5	13.7	2.1	1.6	1.7
Inside	Middle	11.6	31.3	26.8	2.9	14.1	-	2.6	2.1
Catalyst Surface	Bottom	6.3	31.8	35.2	13.2	11.8	-	-	-
60μm	Top	42.2	34.8	14.4	3.1	2.8	2.5	-	-
Inside	Middle	40.0	22.0	6.5	6.7	4.1	1.4	3.9	1.2
Catalyst Surface	Bottom	56.4	33.1	3.2	4.3	2.8	2.5	-	-
Catalyst	Top	67.1	27.1	-	-	2.1	3.6	-	-
Center	Middle	63.0	32.6	-	-	2.1	2.4	-	-
	Bottom	62.2	30.6	-	-	2.0	5.1	-	-

TABLE XXXIX (Continued)

Cursor Position	Catalyst Position	Area Percent							
		Al	S+Mo	Fe	Ti	Si	Ni	Ca	K
Run ZBH (Composite Catalyst Bed)									
Top Reactor									
Overall	Top	36.7	32.1	13.3	2.3	6.7	2.4	4.1	2.1
Surface	Middle	21.1	29.5	23.2	6.9	12.5	1.3	4.3	2.6
Scan	Bottom	10.4	21.2	27.9	3.0	26.8	1.0	3.8	2.9
10 µm	Top	4.2	32.7	51.9	-	7.4	7.4	1.7	2.0
Inside	Middle	6.7	32.5	40.9	-	15.2	-	1.2	2.1
Catalyst	Bottom	11.6	31.3	26.8	-	6.5	3.4	-	-
Catalyst	Top	56.5	27.7	3.9	3.6	2.3	2.7	2.9	-
Center	Middle	47.3	26.7	23.6	3.3	9.2	1.0	3.7	1.1
	Bottom	67.4	27.9	1.0	-	1.7	2.4	-	-
Bottom Reactor									
Overall	Top	17.9	24.9	12.1	11.2	15.4	2.5	3.9	3.3
Surface	Middle	16.5	32.8	15.5	18.1	9.7	3.5	4.8	2.2
Scan	Bottom	20.0	31.2	14.1	14.6	9.5	4.3	5.2	2.1
10 µm	Top	12.6	21.9	30.5	4.3	3.5	-	3.0	4.0
Inside	Middle	16.5	22.0	15.0	3.0	3.1	1.5	5.1	4.3
Catalyst	Bottom	30.7	48.0	12.9	2.9	4.7	6.5	-	-
Catalyst	Top	68.0	20.7	2.0	1.0	-	3.5	-	-
Center	Middle	72.9	21.8	1.9	1.6	-	1.7	-	-
	Bottom	73.1	22.0	1.8	-	-	3.6	-	-
Run ZBI (Two Temperature Zone Experiment)									
Low Temperature Reactor (260°C)									
Overall	Top	29.2	41.2	23.2	1.0	9.7	2.3	1.2	1.8
Surface	Middle	40.8	36.3	16.0	-	6.2	3.5	-	-
Scan	Bottom	27.5	34.0	23.1	1.8	8.4	-	2.3	2.3
10 µm	Top	62.7	26.8	5.0	-	2.4	2.9	-	-
Inside	Middle	58.9	31.1	3.6	-	2.4	2.7	-	-
Catalyst Surface	Bottom	59.8	8.9	6.9	-	2.4	1.8	-	-
Catalyst	Top	65.8	26.4	1.9	-	2.3	3.4	-	-
Center	Middle	59.9	31.1	3.6	-	2.2	2.9	-	-
	Bottom	63.2	26.8	2.3	-	2.3	3.3	-	-

TABLE XXXIX (Continued)

Cursor Position	Catalyst Position	Area Percent							
		Al	S+Mo	Fe	Ti	Si	Ni	Ca	K
High Temperature Reactor (400°C)									
Overall	Top	37.6	36.1	9.9	1.7	4.3	2.2	2.3	3.8
Surface	Middle	46.9	34.1	5.2	3.9	3.8	3.0	1.5	1.0
Scan	Bottom	64.7	28.7	-	-	2.4	3.4	-	-
10 µm	Top	55.9	28.1	2.9	2.4	2.3	3.2	-	4.5
Inside	Middle	62.3	28.9	1.9	1.8	2.0	2.5	-	0.8
Catalyst Surface	Bottom	33.3	26.8	3.1	3.1	2.7	2.2	2.3	1.3
Catalyst	Top	72.3	23.1	-	-	2.1	2.3	-	-
Center	Middle	64.7	28.7	-	-	2.4	3.4	-	-
	Bottom	66.3	26.3	-	-	2.2	2.5	-	-

VITA

Opinder Kishan Bhan

Candidate for the Degree of

Doctor of Philosophy

Thesis: AN INVESTIGATION OF THE ACTIVITY OF COMPOSITE CATALYST BEDS FOR HYDROTREATMENT OF A COAL-DERIVED LIQUID

Major Field: Chemical Engineering

Biographical:

Personal Data: Born in Srinagar, Kashmir, March 17, 1956 to Brij Krishan Bhan and Mohini Bhan.

Education: Attended Tyndle Biscoe Memorial School, Srinagar, Kashmir; received the Degree of Bachelor of Engineering in Chemical Engineering from University of Kashmir, Srinagar, India in August, 1978; received the Degree of Master of Science in Chemical Engineering from Oklahoma State University, Stillwater, Oklahoma, May, 1981; completed the requirements for the Degree of Doctor of Philosophy at Oklahoma State University in December, 1983.

Professional Experience: Engineering Trainee, Bhabha Atomic Research Center, Bombay, India, Summer of 1977; Graduate Teaching Assistant, School of Chemical Engineering, Oklahoma State University, Stillwater, Oklahoma, January, 1979 to December, 1979; Research Assistant, School of Chemical Engineering, Oklahoma State University, Stillwater, Oklahoma, January, 1980 to May, 1983; Research Engineer, United States Department of Energy, Bartlesville, Oklahoma, August, 1983 to present.

Membership in Scholarly or Professional Societies: Omega Chi Epsilon, Chemical Engineering honor society; American Institute of Chemical Engineers.